Journal of International Environmental Application and Science *ISSN-2636-7661*

Publishing Office: *Department of Industrial Engineering, Engineering Faculty, King Abdulaziz University, P.O. Box: 80204 Jeddah 21589 Saudi Arabia*; Tel: +966 533 107628; Fax: +966 2 2486695.

Frequency: Journal of International Environmental Application and Science (ISSN 2636-7661) is published 4 times per year.

Aims and Scope: Journal of International Environmental Application and Science is dedicated to detailed and comprehensive investigations, analyses and appropriate reviews of the interdisciplinary aspects of renewable sources, municipal and industrial solid wastes, waste disposal, environmental pollution, environmental science and education, biomass, agricultural residues, energy sources, hazardous emissions, incineration, environmental protection topics included experimental, analytical, industrial studies, hydrological recycling, water pollution, water treatment, air pollution, gas removal and disposal, environmental pollution modelling, noise pollution and control. Suitable topics are also included regarding the efficient environmental management and use of air, water and land resources.

Publication information: Please address all your requests regarding orders and subscription queries to: *Dr. S. Dursun*, Environmental Engineering Department, Engineering and Natural Science Faculty, Konya Technical University, Konya, TURKİYE. Tel: +90 3332 2051559, Fax: +90 332 2410635, Mobil: + 90 536 5954591.
E-mail: sdursun@ktun.edu.tr

Guide for Authors

Submission of Papers: Manuscripts for publication may be sent to the Editor-in-Chief, a member of the Editorial Board. Submission address is: Editor-in-Chief, Dr. S. Dursun, Environmental Engineering Department, Engineering & Natural Science Faculty, Konya Technical University, Konya, TURKEY. Manuscripts can also be sent to any member of the Editorial Board (see inside front cover for addresses). Although this journal is international in scope, all articles must be in the English language. Potential contributors whose first language is not English are urged to have their manuscript competently edited prior to submission. Papers should be written in the third person in an objective, formal and impersonal style.

Manuscript Preparation:

General: Manuscripts must be typewritten, double-spaced with wide margins on one side of white paper. Good quality printouts with a font size of 12 pt are required. The corresponding author should be identified (include E-mail address, Telephone and Fax number). Full postal addresses must be given for all co-authors. Two hard copies of the manuscript should be submitted by regular mail.

Abstracts: Each manuscript must be including a brief abstract and a short list of keywords.

Text: Follow this order when typing manuscripts: Title, Authors, Affiliations, Abstract, Keywords, Introduction, Main text, Conclusion, Acknowledgements, Appendix, References, Vitae and Figure Captions followed by the Figures and Tables. Pages should be numbered consecutively. The corresponding author should be identified with an asterisk and footnote.

Symbols and Units: All Greek letters and unusual symbols should be identified by name in the margin, the first time they are used. SI units should be used wherever possible, as recommended in ISO 1000 and BS 5555.

References: All publications cited in the text should be presented in a list of references following the text of the manuscript. In the text refer to the author's name (without initials) and year of publication (*e.g.* "since Dursun (1993) has shown that..." or "This is in agreement with results obtained later (Boddy, 1984)". For three or more authors use the first author followed by "*et al.*", in the text. The list of references should be arranged alphabetically by authors' names. The manuscript should be carefully checked to ensure that the spelling of authors' names and dates are exactly the same in the text as in the reference list.

References should be given in the following form:

Boddy L, (1984) The micro-environment of basidiomycete mycelia in temperate deciduous woodlands. In: *The Ecology and Physiology of the Fungal Mycelium* (Ed. by D.H. Jennings & A.D.M. Rayner), pp. 261-289. British Mycological Society Symposium 8, Cambridge University Press, Cambridge.

Dursun S, Ineson P, Frankland JC, Boddy L, (1993) Sulphite and pH effects on CO_2 evolution from decomposing angiospermous and coniferous tree leaf litters. *Soil Biology & Biochemistry* **25**, 1513-1525.

Ergas SJ, Schroeder E, Chang D, Scow K, (1994) Spatial distributions of microbial populations in biofilters. In: Proceedings of the *78th Annual Meeting and Exhibition of the Air and Waste Management Association*, pp. 19-24, Cincinnati, OH.

Hickey M, King C, (1988) *100 Families of Flowering Plants*. Cambridge University Press, Cambridge.

Littlejohn D, Wang Y, Chang S-G, (1993) Oxidation of aqueous sulphite ion by nitrogen dioxide. *Environmental Science & Technology* **27**, 2162-2167.

Illustrations: All illustrations should be provided in camera-ready form, suitable for reproduction (which may include reduction) without retouching. Photographs, charts and diagrams are all to be referred to as “Figure” and should be numbered consecutively in the order to which they are referred. They should be accompanying the manuscript, should be included within the text.

Tables: Tables should be numbered consecutively and given a suitable caption, and each table should be included within the text. Footnotes to tables should be typed below the table and should be referred to by superscript lowercase letters.

Electronic Submission: Authors may submit electronic copy of their manuscript by e-mail or online submission on WEB site of the JIEAS. The final version of the manuscript should be submitted on floppy disk or CD. The electronic copy should match the hardcopy exactly. MS Word is recommended for software for article submission.

Proofs: Proofs will send to the author and should be returned 48 hours of receipt. Corrections should be restricted to typesetting errors; any others may be charged to the author. Any queries should be answered in full.

Subscription: Subscription for the issue contains author’s article published in “*Journal of International Environmental Application and Science*” is €100.00 which will be sending to the corresponding author.Journal of International Environmental Application and Science (ISSN 1307-0428) is published since 2006. Subscription rates for a year are: Institutions: € 300.00 (four issues per a year) Individuals: € 150.00 (four issues per a year)

Correspondence: Papers should be upload DergiPark WEB Page system to: https://dergipark.org.tr/en/journal/759/submission/step/manuscript/new in Microsoft Office Word 2007 format.

Website*:** *http://www.jieas.com*; *https://dergipark.org.tr/en/pub/jieas* ***E-Mail: *sdursun@ktun.edu.tr*

“Journal of International Environmental Application and Science” is indexed in:
“**Global Impact Factor**, **EBSCO, CAS Source Index (A Division of the American Chemical Society), Index Copernicus, ProQuest, CABI, Ulrich's™ Serials Analysis System, SCIRUS, ArgosBiotech, NAAEE, The University of Queensland's Institutional, The NAL Catalog (AGRICOLA), WORLDCAT Catalog, LexisNexis, The National Library of Finland, National Library of Australia, DergiPark Turkey”** *Journal Indexing List.*

C O N T E N T S

J. Int. Environ. Appl. and Sci., Vol. 20 No. 1 pp: 1-115 March 2025

J. Int. Environmental Application & Science, Vol. 20: 1-18 (2025)
Research Paper

Groundwater Quality Assessment in the Upper Denkyira Districts of Ghana

Victor Ofori Agyemang*

Hydrogeological Unit, Community Water and Sanitation Agency, P. O. Box 128, Damongo, Ghana

Received October 2, 2024; Accepted February 17, 2025

Abstract: The Upper Denkyira East and West Districts heavily rely on groundwater for all of their various water needs. The rising levels of surface water pollution brought on by mining, farming, improper waste disposal, and galamsey activities necessitate evaluating the quality of the groundwater for drinking, domestic use, and irrigation. The goal of the study was to assess the suitability of groundwater for drinking, domestic use, and irrigation purposes. Groundwater in the area can be classified as mixed water, NaCl, $CaHCO_3$, and $CaMgSO_4$. Three processes including rock mineral dissolution, ion exchange, and the effects of anthropogenic activities are major factors influencing the chemistry and overall quality of the groundwater in the area. The water quality index indicates that 38%, 38%, 3%, and 21% of the water samples are of excellent, good, poor, and very poor quality respectively for drinking. The groundwater is unfit for drinking without prior treatment due to its low pH, high pH, high Fe, high Mn, and high PO_4^{3-} levels. The quality of groundwater is impacted by both geological processes and anthropogenic activities like improper agrochemical application, galamsey, and improper waste disposal. The study discovered that 48% of the groundwater types were excellent, 34% were good, 14% were moderate, and 3% were poor based on IWSI. The IWSI was calculated using EC, SAR, Na%, RSC, KI, PI, MH, and CR. The IWSI results and the USSL and Wilcox diagrams demonstrated that the groundwater falls within the excellent to good categories. The study has shown that the IWSI method is a reliable technique for assessing water quality irrigation.

Keywords: *Upper Denkyira Districts, Groundwater Quality index, Irrigation Water Suitability Index, Anthropogenic Activities, Birimian*

Introduction

Water is a natural resource essential for human survival, socioeconomic development, factory operation, aquatic life survival, etc. The quality of water is determined by its intended usage; however, for water to be useful the physical, chemical, and biological parameters should have concentrations within a certain limit as approved by the right authority. Increasing or decreasing the centration of a water parameter may render water unfit for its intended usage. Therefore, the definition of water quality is complex since it depends on its desired use and other factors (Babiker et al., 2007). The challenge of not meeting water supply demand calls for effective techniques that serve as keys to the sustainability of water resources. Hence, there is a need for data collection, analysis, and interpretation to make informed decisions on water resources. This is needed for groundwater resource protection and the overall management of water resources.

In modern days the increasing growth of the global population size and advancement in all areas of technology including agriculture, mining, road construction, etc. have impacted water bodies such that some are unsafe for human consumption without treatment. The rate at which this contamination is occurring is so alarming that the whole environmental contamination is globally seen as a major issue for human survival. For example, in Ghana, the recent outbreak of illegal small-scale mining has destroyed the environment and strongly impacted water bodies. This impact includes the introduction of heavy metals and other poisonous substances into water bodies through runoff from agrochemical applications on farmland, improper disposal of domestic and industrial waste, etc.; making them unfit for human consumption (Raju *et al.*, 2011). This calls for effective groundwater quality monitoring for early detection of contamination and this involves continuous groundwater quality assessment. Therefore, a lot of researchers have conducted research in this field of study in different parts of the globe. This is to help address the increasing challenges affecting groundwater management due to geogenic processes and human activities. For example, the studies of Baba and Tayfur in Turkey and Li *et al.* in China helped

*Corresponding: E-Mail: oforiagyemangvictor@yahoo.com, Tel: +233248136427

reveal the groundwater quality issues in the respective study areas and their possible public health effects (Li *et al*., 2010a; Baba & Tayfur, 2011).

Different authors have successfully applied the GIS technique in groundwater studies to integrate different parameters for effective decision-making (Goodchild, 2000). The technique also bridges the gap between water professionals and other professional groups when it comes to communication about water quality issues (Twigg, 1990). For instance, the application of GIS successfully revealed public exposure to polluted water, the spatial distribution of the degree of contamination, and the affected communities (Aral & Maslia, 1996).

Most developing countries like Ghana heavily depend on groundwater due to its availability and relatively low treatment cost. Groundwater is used for drinking, domestic, and agricultural purposes in most developing countries (Margat *et al*., 2013). This has resulted in increasing demand for the resource globally (EEA, 1999; UNECE, 1999). This shows the importance of groundwater and the need to protect it from contamination. This calls for data collection, analysis, and interpretation for effective decision-making. Ghanaians primarily use groundwater resources for drinking, domestic use, and agriculture, according to Gyau-Boakye *et al*. (2008). This is partly because Ghana Water Company Limited (GWCL) serves only the urban areas. Groundwater is the main source of water for the majority of rural water supplies developed by the Community Water and Sanitation Agency (CWSA), non-governmental organizations, faith-based organizations, etc., according to Gyau-Boakye *et al.* (2008). Like many other districts in Ghana, the Upper Denkyira East and West Districts heavily rely on groundwater for the majority of their water needs.

Most of their activities, like improper agrochemical application, galamsey, and improper waste disposal have the potential to contaminate groundwater, endangering the ability of the groundwater resource to remain pure. These towns are primarily agricultural, and the gold minerals in their lands are abundant. The suitability of groundwater for drinking, domestic use, and agricultural use, as well as any potential anthropogenic effects on the chemistry of the groundwater, are important to understand. This will contribute to the public's access to potable water and the efficient management of water resources.

The groundwater resource of the aquifers in the districts, however, is not well known. The purpose of the study was to characterize the chemical parameters, identify the factors influencing groundwater chemistry, and assess the suitability of the groundwater for irrigation, domestic use, and drinking. This is essential to meet Sustainable Development Goal Number Six mainly on clear water and sanitation. The hydrogeology of the Districts is mainly controlled by the underlying Birimian and Tarkwaian formations. These rocks have limited primary porosity and permeability; hence, their hydraulic properties are controlled mainly by the secondary hydraulic properties. Therefore, the flow of groundwater occurs mainly through the fracture zones and other discontinuities instead of interstitial flow (CAGL, 2010). While Coffey observed that the groundwater flows toward the Offin River, (CAGL, 2010) observed a radial flow of groundwater within the Districts. Also, while JMSL (1993) noticed aquifer recharge of 3-5% of the total precipitation CAGL (2010) observed 15% of total precipitation.

Materials and Methods

Study area

Situated on a forest-cut plateau, the study area features undulating steep-sided hills and valley topography. The highest rise is about 250 m high. The primary drainage sources for the region are the Offin and Dia Rivers and their tributaries, Ninta, Subin, and Afiefi. The area is in the semi-equatorial zone, with mean annual temperatures of 30°C for the hottest month and 26°C for the coolest month during the wet and dry seasons, respectively (GSS, 2021). With an average yearly rainfall of 1,200 mm to 2,000 mm, the region experiences two different rainfall regimes (GSS, 2021). The first rainy regime starts in May or June, the second begins in September or October, and the dry season starts in November or February. Plantains, cocoa, cassava, and other crops are common in the districts. The districts rank among the top cocoa-producing districts in the Central Region of Ghana, which is significant. Due to the large gold reserves within the districts, many mining companies and small-scale illegal miners, known locally as galamsey, have been drawn to the area. The primary geological components of the region are the Tarkwaian and Birimian Formations (Fig. 1).

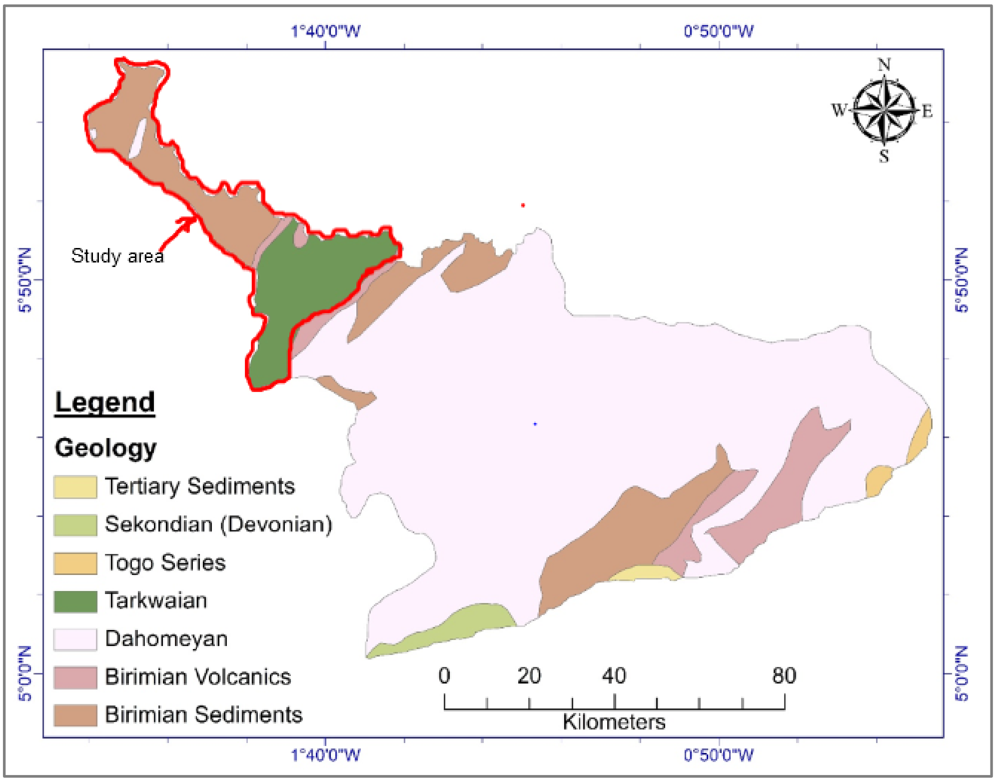

Figure 1. Geological Map of Central region showing the study area (Modified after Osiakwan *et al*., 2022)

Hydrogeology

The study area is underlain by the northeastern and southwest-oriented Middle Precambrian Birimian and Tarkwaian Formation hydrogeological units (Fig. 1). Despite having distinct dates, phyllite may be found in relative abundance in both the Tarkwaian and Birimian Formations. The Birimian formation contains metamorphosed volcanic and sedimentary rocks. Granitoid invasion, folding, and transformation under the greenschist-facies condition occurred during the Eburnean (Junner, 1935; Leube *et al*., 1990). The folded and foliated rocks of the Birimian formation enhance the permeability of the rocks for groundwater storage and flow in conjunction with the faults, folds, foliations, and joints (Junner, 1935). Because of the considerable shearing, schists are more common where the rocks and granitic intrusives of the Birimian Sedimentary Basin meet.

Because the Dixcove granite (G2) is a complex rock that intrudes into the Birimian metavolcanic, the volcanic belts are granitoid. These rocks are frequently tonalitic, consisting of granodiorites, biotite granite, or soda-rich hornblende that grade into hornblende diorite and quartz diorite. The study area has a variety of rocks, including granite, sandstones, mudstones, siltstones, phyllites, slates, schists, tuffs, conglomerates, and greywackes. Thus, the minerals commonly discovered in the area include orthoclase, plagioclase, quartz, biotite, muscovite, amphibole, hornblende, calcite, silica, and chlorite. The Birimian rocks have poor correlations between borehole production and depth, according to Anornu et al. (2009). The transmissivity of boreholes ranges from 0.12 to 125 m2/day based on the results of pumping tests conducted by Anornu *et al.* (2009).

Different sandstones, conglomerates, and argillites make up the Tarkwaian Formation. Griffiths et al. (2002) claim that after deposition in alluvial fans, the conglomeratic units of the Tarkwaian Formation were modified by braided stream channels. In the latter, concentrated fine gold particles are considered present in the channel conglomerates. The northeastern folding of the Tarkwaian increases the groundwater potential (Kesse, 1985). Additionally, according to the CSIR-WRI Database (2007), the presence of a buried river channel (Dickson and Benneh, 1988), substantial weathering, and the availability of quartz veins are characteristics of the Birimian and Tarkwaian Formations that contribute to the comparatively high groundwater potential of the area (Kortatsi, 1994). Figure 2 shows the directions of groundwater flow within the study area. The groundwater flows into the Offin River within the study area.

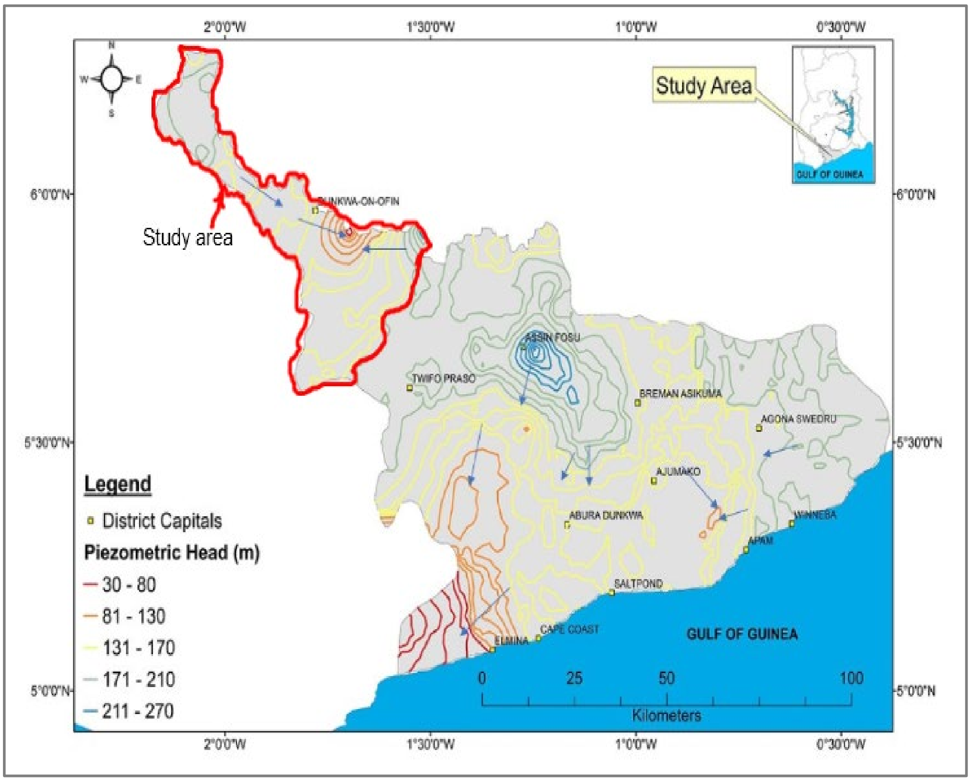

Figure 2. Groundwater flow directions of Central Region showing the study area (Modified after Osiakwan *et al.*, 2022)

Method

The data used in this study was provided by the Central Regional Office of Community Water and Sanitation Agency (CWSA) in Cape Coast. Physico-chemical parameter data from 29 boreholes were obtained from CWSA in November 2020. The data was gathered as part of several initiatives to provide the target communities with potable water. The Geographic Positioning System (GPS) was used to record the coordinates of the boreholes where the samples were taken. Groundwater samples were taken in 500 ml high-density polyethylene sampling bottles for in-lab testing. Typically, the samples were taken after a long pumping session or a pumping test. The samples were preserved for heavy metal analysis, and 10 ml of 69% nitric acid was used to prepare them for the analysis. The bottles were labeled to identify the samples while the necessary field observations and other data were being recorded in the field notebook. Physical parameters such as pH, Total Dissolved Solids (TDS), and Electrical Conductivity (EC) were measured in situ using a portable meter (Hanna instrument), using the guidelines of the World Health Organization (WHO, 2008) and American Public Health Association (APHA, 1995). The samples were kept in an ice chest with ice packs during transportation to the Ghana Water Company Limited (GWCL) Laboratory in Cape Coast for additional analysis.

The recommended standards from APHA (1995) were used to analyze the groundwater samples. TDS, EC, temperature, and pH were among the physical parameters examined using the probe method. Chemical parameters F^-, Cl^-, SO_4^{2-}, NO_3^-, NO_2^-, PO_4^{3-}, and CO_3^{2-} were examined using ion chromatography, while Fe, Mn, and Ca^{2+} were examined using Atomic absorption spectrometry (AAS). $CaCO_3$ mg/L was changed into HCO_3^- using the formula proposed by Hem (1985). The measurement of Total Suspended Solid (TSS) was done using photometric method 8006, the measurement of Total Hardness (TH) was done using titrimetric method, the measurement of alkalinity was done using titration method, the measurement of turbidity was done using absorptiometric method, the measurement of color was done using cobalt standard method, the measurement of salinity was done using electrical conductivity method, measurement of sodium and potassium was done using flame photometer. The calculated Charge Balance Error (CBE) of the samples was used to evaluate the accuracy of the laboratory data, and it was found that the samples were accurate to within ±10% (Celesceri *et al.*, 1998) as shown in Table 1.

Table 1. Calculated results of charge balance error

No	Community	Na	K	Ca	Mg	NH_4	Cl	SO_4	NO_2	HC_3	CO_3	TZ^+	TZ^-	CBE (%)
1	Subinsu	2.91	0.19	1.00	1.33	0.00	1.76	1.31	0.00	2.69	0.00	5.44	5.75	-2.84
2	Barrier	0.57	0.06	0.17	0.41	0.00	0.45	0.33	0.00	0.49	0.00	1.20	1.28	-3.00
3	Sobroso	0.83	0.07	0.46	0.09	0.00	0.28	0.17	0.00	0.05	1.08	1.45	1.59	-4.60
4	Zion Camp	0.76	0.07	1.20	0.17	0.00	0.68	0.52	0.00	1.04	0.00	2.20	2.24	-0.90
5	Achiase	0.53	0.01	0.08	0.16	0.00	0.14	0.11	0.00	0.44	0.00	0.78	0.69	6.45
6	Fosu Dankwa	0.07	0.02	2.41	1.03	0.02	0.17	0.36	0.00	3.10	0.00	3.53	3.64	-1.58
7	Zion 2	0.65	0.09	0.32	0.15	0.00	0.34	0.05	0.00	0.37	0.40	1.21	1.15	2.62
8	Akyerekrom	0.20	0.03	0.70	0.10	0.00	0.40	0.02	0.00	0.53	0.00	1.02	0.95	3.45
9	Zion 1	0.30	0.06	0.12	0.20	0.00	0.33	0.00	0.00	0.24	0.00	0.67	0.57	8.38
10	Congo 1	0.24	0.03	0.20	0.33	0.00	0.17	0.13	0.00	0.56	0.00	0.80	0.86	-3.55
11	Gyampokro1	0.37	0.06	0.12	0.20	0.00	0.34	0.02	0.00	0.36	0.00	0.75	0.72	2.16
12	Konaboe	0.37	0.06	1.49	0.48	0.00	0.37	0.16	0.00	1.84	0.00	2.41	2.37	0.78
13	Abudukrom	0.75	0.06	0.44	0.20	0.88	0.03	0.00	0.00	0.74	0.00	1.45	1.66	-7.90
14	Imbrain Clinic	0.37	0.03	0.40	0.16	0.00	0.28	0.34	0.00	0.40	0.00	0.96	1.02	-3.14
15	Kruwa	0.52	0.08	1.03	0.17	0.00	0.31	0.52	0.00	0.81	0.00	1.80	1.64	4.81
16	Kyebi	2.04	0.35	2.69	3.28	0.00	3.83	2.02	0.00	1.75	0.00	8.35	7.60	4.68
17	Tegyamoso	0.73	0.04	0.43	0.56	0.00	0.28	0.22	0.00	1.09	0.00	1.75	1.59	4.84
18	Betease	0.80	0.13	0.24	0.13	0.00	0.62	0.02	0.00	0.68	0.00	1.29	1.32	-1.18
19	Adedietem	0.44	0.07	0.91	0.36	0.00	0.45	0.57	0.00	0.91	0.00	1.78	1.94	-4.27
20	Amobaka	0.81	0.02	0.20	1.09	0.00	0.68	0.18	0.00	1.40	0.00	2.12	2.26	-3.08
21	Adeade	0.80	0.01	0.04	0.37	0.00	0.28	0.23	0.00	0.60	0.00	1.22	1.11	4.66
22	Kyerepo	0.99	0.02	0.56	0.85	0.00	0.20	0.22	0.00	2.00	0.00	2.42	2.41	0.06
23	Ampabeng	1.11	0.05	0.16	0.29	0.00	0.14	0.08	0.00	1.24	0.00	1.62	1.46	6.14
24	Aniantetem	1.23	0.02	0.24	0.41	0.00	0.88	0.17	0.00	0.76	0.00	1.90	1.81	2.34
25	Ntomfom	0.13	0.02	0.87	0.73	0.00	0.43	0.27	0.00	1.24	0.00	1.74	1.94	-5.52
26	Kotedaso	0.43	0.07	0.42	0.55	0.01	0.28	0.18	0.00	0.88	0.00	1.48	1.35	4.60
27	Ananekrom	0.22	0.03	0.34	0.83	0.00	0.28	0.20	0.00	0.80	0.00	1.41	1.29	4.49
28	Bethlehem	0.65	0.05	0.15	0.18	0.00	0.51	0.12	0.00	0.45	0.00	1.02	1.08	-2.52
29	Amoaman	0.10	0.02	0.40	0.22	0.00	0.17	0.07	0.00	0.42	0.00	0.73	0.66	5.07

Water Quality Index (WQI)

The WQI was assessed using the following parameters pH, TH, Ca^{2+}, Mg^{2+}, HCO_3^-, Cl^-, TDS, F^-, NO_3^-, SO_4^{2-}, Fe, Na^+, Mn and PO_4^{3-} and following steps below;

a. Assignment of Weights (w_i) to the various groundwater parameters based on their potential impact on human health (Table 2). The weights to the various parameters were assigned based on literature review and public health experts input.
b. Calculation of Relative weight (W_i);
$$W_i = \frac{w_i}{\sum_{i=1}^{n} w_i} \quad (1)$$
c. The Quality rating (q_i) calculation;
$$q_i = 100 * \left(\frac{C_i}{S_i}\right) \quad (2)$$
d. Calculation of sub-index (SI) of various parameters;
$$SI_i = W_i * q_i \quad (3)$$
e. Calculation of Water Quality Index (WQI);
$$WQI = \sum SI_i \quad (4)$$

Where SI is the sub-index for the different parameters, S_i is the WHO value in mg/L, C_i is the lab concentration in mg/L, W_i is the relative weight, W_i is the assigned weight, and n is the number of parameters (Couillard & Lefebre, 1985).

Irrigational Water Suitability Index (IWSI)

To assess the suitability of the groundwater for irrigation use, an effort was made to integrate the effects of eight parameters frequently used to evaluate irrigational water to create IWSI. The creation of IWSI involved the computation of the eight irrigational water quality assessment parameters including EC, Sodium Absorption Ratio (SAR), Sodium Percentage (Na%), Residual Sodium Carbonate (RSC), Kelly Index (KI), Permeability Index (PI), Magnesium Hazard (MH) and Corrosivity Ratio (CR) using equations (5) to (11) and expressing all the ionic concentrations in meq/L. After that, an equal weight of 5 was assigned to all eight parameters. The parameters were classified based on their existing classification, and a rate of 1-5 was assigned to the classes based on their impact on water quality. Equation (12) was used to calculate the IWSI after the weights and ratings for each factor were assigned. Higher values achieved through this method indicate a greater likelihood of suitable groundwater quality for irrigational purposes.

Table 2. Groundwater quality parameters used for calculation of water quality index

Parameter	Weight (w_i)	Relative weight (W_i)	WHO (2012)
pH	4.00	0.09	6.5-8.5
TH	3.00	0.07	500.00
Ca^{2+}	2.00	0.04	75.00
Mg^{2+}	2.00	0.04	150.00
Na^{+}	3.00	0.07	200.00
Cl^{-}	4.00	0.09	250.00
TDS	4.00	0.09	1500.00
F^{-}	4.00	0.09	1.50
NO_3^{2-}	5.00	0.11	50.00
SO_4^{2-}	4.00	0.09	250.00
Mn	3.00	0.07	0.10
Fe	3.00	0.07	0.30
PO_4^{3-}	4.00	0.09	0.10
TOTAL	**45.00**	**1.00**	

$$SAR = \frac{rNa^{+}}{\sqrt{(rCa^{2+}+rMg^{2+})/2}} \quad (5)$$

$$\mathrm{Na\%} = 100 * \frac{\mathrm{rNa^{+}}}{\mathrm{rCa^{2+}+rMg^{2+}+rNa^{+}+rK^{+}}} \quad (6)$$

$$\mathrm{MH} = \frac{\mathrm{rMg^{2+}}}{\mathrm{rCa^{2+}+rMg^{2+}}} * 100 \quad (7)$$

$$\mathrm{PI} = 100 * \frac{\mathrm{rNa^{+}} + \sqrt{\mathrm{rHCO_3^{-}}}}{\mathrm{rCa^{2+}+rMg^{2+}+rNa^{+}}} \quad (8)$$

$$\mathrm{RSC} = (\mathrm{rCO_3^{2-}} + \mathrm{rHCO_3^{-}}) - (\mathrm{rCa^{2+}} + \mathrm{rMg^{2+}}) \quad (9)$$

$$CR = \left(\frac{\frac{rCl^{-}}{35.5} + 2\left(\frac{rSO_4^{2-}}{96}\right)}{2\left(rHCO_3^{-}+rCO_3^{2-}\right)}\right) * 100 \quad (10)$$

$$\mathrm{KI} = \frac{r\mathrm{Na^{+}}}{\mathrm{rCa^{2+}+rMg^{2+}}} \quad (11)$$

$$IWSI = \sum_{j=1}^{m}\sum_{i=1}^{n}(W_i * r_j) \quad (12)$$

Where n is the total variables, m is the total variable classes, W_i is the weight of the i[th] desired variable, r_j is the weight of the j[th] variable class, and IWSI is the irrigation water suitability index. Table 3: presents the weights assigned to the different parameters and rating of their subclasses

Table 3. Weights assigned to different parameters and rating of their subclasses

Parameter	Weight (W)	Classes	Rate (r)	W*r
EC (Wilcox, 1955)	5	<1000	5	25
		1000-2000	4	20
		2000-3000	3	15
		3000-4000	2	10
		>4000	1	5
SAR (USSL, 1954)	5	<2	5	25
		2-10	4	20
		10-18	3	15
		18-26	2	10
		>26	1	5
Na% (Wilcox, 1955)	5	< 60	5	25
		>60	1	5
RSC (Raghunath, 1987)	5	<1.25	5	25
		1.25-2.5	3	15
		>2.5	1	5
KI (Kelley, 1940)	5	<1	5	25
		>1	1	5
PI (Doneen, 1962)	5	<25	1	5
		25-75	3	15
		>75	5	25

MH (Paliwal, 1972)	5	<50	5	25
		>50	1	5
CR (Ryzner, 1944)	5	<1	5	25
		>1	1	5

To show the spatial distribution of the WQI and IWSI values, numerical weight were assigned to the various classes as codes as shown in Table 4.

Table 4. Computed values of WQI, IWSI and their assigned codes

WQI			IWSI		
Classes	**Interpretation**	**Code**	**Classes**	**Interpretation**	**Code**
0-50	Excellent	1	90-100	Excellent	1
50-100	Good	2	80-90	Good	2
100-200	Poor	3	70-80	Moderate	3
200-300	Very poor	4	60-70	Poor	4
>300	Unsuitable	5	<60	Unsuitable	5

Results

A statistical breakdown of the hydrochemical data used in this study is shown in Table 5. The table shows that, according to WHO (2012), some samples are below the parameters' upper permissible limits while others are above them. The pH of the groundwater ranged from 5.24 to 9.40, with a mean of 6.17. The dissolution of minerals in groundwater is impacted by pH, which also affects the chemistry and overall quality of the groundwater for a range of intended uses. (Freeze, 1979; Langmuir, 1997) The majority of groundwater samples have pH values that range from neutral to acidic. The pH range for drinking water is 6.5 to 8.5, as per the WHO (2012). The low pH levels of groundwater are attributed, in part, to CO_3^{2-}charged precipitation (Anku *et al*., 2009; Chegbeleh *et al*., 2020). The EC ranged from 54.10 to 758.00µS/cm, with a mean of 198.18µS/cm. The EC values meet the 2500µS/cm drinking water standard recommended by the WHO. The TDS values, which ranged from 29.80 mg/L to 501 mg/L with a mean of 127.21 mg/L, were all below the recommended level of 1000 mg/L.

Table 5. Statistical summary of the groundwater data

Parameter	Unit	Minimum	Maximum	Mean	Std. Deviation	WHO (2012)
Alkalinity	mg/L	9.80	155.00	48.32	35.29	
HCO_3^-	mg/L	3.17	189.00	59.07	43.85	
Ca^{2+}	mg/L	0.80	53.70	12.25	13.00	75.00
Ca^{2+} Hardness	mg/L	2.00	134.00	29.86	32.74	
Cl^-	mg/L	0.00	32.50	1.53	6.36	250.00
CO_3^{2-}	mg/L	1.00	134.00	18.11	24.97	
Colour	PCU	2.50	50.00	10.10	12.67	15.00
EC	µS/cm	54.10	758.00	198.18	150.25	2500.00
F^-	mg/L	0.01	1.32	0.27	0.31	1.50
Fe	mg/L	0.01	1.59	0.39	0.46	0.30
PO_4^{3-}	mg/L	0.00	0.81	0.33	0.28	0.10
K^+	mg/L	0.40	13.50	2.44	2.61	30.00
Mg^{2+}	mg/L	1.10	39.30	6.37	7.49	150.00
Mg^{2+} Hardness	mg/L	0.01	162.00	25.99	31.64	
Mn	mg/L	0.01	2.78	0.29	0.53	0.10
Na^+	mg/L	1.50	67.00	15.49	13.67	200.00
NH_4^-	mg/L	0.00	15.90	0.56	2.95	
NO_2^-	mg/L	0.00	0.26	0.03	0.05	3.00
NO_3^-	mg/L	0.00	42.00	4.32	8.35	50.00
pH	pH unit	5.24	9.40	6.17	0.89	6.50-8.50
SO_4^{2-}	mg/L	0.00	96.90	14.15	20.16	250.00
TDS	mg/L	29.80	501.00	127.21	109.27	1500.00
TH	mg/L	12.00	296.00	56.86	57.77	500.00
TSS	mg/L	1.00	321.00	25.72	65.38	500.00
Turbidity.	mg/L	1.00	64.00	23.01	11.55	5.00

Hydrochemical facies of the groundwater

According to the Piper (1944) diagram, the main groundwater types in the study area are mixed, NaCl, $NaHCO_3$, $CaMgSO_4$, and $CaMgHCO_3$ (Fig. 3). Plotting Cl^- versus Na^+ reveals that there is no obvious linear relationship between the two variables (Fig. 4).

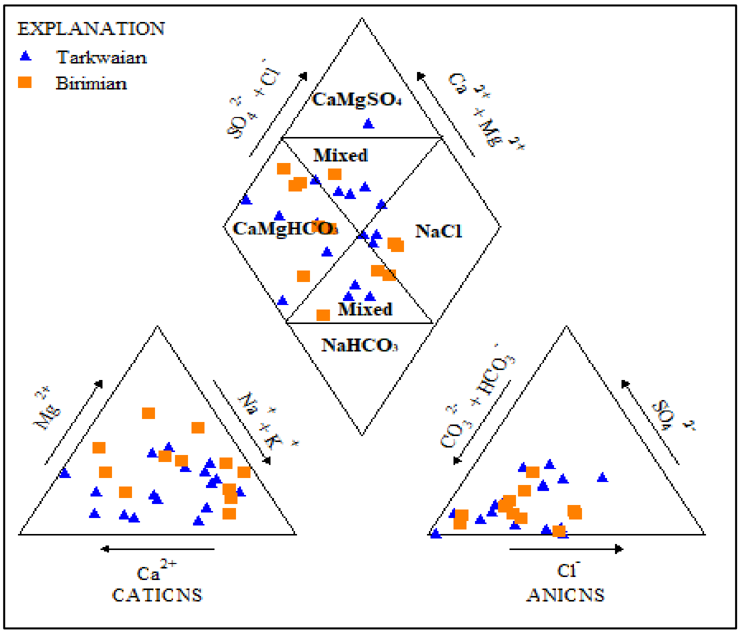

Figure 3. A Piper (1944) diagram showing the groundwater types

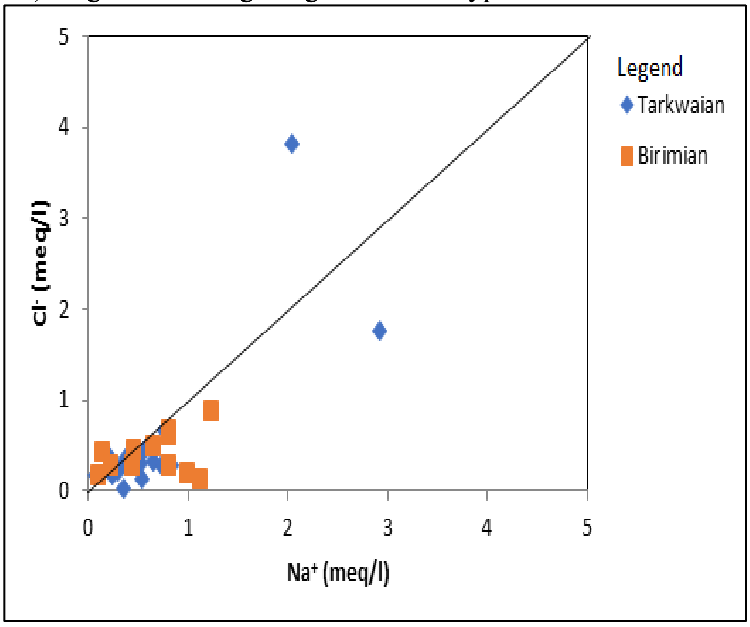

Figure 4. A plot of Cl^- against Na^+ of groundwater in study area.

Hydrogeological Processes

The plot of Gibbs (1970) diagrams (Fig. 5) illustrates how the weathering of rocks has a significant impact on the chemistry of groundwater. Because most samples were below the equiline and few samples were above it, the plot of (HCO_3^- + SO_4^{2-}) vs. (Ca^{2+} + Mg^{2+}) revealed an excess of (HCO_3^- + SO_4^{2-}) over (Ca^{2+} + Mg^{2+}) as shown in Fig. 6. Figure 7 shows a plot of (Ca^{2+} + Mg^{2+}) versus the total cation (TZ^+) and all the samples have more TZ^+ than (Ca^{2+} + Mg^{2+}). The CAI 1 and CAI 2 plots show that only a small fraction of samples have positive values for either index (Fig. 8). Equations 13 and 14 were used to calculate the CAI 1 and CAI 2, respectively.

$$\text{CAI 1} = \frac{\text{rCl}-(\text{rNa}+\text{rK})}{\text{rCl}} \quad (13)$$

$$\text{CAI 2} = \frac{\text{rCl}-(\text{rNa}+\text{rK})}{\text{rSO}_4+\text{rHCO}_3+\text{rCO}_3+\text{rNO}_3} \quad (14)$$

(All values are measured in meq/L)

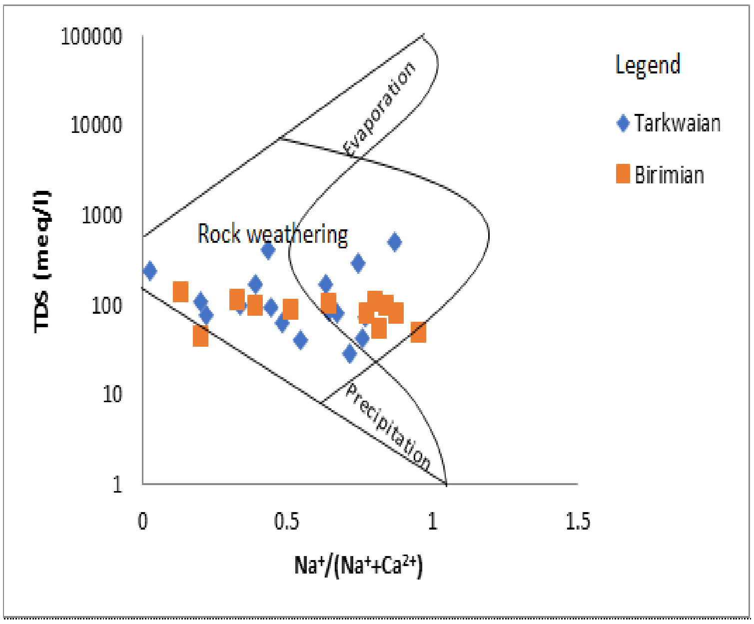

Figure 5. A plot of TDS vs. $Na^+/(Na^++Ca^{2+})$ of groundwater in the study area

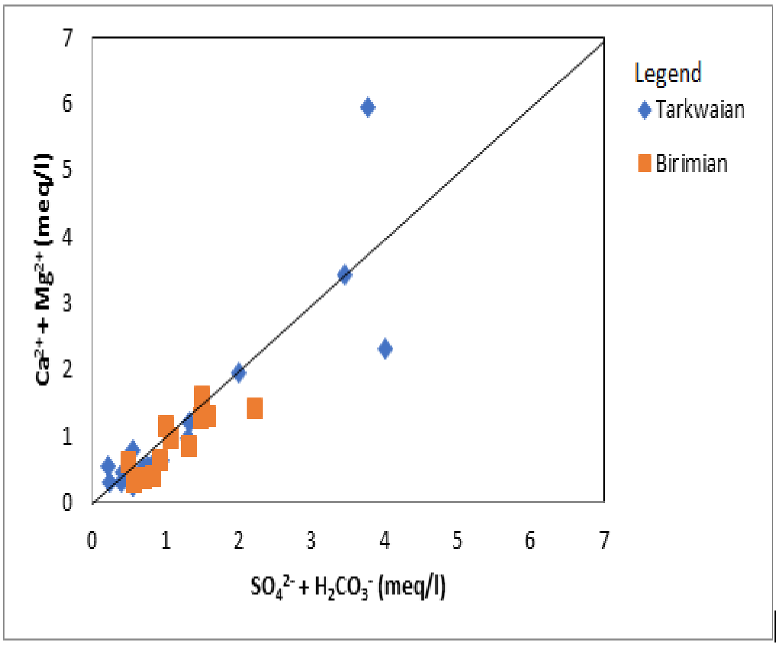

Figure 6. A plot of $(Ca^{2+}+Mg^{2+})$ vs. $(SO_4^{2-}+HCO_3^-)$ of groundwater in the study area

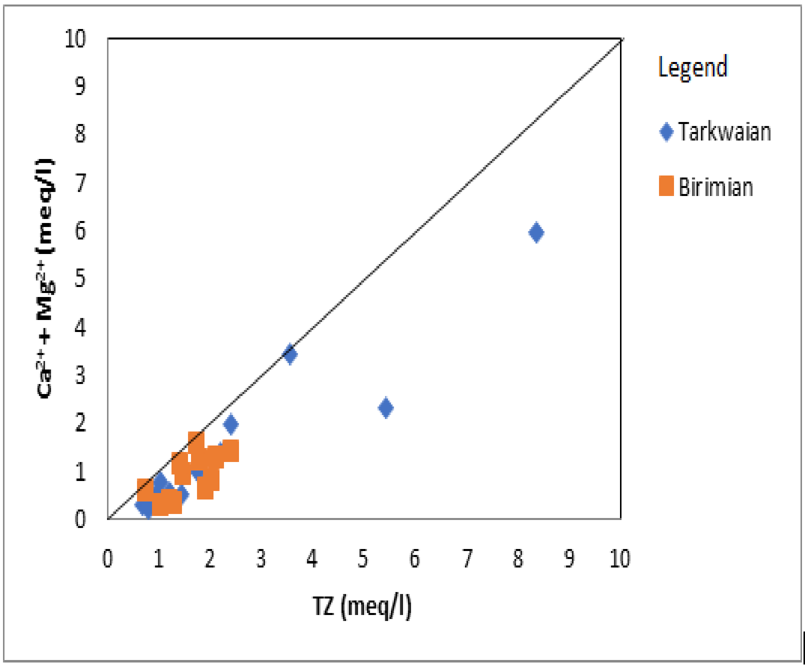

Figure 7. A plot of (Ca^{2+}+Mg^{2+}) vs. TZ^{+} of groundwater in the study area

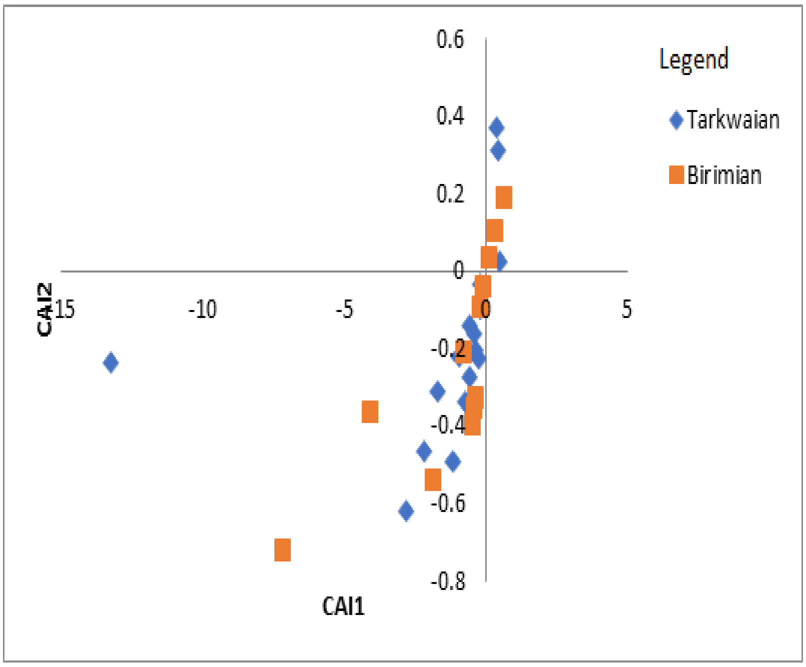

Figure 8. CAI1 vs. CAI2 of groundwater in the study area.

Groundwater suitability

For holistic management of groundwater resources, the recharge zone, discharge zone, and flow paths should be identified. The recharge zones must be protected against potential contamination of the groundwater. For example, the application of fertilizers and manure, improper disposal of waste, and galamsey activities which are common in the study area and have the potential to contaminate the groundwater should be avoided at the recharge zones. This will help in the prevention of contaminating the aquifer system through the flow path from the recharge zone to the discharge zone. Therefore, the study applied the WQI and IWSI techniques to assess the quality of the groundwater for drinking and irrigational purposes respectively. The calculated results of WQI and IWSI are presented in Table 6. About 38% excellent water type, 38% good water, 21% poor water and 3% very poor water based on the WQI (Fig. 9). It also shows 48% excellent water type, 34% good water, 14% moderate water type and 3%

poor water type based on IWSI (Fig. 10). The irrigational water suitability index was divided into the following ranges using the overall maximum potential value of 200 (i.e. 5×5×8=200). Excellent (>90%), Good (80–90%), Moderate (70–80%), Poor (70–80%), and Unsuitable (<70%) are the five categories. The spatial variation of the water quality index and the irrigational water quality index are depicted in Figures 9 and 10. The USSL (1954) and Wilcox (1955) diagrams are shown in Fig. 11 and Fig. 12.

Table 6. Calculated results of WQI and IWSI

No	Latitude	Longitude	WQI		IWSI										
			%	Code	EC	SAR	Na%	RSC	KI	PI	MH	CR	IWSI	%	Code
1	5.888823	-1.75399	108.61	3	149	3.81	53.59	0.36	1.25	86.78	57.14	10.32	140	70	3
2	5.978427	-1.7778	74.65	2	544	1.49	47	-0.09	0.98	110.55	70.61	0.48	180	90	1
3	5.888823	-1.75399	102.73	3	137	2.22	57.09	0.58	1.5	76.5	16.62	0.65	180	90	1
4	5.873235	-1.64606	90.71	2	157	1.3	34.56	-0.32	0.56	83.79	12.2	1.56	160	80	2
5	5.933146	-1.86322	53.37	2	309	2.19	68.27	0.2	2.24	154.91	66.43	0.14	160	80	2
6	5.92318	-1.6077	93.25	2	209	0.07	1.85	-0.34	0.02	52.03	30.01	1.9	170	85	2
7	5.855725	-1.6152	19.61	1	91	1.9	53.7	0.3	1.39	112	31.91	0.4	180	90	1
8	5.887208	-1.62935	18.36	1	203	0.44	19.2	-0.26	0.25	93.43	12.58	0.31	200	100	1
9	5.859436	-1.64566	34.39	1	89	1.05	43.82	-0.08	0.92	127.49	62.5	0.08	180	90	1
10	5.847507	-1.64911	245.13	4	194	0.65	29.77	0.03	0.45	127.89	62.5	0.21	180	90	1
11	5.874987	-1.70158	26.16	1	150	1.31	49.04	0.04	1.15	140.68	62.5	0.18	160	80	2
12	5.815628	-1.6914	37.36	1	181	0.53	15.54	-0.13	0.19	73.81	24.56	1.27	170	85	2
13	5.817042	-1.71869	23.01	1	399	0.87	33.23	0.3	0.54	133.33	31.25	0.04	200	100	1
14	5.811346	-1.76584	82.94	2	232	0.99	38.45	-0.16	0.66	107.99	28.36	0.3	200	100	1
15	5.798412	-1.76106	65.74	2	134	0.95	28.94	-0.39	0.44	82.68	13.93	0.79	200	100	1
16	5.768424	-1.7943	102.96	3	131	1.67	24.47	-4.21	0.34	42.08	54.95	13.15	150	75	3
17	5.766016	-1.84052	53.03	2	153	1.47	41.75	0.11	0.74	103.5	56.78	0.68	180	90	1
18	6.153626	-2.04054	124.35	3	167	2.65	61.86	0.32	2.19	139.47	34.25	0.61	160	80	2
19	6.184009	-2.09068	159.61	3	91.5	0.79	24.95	-0.36	0.35	81.68	28.25	1.12	180	90	1
20	6.199853	-2.17885	66.75	2	76.2	1.42	38.13	0.11	0.63	94.84	84.52	1.6	160	80	2
21	6.182736	-2.09267	31.57	1	54.1	2.51	65.74	0.19	1.97	130.49	90.16	0.38	140	70	3
22	6.234641	-2.10499	98.37	2	74.5	1.67	41.02	0.59	0.7	100.18	60.28	1.01	160	80	2
23	6.14823	-2.04018	115.53	3	78.8	2.41	55.14	0.39	1.31	113.31	81.21	0.35	160	80	2
24	6.088327	-2.10479	50.47	2	202	3.07	65.04	0.11	1.9	111.89	62.98	1.08	120	60	4
25	6.204763	-2.12468	46.05	1	162	0.21	7.51	-0.35	0.08	72.29	45.6	1.1	170	85	2
26	6.099691	-2.14141	79.1	2	116	0.88	29.45	-0.09	0.45	97.74	56.7	0.51	180	90	1
27	6.078153	-2.05409	87.97	2	185	0.4	15.41	-0.36	0.19	80.56	70.82	0.49	180	90	1
28	6.231055	-2.11934	44.49	1	758	2.29	63.73	0.12	2.01	135.2	53.85	0.38	140	70	3
29	6.27263	-2.06824	33.97	1	320	0.26	13.66	-0.19	0.16	105.61	35.42	0.13	200	100	1

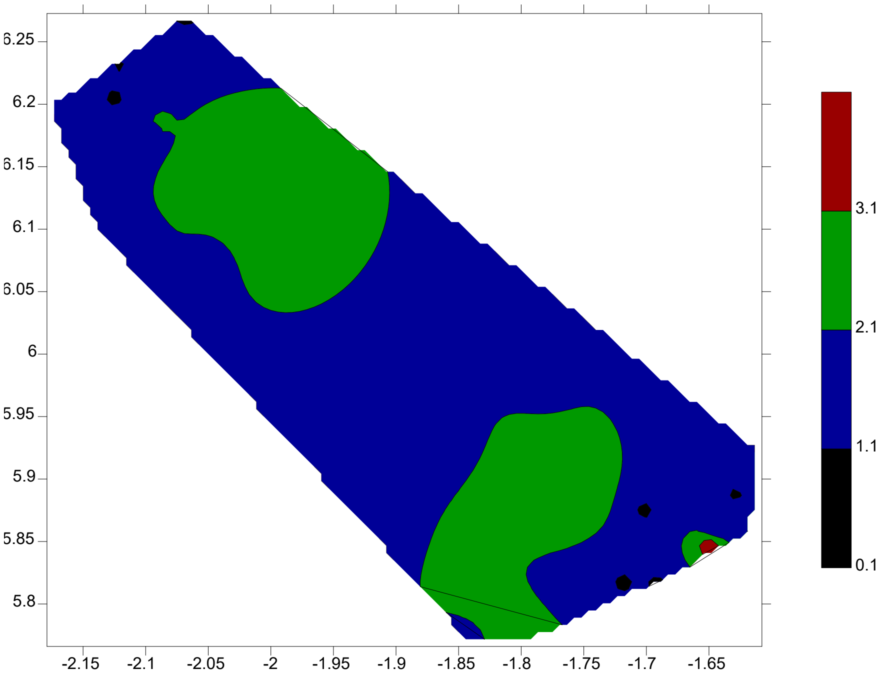

Figure 9. Spatial distribution of WQI of groundwater in the study area

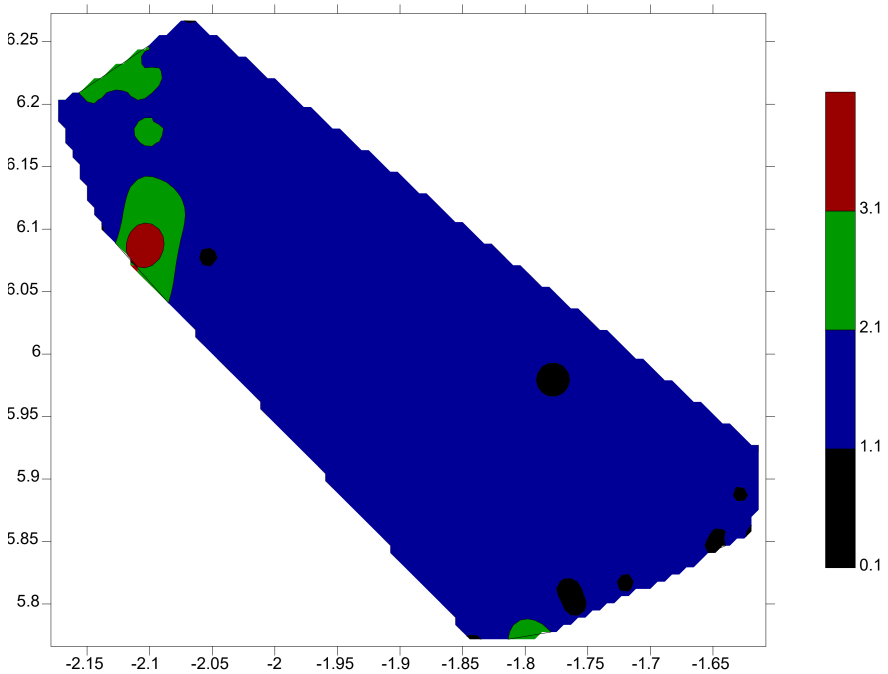

Figure 10. Spatial distribution of IWSI of groundwater in the study area

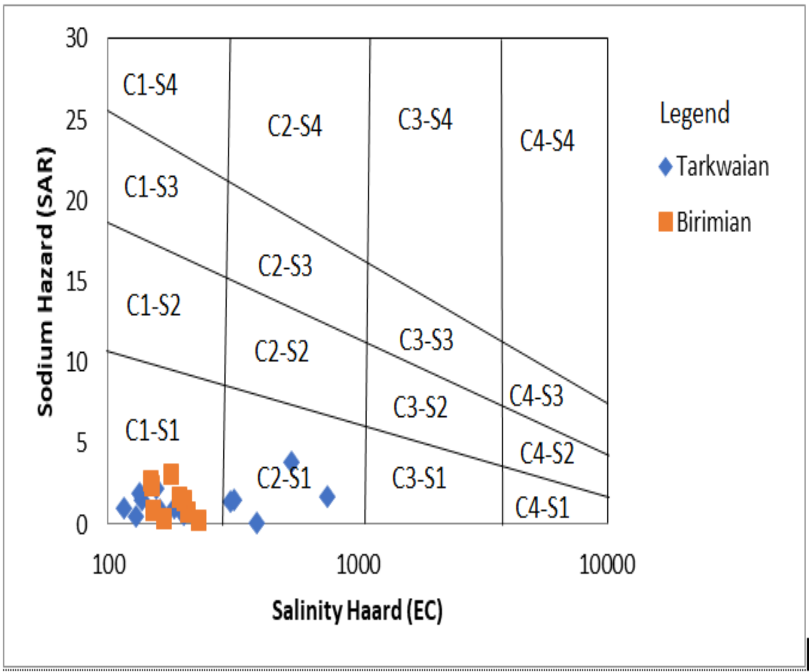

Figure 11. A plot of EC vs. SAR (After USSL, 1954) of groundwater in the study area

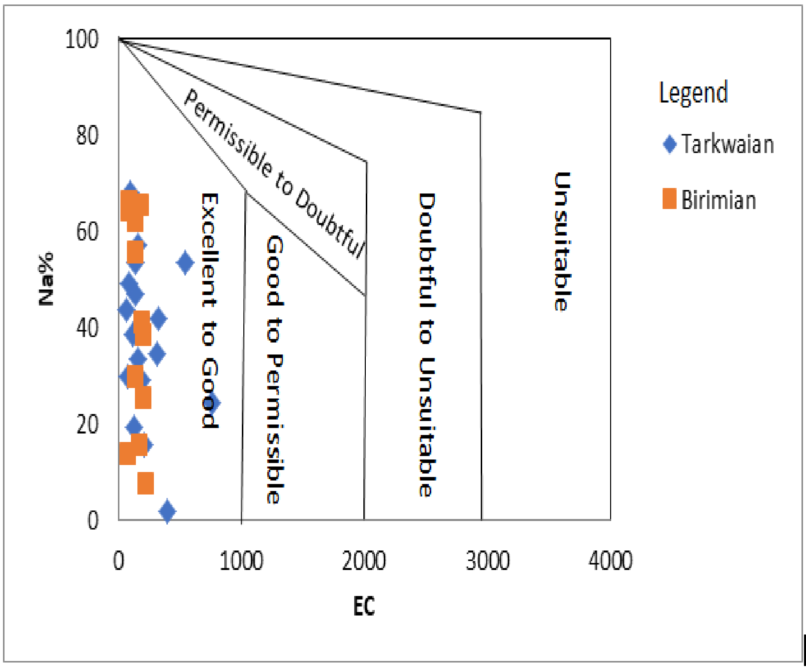

Figure 12. A plot of EC vs. Na% (After Wilcox, 1955) of groundwater in the study area.

Discussion

The generally low EC and TDS show that the study area is a recharge zone. Since fewer rock-water interactions have occurred, the concentration of various constituents in freshwater that enter the water table has not increased. The concentrations of the various groundwater parameters are lowered by the freshwater due to the frequent rainfall in the study area. All parameters are within the recommended limits of the WHO (2012) for drinking water, apart from pH, Mn, Fe, and PO_4^- of some samples. The Mn concentration was greater than the recommended level of 0.10 mg/L, ranging from 0.01-2.78 mg/L with a mean of 0.29 mg/L (WHO, 2012). With a mean of 0.39 mg/L and a recommended value of 0.30 mg/L, the range of Fe concentrations was 0.01 to 1.59 mg/L. The concentration of PO_4^{3-} ranged from 0 to 0.81 mg/L, with a mean that was 0.33 mg/L higher than the recommended value of 0.10 mg/L.

Hydrochemical facies of the groundwater

The major groundwater types in the districts are NaCl, $NaHCO_3$, $CaMgSO_4$, $CaMgHCO_3$, and mixed water types. The formation of NaCl water may be influenced by the dissolution of minerals such as halite. However, the lack of a well-defined relationship between the Cl^- and Na^+ reveals that their entry into the water is not by dissolution of rocks like halite (Hem, 1985). $NaHCO_3$ groundwater type may be produced from the dissolution of Na-bearing silicates as meteoric water charged with carbonic acid dissolving Na^+ (Garrels and Mackenzie, 1967). However, the dissolution of albite and augite rich in Na+ and the presence of CO_2 may have also contributed to the occurrence of $NaHCO_3$ in the study area.

Considering the occurrence of $CaHCO_3$ and NaCl in the study area the $NaHCO_3$ may have also occurred through the ion exchange reaction whereby $CaHCO_3$ evolve to $NaHCO_3$ by interacting with NaCl water types. This occurs when the Na increases along the flow path of the groundwater and gains dominance over the Ca^{2+} through an ion exchange process. Through this process, the NaCl water within the aquifer system is diluted by fresh water to form a mixed water type before the formation of the $NaHCO_3$ water type. The mixing of various types of water has a significant impact on the chemical composition of the groundwater in the study area. Mixed water types have no single ion that shows dominance; hence, they do not have any specific feature that is particular to them. The mixed water could result from the weathering of different minerals and/or the mixing of two chemically distinct groundwater types.

Hydrogeological Processes

The moderate TDS and moderate $Na^+/(Na^+ + Ca^{2+})$ ratio in the Gibbs (1970) diagram demonstrate that the primary factor regulating groundwater chemistry is the dissolution of rock minerals through rock-water interaction. There was an excess of (HCO_3^- + SO_4^{2-}) over (Ca^{2+} + Mg^{2+}) as seen in the (HCO_3^- + SO_4^{2-}) vs. (Ca^{2+} + Mg^{2+}) plot. According to Tiwari and Singh (2014), the effects of silicate mineral weathering, carbonate weathering, and potential ion exchange processes on groundwater chemistry were identified. However, silicate weathering dominates, especially within the Birimian Supergroup. The minerals quartz, hornblende, biotite, and other materials may be responsible for the high SO_4^{2-} + HCO_3^- concentration. Silicate weathering produces secondary minerals like clays such as kaolinite, and iron oxides since the Al-compounds are insoluble (Appelo and Postma, 2005). The process increases the cation and silica concentrations of the groundwater. However, the secondary data used for this study did not have silica concentration.

The amount of silica in groundwater is controlled by the weathering of silicate minerals and the presence of multivalent ions like Al^{3+}, Ca^{2+}, Mg^{2+}, and Fe^{3+} that affect the solubility of silica (Hem, 1985; Hann, 1993; Jansen et al., 2010). The results of the study suggest that silicate weathering is a significant process influencing the chemistry of the groundwater because the concentrations of alkalis are higher than the concentrations of the major ions (Fig. 7). Under specific conditions, groundwater can exchange ions with the host aquifer system, particularly with clay particles (Schoeller, 1965). Generally, Mg^{2+} or Ca^{2+} from aquifer material exchanged with Na^+ or K^+ in groundwater results in negative values for the two indices (Schoeller, 1965). Na^+ or K^+ from aquifer material exchanged with Mg^{2+} or Ca^{2+} in groundwater results in positive values for the two indices. Reverse ion exchange consequently has a significant impact on the chemistry of the groundwater in the districts.

Groundwater suitability

Factors that affect groundwater quality include the composition of recharge water, mineralogy of the aquifer system, climatic conditions, topography, possible impacts of anthropogenic activities, etc. These factors may cause the concentrations of certain minerals to increase above the recommended permissible limits. This causes groundwater contamination affecting environmental and human health (Kumar and Riyazuddin, 2008).

Suitability of groundwater for drinking and domestic purposes

The people of the study area hugely depend on groundwater for their water needs including drinking, domestic, agriculture, and industrial purposes. The overdependence on groundwater in the area is partly due to the high pollution of the existing surface water bodies due to galamsey activities. This has resulted in the outbreak of waterborne and related diseases such as diarrhea, dysentery, cholera, and guinea worm in the area (Ganyaglo *et al*., 2011). This means that the groundwater resource in the districts is prone to anthropogenic contamination. Unfortunately, monitoring of groundwater quality has not been effective in Ghana even though most people in the rural areas use groundwater without prior treatment. One of the major challenges associated with the overdependence on the groundwater resources in the area is the insufficient knowledge of the aquifer system, the groundwater quality, and the possible impact of anthropogenic activities on the groundwater quality in the area.

The study found that 38% of the groundwater in the districts is of excellent quality for domestic and drinking purposes; 38% has good quality; 21% has poor quality and 3% has very poor quality. This indicates that the groundwater is generally suitable for drinking, but certain parameters that are above the recommended values should be treated. The generally high groundwater quality may be attributed to the low concentrations of the groundwater parameters. On the other hand, the groundwater in some communities is unfit for drinking without prior treatment due to its low pH, high pH, high Fe, Mn, and PO4- levels. Both natural/geogenic processes and anthropogenic activities, such as the use of agrochemicals, pit latrines, and improper waste disposal, have an impact on the quality of groundwater in the districts. Considering Figure 2, the groundwater flows toward the Offin River, accounting for the relatively pure groundwater compared to the contaminated surface water bodies in the area.

The groundwater quality in the Birimian and Tarkwaian geological formations is similar. The high Fe, Mn, and PO4- consecrations of the groundwater in the districts are due to the dissolution of Fe and Mn-containing minerals of the host aquifer systems and anthropogenic activities. The poor groundwater quality for drinking was seen at Subinsu, Sobroso, Fosu Dankwa, Congo 1, Kyebi, Betease, and Ampabeng in the southern part of upper Denkyira east. This shows the impact of anthropogenic activities on the groundwater quality in those communities at the local scale. In their studies of heavy metals in drinking water, their effects on human health, and their treatment techniques Jamshaid et al (2018) observed that both Fe and Mn have essential roles to play in the normal functioning of the body when their concentrations are within a certain recommended range.

However, inadequate supply and excess of the two can affect the normal functioning of the body. High concentrations of Fe and Mn in drinking water can cause an increased risk of certain diseases in consumers. Fe and Mn may be found naturally in groundwater in low concentrations. They cause taste and staining problems with groundwater (Jamshaid et al., 2018). Mn has a very essential role to play in the human body when the concentration is low (Jamshaid et al., 2018). However, the excessive intake of Mn can cause different diseases such as nervous system disorder and Parkinson's disease (Jamshaid et al., 2018). Also, Fe is one of the essential elements needed for the proper functioning of the human body. It helps in the production of haemoglobin which is the protein responsible for carrying oxygen from the lungs to the other parts of the body. However, excess Fe may cause hypothyroidism, heart failure, osteoarthritis, depression, osteoporosis, infertility, and abdominal pain (Jamshaid et al., 2018).

Irrigational water suitability assessment

It is crucial to remember that figuring out the quality of groundwater is difficult because it depends on a variety of factors, such as the intended use of the water and the specific water quality parameters involved. Due to this complexity, it is challenging for researchers and water professionals to communicate their research findings with decision-makers who might not be technically savvy in water science. In this case, the water quality index method can bridge the communication gap. It provides values of the overall water quality at a particular time and location based on selected water quality parameters (Yogendra and Puttaiah, 2008). The study discovered that 48% of the groundwater types were excellent, 34% were good, 14% were moderate, and 3% were poor based on IWSI. This shows that the quality of the groundwater is good for irrigation use. To verify the accuracy of the new method, USSL and Wilcox diagrams were also employed. Groundwater falls into the C1-S1 and C2-S1 categories in the USSL diagram, but the Wilcox diagram places it in the excellent to good category. This indicates that the two diagrams also show 'excellent to good' groundwater types for irrigation use, just as the IWSI method had shown. This demonstrates the dependability of the IWSI technique. The groundwater quality of the Tarkwaian and Birimian geological formations is comparable.

Conclusion

Groundwater suitability for drinking, domestic use, and irrigation purposes in the Upper Denkyira East and West Districts has been assessed. Groundwater types in the districts are mixed water, NaCl, $CaHCO_3$, and $CaMgSO_4$. Rock weathering, ion exchange, and impacts of anthropogenic activities like improper agrochemical application, galamsey, and improper waste disposal are the major processes affecting groundwater quality. The study found that 38% of the groundwater in the districts is of excellent quality for domestic and drinking purposes; 38% has good quality; 21% has poor quality and 3% has very poor quality. The groundwater is generally suitable for drinking but the low pH, high pH, high Fe, high Mn, and high PO_4^{3-} levels of some samples make them unsuitable for drinking without prior treatment. These observations agree with the findings of early studies. The study discovered that 48% of the groundwater types were excellent, 34% were good, 14% were moderate, and 3% were poor based on IWSI. The IWSI was calculated using EC, SAR, Na%, RSC, KI, PI, MH, and CR. The USSL diagram and the Wilcox diagram confirmed that the groundwater falls within the excellent to good categories. This revealed the IWSI agrees with USSL and Wilcox diagrams; the technique is effective for groundwater suitability assessment for irrigational use. The groundwater quality of the Tarkwaian and Birimian geological formations is comparable.

Acknowledgment: *The author is appreciative to the Management of the CWSA, Cape Coast for making data for this study available.*
Funding: *The author received no funding for this study.*
Conflict of Interest: *The author declares that he has no conflict of interest.*
Availability of data: *All data used for this study are included within the manuscript.*

References

Ahmed MF, (2002) An assessment of arsenic problems in Bangladesh. In: Proceedings of the International Workshop on Arsenic Mitigation, Dhaka, Bangladesh, 14-16 January 2002. Dhaka: Ministry of Local

Government, Rural Development and Cooperatives, Government of Bangladesh, 2002: 15-20. https://www.ircwash.org/sites/default/files/Ahmed-2002-Arsenic.pdf

Alagbe SA, (2006) Preliminary evaluation of hydrochemistry of the Kalambaina formation, Sokoto Basin, Nigeria. *Environ Geol* 51: 39–45. DOI: 10.1007/s00254-006-0302-5. https://link.springer.com/content/pdf/10.1007/s00254-006-0302-5.pdf

America Public Health Association (1995) Standard methods for the examination of water and wastewater, 19th edition, Washington, DC.

Anku YS, Banoeng-Yakubo B, Asiedu DK, Yidana SM, (2009) Water quality analysis of groundwater in crystalline basement rocks, northern Ghana. *Environmental Geology*. 2009;58(5):989–997. doi: 10.1007/s00254-008-1578-4.

Anornu GK, Kortatsi BK, Saeed ZM, (2009) Evaluation of groundwater resources potential in the Ejisu-Juaben District of Ghana. Afr. J. Environ. Sci. Technol. 3 (10): 332 - 340. https://doi.org/10.5897/AJEST09.048

Appelo CAJ, Postma D, (2005) Geochemistry, groundwater and pollution, 2nd edition. https://www.usb.ac.ir/FileStaff/4685_2019-6-10-0-15-56.pdf

Aral MM, Maslia ML, Ulirsch GV, Reyes JJ (1996) Estimating Exposure to Volatile Organic Compounds from Municipal Water-Supply Systems: Use of a Better Computational Model. Archives of Environmental Health: An Int. J., 51(4), 300-309. DOI: 10.1080/00039896.1996.9936029

Baba A, Tayfur G, (2011) Groundwater contamination and its effect on health in Turkey. Environmental Monitoring and Assessment Environ Monit Assess, 183(1-4), 77-94. http://doi.org/10.1007/s10661 -

Babiker IS, Mohamed AM, Hiyama T, (2007) Assessing groundwater quality using GIS. Water Resour. Manage. 21(4): 699 –715. https://doi.org/10.15832/ankutbd.744844

Cederstorm DJ (1946) Genesis of groundwater in the coastal plain of Virginia. Environmental Geology 41:218–245. https://doi.org/10.2113/gsecongeo.41.3.218

Celesceri L, Greenberg AE, Eaten AD (1998) Standard methods for the examination of water and wastewater. American Public Health Association, Washington, p 134. https://www.google.com.tr/search?hl=tr&tbo=p&tbm=bks&q=inauthor:%22American+Public+Health+Association%22

Central Ashanti Gold Limited (2010) Environmental impact statement central Ashanti Gold Project. Volume 1 Final. March 2010. https://perseusmining.com/wp-content/uploads/2019/07/Binder-Edikan-ESIA-Report-EIS-Western-Side-Final-Eng.pdf

Couillard D and Lefebvre Y (1985) Analysis of Water Quality Indices. Journal of Environmental Management 21:161-179. https://www.scirp.org/reference/referencespapers?referenceid=1938756

CSIR-WRI Database (2007) Existing Boreholes in Upper Denkyira District. https://doi.org/10.1007/s13201-021-01462-w

Dickson KB, Benneh G, (1980) "A New Geography of Ghana," Longman, London. European Environment Agency (1999) Groundwater Quality and Quantity in Europe: Data and Basic Information. Technical report, Copenhagen. https://ir.knust.edu.gh/bitstreams/a74fdb82-a426-4ccd-b7b8-0281f7e7750b/download

Domenico PA, Schwartz FW (1990) Physical and chemical hydrology. Wiley, New York. https://health.hawaii.gov/heer/files/2021/07/Domenico1990.pdf

Doneen LD (1964) Water quality for agriculture. Department of Irrigation, University of California, Davis, p 48 https://www.sciepub.com/reference/67145

Drever JI (1988) The geochemistry of natural waters. 2nd edn. Prentice-Hall, New York.

Freeze RA, Cherry JA (1979) *Groundwater*. NJ, USA: Prentice-Hall, Inc. Englewood Cliffs; 1979.

Ganyaglo SY, Osae S, Dampare SB, Fianko JR, Bhuiyan MAH, Gibrilla A, Bam E, Ahialey E, Osei J. (2012) Preliminary groundwater quality assessment in the central region of Ghana. Environ Earth Sci 66:573–587 DOI 10.1007/s12665-011-1266-7

Garrels RM. and Mackenzie ET (1967) Origin of the chemical compositions of some springs and lakes. Advance Chemical. Ser. 67: 222-242. Géology Minière, France. 88:40 p.

Ghana Statistical Service (2021) 2020 Population and Housing Census Summary Report on Final Results. Medialite Co. Ltd., Accra.

Gibbs RJ (1970) Mechanisms controlling world water chemistry. Science Journal 170:795–840.

Goodchild, M. F. (2000) Part 1 Spatial analysts and GIS practitioners. J. Geog. Sys., 2(1), 5-10.

Griffis RJ, Barning K, Agezo FL, Akosah FK (2002) Gold deposits of Ghana. Minerals Com. Report.

Gupta PK (2005) Methods in environmental analysis: water, soil and air. Agrobios, pp 1–127

Gyau-Boakye PK, Kankam-Yeboah PK, Darko S, Dapaah-Siakwan and Duah AA (2008) Groundwater as a vital resource for rural development: example from Ghana, In: Adelana S.M.A. and MacDonald A.M. Appl. Groundwater Stud. in Af.. Int. Appl. Hydro. Selected Papers on *Hydrogeol.*, **13**, 149-170.

Hann WM, (1993) Dispersant: Kirk-Othmer Encyclopedia of Chemical Technique. Volume 8. 2nd Edition. New York: John Wiley and Sons, pp. 293-311.

Hem JD (1991) Study and interpretation of the chemical characteristics of natural waters, Book 2254, 3rd edn. Scientific Publishers, Jodhpur. Holden WS (1971) Water treatment and examination. London.

Hem JD, (1985) Study and Interpretation of the Chemical Characteristics of Natural Water. 3rd Edition. U.S. Geological Survey Water-Supply Paper 2254, P. 263.

ISI (1983) Indian standard specification for drinking water. IS: 10500, Indian Standard Institute, India.

Jamshaid M, Khan AA, Ahmed K, Saleem M (2018) Heavy metal in drinking water its effect on human health and its treatment techniques. Int. J Biol Sci. 2018;12: 223-240.

Jansen N, Hartmann J, Lauerwald R, Durr HH, Kempe S, Loos S, Middelkoop H (2010) Dissolved silica mobilization in the conterminous USA. Chemical Geology, 270: 90-109.

Junner NR, (1935) Gold in the Gold Coast, Me,morandum no. 4, Accra, 67pp.

Karanth KR (1987) Groundwater assessment, development and management. Tata McGraw Hill publishing Company Limited, New Delhi.

Karanth KR (1997) Groundwater assessment, development and management. Tata McGraw-Hill, New Delhi.

Kesse GO (1985) The Mineral and Rock Resources of Ghana, Ballkema Publishers, Rotterdam, 610pp.

Kortatsi BK (1994) Groundwater utilization in Ghana, Proceedings of the Helsinki Conference, IAHS Publ. No. 222.

Kumar RA, Riyazuddin P (2008) Application of chemometric techniques in the assessment of groundwater pollution in a suburban area of Chennai city, India Current Science, Vol. 94, No. 8 (25 April 2008), pp. 1012-1022. https://www.jstor.org/stable/24100795

Langmuir D. *Aqueous Environmental Geochemistry*. River, NJ, USA: Prentice Hall Upper Saddle; 1997.

Leube A, Hirdes W, Mauer R, Kesse GO, (1990) The Early Proterozoic Birimian Supergroup of Ghana and Some Aspects of Its Associated Gold Mineralization. *Precambrian Res.* **46**, 139–165. https://doi.org/10.1016/0301-9268(90)90070-7

Li PY, Qian H Wu JH, (2010) Groundwater Quality Assessment Based on Improved Water Quality Index in Pengyang County, Ningxia, Northwest China. *E-J. Chem.,* **7**(S1). https://doi.org/10.1007/s12403-020-00345-w

Margat J, van-der JG, (2013) *Groundwater around the World*. CRC Press, Balkema. https://www.un-igrac.org/sites/default/files/resources/files/Groundwater_around_world.pdf

Nagaraju AS, Killham SK, Hudson-Edwards K, (2006) Hydrogeochemistry of Waters of Mangampeta Barite Mining Area, Cuddapah Basin, and Hra Pradesh, India. *Turkish J. Engen. & Environ. Sci..* **30**: 203-219. https://online-journals.tubitak.gov.tr/engineering/index.htm

Narsimha A, Sudarshan V, Swathi P, (2013) International Journal of Research in Chemistry and Environ., (2), 196-200.

Osiakwan GM, Gibrilla A, Kabo-Bah AT, Appiah-Adjei EK, Anornu G, (2022) Delineation of groundwater potential zones in the Central Region of Ghana using GIS and fuzzy analytic hierarchy process. *Model. Earth Sys. & Environ.* **8**, 5305–5326. https://erem.ktu.lt/index.php/erem/article/view/33628/16076

Paliwal KV, Singh S, (1967) Effect of Gypsum Application on the Quality of Irrigation Water. *The Madras Agric. J.* **59**:646647. https://www.scirp.org/reference/referencespapers?referenceid=1927067

Piper AM, (1944) A graphic procedure in the geochemical interpretation of water analyses. *Trans. Am. Geoph. Union,* **25**, 914–928. https://doi.org/10.1029/TR025i006p00914

Rahman M, (2002) Arsenic Contamination of Drinking-water in Bangladesh: A Public-health Perspective. *J Health Popul Nutr.* Sep; **20**(3):193-197. ISSN 1606:0997. https://www.jstor.org/stable/23498798?seq=1

Raju NJ, Shukla UK, Ram P, (2011) Hydrogeochemistry for the assessment of groundwater quality in Varanasi: a fast-urbanizing center in Uttar Pradesh, India. Environ. Monit. & Assess., 173: 279–300. https://doi.org/10.1007/s10661-010-1387-6

Reghunath R, Murthy TRS, Raghavan BR, (2002) The utility of multivariate statistical techniques in hydrogeochemical studies: an example from Karnataka, *India. Water Res* **36**: 2437-2442. https://www.scirp.org/reference/referencespapers?referenceid=1763574

Schoeller H, (1965) *Qualitative evaluation of groundwater resource. In: Methods and techniques of groundwater investigation and development.* UNESCO, pp 54-83.

Stumm W, Morgan JJ (1981) *Aquatic Chemistry*, 2nd Edn. Wiley, New York. https://www.scirp.org/reference/referencespapers?referenceid=2052039

Sundaray SK, Nayak BB, Bhatta D (2009) Environmental studies on river water quality with reference to suitability for agricultural purposes: Mahanadi River estuarine system, India—a case study. *Environ Monit Assess* **155**:227–243. https://doi.org/10.1007/s10661-008-0431-2

Tank DK, Chandel CPS, (2010) A hydrochemical elucidation of the groundwater composition under domestic and irrigated land in Jaipur City. *Environ. Moni. Assess*. **166**(1–4):69–77. DOI: 10.1007/s10661-009-0985-7

Thorne DW, Peterson HB (1954) *Irrigated soils. Constable and Company,* London. http://dx.doi.org/10.1097/00010694-195411000-00021

Tiwari AK, Singh AK, (2014) Hydrogeochemical Investigation and Groundwater Quality Assessment of Pratapgarh District, Uttar Pradesh. *J. Geolo.Soc. India,* **83**(3):329-343p. https://doi.org/10.1007/s12594-014-0045-y

Todd DK (1980) Groundwater hydrology. Wiley, New York. https://www.scirp.org/reference/referencespapers?referenceid=2402271

Twigg L. (1990) Health based geographical information systems: Their potential examined in the light of existing data sources. Social Science & Medicine, 30(1), 143-155. https://ideas.repec.org/a/eee/socmed/v30y1990i1p143-155.html#download

United Nations Educational, Scientific and Cultural Organization (2004) G*roundwater Resources of the World and their Use.* Zektser I.S., Everett L.G., eds. IHP-VI, Series on Groundwater No. 6. ISBN 92-9220-007-0. Paris. https://policycommons.net/artifacts/8956437/groundwater-resources-of-the-world-and-their-use/9822992/

United States Environmental Protection Agency, (1998) *Land farming. Office of the Underground Storage Tank*, US Environmental Protection Agency. 510-B-95-007. https://www.waterboards.ca.gov/ust/training/docs/epa910b92001ustcat00.pdf

United States Salinity Laboratory (1954) *Diagnosis and Improvements of Saline and Alkali Soils.* US Department of Agricultural Soils, US Department of Agricul-tural Handbook 60, Washington. https://www.scirp.org/reference/referencespapers?referenceid=83271

US Salinity Laboratory Staff (1954) D*iagnosis and improvement of saline and alkali soils*. US Department of Agricultural Soils. US Department of Agricultural Handbook 60, Washington. https://www.ars.usda.gov/ARSUserFiles/20360500/hb60_pdf/hb60complete.pdf

Wilcox LV, (1955) *Classification and use of irrigation waters.* U.S. Department of Agriculture Circular 969. Washington, DC: U.S. Dept. Agric., pp. 19. https://www.scirp.org/reference/referencespapers?referenceid=1342379

World Health Organization (1984) *Guidelines for Drinking Water Quality.* World Health Organization, Geneva. https://www.who.int/publications/i/item/9241541687

World Health Organization (2008) *Guidelines for drinking-water quality: incorporating 1st and 2nd addenda,* Vol.1, Recommendations 978 92 4 1547611. https://iris.who.int/bitstream/handle/10665/204411/9789241547611_eng.pdf

Yogendra K, Puttaiah ET, (2008) Determination of water quality index and suitability of an urban waterbody in Shimoga Town, Karnataka, *Proceedings of 12th World Lake Conference,* pp. 342-346. https://ouci.dntb.gov.ua/en/works/45E2yDj4/

Zaporozec A, (1972) Graphical interpretation of water quality. *Groundwater*. **10**(2):32-43. https://doi.org/10.1111/j.1745-6584.1972.tb02912.x

J. Int. Environmental Application & Science, Vol. 20: 19-37 (2025)
Research Paper

Groundwater Quality Assessment in the Central Region of Ghana

Victor Ofori Agyemang*

Hydrogeological Unit, Community Water and Sanitation Agency, P. O. Box 128, Damongo, Ghana

Received October 17, 2024; Accepted February 24, 2025

Abstract: In the central region of Ghana, a study that applied two water quality indicators and a risk index to groundwater was successfully completed. The weighted arithmetic water quality index (WAQWI), the water quality index (WQI), and the water quality risk index for human consumption (IRCA) were all employed in the study. In the research area, there are four different forms of groundwater: Ca-Mg-SO_4, Na-Cl, Ca-Mg-HCO_3, and mixed water. Rock weathering is the primary process regulating the chemical of the groundwater. Evaporation, ion exchange, and the effects of anthropogenic activities are other processes that may be controlling the geochemistry. According to the WQI, 6% of the groundwater samples had excellent quality, 54% had good quality, 22% had poor quality, 9% had very poor quality, and 9% were unfit for drinking without treatment. According to the WAQWI, 71% of groundwater are of outstanding quality, followed by 19% of acceptable quality, 4% of bad quality, and 6% of unsuitable quality. IRCA calculations showed that 2% of the samples included water that posed no risk to human health, 20% contained water that was low risk, 2% contained water that was medium risk, 75% contained water that was high risk, and 1% contained water that was unfit for human consumption. The IRCA indicates that there is a generally high level of health risk associated with using the groundwater for drinking without prior treatment, even though the two indices indicate that the groundwater is generally good for that purpose.

Keywords: *Groundwater, Water Quality Index, Weighted Arithmetic Water Quality Index, Water Quality Risk Index for Human Consumption, Central Region, Ghana, World Health Organization*

Introduction

Natural resources like water are crucial to human existence. For the general welfare, clean water is crucial. Since water reacts with and dissolves many chemicals from the atmosphere, surface, and subsurface, it does not exist in its purest form. The chemistry and general quality of water are altered due to the dissolution of gaseous chemicals in the atmosphere, organic materials, and inorganic materials from the earth's surface and subsurface (Raju, 2007; Wang, 2013). Different anthropogenic activities may have an impact on the chemistry and general quality of water supplies. Groundwater frequently has a distinct hydrochemistry and quality due to interactions between the water and its environment (Back, 1966; Drever, 1982). Ion exchange between water and the aquifer system, the dissolving of rock minerals and the effects of human activity are some of the ways that water interacts with its surroundings (Faure, 1998). It is important to keep in mind that even elements that are beneficial to human health when present in low quantities can have major negative effects on public health when present in high concentrations (Raju, 2012).

The practices of water safety are therefore required, which ensure that the entire water supply chain is watched to prevent water contamination or to discover pollution early enough to allow for remediation. The protection of the water source and the entire water supply chain is ensured by water safety procedures. Therefore, in order to effectively manage water resources, it is necessary to comprehend both the natural processes that control the chemistry and general quality of the water as well as the potential effects of human activity (Raju et al., 2011). Around two billion people lack access to suitable water sources on a global scale (UN, 2014, 2021). People use water from various sources for drinking and other domestic tasks including cooking, personal hygiene, washing utensils, etc. Water can come from either a surface or a subsurface source.

Unfortunately, using water of poor quality might harm a person's health. Water pollution influences the usage of the water for different purposes, necessitating effective water quality

*Corresponding: E-Mail: oforiagyemangvictor@yahoo.com, Tel: +233248136427

monitoring to assure water safety or early detection of contamination and remediation. This necessitates the use of an efficient monitoring tool, such as the Water Quality Index and the IRCA, which offer an efficient evaluation of the usage of the water resources for drinking (Torres et al., 2010; Castro et al., 2014). Water resources can get contaminated in a variety of ways, including through human activities and natural processes, and the contaminants can be either organic or inorganic. The WHO has released a water safety plan (WSP) for effective management of drinking water to enable risk assessment and proper management of water resources to satisfy the need for supplying high-quality water from the source to the consumer. The development of the water safety team, defining the current water system (DWSS), identifying hazards and risky events, assessing risks, and risk management planning are the five stages that typically make up the WSP (Perez et al., 2020).

Rural areas in underdeveloped nations like Ghana frequently lack access to sufficiently treated water for home use, so they supplement it with groundwater by drilling boreholes. To ensure that the public has access to safe water, this necessitates the efficient implementation of water safety measures. Due to the availability of groundwater, population growth, and the generally poor quality of surface water, groundwater use is increasing nowadays. According to statistics, 60% of the projected 982 km^3/year rate of groundwater extraction is used for agricultural activities, with the remaining 40% being used for drinking and domestic purposes (NGWA, 2016). However, in developing nations, more than 50% of the groundwater that is taken is used for drinking (NGWA, 2016).

People in the research area rely on groundwater for domestic and agricultural purposes, among other uses. The region's surface water bodies are becoming more and more polluted because of galamsey operations, making it harder to supply drinkable water. This necessitates the adoption of proper tools to assess the Region's water resources. Water safety practices are advised to ensure the appropriate management of the region's groundwater resources. Diverse professional organizations, including those involved with water, the environment, engineering, politics, public health, social science, and policymaking, must collaborate on this. Sadly, not all professionals are familiar with the idea of water quality. As a result, the gap between the water experts and the other stakeholders widens. An efficient method called the water quality index is utilized to close that gap (Shah and Joshi, 2017).

Examples of WQI include the National Sanitation Foundation index (NSF WQI method), the Weighted Arithmetic Water Quality Index (WAQWI) technique, the Canadian Council of Ministers of the Environment Water Quality Index (CCME WQI), the Water Quality Index, and others. The Canadian Council of Environment Ministers created the CCME WQI to assess the ecological quality of water (Agarwal et al., 2020; Saffran et al., 2001). The WAQWI uses measures of regularly measured water quality to express the degree of purity (Tygai *et al.*, 2013). Though this tool employs fewer parameters than comparable WQIs, it nevertheless permits the use of several physical, chemical, and bacteriological properties of the water (Saha et al., 2019). The WQI tool has been used in numerous water studies throughout the world. The Canadian Council of Environment Ministers created the CCME WQI to assess the ecological quality of water (Agarwal et al., 2020; Saffran et al., 2001).

In his research, Agyemang (2019) used WQI methodologies to evaluate the drinking water quality in the Afigya Kwabre District. He noted that 80% fell into the "excellent" group, 7.5% into the "good," 5% into the "poor," and 7.5% into the "unsuitable" category. He blamed anthropogenic activities and the comparatively high quantities of iron and lead in the groundwater for the poor water quality in some localities. Again, Agyemang (2020) applied the method to determine if groundwater in Agona East District of Ghana was suitable for drinking and found that every water sample fell into the good category. Boah et al. (2015) used the WAQWI approach to evaluate the Vea Dam's water quality for drinking purposes in Ghana's Upper East Region and discovered that the area's water had a WAQWI value of 54.21, meaning it was unfit for consumption without prior treatment.

Out of these studies, 82% employed the techniques to characterize the quality of river water, while 18% applied the tools to characterize the other forms of water, such as groundwater for drinking, household use, and irrigation (Shah and Joshi, 2017; Ahmed et al., 2020; Uddin et al., 2021). The CCME WQI and NSF-WQI methodologies, according to Uddin et al. (2021), account for around 50% of all research conducted utilizing the WQI tool globally. While many researchers have found success using a single tool, some have integrated two or more of the many WQI techniques to assess the water quality (Finotti et al., 2015; Jahan and Strezov 2017; Sim & Tai, 2018; Zooalnoon & Musa 2019; Alexakis, 2020). Once more, the water quality risk index for human consumption is a useful technique to analyze the potability of water for human drinking and to determine the degree of risk of illness incidence associated with water consumption (Garcia-Avila *et al*., 2022). The IRCA is a tool for determining if water is fit for human consumption. The allocated scores to the various parameters, which are established by Resolution 2115 of 2007, are used in the calculation of the IRCA (Duarte *et al*., 2022).

Study area

The purpose of this study was to use the IRCA technique to analyse the amount of health risk related to drinking groundwater and two different water quality indices to determine whether the groundwater was suitable for consumption. The fact that some people in the Region drink untreated, raw groundwater makes the use of the IRCA in this study necessary. In order to manage water resources holistically, water quality indices method is particularly good in expressing the water quality. The tool may show the water resource's quality in time and space when used with the GIS approach (Kumar & Sharma, 2019; Kamboj & Kamboj 2019). In various locations of the world and for various purposes, different writers have evaluated water quality using various types of WQI (Nayak & Patil, 2015). The methods used to evaluate the water quality, and the numerous characteristics utilized for the index are what differentiate different water quality indices (Ahn *et al.*, 2018; Garcia-Avila *et al.*, 2018).

Materials and Methods

The Central Region is bordered by latitudes 5° 05' 48.484" N and 5° 56' 23.525" N, and longitudes 1° 49' 53.868" W and 0° 23' 59.586" W (Fig.1). The area is located in the evergreen and semi-deciduous forest zones of the dry equatorial climate region. The dry and wet seasons are the two predominant in the region with a typical annual rainfall range of 1000-2000 mm. The dry season runs from December to February while the wet seasons run from May to June as well as September to October. The average yearly temperature is between 24 ºC and 30 ºC, with the peak months being March and August, respectively.

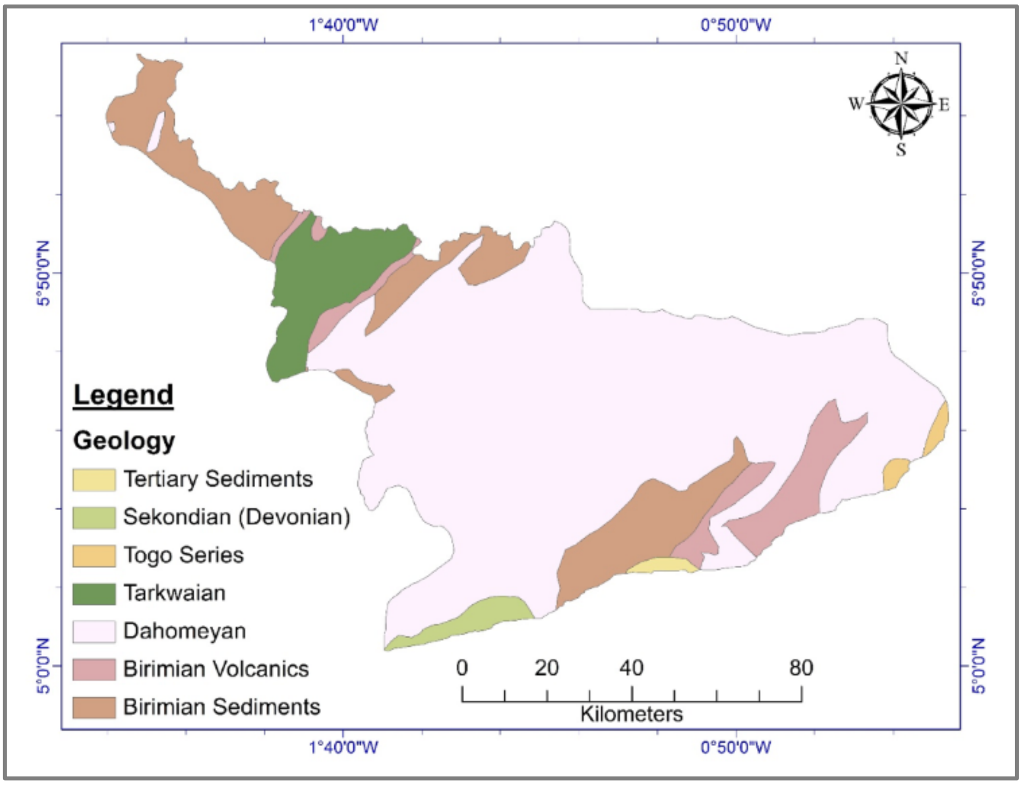

Figure 1. Geological map of Central region (Osiakwan *et al.*, 2022)

The majority of the water needs for the towns in the region are largely met by groundwater resources. This is because the reliance on transient surface water, which depends on rainfall for their replenishment, causes periodic water shortages in the settlements. Additionally, the majority of surface water bodies are so contaminated that some of them are unusable for specific purposes, so the population now relies excessively on boreholes fitted with hand pumps to supply its water demands. The development of groundwater is the most reliable source of efficient water supply in the region to accomplish the SDG targets due to the lack of reliable surface water sources. As part of the small towns water supply initiative, the Community Water and Sanitation Agency provided piped water to a few settlements in the region (CWSA, 2018).

The geology of an area determines the groundwater potential of the study area as the rocks determine the recharge rate, storativity, transmissivity, etc. (Shaban *et al.* 2006). Nearly 96% of the area is composed of Precambrian crystalline igneous and metamorphic rocks, which comprise the Upper Birimian, Lower Birimian, Tarkwaian, Togo, and Sekondian deposits. Sekondian and Tertiary deposits from the Cenozoic and Palaeozoic periods can be found along the coast. The central portion between Anomabo and Mankessim has Tertiary sedimentary strata, while the Sekondian lies west of the area (GGS, 2009). The Ashanti and Kibi-Winneba belts in the north are linked to the Upper Birimian formations, which are distinguished by lava rock types and metamorphosed tuffs, in a north-east-south-west direction. Dapaah-Siakwan and Gyau-Boakye (2000) state that isoclinal, folded, and metamorphosed schist, slate, and phyllite with interbedded greywacke comprise the Lower Birimian formation. Additionally, batholithic masses of gneisses, migmatites, and biotite granitoids intrude across the whole Birimian formation decreasing the groundwater potential. High-yielding boreholes, with an average of 12.7 m^3/hr and a range of 0.41 m^3/hr to 29.8 m^3/hr, are found in the Birimian strata, which feature considerable foliation and fractures (Dapaah-Siakwan and Gyau-Boakye 2000).

Early Proterozoic rocks from the Birimian, Kibi-Winneba, and Ashanti belts form the region's subsurface (Leube *et al.*, 1990). The Cape Coast-type biotite granites/gneisses are the primary rock type in the region. Volcaniclastics, schists, amphibolites, sandstone, conglomerate, and shale with mafic dykes are some of the additional rocks found in the region. Since the rocks in the region lack primary porosity and permeability, the hydrogeology of the region is primarily governed by secondary porosity and permeability brought about by weathering and the development of secondary structures such joints, shear zones, folds, fissures, faults, and fractures.

Method

The hydrogeochemical data for this study was obtained from the Community Water and Sanitation Agency (CWSA), Cape Coast. The CWSA provided data from a total of 136 boreholes that were sampled for physico-chemical parameters. The information was gathered as part of numerous initiatives designed to get potable water to the target populations. The samples were taken from boreholes that were situated in several Central Region recipient villages, and the locations of those boreholes were recorded using a Global Positioning System (GPS). 500 ml high-density polyethylene sampling vials were used to collect groundwater samples for in-lab testing. Most of the time, the samples were taken following a lengthy pumping period (i.e. after the pumping test). The samples must be preserved for heavy metal examination. Hence, 10 ml of 69% nitric acid were applied to the samples. While the necessary field observations and other information were being entered in the field notebook, the bottles were labelled to identify the samples.

Following the recommendations of WHO (2008) and APHA (1995), physical parameters such as pH, Total Dissolved Solids (TDS), and Electrical Conductivity (EC) were measured on the field using a portable meter (Hanna equipment). The samples were taken to the Ghana Water Company Laboratory in Cape Coast for additional analysis while being maintained in an ice chest with ice packs. The groundwater samples were analyzed in the lab using the APHA (1995) recommended standards. The probe method was used to analyze the physical parameters, including TDS, EC, temperature, and pH. Ion chromatography was used to examine some of the chemical parameters, including F^-, Cl^-, SO_4^{2-}, NO_3^-, NO_2^-, PO_4^{3-}, and CO_3^{2-}, while flame atomic absorption spectrometry (AAS) was used to analyse others, including Fe, Mn, and Ca^{2+}. The formula suggested by Hem (1985) was used to convert $CaCO_3$ mg/l into HCO_3^-.

TSS was measured using photometric method 8006, TH was measured using titrimetric method, alkalinity was measured using titration method, turbidity was measured using absorptiometric method, colour was measured using cobalt standard method, salinity was measured using electrical conductivity method, whiles sodium and potassium were measured using flame photometer. Ionic balance of the samples was estimated to evaluate the quality of the laboratory data, and samples were within the range of 10% (Celesceri et al., 1998).

The factors in Table 1 were used to calculate the water quality index in this study, and by utilizing the following formula steps;

a. Assignment of weight (w_i) to the various parameters based on their perceived impact on human health.

b. Relative weight (W_i) calculation using;

$$W_i = \frac{w_i}{\sum_{i=1}^{n} w_i} \quad (1)$$

c. Calculation of quality rating scale (qi) using;

$$q_i = 100 * \left(\frac{C_i}{S_i}\right) \quad (2)$$

d. Calculation of sub-index of each parameter SI using;

$$SI_i = W_i * q_i \quad (3)$$

e. WQI calculation using;

$$WQI = \sum SI_i \quad (4)$$

Where w_i is the assigned weight, W_i is the relative weight, n is the number of parameters, q_i is the quality rating, S_i is the WHO (2012) value in mg/l and C_i is the concentration from the laboratory in mg/l, SI is the sub-index for the various parameters and WQI is the Water Quality Index (Couillard and Lefebre, 1985).

Table 1. Groundwater quality parameters used for calculation of water quality indices

Parameter	Unit	Weight (wi)	Relative weight (Wi)	WHO (2012)
pH	pH unit	4	0.07	6.5-8.5
TH	mg/l	3	0.05	500.00
Ca^{2+}	mg/l	2	0.03	75.00
Mg^{2+}	mg/l	2	0.03	150.00
Na^{+}	mg/l	3	0.05	200.00
Cl^{-}	mg/l	4	0.07	250.00
TDS	mg/l	4	0.07	1500.00
F^{-}	mg/l	4	0.07	1.50
NO_2^{-}	mg/l	5	0.08	3.00
NO_3^{-}	mg/l	5	0.08	50.00
SO_4^{2-}	mg/l	4	0.07	250.00
Mn	mg/l	3	0.05	0.10
Fe	mg/l	3	0.05	0.30
PO_4^{3-}	mg/l	4	0.07	0.10
Turbidity	mg/l	5	0.08	5
Colour	CPU	2	0.03	15
$CaCO_3$	mg/l	2	0.03	200
TOTAL		**59**	**1.00**	

To calculate the WAQWI the following steps were taken below and parameters of Table 1;

a. Selection of water quality parameters based on their perceived impact on human health.

b. Calculation of proportionality constant (K) using;

$$K = \frac{1}{\frac{1}{\sum_{i}^{n} S_i}} \quad (5)$$

c. Calculation of quality rating (Q_i) using;

$$Q_i = \frac{C_i - V_i}{S_i - V_i} * 100 \quad (6)$$

d. Calculation of unit weight (W_i) for the nth parameter

$$W_i = \frac{K}{S_i} \quad (7)$$

e. Calculation of WAQWI

$$WAQWI = \frac{\sum W_i * Q_i}{\sum W_i} \quad (8)$$

Where K is the constant proportionality, S_i is the value of the water quality parameter obtained from the recommended standard WHO standard for drinking water, Q_i is the quality rating, C_i is the concentration of each physical or chemical parameter in each water sample in mg/l, V_i is the ideal value of the parameter in pure water ($V_i = 0$) and is considered as 7.0 for pH, W_i is the unit weight and WAQWI is the Weighted arithmetic Water Quality Index. The IRCA was calculated using the equation (García-Ubaque et al., 2018) and parameters in Table 2.

$$\%IRCA = \frac{\text{Risk score for unacceptable parameters}}{\text{Risk score for all parameters analysed}} * 100 \quad (9)$$

Table 2. IRCA's risk scores (MAVD, 2021).

Parameter	Unit	Risk score
pH	pH unit	1.5
TH	mg/l	1
Ca^{2+}	mg/l	1
Mg^{2+}	mg/l	1
Na^+	mg/l	1
Cl^-	mg/l	1
TDS	mg/l	1
F^-	mg/l	1
NO_2^-	mg/l	1
NO_3^-	mg/l	1
SO_4^{2-}	mg/l	1
Mn	mg/l	1
Fe	mg/l	1.5
PO_4^{3-}	mg/l	1
Turbidity	mg/l	15
Colour	CPU	6
$CaCO_3$	mg/l	1
TOTAL		**39**

Results

The statistical analysis of the groundwater data is shown in Table 3. The Table lists the several parameters that were employed in this research, along with the concentration range for each and the corresponding WHO (2012) acceptable limits. It has been noted that some samples have values that are below the acceptable limits and others have values that are above the acceptable limits.

In this study, the correlation technique was used to demonstrate the relationship that currently exists between the water quality metrics (McGrorya, 2020). This method is helpful in determining where groundwater pollution originates (Hussain, 2019). It has been effectively applied by several authors in groundwater quality research (Varol and Davraz, 2014; Agyemang 2022). The correlation outcome is shown in Table 4.

The $CaMgSO_4$, NaCl, $CaMgHCO_3$, and Mixed water types are present in the study area, according to the Piper (1944) diagram plot in Fig. 2. The majority of the samples exhibit excess Cl^- concentration above the Na^+ concentration, as shown by the plot of Na^+ vs. Cl^- in Fig. 3. By plotting the Gibb diagrams, it can be seen that rock weathering and, to a lesser extent evaporation, are the key factors influencing the chemistry of groundwater (Fig. 4 a, b). The influence of silicate weathering, carbonate weathering, and ion exchange process are displayed in the plot of CAI I vs. CAI II in Fig. 5. The study area's typical type of rock weathering process was investigated using the plot of Ca^{2+}+Mg^{2+} against SO_4^{2-}+$H_2CO_3^-$, as shown in Fig 6. The diagram showed that some of the samples are above the equiline, while others are on it. The dissolution of carbonate and/or sulphate minerals is indicated by a plot of the sample on the equiline where SO_4^{2-}+HCO_3^- = Ca^{2+}+Mg^{2+}, the carbonate and sulphate mineral dissolution and/or ion exchange is indicated by excess SO_4^{2-}+HCO_3^- over Ca^{2+}+Mg^{2+}, and the dissolution of silicate minerals is indicated by excess Ca^{2+}+Mg^{2+} over SO_4^{2-}+HCO_3^- (Tiwari and Singh, 2014). Samples that are found above the equiline (i.e., Ca^{2+}+Mg^{2+} above SO_4^{2-}+HCO_3^-) indicate the occurrence of silicate weathering. It suggests that silicate mineral dissolution and/or ion exchange mechanisms predominate in the area.

Table 3. Statistical summary of the groundwater data

Parameter	Unit	Minimum	Maximum	Mean	Std. Deviation	WHO (2012)
pH	pH unit	4.75	9.40	6.35	0.69	6.50-8.50
Colour	CPU	1.00	188.00	9.70	16.86	15.00
EC	µS/cm	44.80	24900.00	893.81	2634.13	1000.00
TDS	mg/l	26.90	13695.00	495.38	1448.12	1500.00
TH	mg/l	6.00	9200.00	272.93	955.83	500.00
TSS	mg/l	1.00	321.00	9.52	30.73	500.00
Turbidity	mg/l	0.750	484.00	22.33	38.79	5.00
Ca hardness	mg/l	2.000	4509.00	142.27	483.30	200.00
Mg hardness	mg/l	0.005	5292.00	128.86	514.97	
Ca^{2+}	mg/l	0.800	1804.00	56.76	193.27	75.00
$CaCO_3$	mg/l	9.800	390.00	91.94	68.91	200.00
Cl^-	mg/l	3.000	8660.00	219.01	979.32	250.00
CO_3^{2-}	mg/l	0.000	32.50	0.27	2.70	
F^-	mg/l	0.001	150.00	2.65	17.60	1.50
Fe	mg/l	0.008	56.90	0.92	4.53	0.30
H_2CO_3	mg/l	0.000	476.00	110.23	84.83	
H_2PO_4	mg/l	0.001	61.70	0.88	5.02	0.10
K^+	mg/l	0.400	57.50	5.69	7.57	30.00
Mg^{2+}	mg/l	1.000	1286.00	31.20	124.77	150.00
Mn	mg/l	0.003	10.70	0.37	1.09	0.10
Na^+	mg/l	1.500	2688.00	81.53	277.76	200.00
NH_4^-	mg/l	0.001	15.00	0.13	1.23	
NO_2^-	mg/l	0.001	0.70	0.07	0.12	3.00
NO_3^-	mg/l	0.001	134.00	3.50	12.35	50.00
SO_4^{2-}	mg/l	0.001	3127.00	58.05	254.32	250.00

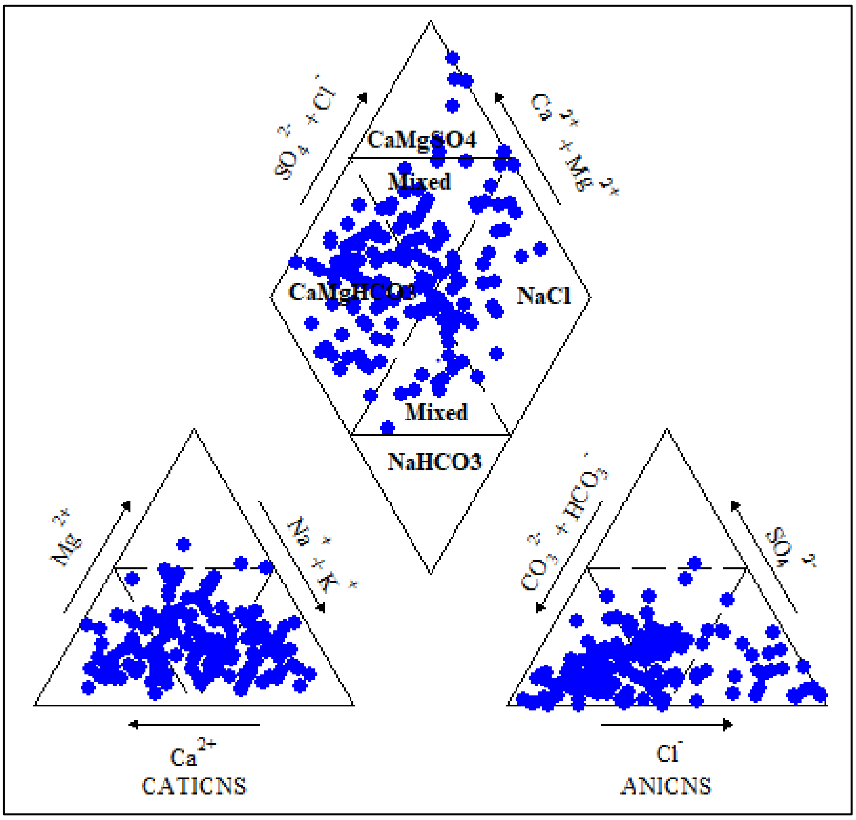

Figure 2. Piper diagram showing groundwater types in the study area.

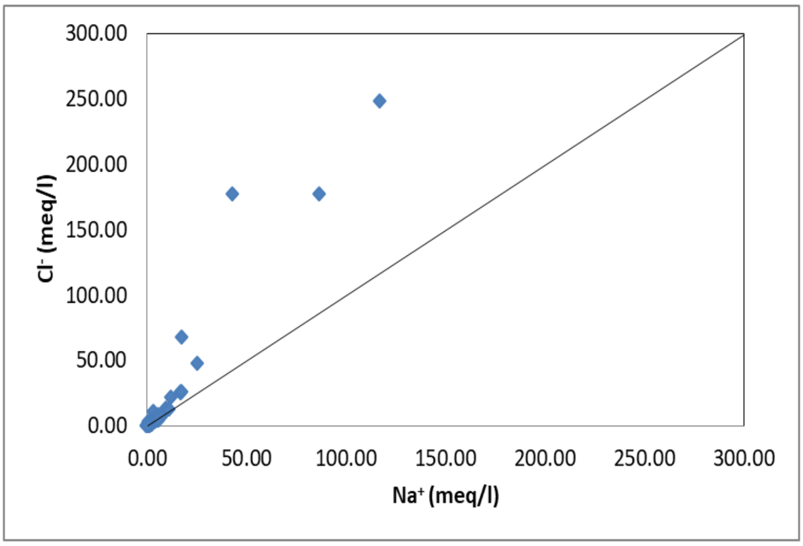

Figure 3. a plot of Cl^- vs. Na^+ concentrations

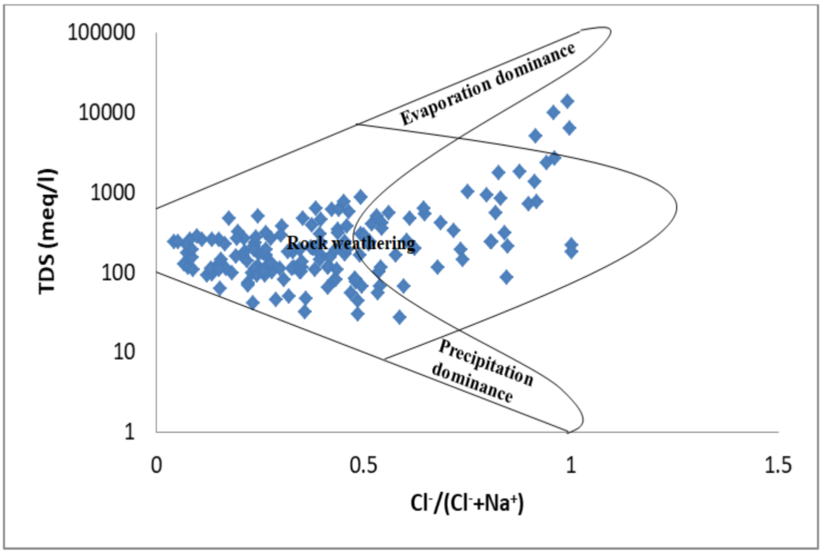

Figure 4.a A plot of TDS vs. $Cl^-/(Cl^-+Na^+)$

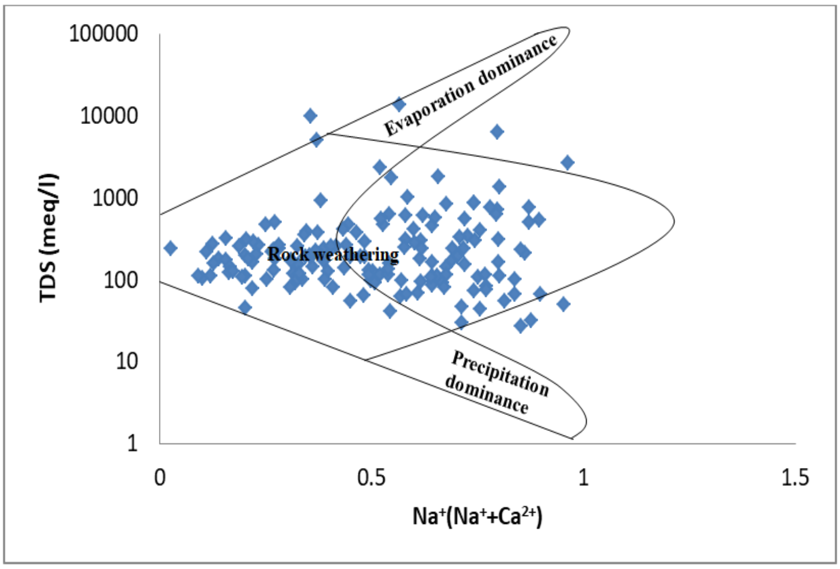

Figure 4.b A plot of TDS vs. $Na^+/(Na^++Ca^{2+})$

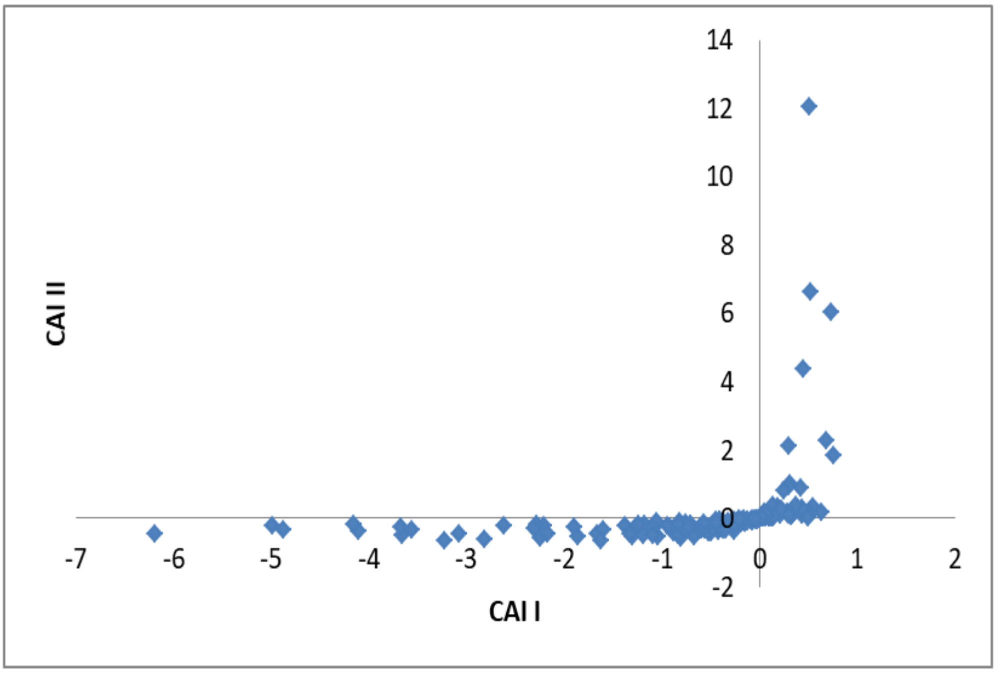

Figure 5. a plot of CAI I vs. CAI II

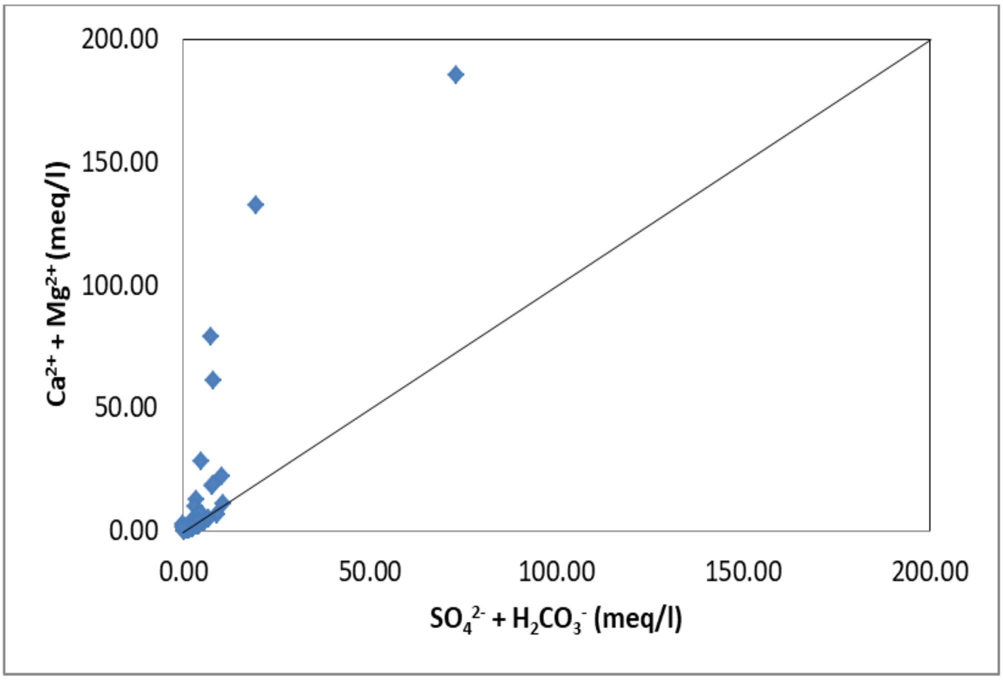

Figure 6. plot of (Ca^{2+}+Mg^{2+}) vs. (SO_4^{2-}+$H_2CO_3^-$)

The classification of the computed WQI, WAQWI, and IRCA values for the groundwater samples are shown in Table 5. To show the spatial variation of the various classes of water quality indices, codes of 1-5 were assigned to the classes as shown in Table 5. The spatial distribution maps of the indices are shown in Figures 7, 8, and 9. Additionally, Fig. 10 illustrates how the WQI, WAQWI, and IRCA tools broke down the major groups. To show the spatial distribution of the WQI, WAQWI, and IRCA values, numerical weight were assigned to the various classes as codes as shown in Table 5.

Table 4. Correlation Table of physicochemical parameters

	Turb.	**Col.**	**pH**	**EC**	**TSS**	**TDS**	**Na**	**K**	**Ca**	**Mg**	**Fe**	**NH_4**	**Cl**	**SO_4**	**PO_4**	**Mn**	**NO_2**	**NO_3**	**TH**	**$CaCO_3$**	**Ca_hard.**	**Mg_hard.**	**F**	**H_2CO_3**	**CO_3**
Turb.	1.00	**0.85**	0.14	0.01	0.08	0.01	0.00	-0.03	-0.01	0.00	**0.91**	0.01	0.00	0.01	0.00	0.47	0.08	-0.03	0.00	-0.03	0.00	0.00	-0.02	-0.04	0.08
Col.		1.00	0.13	-0.01	0.20	-0.01	-0.02	0.01	-0.03	-0.01	**0.84**	-0.04	-0.03	-0.01	-0.04	0.44	0.03	-0.06	-0.02	0.04	-0.02	-0.02	-0.04	0.04	0.06
pH			1.00	0.03	-0.15	0.03	0.03	0.11	0.04	0.02	0.12	0.17	0.01	0.03	0.13	0.16	0.11	0.08	0.03	0.32	0.04	0.02	0.12	0.27	0.42
EC				1.00	-0.05	1.00	**0.93**	**0.53**	**0.97**	**0.86**	-0.01	-0.02	**0.98**	**0.72**	-0.03	0.03	-0.05	0.01	**0.95**	0.32	**0.97**	**0.86**	0.06	0.33	-0.03
TSS					1.00	-0.05	-0.03	-0.02	-0.05	-0.03	0.03	-0.03	-0.03	-0.03	-0.03	-0.02	-0.06	0.02	-0.04	-0.10	-0.05	-0.03	-0.04	-0.09	-0.02
TDS						1.00	**0.93**	**0.52**	**0.97**	**0.86**	-0.01	-0.02	**0.98**	**0.72**	-0.03	0.03	-0.05	0.01	**0.95**	0.32	**0.97**	**0.86**	0.06	0.33	-0.03
Na							1.00	**0.59**	**0.83**	**0.74**	0.00	-0.03	**0.96**	**0.51**	-0.03	0.04	-0.06	0.01	**0.82**	0.18	**0.83**	**0.74**	0.07	0.18	-0.02
K								1.00	0.45	0.37	0.00	-0.01	**0.52**	0.24	-0.01	0.02	-0.06	0.03	0.42	0.38	0.44	0.37	0.12	0.38	-0.04
Ca									1.00	**0.84**	-0.01	-0.01	**0.92**	**0.80**	-0.02	0.03	-0.06	0.01	**0.96**	0.36	**1.00**	**0.84**	-0.01	0.37	-0.03
Mg										1.00	-0.02	-0.02	**0.87**	**0.89**	-0.03	0.04	-0.08	0.01	**0.96**	0.37	**0.84**	1.00	0.10	0.37	-0.02
Fe											1.00	0.00	-0.02	0.00	0.00	**0.52**	0.04	-0.01	-0.02	0.01	-0.01	-0.02	-0.01	0.02	-0.01
NH_4												1.00	-0.02	-0.02	**0.58**	-0.04	**0.53**	**0.93**	-0.02	0.02	-0.03	-0.03	**0.74**	-0.13	-0.01
Cl													1.00	**0.69**	-0.03	0.03	-0.07	0.01	**0.93**	0.23	**0.92**	**0.87**	0.06	0.24	-0.02
SO_4														1.00	-0.03	-0.01	-0.05	-0.01	**0.88**	0.39	**0.80**	**0.89**	0.00	0.39	-0.02
PO_4															1.00	-0.03	0.48	**0.66**	-0.03	-0.02	-0.03	-0.03	**0.56**	-0.13	-0.01
Mn																1.00	-0.02	-0.05	0.03	0.22	0.03	0.04	-0.05	0.23	-0.03
NO_2																	1.00	**0.54**	-0.07	-0.07	-0.07	-0.08	0.41	-0.15	0.00
NO_3																		1.00	0.01	0.00	-0.01	0.01	**0.72**	-0.14	-0.02
TH																			1.00	0.39	**0.96**	**0.96**	0.05	0.39	-0.03
$CaCO_3$																				1.00	0.37	0.37	0.02	**0.99**	-0.07
Ca_hard.																					1.00	**0.84**	-0.03	0.37	-0.03
Mg_hard.																						1.00	0.10	0.37	-0.02
F																							1.00	-0.10	-0.01
H_2CO_3																								1.00	-0.12
CO_3																									1.00

Bolded values showed significant correlations

Table 5. WQI, WAQWI and IRCA classifications (Couillard & Lefebre, 1985; Tygai, 2013; MAVD, 2021)

Classification	Assigned code	WQI	WAQWI	IRCA
Excellent	0.1-1.0	0-50	0-25	0-5
Good	1.1-2.0	50-100	25.1-50	5.1-14
Poor	2.1-3.0	100-200	50.1-75	14.1-35
Very Poor	3.1-4.0	200-300	75.1-100	35.1-80
Unsuitable	4.1-5.0	>300	>100	80.1-100

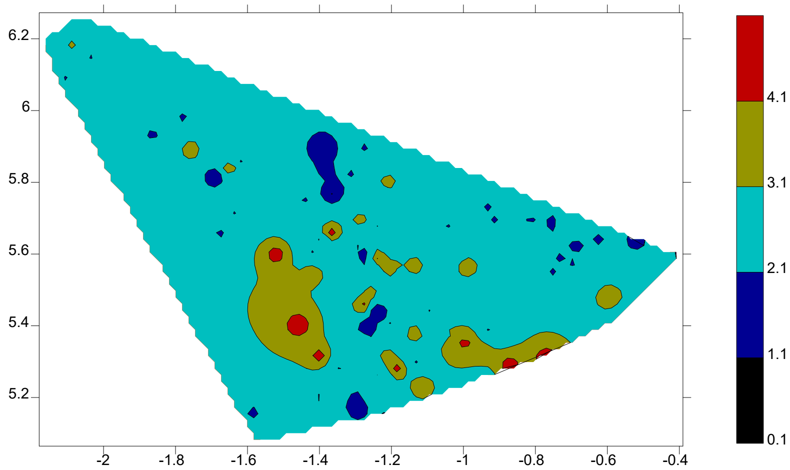

Figure 7. Spatial distribution of WQI

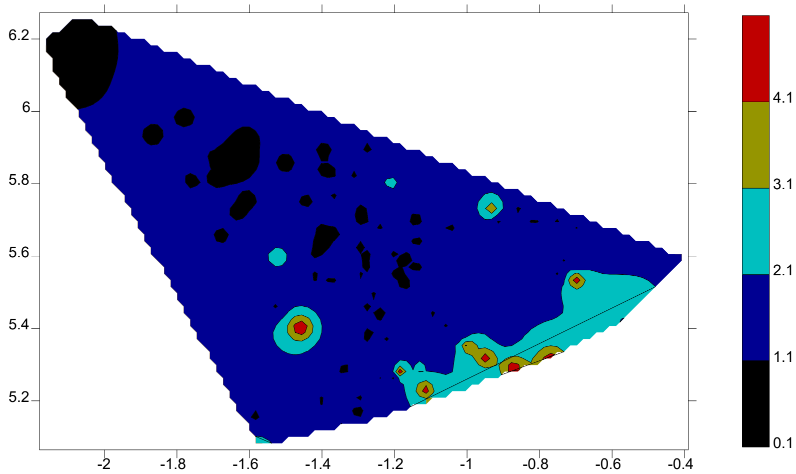

Figure 8. Spatial distribution of WAQWI

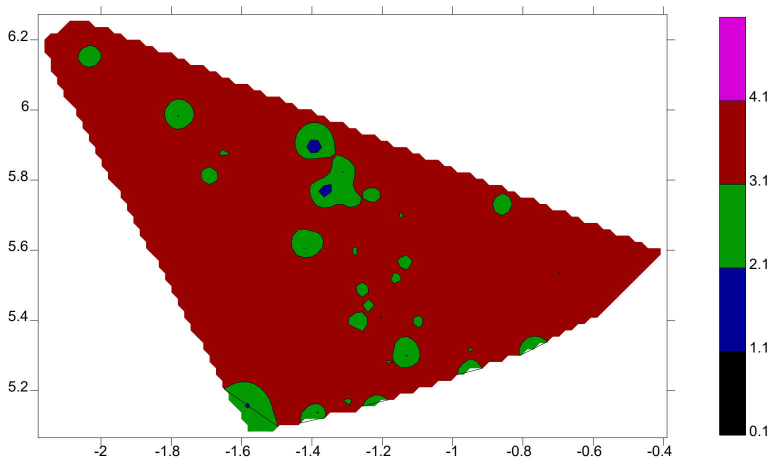

Figure 9. Spatial distribution of IRCA

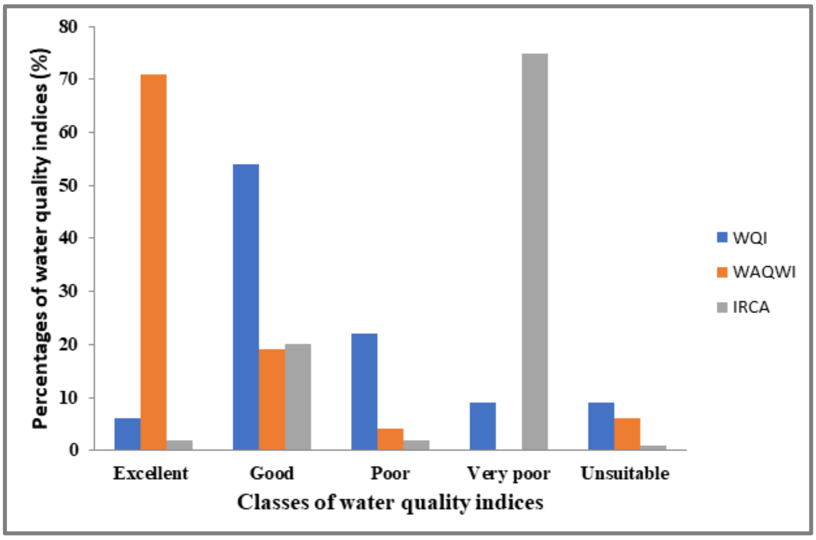

Figure 10. Classification of the water quality indices and IRCA

Discussion

The average pH of the groundwater is 6.351 pH units, with a range of 4.750 pH units to 9.400 pH units. This demonstrates that certain samples have pH levels that are either below or over the 6.5–8.5 limits for drinking water recommended by the WHO (2012). This indicates that some of the samples are basic and some are acidic, making them unfit for drinking without treatment. TDS has a range of 26.900 to 13695.000 mg/l with a mean of 495.378 mg/l. While some of the samples are below the 1500 mg/l drinking water recommendation, several are far above the limit. The mean EC value for the groundwater samples is 893.812 S/cm, with a range of 44.800 S/cm to 24900.000 S/cm. This indicates that a few of the samples are greater than the suggested value of 1000 S/cm. The range of TH was 6.000-9200.000 mg/l with a mean of 272.930 mg/l indicating that some of the samples have higher TH values than the recommended value of 500 mg/l.

TSS has a range of 1.000 mg/l to 321.000 mg/l. with an average of 9.520 mg/l. This demonstrates that all of the samples have readings below the suggested level of 500 mg/l. Turbidity ranges from 0.750 to 484.000 mg/l, with a mean of 22.330 mg/l. This demonstrates that some of the samples have readings that are higher than the advised level of 5 mg/l. With a mean of 9.701 CPU, the samples' color runs from 1.000 CPU to 188.000 CPU. This indicates that some of the samples have color values over the suggested level of 15 CPU. It is apparent that the groundwater's physical properties have quite large changes when considered their concentration. This observation may be explained by the various geographic locations of the borehole samples used in the study inside the recharge zone or discharge zone of the aquifer systems.

Potassium has a concentration range of 0.400–57.500 mg/l, with a mean of 5.686 mg/l. Some of the samples show readings that are higher than the safe drinking water standard of 30 mg/l. Na^+ has an average concentration of 81.532 mg/l with a range of 1.500 mg/l to 2688 000 mg/l. This indicates that a few samples contain concentrations that are extremely high compared to the suggested value of 200 mg/l. Ca^{2+} ranges from 0.800 to 1804.000 mg/l with a mean of 56.763 mg/l, indicating that certain sample values are higher than the recommended value of 75 mg/l. With a mean of 31.202 mg/l, Mg^{2+} has a range of 1.000 mg/l to 1286.000 mg/l. This indicates that a few samples contain high concentrations that are over the recommended level of 150 mg/l. With a mean of 0.372 mg/l, the Mn content ranges from 0.003 mg/l to 10.700 mg/l. This demonstrates that some samples have levels higher than the 0.10 mg/l threshold for drinking water.

With a range of 0.008 mg/l to 56.900 mg/l and a mean of 0.918 mg/l, the Fe content indicates that some samples may have values higher than the advised threshold of 0.30 mg/l. The range of Cl^- concentrations, from 3.000 mg/l to 8660.000 mg/l, with a mean of 219.009 mg/l, suggests that some samples have values higher than the recommended value of 250 mg/l. The CO_3^{2-} range has a mean of 0.271 mg/l and a range of 0-32.500 mg/l. $H_2CO_3^-$ concentrations range from 0 to 476.000 mg/l, with a mean of 110.226 mg/l. The average NH_4^- content is 0.131 mg/l, however it ranges from 0.001 mg/l to

15.000 mg/l. The range of NO_2^- concentration is 0.001-0.700 mg/l, and the mean value is 0.065 mg/l, which means that some samples had levels higher than the recommended amount of 3 mg/l. The range of NO_3^- is 0.001-134.000 mg/l, and the mean value is 3.504 mg/l, indicating that some samples have NO_3^- concentrations that are higher than the advised value of 50 mg/l. With a mean concentration of 58.046 mg/l, the range of SO_4^{2-} is 0.001-3127.000 mg/l. This demonstrates that some samples have values that are higher than the suggested level of 250 mg/l. PO_4 concentrations range from 0.001-61.700 mg/l, with a mean of 0.878 mg/l. This indicates that some of the samples had readings that are higher than the advised level of 0.10 mg/l. F^- concentrations range from 0.001 to 15 000 mg/l, with a mean of 2.647 mg/l. This demonstrates that some samples have results over the suggested level of 1.5 mg/l.

Similar to the physical characteristics, the spatial distribution of the sampled boreholes for this study may also be responsible for the large fluctuations in the cations and anion concentrations within the groundwater. Groundwater cation and anion concentration variations may be caused by a variety of factors, including rock weathering, ion exchange, precipitation, evaporation, and impacts of anthropogenic activities. According to the study, the groundwater types in the area include Ca-Mg-SO_4, Na-Cl, Ca-Mg-HCO_3, and mixed water types and the processes that control the groundwater chemistry include silicate weathering, carbonate weathering, ion exchange, and the potential effects of anthropogenic activities like improper waste disposal, the use of pit latrines, open defecation, mining, and galamsey activities. To examine the impact of ion exchange on groundwater chemistry, a plot of CAI I vs. CAI II was employed. According to Schoeller (1965), CAI I and CAI II positive values indicate that Na^+ or K^+ in groundwater exchanges with Mg^{2+} or Ca^{2+} in the aquifer system, and negative values indicate that Mg^{2+} or Ca^{2+} in groundwater exchanges with Na^+ and K^+ in the rocks. Positive numbers indicate ion exchange, while negative values indicate reverse ion exchange. Reverse ion exchange predominat the groundwater from the study area.

Correlation Analysis

The use of the correlation analysis technique revealed a substantial association between turbidity, Fe, and colour, suggesting that the content of Fe in the groundwater regulates turbidity. Strong correlations between colour and Fe imply that the groundwater's Fe concentration affects the color. The EC is correlated with Mg^{2+} hardness, Na^+, K^+, Ca^{2+}, Mg^{2+}, Cl^-, SO_4^{2-}, TH, and Ca^{2+} hardness, indicating that the amounts of these substances affect the groundwater's EC. As shown by the factor analysis and cluster analysis approaches, geogenic processes and human activities may be in control of the concentrations of Na^+, K^+, Ca^{2+}, Mg^{2+}, Cl^-, and SO_4^{2-} in the groundwater. As a result, these factors affect the EC of the groundwater. The fact that TDS closely correlates with Na^+, K^+, Ca^{2+}, Mg^{2+}, Cl^-, SO_4^{2-}, Ca hardness, and Mg hardness suggests that the concentrations of Na^+, K^+, Ca^{2+}, Mg^{2+}, Cl^-, and SO_4^{2-} in the groundwater affect the TDS of the groundwater. This indicates that anthropogenic activities as well as rock weathering affect the TDS.

The correlations among cations and anions reflect the effect of weathering of the source rocks. The relationship between K^+ and Cl^- shows that anthropogenic activities have an impact on the chemistry of groundwater and the overall quality of groundwater. The relationship between Ca^{2+} and Cl^-, SO_4^{2-}, Mg^{2+}, TH, Ca^{2+} hardness, and Mg^{2+} hardness suggests that the weathering of rocks has an effect on the quality of the groundwater. Mg correlates with Cl^-, SO_4^{2-}, TH, Ca^{2+} hardness, and Mg^{2+} hardness, illustrating how the weathering of rocks affects the quality of groundwater. Fe and Mn are correlated, which shows that weathering of rocks has an effect of the groundwater chemistry. The relationship between NH_4^+ and F^-, NO_2, NO_3, and PO_4 indicates that anthropogenic activities, such as applying fertilizer to farmland, poor hygienic conditions around boreholes, using chemicals for galamsey activities, using pit latrines, etc., have an impact on the chemistry and general quality of groundwater.

The relationship between Cl^- and SO_4^{2-}, TH, Ca^{2+} hardness, and Mg^{2+} hardness suggests that anthropogenic activities have an impact on groundwater quality. The correlation between SO_4^{2-} and TH, Ca^{2+} hardness and Mg^{2+} hardness suggests that SO_4^{2-} may have an impact on groundwater hardness. PO_4 correlates with NO_3 and F^-, demonstrating how human activities affect the quality of groundwater. The relationship between NO_2 and NO_3 implies that the conversion of NO_3 to NO_2 is the primary factor affecting the content of NO_2 in groundwater. NO_3 correlates with F-, demonstrating that anthropogenic sources account for the majority of the NO_2 entering the groundwater system. A portion of the concentration is changed into NO_2 upon the introduction of NO_3. The use of the correlation analysis technique confirms the potential impact of ion exchange, rock weathering, and human activity on the region's groundwater chemistry and general quality. The various associations point to the potential effects of mineral dissolution and human activities including improper waste disposal, a lack of hygienic conditions around boreholes, and the use of fertilizers on agricultural land on the chemistry of groundwater (Driscoll et al., 1989; Koh et al., 2010; Tiwari and Singh, 2014).

Water quality index (WQI)

The WQI scores are divided into five groups based on various ratings. When the value falls between 0 and 50, it is considered to be water of excellent quality for drinking, between 50 and 100, it is considered to be good for drinking, between 100 and 200, it is considered to be water of poor quality for drinking, between 200 and 300, it is considered as water of very poor quality and above 300, it is considered to be water of unsuitable quality (Couillard and Lefebre, 1985). The WQI determined that 6% of the groundwater samples had excellent quality, 54% had good quality, 22% had poor quality, 9% had very poor quality, and 9% were unfit for drinking purposes based on this classification. By making a thematic map, the spatial distribution of the WQI is displayed. The majority of the water quality readings fall between 50% and 100%. Poor and very poor water types can be found in coastal areas and some central regions. This observation might be explained by the interactions between groundwater and seawater near the coastline areas of the region. The low groundwater quality along the coast may be caused by a potential seawater intrusion. However, the occurrence of poor, extremely poor, and unsuitable water types in the region's central part may be attributed to the effects of anthropogenic activities. The majority of the locals are farmers, and they treat the farmland with various pesticides and animal dung. Once more, sloppy small-scale mining operations are widespread in the Region, and this may also be the reason for the area's documented groundwater quality issues.

Weighted arithmetic Water Quality Index (WAQWI)

When there are no contaminants in the water, the quality rating in the WAQWI calculation is zero, and it is 100% when the parameter has the recommended value of the WHO (2012). However, as contamination levels increases, the quality rating's worth decreases. Garcia-Avila et al. (2018) claim that a water quality parameter's relative weight is inversely related to the WHO's suggested values. The final WAQWI scores are divided into five categories with varying ratings. When the value is between 0 and 25, it is graded as A, meaning the water is excellent for drinking. When the value is between 26 and 50, it is graded as B, meaning the water is good for drinking. When the value is between 51 and 75, it is graded as grade C, meaning the water is poor. When the value is between 76 and 100, it is graded as D, meaning the water is very poor. When the value is above 100, it is graded as grade E, meaning the water is unsuitable for drinking without treatment (Tygai, 2013). According to the study, 71% of the groundwater in the study region is of grade A water type, followed by 19% grade B, 4% grade C, 0% grade D, and 6% grade E. This implies that the groundwater in the research area is generally suitable for human consumption. However, since the quality varies by location, it is necessary to test the water before consuming it. In some areas, the water is of poor quality.

IRCA determination

The IRCA, which has a value range of zero to one hundred, is one of the water quality indices used to evaluate the quality of drinking water. Like all water quality indices, it breaks down complex data on drinking water samples' water quality into a number that can be easily understood by various professional groups. The index makes use of variables whose potential effects on human health have been given a risk score. Depending on the range that the IRCA values fall into, they are divided into five groups. The value is considered to pose no risk to human health when it falls within the range of 0 to 5, low risk when it falls within the range of 5.1 to 14, medium risk when it falls within the range of 14.1 to 35, high risk when it falls within the range of 35.1 to 80, and sanitarily infeasible when it falls within the range of 80.1 to 100 (MAVD, 2021). In Table 2, the parameters that were utilized to calculate the IRCA are listed along with the corresponding risk score.

According to the IRCA calculations, 2% of the samples contain water that poses no risk to human health, 20% contain water that is low risk, 2% contain water that is medium risk, 75% contain water that is high risk, and 1% contains water of unsuitable quality for drinking. This indicates that the bulk of the samples have high-risk potential for human consumption and that the groundwater is not appropriate for drinking without prior treatment. The observation is related to the majority of the samples' generally low pH values and high observed values of turbidity, color, Mn, Fe, and PO_4 in comparison to WHO (2012) recommended values.

The weights assigned to the various water quality parameters are based on their potential effects on human health, similar to other water quality indices. High potential parameters are given higher weights, whilst low potential parameters are given lower weights. The monitoring of water quality in Colombia from 2008 to 2012, according to Garca-Ubaque et al. (2018), showed that the calculated IRCA value was around 13.4%, which denotes water of a low-risk level. Since the water sources in Sincern and Gambote municipalities provide a significant risk to human health, Duarte-Jaramillo et al. (2021) investigated them and concluded that the sources should not be used for drinking. The domestic water supply network in Azogues, Ecuador, was evaluated by Garcia-Avilla et al. (2022), who found that the samples exhibited IRCA levels between 0 and 5%. As a result, the water that was being provided was deemed safe for consumption and assigned the water type designation "No-risk."

Comparison of the WQI, WAQWI and IRCA

The Water action decade (2018–2028) was established by the UN general assembly in response to a trend that raises the possibility of an impending global water catastrophe (UNDESA, 2014; 2021). Achieving universal access to clean water and sanitary facilities is a specific goal of Sustainable Development Goal (SDG) 6. According to research, there are two billion people without access to clean drinking water worldwide (UNDESA, 2021). Studies in a few African nations have shown that some of them are already dealing with water issues (Sachs et al., 2021). According to the survey, roughly eight countries rely on less than 50% of the minimum facilities they need for drinking water, while over fifteen countries rely on less than 60% of the necessities (SDG Index, 2021).

The spread of galamsey activities in Ghana has had a significant negative impact on the environment and water resources. Most of the water bodies that formerly provided an alternative source of water for the population have become so polluted as a result that some of them are no longer suitable for certain purposes. As a result, there is now less water available and there are problems with the water's quality. According to the WQI, 6% of the groundwater samples had excellent quality, 52% had good quality, 34% had poor quality, 3% had very poor quality, and 5% were unfit for drinking purposes. According to the WAQWI, 71% of groundwater samples are grade A, followed by 19% grade B, 4% grade C, 0.00% grade D, and 6% grade E. According to the IRCA calculations, 2% of the samples contain water that poses no risk to human health, 20% contain water that is low risk, 2% contain water that is medium risk, 75% contain water that is high risk, and 1% contains water that is unfit for human consumption.

According to this observation, approximately 58% of groundwater samples based on WQI, 90% based on WAQWI, and just 22% based on IRCA are suitable for human consumption. This discovery demonstrates that while the two water quality indexes differ greatly from the IRCA, they do share some characteristics. The findings of the study by Osiakwan et al. (2021), which applied the entropy-based groundwater quality index (IEBGWQIs) for the assessment of groundwater quality for drinking purposes in the Central Region of Ghana, are consistent with the results of the two water quality indices. According to their research, the groundwater quality of the samples taken was evaluated to be excellent, good, average/medium, poor, or extremely poor in 59.4%, 20.3%, 7.8%, 2.6%, and 9.9% of the groundwater samples, respectively.

Additionally, as observed in the spatial distribution maps of the two indices employed in this study, the areas around the coast have very poor groundwater quality while the northern part has outstanding groundwater quality. The bulk of the groundwater samples fall within the excellent category, according to the results from the WAQWI. As a result, consuming the groundwater is generally safe. In their investigations, Agarwal et al. (2020) used WAWQI and CCME WQI methodologies to examine the water quality in India and found that, respectively, 82% and 77% of the samples had poor to inappropriate water types. The observations between the two water quality indicators did not differ significantly, as the current study has shown.

It is important to note that the groundwater samples are untreated raw samples. The fact that some of the samples had poor to unacceptable quality for drinking is therefore not surprising. This explains why the IRCA technique which is often used to evaluate the quality of drinking supply water that may have undergone some type of treatment indicated the extremely poor quality of groundwater. According to the study, in order to protect the public's health, the groundwater in the studied region needs to be treated before being utilized for drinking purpose. The Region has a total population of approximately 2859821 and a land area of approximately 9826 km^2 (GSS, 2021). For their water needs, the majority rely on groundwater supplies. The rural communities are more susceptible to water-related public health problems due to the potential of contaminated groundwater and often lack of treatment before drinking.

Conclusion

In the Central Region of Ghana, a comparative research of groundwater quality has been conducted utilizing two groundwater risk indices and two water quality indices. The area's groundwater types include $CaMgSO_4$, NaCl, $CaMgHCO_3$, $NaHCO_3$, and Mixed water types. Silicate weathering, carbonate weathering, ion exchange, and potential anthropogenic activity effects, such as poor hygiene around boreholes, the use of agrochemicals on farmlands, improper waste disposal, the use of pit latrines, open defecation, mining, and galamsey activities, control the groundwater chemistry. According to the WQI, 6% of the groundwater samples had excellent quality, 54% had good quality, 22% had poor quality, 9% had very poor quality, and 9% were unfit for drinking without treatment. According to the WAQWI, 71% of groundwater samples are of outstanding quality, followed by 19% of acceptable quality, 4% of bad quality, and 6% of unsuitable quality. IRCA calculations showed that 2% of the samples included water that posed no risk to human health, 20% contained water that was low risk, 2% contained water that was medium risk, 75% contained water that was high risk, and 1% contained water that was unfit for human consumption.

The WQI and WAQWI water quality indices display a comparable pattern. However, the IRCA in the study area has a different pattern. The IRCA indicates that there is a generally high level of health risk associated with using the groundwater for drinking without prior treatment, despite the fact that the two indices indicate that the groundwater is generally good for that purpose. The observation is related to the majority of the samples' generally low pH values and high observed values of turbidity, color, Mn, Fe, and PO_4 in comparison to WHO (2012) recommended values. The study has demonstrated the value of WQI, WAWQI, and IRCA as instruments for evaluating and comprehending groundwater quality for drinking purpose. Particularly, in developing nations like Ghana, their use is helpful in achieving the SDG 6.

Acknowledgment: *The author is appreciative to the Management of the CWSA, Cape Coast for making data for this study available.*

Compliance with Ethical Standards

Funding: *The author received no funding for this study.*

Conflict of Interest: *The author declares that he has no conflict of interest.*

References

Agarwal M, Singh M, Hussain J, (2020) Evaluation of groundwater quality for drinking purpose using different water quality indices in parts of Gautam Budh Nagar district, India. *Asian J. Chem.* **32**(5):1128–1138. https://asianpubs.org/index.php/ajchem/article/view/2486/2485

Agyemang (2020) Hydrochemical characterization and assessment of groundwater suitability for drinking, domestic and irrigation purposes in the Agona East District, Ghana. Iconic *Res. & Engin. J.* **3** (7), 112-125. https://www.irejournals.com/paper-details/1701878.

Agyemang VO (2019) Hydrochemical Assessment of Groundwater Quality for Drinking, Domestic and Irrigation Purposes in Afigya Kwabre District, Ghana. *J Hydrogeol Hydrol Eng* 8:3. https://www.scitechnol.com/peer-review/hydrochemical-assessment-of-groundwater-quality-for-drinking-domestic-and-irrigation-purposes-in-afigya-kwabre-district-ghana-Ju3M.php?article_id=9677

Agyemang VO, (2022) "Application of geostatistical techniques in the assessment of groundwater contamination in the Afigya Kwabre District of Ghana". *Applied Water Science* volume 12, Article number: 53 (2022). https://link.springer.com/article/10.1007/s13201-022-01582-x

Ahmed J, Wong LP, Chua YP, (2020) Drinking water quality mapping using water quality index and geospatial analysis in primary schools of Pakistan. Water (Basel). 12:3382. https://www.mdpi.com/2073-4441/12/12/3382

Ahn J, Na Y, Park SW, (2018) Assessment of water quality in an artificial urban canal: a case study of Songdo City in South Korea. *Environ Eng Res.* 24(4):582–590. https://www.eeer.org/new/journal/view.php?number=990

Alexakis DE. Meta-evaluation of water quality indices, application into groundwater resources. Water (Basel). 2020;12:1890. https://www.mdpi.com/2073-4441/12/7/1890

America Public Health Association (1995) Standard methods for the examination of water and waste water, 19th edition, Washington, DC. https://srjcstaff.santarosa.edu/~oraola/Assets/APHA_SM_20.pdf

Back W. (1966). Hydrochemical facies and ground-water flow patterns in northern part of Atlantic Coastal Plain. U .S. Geological Survey 498-A.42. https://doi.org/10.3133/pp498A

Boah DK, Twum SB, Pelig-Ba KB (2015) Mathematical Computation of Water Quality Index of Vea Dam in Upper East Region of Ghana. Environmental Sciences, Vol. 3, 2015, no. 1, 11 – 16. https://www.semanticscholar.org/paper/Mathematical-Computation-of-Water-Quality-Index-of-Boah-Twum/3d2b642173c9f8bafa1265b0c6a73f42e8f14c78

Castro M, Almaida J, Ferrer J, and Díaz D (2014) Indicadores de la calidad del agua: Evolución y tendencias a nivel global Ingeniería Solidaria, vol. 10, no. 17, December 2014. DOI: 10.16925/in.v9i17.811

Celesceri L, Greenberg AE, Eaten AD, (1998) Standard methods for the examination of water and waste water. *American Public Health Association*, Washington, p 134. https://srjcstaff.santarosa.edu/~oraola/Assets/APHA_SM_20.pdf

Couillard D, Lefebvre Y, (1985). Analysis of Water Quality Indices. Journal of Environmental Management 21:161-179. https://www.semanticscholar.org/paper/Analysis-of-water-quality-indices-Couillard-Lefebvre/da385bcfdefd5a823feb6c65aa03744bba5317c5

CWSA (2018) Community water and sanitation agency (CWSA). 2018 Annual Report. https://www.cwsa.gov.gh/publications/annual-reports/

Dapaah-Siakwan S, Gyau-Boakye P (2000) Hydrogeologic framework and borehole yields in Ghana. Hydrogeol J 8(4):405–416. https://doi.org/10.1007/PL00010976

Drever, J. I. (1982). The Geochemistry of Natural Waters. Prentice-Hall, New Jersey. https://doi.org/10.4319/lo.1983.28.3.0600a

Duarte L, Mendoza MA, Jaramillo BE, González A, (2022) Water quality in the municipalities of Sincerín and Gambote, Bolívar, Colombia (2017-2018)", Revista Facultad de Ingeniería Universidad de Antioquia, no. 103, pp. 77-87, Apr-Jun 2022. DOI:10.17533/udea.redin.20210217

Duarte-Jaramillo L., Mendoza-Atencio MA, Jaramillo-Colorado BE, González-Álvarez A (2021) Water quality in the municipalities of Sincerín and Gambote, Bolívar, Colombia (2017-2018) Revista Facultad de Ingeniería Universidad de Antioquia, no. 103, pp. 77-87, 2022. Facultad de Ingeniería, Universidad de Antioquia https://doi.org/10.17533/udea.redin.20210217

Faure G., (1998) Principles and Applications of Geochemistry, 2nd ed. Prentice-Hall, Englewood Cliffs, New Jersey. https://www.geokniga.org/bookfiles/geokniga-principles-geochemistry.pdf

Finotti AR, Finkler R, Susin N, et al. Use of water quality index as a tool for urban water resources management. Int J Sustain Dev Plan. 2015;10:781–794. DOI: 10.2495/SDP-V10-N6-781-794

García-Ávila F, Ramos-Fernández L, Pauta D, et al. (2018) Evaluation of water quality and stability in the drinking water distribution network in the Azogues City, Ecuador. Data Brief. 2018;18:111–123. DOI: 10.1016/j.dib.2018.03.007

García-Ávila F, Zhindón-Arévalo C, Valdiviezo-Gonzales L, Cadme-Galabay M, Gutiérrez-Ortega H, del Pino LF (2022) A comparative study of water quality using two quality indices and a risk index in a drinking water distribution network, Environmental Technology Reviews, 11:1, 49-61. DOI: 10.1080/21622515.2021.2013955

Garcia-Ubaque, García-Ubaque, Rodríguez-Miranda, Pacheco-García, García-Vaca (2018). Limitations of the Water Quality Risk Index as an estimator of quality for human consumption. Rev. salud pública [online]. 2018, vol.20, n.2, pp.204-207. ISSN 0124-0064.

https://doi.org/10.1016/j.dib.2018.03.007
Ghana Geological Survey (GGS) (2009) Geological Map of Ghana—Scale 1:1,000,000. Geological Survey Department (GSD). https://searchworks.stanford.edu/view/8826218
Ghana Statistical Service (2021) Ghana 2021 population and housing census General Report Volume 3A. Population of Regions and Districts. November 2021. https://statsghana.gov.gh/gssmain/fileUpload/pressrelease/2021%20PHC%20General%20Report%20Vol%203A_Population%20of%20Regions%20and%20Districts_181121.pdf
Hussain MS, Abd-Elhamid HF, Javadi AA, Sherif MM, (2019). Management of Seawater Intrusion in Coastal Aquifers: A Review. Water, 11(12) *(Advances in Groundwater and Surface Water Monitoring and Management),* 2467. https://doi.org/10.3390/w11122467
Jahan S, Strezov V. Water quality assessment of Australian ports using water quality evaluation indices. PLoS One. 2017;12(12):1–15. DOI: 10.1371/journal.pone.0189284
Kamboj N, Kamboj V. Water quality assessment using overall index of pollution in riverbed-mining area of Ganga-River Haridwar, India. Water Sci. 2019;33(1):65–74. https://doi.org/10.1080/11104929.2019.1626631
Kumar R, Sharma RC. Assessment of the water quality of glacier-fed lake Neel Tal of Garhwal Himalaya, India. Water Sci. 2019;33(1):22–28. https://doi.org/10.1080/11104929.2019.1631554
Leube A, Hirdes W, Mauer R, Kesse GO, (1990). The Early Proterozoic Birimian Supergroup of Ghana and Some Aspects of Its Associated Gold Mineralization. *Precambrian Res.* 46, 139–165. https://doi.org/10.1016/0301-9268(90)90070-7
Liu Y, Yu H, Sun Y, et al. Novel assessment method of heavy metal pollution in surface water: a case study of Yangping River in Lingbao City, China. Environ Eng Res. 2017;22(1):31–39. DOI: https://doi.org/10.4491/eer.2016.015
McGrorya E, Holianb E, Morrison L, (2020) Assessment of groundwater processes using censored data analysis incorporating non-detect chemical, physical, and biological data. *Journal of Contaminant Hydrology.* Volume 235, November 2020, 103706. https://doi.org/10.1016/j.jconhyd.2020.103706
Ministry of Environment, Housing and Territorial Development (MAVD); Republic of Colombia. Resolution 2115 of 22 June 2007; 2021. https://media.rff.org/documents/RFF-Rpt-SINA.pdf
National Groundwater Association News (2016) Groundwater 54(2):150-150. https://www.ngwa.org/publications-and-news/Newsroom
Nayak JG, Patil LG. A comparative study of prevalent water quality indices in streams. Int J Eng Adv Technol. 2015;4(3):208–212. DOI: 10.1080/21622515.2021.2013955
Osiakwan GM, Appiah-Adjei EK, Kabo-Bah AT, Gibrilla A, Anornu G, (2021) Assessment of groundwater quality and the controlling factors in coastal aquifers of Ghana: An integrated statistical, geostatistical and hydrogeochemical approach. Journal of African Earth Sciences. Volume 184, December 2021, 104371. https://doi.org/10.1016/j.jafrearsci.2021.104371
Osiakwan GM, Gibrilla A, Kabo-Bah AT, Appiah-Adjei EK, Anornu G (2022). Delineation of groundwater potential zones in the Central Region of Ghana using GIS and fuzzy analytic hierarchy process. Modeling Earth Systems and Environment volume 8, pages 5305–5326. DOI: 10.1007/s40808-022-01380-z
Pérez AV, Carlos JER, Torres PL (2020) Development and implementation of a water-safety plan for drinking-water supply system of Cali, Colombia. International Journal of Hygiene and Environmental Health Volume 224, March 2020, 113422. DOI: 10.1016/j.ijheh.2019.113422
Raju N. J. (2007) Hydrogeochemical parameters for assessment of groundwater quality in the upper Gunjanaeru River basin, Cuddapah District, Andhra Pradesh, South India. Environmental Geology 52:1067-1074. DOI: https://doi.org/10.1007/s00254-006-0546-0
Raju N. J. (2012a) Hydrogeochemical processes in the Pleistocene aquifers of middle Ganga Plain, Uttar Pradesh, India. Environ Earth Sci 65: 1291-1308. DOI: 10.1007/s12665-011-1377-1
Raju N. J., Shukla, U.K., and Ram, P., (2011). Hydrogeochemistry for the assessment of groundwater quality in Varanasi: a fast-urbanizing center in Uttar Pradesh, India. Environmental Monitoring and Assessment, 173: 279–300. https://doi.org/10.1007/s10661-010-1387-6
Sachs J et al (2021) Sustainable development report. Cambridge University Press. https://doi.org/10.1017/9781009106559

Saffran K, Cash K, Hallard K. CCME water quality index 1.0 user's manual. Canadian water quality guidelines for the protection of aquatic life; 2001. p. 1–5. https://ccme.ca/en/res/wqimanualen.pdf

Saha R, Dey N, Rahman M, et al. (2019) Geogenic arsenic and microbial contamination in drinking water sources : exposure risks to the coastal population in Bangladesh. Front Environ Sci. 2019;7(57):1–12. https://doi.org/10.3389/fenvs.2019.00057

SDG Index. Org (2021) Sustainable development report, sustainable development report. https://dashboards.sdgindex.org/

Shaban A, Khawlie M, Abdallah C (2006) Use of remote sensing and GIS to determine recharge potential zones: the case of Occidental Lebanon. Hydrogeol J 14(4):433–443. DOI:10.1007/s10040-005-0437-6

Shah KA, Joshi GS. Evaluation of water quality index for River Sabarmati, Gujarat, India. Appl Water Sci. 2017;7:1349–1358. DOI: 10.1007/s13201-015-0318-7

Sim SF, Tai SE. Assessment of a physicochemical indexing method for evaluation of tropical river water quality. J Chem. 2018;8385369. DOI: 10.1155/2018/8385369

Tiwari AK, Singh AK, (2014) Hydrogeochemical Investigation and Groundwater Quality Assessment of Pratapgarh District, Uttar Pradesh. *Journal of the Geological Society of India*, 83(3):329-343p. DOI:10.1007/s12594-014-0045-y

Torres P, Cruz C.H, Patiño P, Escobar J. C, Pérez A, (2010) Aplicación de índices de calidad de agua -ICA orientados al uso de la fuente para consumo humano Ing. Inv., vol. 30, no. 10, pp. 86-95, Dec. 2010. https://www.researchgate.net/publication/262430438_Aplicacion_de_indices_de_calidad_de_aguaICA_orientados_al_uso_de_la_fuente_para_consumo_humano_Applying_water_quality_indexes_WQI_to_the_use_of_water_sources_for_human_consumption/citations

Tygai S, Sharma B, Singh P, et al. Water quality assessment in terms of water quality index. Am J Water Resour. 2013;1(3):34–38. DOI: 10.12691/ajwr-1-3-3

Uddin MG, Nash S, Olbert AI. (2021) A review of water quality index models and their use for assessing surface water quality. Ecol Indic. **122**:107218. https://doi.org/10.1016/j.ecolind.2020.107218

United Nations Department of Economic and Social Affairs (2014) International decade for action 'Water forlLife' 2005–2015, United Nations Department of Economic and Social Affairs. https://www.un.org/waterforlifedecade/20150327_newsletter.shtml

United Nations Department of Economic and Social Affairs (2021) Ensure availability and sustainable management of water and sanitation for all, United Nations Department of Economic and Social Affairs. https://sdgs.un.org/goals/goal6

Varol S, Davraz A, (2014) Evaluation of the groundwater quality with WQI (Water Quality Index) and multivariate analysis: a case study of the Tefenni plain (Burdur/Turkey). *Environ Earth Sci*. doi:10.1007/s12665-014-3531-z. DOI: https://doi.org/10.1007/s42452-020-03768-x

Wang S. X. (2013) Groundwater quality and its suitability for drinking and agricultural use in the Yanqi basin of Xinjiang Province, Northwest China. Environmental Monitoring Assessment 185:7469–7484 DOI: 10.1007/s10661-013-3113-7

World Health Organization (2008) Guidelines for drinking-water quality: incorporating 1st and 2nd addenda, Vol.1, Recommendations 978 92 4 1547611. https://www.who.int/publications/i/item/9789241547611

World Health Organization (2012) Edition of the Drinking Water Standards and Health Advisories Environmental Protection Agency 822-S-12-001 Washington, DC. https://rais.ornl.gov/documents/2012_drinking_water.pdf

Xin X, Li K, Finlayson B, et al. 2015;Evaluation, prediction, and protection of water quality in Danjiangkou Reservoir, China. Water Sci Eng. 8(1):30–39. https://doi.org/10.1016/j.wse.2014.11.001

Zooalnoon MO, Musa A. Evaluation of produced water quality by using water quality indices in Heglig area, Sudan. J Water Supply: Res Technol – AQUA. 2019;68 (7):607–615. DOI: 10.2166/aqua.2019.088

J. Int. Environmental Application & Science, Vol. 20: 38-55 (2025)
Research Paper

Monetizing Stranded Gas: Economic Analysis of Gas to Liquid Technologies in Nigeria

Igbinere, Sunday Agbons[1,]; Eka, Marvellous Emuobosan[2]*

Department of Petroleum Engineering, University of Benin, Benin City, Nigeria[1,2]

Received December 18, 2024; Accepted February 25, 2025

Abstract: Nigeria, as a nation endowed with vast reserves of stranded hydrocarbon resources and she is faced with the challenge of monetizing these resources, which are often flared due to lack of appropriate infrastructures for utilization. This has led the country into exploring different innovative approaches to unlock the economic potential of these resources. Gas-to-Liquid (GTL) technology has been seen as one of the major technologies that provide answers that can assist the country to grow in its economy. This study delves into the economic analysis of Gas-to-Liquids (GTL) technologies to monetize stranded hydrocarbon reserves in Nigeria. The economic analysis of the GTL technologies in Nigeria was done taking the Fischer-Tropsch GTL (FT-GTL) plant in Niger Delta as a case study. It was economically evaluated for a plant capacity of 1,000 MMSCF/D of natural gas. This plant is primarily affected by the crude oil price. The major aspect of this economic analysis was done by using a Microsoft Excel template developed for this study. The template considered the various variables that affect the variability of the projects such as plant life, construction period, capital expenditure, tax, operating expenditure, depreciation schedules, etc. The economic model used four economic indicators namely net present value (NPV), internal rate of return (IRR), profitability index (PI) and payback period (PP) to analyze both projects in this study. The financial and economic analysis of each indicator was carried out using the technique of discounted cash flow (DCF) analysis. DCF analysis yielded project performance criteria such as net present value (NPV) and internal rate of return (IRR), which were obtained from the projects' cash flow under consideration. Sensitivity analyses were then carried out with different tornado plots by varying the values of some of the economic parameters and determining their impacts on the project performance criteria within predetermined ranges. The results revealed that the higher the CAPEX for each of the cases, the lower the NPV and hence the profitability of the project is seen. For GTL technology to be viable as a project and profitable, the CAPEX is a factor to be extensively considered and reviewed periodically to ensure that it is not unreasonably high. Furthermore, the results of the economic analysis obtained at the different case scenarios using the most likely values of the economic input parameters indicate that FT-GTL profitability is highly dependent on the crude oil price, capital expenditure (CAPEX), operating expenditure (OPEX) and discounting factors should each be given proper considerations and review before embarking on future GTL projects. Increased operating expenditures from the FT-GTL technology reduced the NPV and IRR thereby affecting project profitability and extending the payback period, increasing the time to recoup initial investments of the FT-GTL technology plant.

Keyword: *Fischer-Tropsch, Gas-to-Liquid, CAPEX, OPEX, Net Present Value, Internal Rate of Return, Stranded Hydrocarbon*

Introduction

Natural gas is one of the primary energy sources besides oil, condensate, coal, as well as nuclear energy and renewable source of energy, natural gas is a cleaner and more effective source of energy that is less expensive and emits less greenhouse gases. The current production from conventional sources is not sufficient to satisfy all demands for natural gas (Ikoku, 1992). According to the International Energy Agency (2022), the global annual gas consumption is expected to grow at an annual average rate of 0.8% from 2023 to 2025, reaching around 4240 billion cubic meters by the end of the forecast. Also, the National Oil Spill Detection and Response Agency (NOSDRA) records that

*Corresponding: E-Mail: agbons.igbinere@uniben.edu, Tel: +234 09070858395

oil and gas companies operating in Niger Delta region flared 92.3 million standard cubic feet (Mscf) of gas, between January and April 2023 and this represents an increase of 79.5% against 50.3 Mscf of gas flared in 2022. The need to meet its flare down targets and promote production and use of environmentally friendly fuels serves as a drive for investment in the gas sector of the Niger Delta region economy. Also, with the global depletion of existing oil reserves, there is a drive towards finding the most economically viable way of commercializing our abundant gas reserves in this location. Glebova, (2013) looked at the history and future of Gas-to-liquid (GTL) technology in utilizing stranded hydrocarbon. This GTL technology has been seen as an option for utilization of the significant quantities of natural gas reserves in Niger Delta and to assist its economy to grow, because it is more favorable to liquefied natural gas (Nagi *et al*., 2016). To help decision-makers, this research aims to assess the feasibility and economic effects of GTL technologies in Niger Delta. GTL technology includes synthesizing natural gas to create premium liquid fuels like diesel, jet fuel, and other chemicals with additional value. In the GTL process, natural gas is transformed into syngas and ultimately into high-quality hydrocarbon products. Additionally, GTL technology lowers greenhouse gas emissions and aids in reducing the harmful consequences of climate change.

Natural gas is considered one of the most abundant energy resources worldwide with proven reserves exceeding 6000 trillion cubic feet (Tcf), and approximately 60% of these reserves can be classified as stranded, furthermore, Nigeria is the 10th biggest natural gas holder on the planet and biggest in Africa representing about 3% of the absolute natural gas estimates of 6,923 Trillion cubic feet (TCF) and Nigeria had about 200.4 trillion cubic feet of proven gas reserves in 2019 which later increased to an estimate of about 206.5 trillion cubic (Tcf) of proved natural gas reserves (Chikwe *et al*., 2021). Following Nigeria's gas reserves currently estimated to be at 206.5 TCF (trillion cubic feet) with a projected growth rate of over 70% by 2025. Unfortunately, even with this huge gas reserve, not much has been accomplished in the effective exploitation and utilization of this abundant natural gas reserve of which some of these gas reserves are termed stranded, whose volume and location are often considered as non-commercial and difficult to exploit. Dry natural gas production in Nigeria averaged about 1.5 Tcf between 2012 and 2021, and dry natural gas consumption averaged 649 billion cubic feet (Bcf) over the same period. Significant amounts of natural gas production in Nigeria is either re-injected or flared or abandon (Chikwe *et al*., 2021). Domestically, natural gas is still very undervalued as a major energy resource and various sustainable economic projects can be built around natural gas to drive our economy (Idigbe & Onwuachi-Iheagwara, 2014). GTL technology has the potential to utilize natural gas or any other resource rich in methane *i.e.* refinery gas, gas hydrates and landfills for gainful utilization of the feed stock with value addition to yield middle distillates or any other fuel product, chemical or chemical feedstock (Ahmed *et al*., 2012). GTL technology has the tendency to produce more of lighter petroleum fractions (kerosene and diesel), compared to the refined oil barrel distillates fraction and these GTL distillates can be used immediately or blended with others (Stanley, 2009). According to Oredein, (2013) and Uzuegbunam (2014), the Escravous gas to liquid (EGTL) is expected to convert more than 325 MMcf/d of natural gas to 33,000 bbl/day of GTL diesel; GTL naphtha, which is a feed stock used in plastics manufacturing and liquefied petroleum gas (LPG). Some of Nigeria's oil fields lack the infrastructure to capture the natural gas produced with oil, known as associated gas. According to the most recent data by the World Bank's Global Gas Flaring Reduction Partnership (GGFR), Nigeria flared about 5.318 billion cubic meters (or 188 Bcf) of natural gas in 2022, making Nigeria the ninth-highest natural gas-flaring country in terms of annual natural gas-flaring volume. Some researchers have studied the comparison between LNG and GTL technologies in Niger Delta region (Akpomera & Oghenekevwe 2017).

Gas-to-Liquid (GTL) technology refers to a process that converts natural gas or other gaseous hydrocarbons into clean burning liquid hydrocarbon products. It involves transforming gas molecules into long chain hydrocarbons, such as synthetic crude oil or transportation fuels like diesel or jet fuel (Al-Shalchi, 2006). While Dodaro, (2015) described the Fischer-Tropsch process as a gas to liquid (GTL) polymerization technique that turns a carbon source into hydrocarbons chains through the hydrogenation of carbon monoxide by means of a metal catalyst. This study is also aimed at identifying which parameter such as CAPEX, OPEX, tax rate, GTL premium has the highest impact on the viability of GTL technology in Nigeria. Also to assess the feasibility and cost-effectiveness of GTL technologies in Nigeria and to determine which economic indicator such as the net present value (NPV) and internal rate of return (IRR) has the greatest impact on the viability of the GTL technology in Nigeria, and also to determine the profitability index and payback period.

Research Methodology

This study focused on the application of GTL technologies in Fischer- Tropsch GTL (FT-GTL) plant in Niger Delta, Nigeria. Microsoft excel was used to develop a template that was applied to some of the economic indicators. The template considered the various variables that affect the variability of the projects such as plant life, construction period, CAPEX, tax, OPEX, depreciation schedules, etc. The study model for this project developed from Microsoft Excel incorporated a plant life of 25 years and a construction period of 3 years, while the plant operating time of 330 days/annum, 5-year MACRS depreciation schedule and 100% owner's equity were adopted. A detailed list of all parameters used in this study is shown in table 1 below.

Table 1. Selected Economic Input Data (Capuano, 2018; Economides *et al.*, 2005; Gradassi, 2001; Uzuegbunam, 2014)

S/N	Parameter	Value
1	Plant useful life	25 years
2	Plant construction period	3 years
3	Plant construction spending period per year	25%, 35%, 40% (Year 1, 2 3 respectively)
4	Depreciation schedule	5 – years MACRS
5	**Tax Rates**	
	Company tax	30%
	Royalty rate	5%
6	Plant operating time	330 days per annum
7	Feed gas cost (Base cost)	\$2.50/MMBTU
8	Discount ratio	10%
9	**FT-GTL Estimated CAPEX**	
	Gas utilization	1000 MMscf/d
	FT-GTL plant capacity	100,000 bbl/day
	FT-GTL plant CAPEX	\$5.7 Bn
9	**OPEX**	
	LNG	0.5%/MMBTU
	FT-GTL	\$6.00/bbl
10	Crude oil cost (Base cost)	\$65.00/bbl
11	**FT-GLT Product Per Annum**	
	Diesel	\$4.50/gal
	Naphtha	\$3.00/gal
12	**Product Distribution**	
	Diesel	72%
	Naphtha	28%
13	FT-GTL shipping cost	\$1.50/bbl
	Plant capacity	1000 MMscf/d

The Research Economic Measures of Profitability

The economic model incorporated four economic indicators, namely net present value (NPV), internal rate of return (IRR) and profitability index (PI) as well as payback period to analyze both projects in this study. The financial and economic analysis of each indicator was carried out using the technique of discounted cash flow (DCF) analysis. The DCF is any method of investment project evaluation and selection which adjusts cash flows over time for the time value of money. DCF analysis yielded project performance criteria such as net present value (NPV) and internal rate of return (IRR) which were obtained from the cash flow of the projects under consideration (Onyelucheya & Ibe, 2015). Sensitivity analyses were then carried out with different tornado and spider plots by varying the values of some of the economic parameters and determining their impacts on the project performance criteria within predetermined ranges. Furthermore, bar charts were also used to present the behavior of the different economic indicators and other economic parameters. This was to determine which economic indicator would have the greatest impact on the economics of the GTL project. The composition of the product range produced by a GTL plant can differ based on the specific technology and processes employed. In the case of the EGTL plant, Sasol technology is utilized for the processes. According to a study conducted by Smith and Asaro (2005), the product slate for Sasol technology consists of approximately 28% naphtha and 72% middle distillates. This research work assumed a product slate of 72% for diesel and 28% for that of naphtha.

Net Present Value (NPV): The present value (NPV) of an investment proposal is the present value of the proposal's net cash flows less the proposal's initial cash outflow. Net present value was obtained by summing the discounted cash flows for each year for the lifespan of the project.

$$NPV = -1 + \sum_{i=1}^{n} \frac{DCF_i}{(1+i)^n} \tag{1}$$
$$I = CAPEX + OPEX \tag{2}$$

Where NPV is the net present value, I is the project investment, DCF is the discounted cash flow, ἱ is the interest rate, while CAPEX and OPEX are the capital expenditure and operating expenditure respectively.

Internal Rate of Return (IRR) or Discounted Cash-Flow Rate of Return (DCFROR): This is the interest rate that makes the cumulative NPV of the project equal zero. It is a measure of the interest rate the project can pay and still break even by the end of the project life. A project is judged to be worthwhile in economic terms if the IRR is greater than the cost of capital, otherwise it should be rejected (Gradassi, 2001; Nwankwo, 2008; Onyelucheya and Ibe, 2015). The general criterion used for economic evaluation of an investment by means of IRR is to compare the obtained IRR with a required rate of return known as the hurdle rate or discount rate and the discount rate was assumed to be 10%.

$$IRR = \sum_{t=0}^{n} \frac{CF_t}{(1+IRR)^t} \tag{3}$$

Where IRR is the internal rate of return, CF_t is the cash flow at time t and t is the time period considered.

Profitability Index (PI): The Profitability Index (PI) is the ratio of the present value of future net cash flows to the initial cash out flows. It measures the ratio of the net present value to the initial investment or capital expenditure (CAPEX) of a project. It is also known as the benefit-cost ratio. The acceptance criterion for the profitability index of an investment proposal is to accept the proposal if the profitability index ($PI \geq 1$) or reject the proposal if otherwise.

Payback Period (PP)*:* The Payback Period is the time required for the cumulative net earnings to equal the initial outlay; it is the length of time required to get our investment capital back. It is the time until the cash flow recovers the initial investment or CAPEX of the project and it is estimated by dividing CAPEX into the profit after taxes results. The shorter the payback period, the higher the project is rated. On the other hand, if the calculated period is deemed too long, the project is rejected.

Evaluating the Capital Expenditure (CAPEX)

The capital expenditure (CAPEX) for this project using the FT-GTL plants was based on the cost of a gas to liquid (GTL) plant located in Niger Delta of Nigeria and which has started production. The current CAPEX for the EGTL plant is about $10 billion and it processes about 475 MMscf/d of feed gas (Uzuegbunam, 2014). It is also able to produce about 33,000 bbl/day of GTL product and the base cases to be used in this research work will be the CAPEX and capabilities of the GTL plants that will be capable of processing 1000 MMscf/d of feed gas. This will be done using the power law and sizing model.

The Power Law and Sizing Model*:* This is also known as the exponential rule or the six-tenth rule. It is a nonlinear correlation that's frequently used to estimate the cost of a new process facility based on the cost of an existing known capacity (Hendrix and Au, 2003; Kerzner, 2001). Power law (equation 4) will estimate the CAPEX of the FT-GTL plant capable of processing 1000 MMscf/d. Shown below in equation 4 is the mathematical expression of the power law and sizing model.

$$C_b = C_a \left(\frac{Q_b}{Q_a}\right)^m \tag{4}$$

Where C_a is the cost of existing facility, C_b is the estimated cost of new facility, Q_a is the capacity of existing facility, Q_b is the estimated capacity of new facility and m is the correlation exponent, ($0 < m < 1$). For most equipment, m is approximately 0.5, and for chemical processing plant, it is approximately 0.6 (Mian, 2010).

Estimating Operating Expenditure (OPEX)*:* The annual operating expenditure (OPEX) used in this research work includes the cost of materials and supplies as well as the cost of labour, utilities and maintenance, except the cost of feedstock which was separately estimated. Al-Saadoon (2005) gave the annual operating expenditure for large projects to be in the range of 5-7% of the capital expenditure. While Toochukwu *et al*. (2019) and Ubanozie *et al*. (2021) stated that GTL plant OPEX is 5% of CAPEX (excluding the cost of natural gas and cost of O_2 or CO_2). Economides *et al*. (2005) reported the FT-GTL OPEX to be $5.00/bbl while Gradassi (2001) gave the OPEX for FT-GTL as $4.00/bbl. Patel, (2005) reported the operating costs of the FT-GTL plant to be between $4.00/bbl and $5.50/bbl. This research work adopted $6/bbl as the OPEX for the FT-GTL plant project.

Feedgas Cost and Shipping Cost*:* According to Capuano, (2018) of the United States Energy Information Administration (EIA) and Annual Energy Outlook (AEO) in 2018, the annual cost of natural gas used as feed gas in chemical plants is $4.80/MMBtu compared to the original price of $3.80/MMBtu as at 2012. It was projected that the cost will even increase further to $7.65/MMBtu in 2040. Gas prices of $1.00/MMBtu, $2.5/MMBtu and $5.0/MMBtu were adopted for the purpose of this analysis while the base case price shall be $2.5/MMBtu. While that of the shipping cost for the FT-GTL plant project was taken to be $1.50/bbl. For this particular value, two other values were investigated using the tornado graph to analyze the effect of high and low values from the base case on the economics of the GTL project.

Other economic factors considered in this study include sales revenue, product pricing, plant load factors and plant operating time. While others are plant useful life, tax rate, depreciation, plant capacity as well as plant construction schedule. The individual data adopted for these economic factors were based on current international standard values and from literatures. The summary of these parameters is presented in tables 1 to 3.

Table 2. Parameters for the Sensitivity Analysis for FT-GTL

Parameters	Low Case	Base Case	High Case
Crude Oil Price ($/bbl)	30	65	100
Feed Gas Cost ($/MMBTU)	1	2.5	5
OPEX ($/bbl)	4.5	6	10
Shipping Cost ($/bbl)	0.5	1.5	2.5
Discount Rate (%)	8	10	12
Tax Rate (%)	15	30	35
GTL Diesel Premium ($/gal)	3	4.5	6.5
GTL Naphtha Premium ($/gal)	2	3	40
CAPEX ($M/bbl)	0.5	1.0	2.0
Production Capacity (bbl/day)	1,000,000	1,000,000	1,000,000

Table 3. Depreciation schedule

Recovery Year	MACRS Percentages (%)
1	20.00
2	32.00
3	19.20
4	11.52
5	11.52
6	5.76

Results and Analysis

This section features the results obtained from the analysis of the different economic indicators to determine the viability of the implementation of the GTL technology in Niger Delta, Nigeria. In the economic analysis of implementing Gas-to-Liquid (GTL) technology, it's essential to state that these results represent the project's financial viability under various scenarios: a low case, base case and high case as well as the sensitivity to crude oil prices. These results presented in tables 4 to 6 and in figures 1 to 22 were used to analyze the different economic indicators of GTL technology.

Net Present Value

a) **Low Case Scenario ($30/barrel)**: In the low-price scenario, the project may face challenges in achieving a positive NPV. Reduced crude oil prices can result in lower revenue, impacting the project's cash flow. The NPV may be close to breakeven or negative, indicating potential financial risk.
b) **Base Case Scenario ($65/barrel)**: At the base case scenario, with crude oil prices of $65 per barrel, the project exhibits a positive NPV. This suggests that, under current market conditions, the project is economically viable and can generate a positive return on investment.
c) **High Case Scenario ($100/barrel)**: In the high-price scenario, with crude oil prices at $100 per barrel, the project's NPV is significantly higher. The project appears highly profitable in this scenario, with the potential for substantial returns.

Internal Rate of Return

a) **Low Case Scenario ($30/barrel)**: The low-price scenario results in a lower IRR, which may be below the project's required rate of return. This could indicate that the project's economic feasibility is uncertain when crude oil prices are low.
b) **Base Case Scenario ($65/barrel)**: The base case scenario, with crude oil at $65 per barrel, leads to a reasonable IRR. The project appears capable of meeting or exceeding the required return, making it an attractive investment option.
c) **High Case Scenario ($100/barrel)**: In the high case scenario, the high-price scenario, the project's IRR is notably high, indicating strong potential for significant profits and meeting or surpassing investment expectations.

Capital Expenditure (CAPEX)

a) **Low Case Scenario ($30/barrel)**: The low-price scenario, it's crucial to scrutinize the project's CAPEX carefully. With potential challenges in achieving a positive NPV, cost control and efficiency become critical to improve project economics.
b) **Base Case Scenario ($65/barrel)**: At the base case scenario, the CAPEX is manageable and aligns with the expected returns. Project managers should continue to monitor CAPEX to ensure it remains within budget.
c) **High Case Scenario ($100/barrel)**: In the high-price scenario, the project's CAPEX may be easier to justify due to the expected higher returns. However, it's still essential to optimize CAPEX to enhance overall profitability.

The sensitivity analysis of crude oil prices demonstrates that GTL technology projects are highly sensitive to oil price fluctuations. It underscores the importance of risk management and strategies for hedging against adverse price movements. In the low-price scenario, careful cost management and operational efficiency are paramount to ensure the project's viability. The base case represents a reasonably safe investment with positive NPV and IRR. However, ongoing monitoring and adjustments to market conditions are necessary. While in the high-price scenario, the project becomes highly profitable, potentially attracting more investors. The sensitivity analysis provides valuable insights into the financial robustness of GTL technology projects under different crude oil price scenarios. It highlights the need for proactive risk management and cost optimization to ensure long-term economic viability and profitability.

The results presented in table 4 show the net present values for each of the cases over the period of 10 years. Generally, the values show clearly that the whole project requires re-evaluation of the project conditions and values as well as the fiscal policy under which the GTL project is executed. The low case has a total NPV of -$55,623,304,017.39; the base case has a total NPV of -$304,835,553,760.29, while the high case has a total NPV of -$1,543,792,616,284.73. These values indicate that the low case conditions for the GTL technology project execution is the most profitable. However, the negative NPVs show clearly that the project has a lot of financial risk and needs critical reevaluation at every point of the project execution.

Table 4. NPV Analysis for 10 years for Three Case Scenarios

Year	Low Case ($)	Base Case ($)	High Case ($)
1	2,619,888,888.89	3,500,681,818.18	-12,670,714,285.71
2	3,737,720,164.61	3,079,876,033.06	-32,324,846,938.78
3	3,520,389,117.51	-727,669,045.83	-57,840,062,864.43
4	2,118,307,552.48	-7,452,023,085.85	-88,254,360,552.89
5	-333,069,962.40	-16,680,708,052.11	-122,744,598,831.36
6	-3,711,855,513.78	-28,052,136,056.84	-160,607,784,462.17
7	-7,908,461,203.16	-41,249,765,514.84	-201,244,775,481.42
8	-12,824,445,717.63	-55,996,899,236.19	-244,146,097,430.02
9	-18,371,464,289.19	-72,052,056,037.02	-288,879,606,793.55
10	-24,470,313,054.73	-89,204,854,582.84	-335,079,768,644.40
TOTAL	**-55,623,304,017.39**	**-304,835,553,760.29**	**-1,543,792,616,284.73**

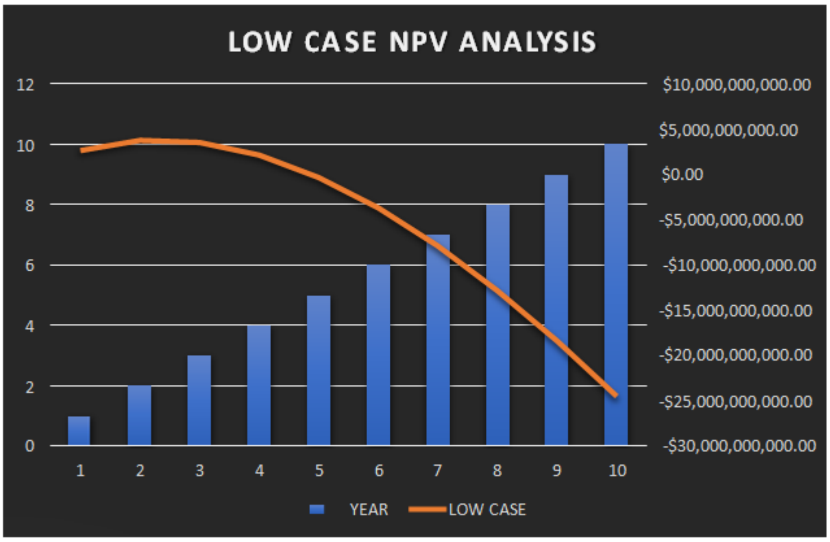

Figure 1. Low Case NPV Analysis for 10 years at $30/bbl

The results presented in figure 1 is a graphical representation of the low case NPV, after a period of 10 years, and it can be seen that there is decline in the NPV as the year of the project progresses. The final value of NPV in the tenth year is -$24,470,313,054.73. This is due to several factors of which the price of crude oil per barrel is a significant factor.

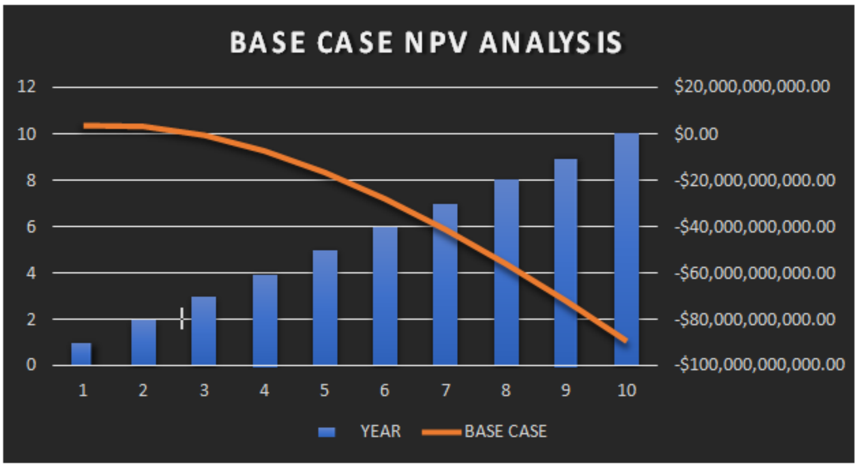

Figure 2. Base Case NPV Analysis for 10 years at $65/bbl

Figure 2 is a graphical representation of the base case NPV, it can also be observed that there is decline in the NPV as the year of the project progresses, but this decline is somewhat more than the low case decline. The final value of NPV at year 10 is -$89,204,854,582.84. This is due to several factors of which the price of crude oil per barrel is also a significant factor.

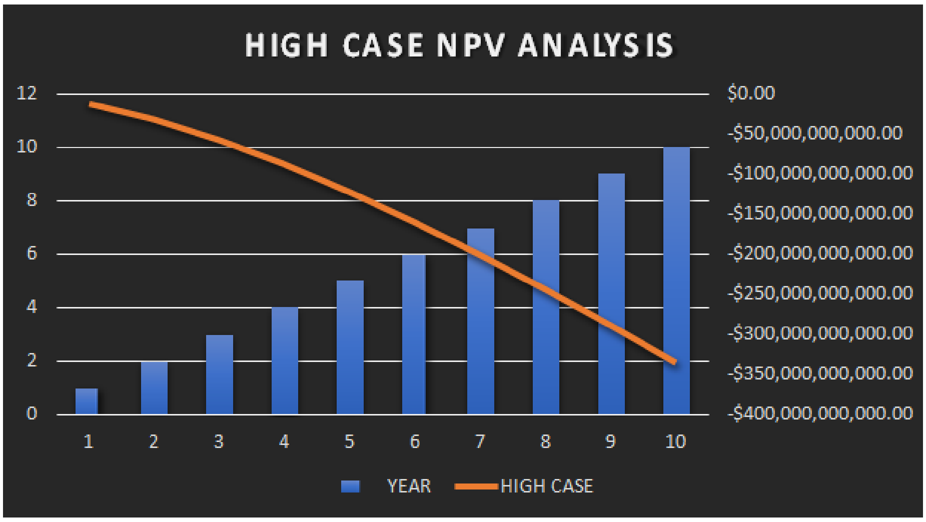

Figure 3. High Case NPV Analysis for 10 years at $100/bbl

Figure 3 is a graphical representation of the high case NPV, it can be seen that there is decline also in the NPV as the year of the project progresses, but this decline is somewhat more than the base case decline. The final value of NPV at year 10 is -$335,079,768,644.40. And which is also due to several factors of which the price of crude oil per barrel is also a significant factor. The results in figure 4 represent the IRR for different case scenarios at different crude oil prizes, and this economic indicator revealed that low crude oil prizes promote the viability of an FT-GTL technology in Niger Delta gas to liquid plant. Internal Rate of Revenue (IRR) is another factor for determining the viability of a project. NPV alone cannot be used to determine the viability of an oil and gas project. A high discounting factor shows a viable project. This means that the low case IRR of 0.1 is the most viable. This might be somewhat different from what is expected as it is believed that at higher crude oil prices, the project should be more viable but it should be noticed that as the prices of crude oil increases for the different cases, other factor also increases as well. NPV and IRR cannot contradict themselves but rather explain and complement themselves. IRR of 0.094 of the base case is also good value as it is very close to 0.1.

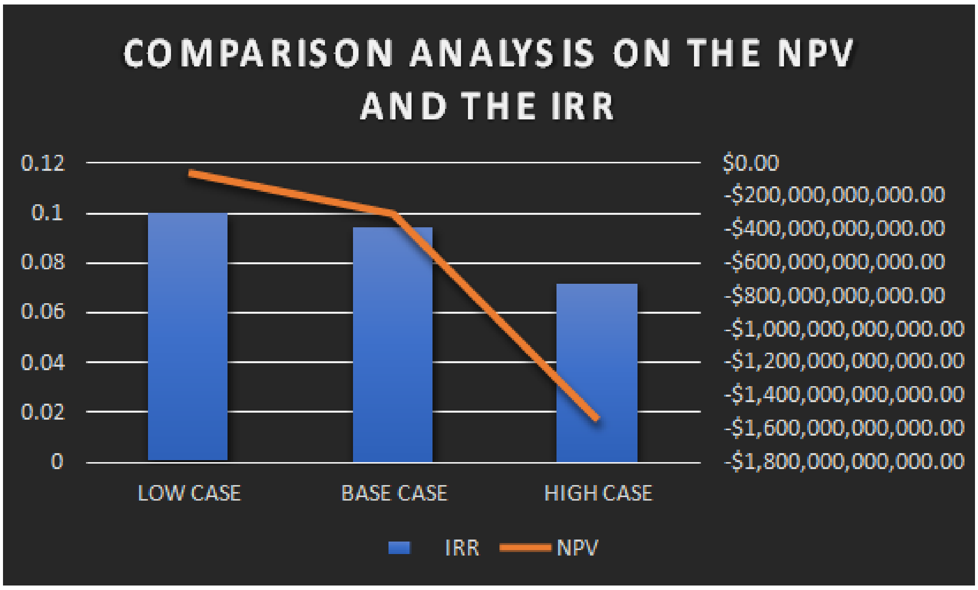

Figure 4: Comparison of NPV and IRR for Three Case Scenarios

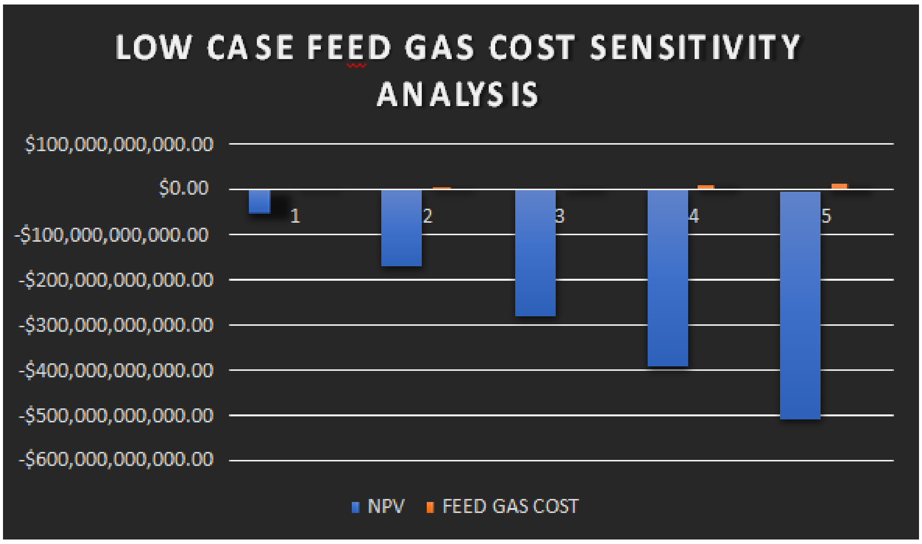

Figure 5. Effect of Feed Gas Cost on NPV for Low Case

Table 5. Analysis of the Feed Gas Cost and Net Present Value

Low Case		Base Case	
NPV ($)	**Feed Gas Cost ($)**	**NPV ($)**	**Feed Gas Cost ($)**
-55,623,304,017.39	4,088,000,000.00	-304,835,553,760.29	7,154,000,000.00
-168,043,304,017.39	6,132,000,000.00	-417,255,553,760.29	9,198,000,000.00
-280,463,304,017.39	8,176,000,000.00	-61,928,053,760.29	11,242,000,000.00
-392,883,304,017.39	10,220,000,000.00	-174,348,053,760.29	13,286,000,000.00
-505,303,304,017.39	12,264,000,000.00	-286,768,053,760.29	15,330,000,000.00

High Case	
NPV ($)	**Feed Gas Cost ($)**
-1,656,212,616,284.73	12,264,000,000.00
-1,768,632,616,284.73	14,308,000,000.00
-1,656,212,616,284.73	16,352,000,000.00
-367,397,616,284.73	18,396,000,000.00
-479,817,616,284.73	20,440,000,000.00
-592,237,616,284.73	22,484,000,000.00

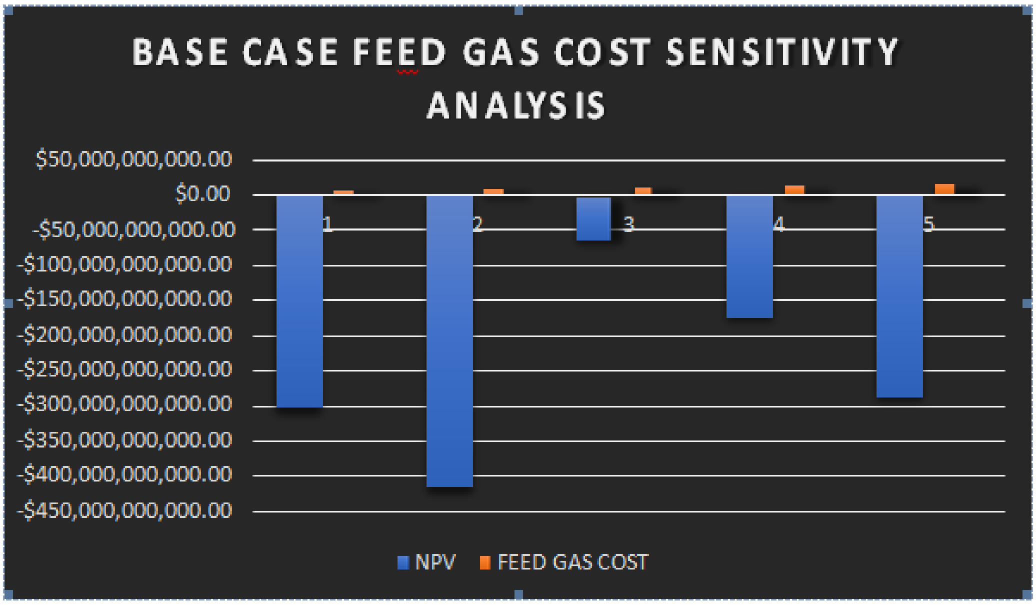

Figure 6: Effect of Feed Gas Cost on NPV for Base Case

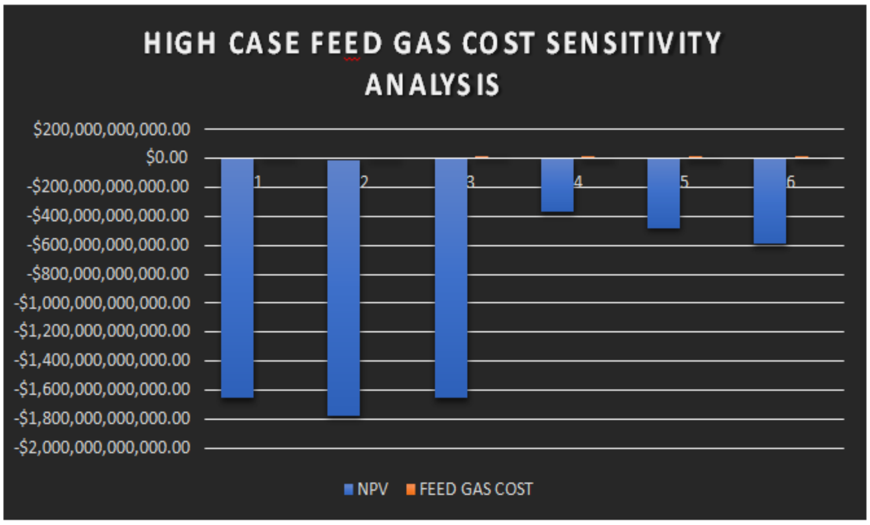

Figure 7. Effect of Feed Gas Cost on NPV for High Case

Figures 5 through 7 explains explicitly the effect of feed gas cost on NPV as it has a direct impact on the overall profitability of the project. At a low feed gas cost of $1/MMBTU, we can see the trend of the NPV. But there is increase in the feed gas cost due to increase in production as the year proceeds and this has a final effect on the NPV. It can be seen from table 5 that with a feed gas cost of $12,264,000,000.00 the NPV is -$505,303,304,017.34 for a low case scenario and this suggest that there is an inverse relationship between the feed gas cost and the NPV. As the feed gas cost increases due to increase in production each year, there is a corresponding NPV. While for a base case presented in figure 6, the feed gas cost of $2.5/MMBTU resulted in an increase due to increase in production, from table 5, the feed gas cost of $15,330,000,000.00 produced an NPV of -$286,768,053,760.29 and also established an inverse relationship between the feed gas cost and the NPV. Similarly from figure 7 and table 5, a high feed gas cost of $5/MMBTU also has the same trend as that of the previous cases. It can be seen here in the high case that with feed gas cost of $22,484,000,000.00 the NPV is -$592,237,616,284.73. This inverse relationship between the feed gas cost and the net present value for an FT-GTL technology is a clear indication of high operating expenses, reduced cash flows. When feed gas cost decreases, operating expenses fall, leading to higher cash flows and consequently results in increase in NPV. This relationship between feed gas cost and net present value is essential for maximizing net present value and maximizing the FT-GTL technology project profitability.

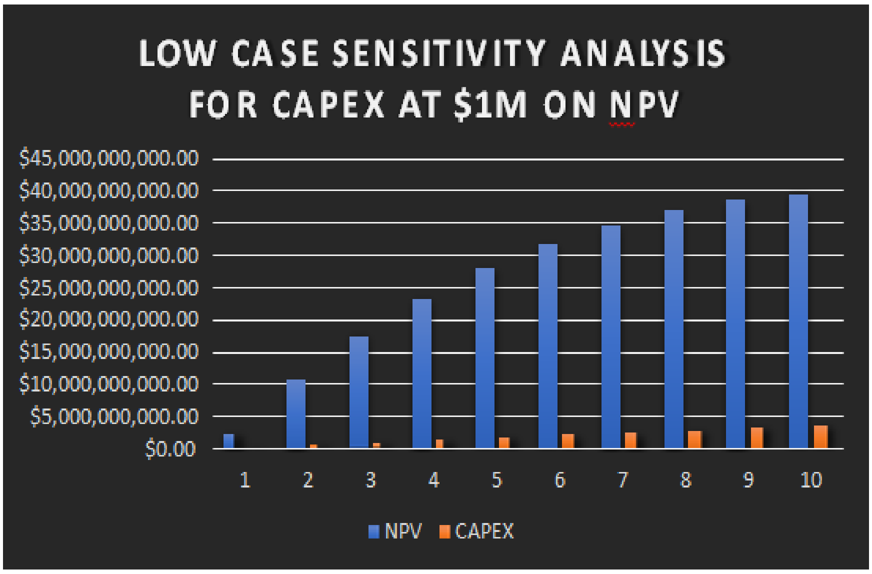

Figure 8. Low Case Sensitivity Analysis for CAPEX at $1M on NPV

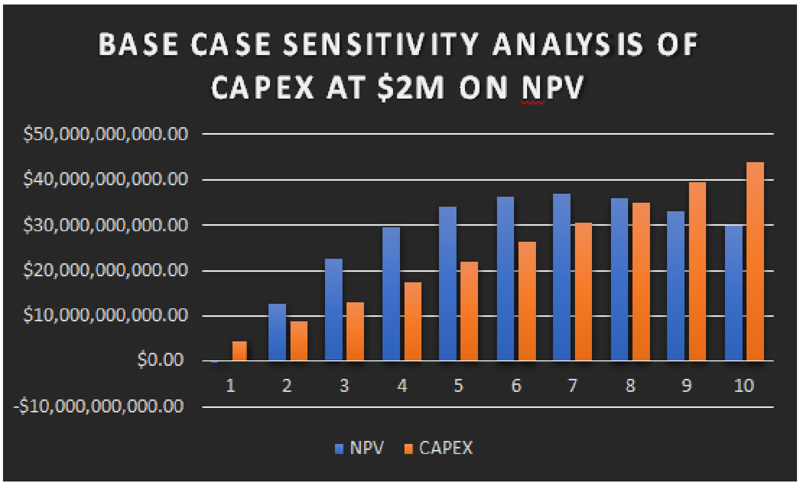

Figure 9. Base Case Sensitivity Analysis for CAPEX at $2M on NPV

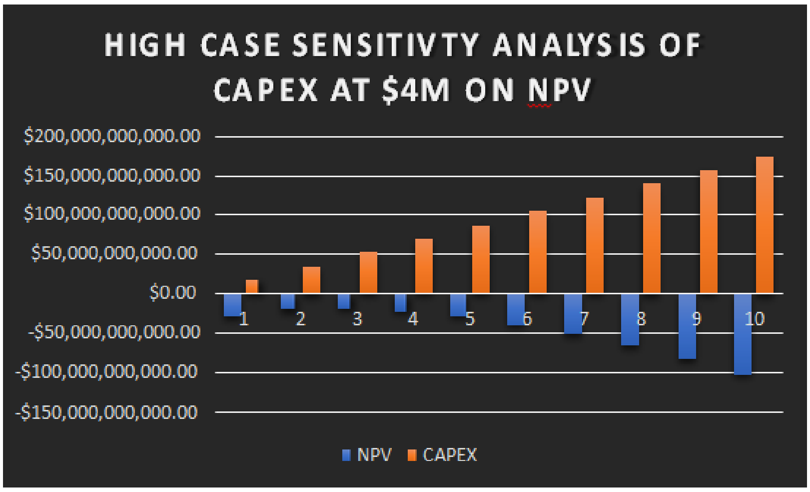

Figure 10. High Case Sensitivity Analysis for CAPEX at $4M on NPV

Capital Expenditure (CAPEX) involves all investments in terms of infrastructure and buildings in a bid to have smooth operation. The highest NPV came at the end of 10 years with a value of $39,733,186,945.27 and the CAPEX being the highest at this point too with a value of $3,650,000,000.00. Figures 4.9 and 4.10 also shows the sensitivity of NPV to increase in CAPEX at increasing CAPEX values.

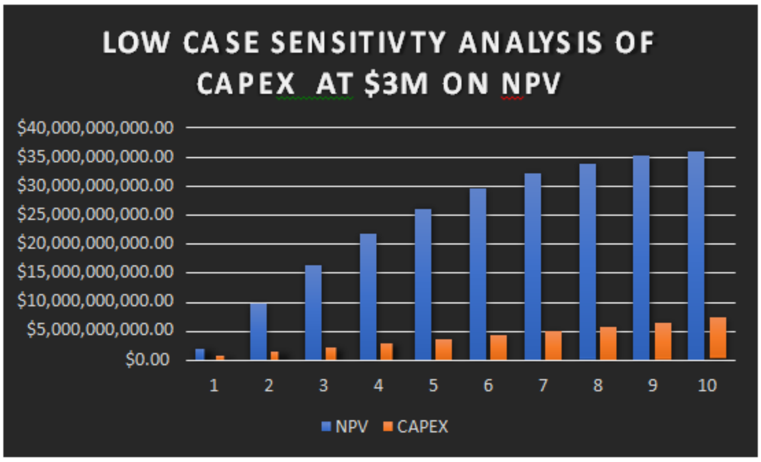

Figure 11: Low Case Sensitivity Analysis of CAPEX at $3M on NPV

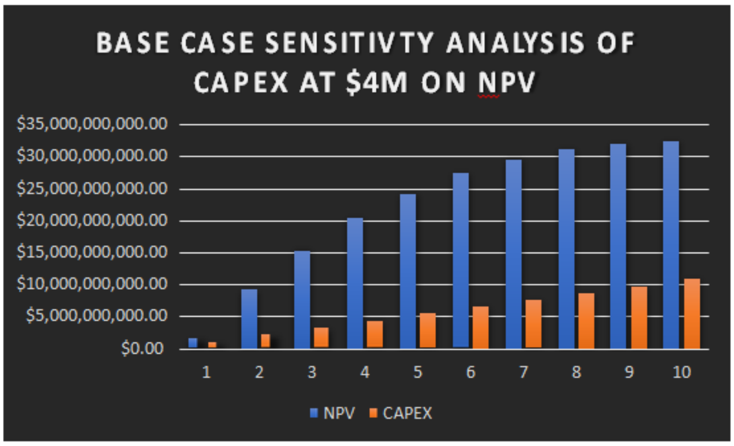

Figure 12. Base Case Sensitivity Analysis of CAPEX at $4M on NPV

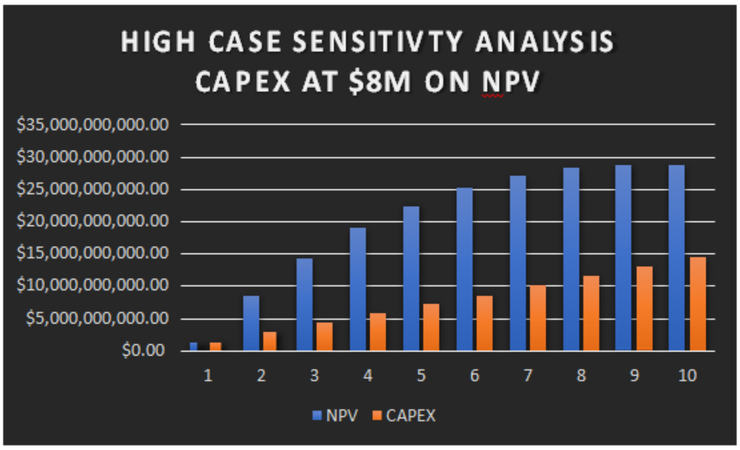

Figure 13. High Case Sensitivity Analysis of CAPEX at $8M on NPV

Figures 8 through 13 show the sensitivity of NPV to the different capital expenditures, also, it has been clearly established that CAPEX is very important to the profitability of a project. This is because CAPEX is part of the investment and this must be reviewed periodically throughout the life of the project to ensure that the payback period is fast and the profitability is maintained and ensured. The higher the CAPEX for each of the cases, the lower the NPV and hence the profitability of the project is seen. For GTL technology to be viable as a project and profitable, the CAPEX is a factor to be extensively considered and reviewed periodically to ensure that it is not unreasonably high.

Table 6. The Effects of Varying Crude Oil Prices on NPV

Low Case		**Base Case**		**High Case**	
Crude Oil Cost ($/bbl)	NPV ($)	Crude Oil Cost ($/bbl)	NPV ($)	Crude Oil Cost ($/bbl)	NPV ($)
40	63,683,927,976.81	65	-304,835,553,760.29	110	46,345,622,086.79
50	182,991,159,971.01	75	278,060,323,827.17	120	140,896,360,458.32
60	302,298,391,965.21	85	-92,873,416,455.76	130	235,447,098,829.85
70	421,605,623,959.42	95	13,107,652,196.51	140	329,997,837,201.37
80	540,912,855,953.62	105	119,088,720,848.77	150	424,548,575,572.90

From table 6, it is seen clearly that the higher the cost of crude oil, with other factors remaining constant, the NPV will appreciably increase and hence ensure the profitability of the project. The major work in the FT-GTL technology in assessing the viability is to increase the prices of crude oil per barrel and make other factors constant so as to have more revenue generated from the sales of hydrocarbon.

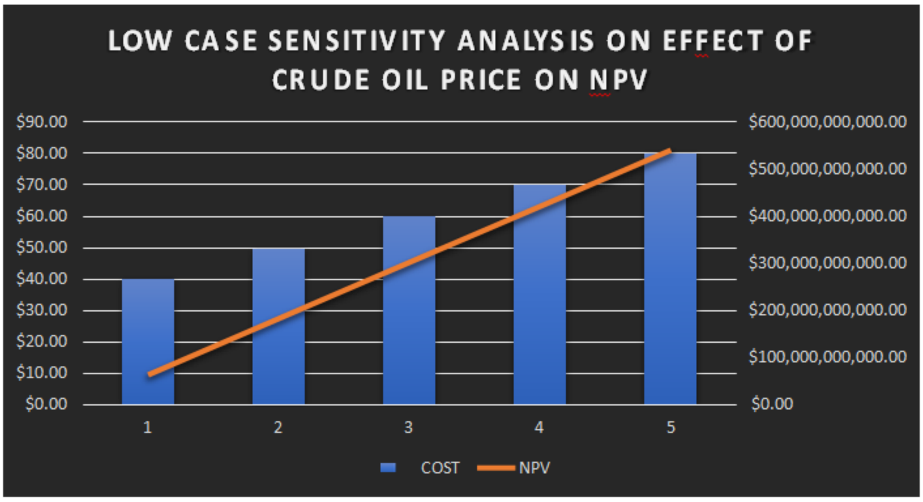

Figure 14. Low Case Analysis of the Effect of Crude Oil Prices on NPV

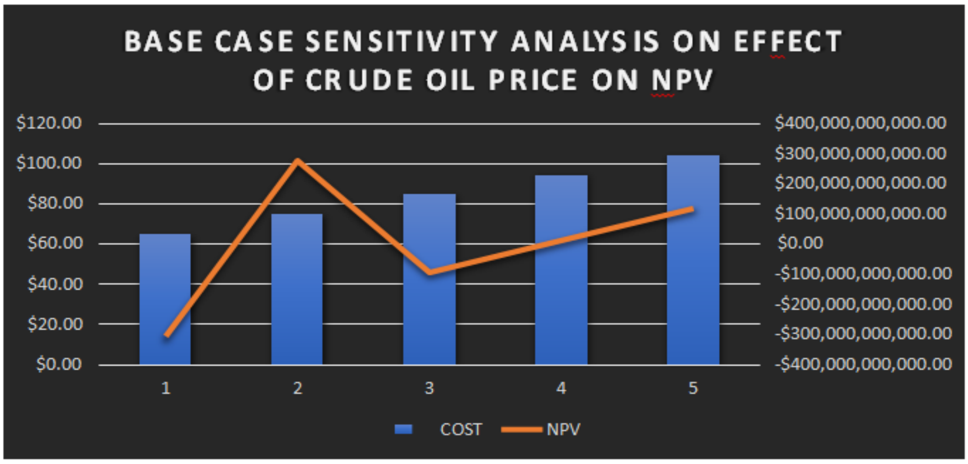

Figure 15. Base Case Analysis of the Effect of Crude Oil Prices on NPV

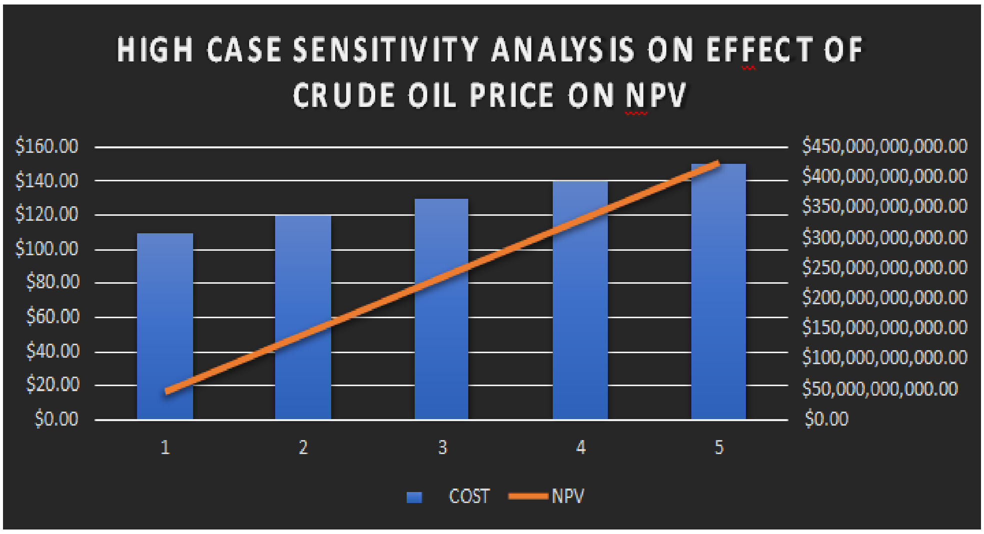

Figure 16. High Case Analysis of the Effect of Crude Oil Prices on NPV

Figures 14 to 16 also establish the direct relationship between the prices of crude oil and its NPV for all the cases considered. There is an upward rise in the NPV as the prices of crude oil increases and this is also shown in table 6.

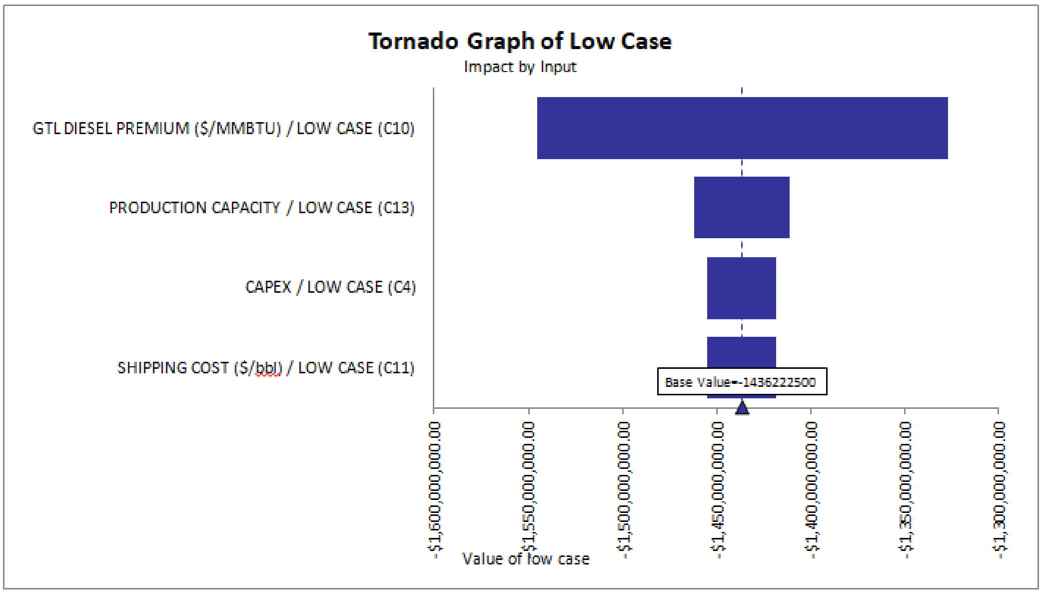

Figure 17. A Tornado Plot of Sensitivity of the Factors on NPV for Low Case

The results presented in figure 17 revealed the first three factors that have the highest impact on the NPV are the GTL diesel premium, the production capacity and the CAPEX. That was why as stated earlier that the increase in prices of crude oil will mean a commensurate increase in the NPV if other factors such as these are kept constant. For our case scenario considered in this GTL technology, the factors with highest impact are shown in the tornado plots. While for figure 18, the first three factors with highest impact on the net present value are GTL diesel premium, OPEX and shipping cost. Changes in these inputs variables greatly affect the NPV and the greatest impact is the GTL diesel premium. In the base case, OPEX is next in line in terms of its impact on NPV and the order of impact decreases from top to the bottom of the tornado plot. This is similarly seen in figure 19; however, the order of impact by these factors differs slightly.

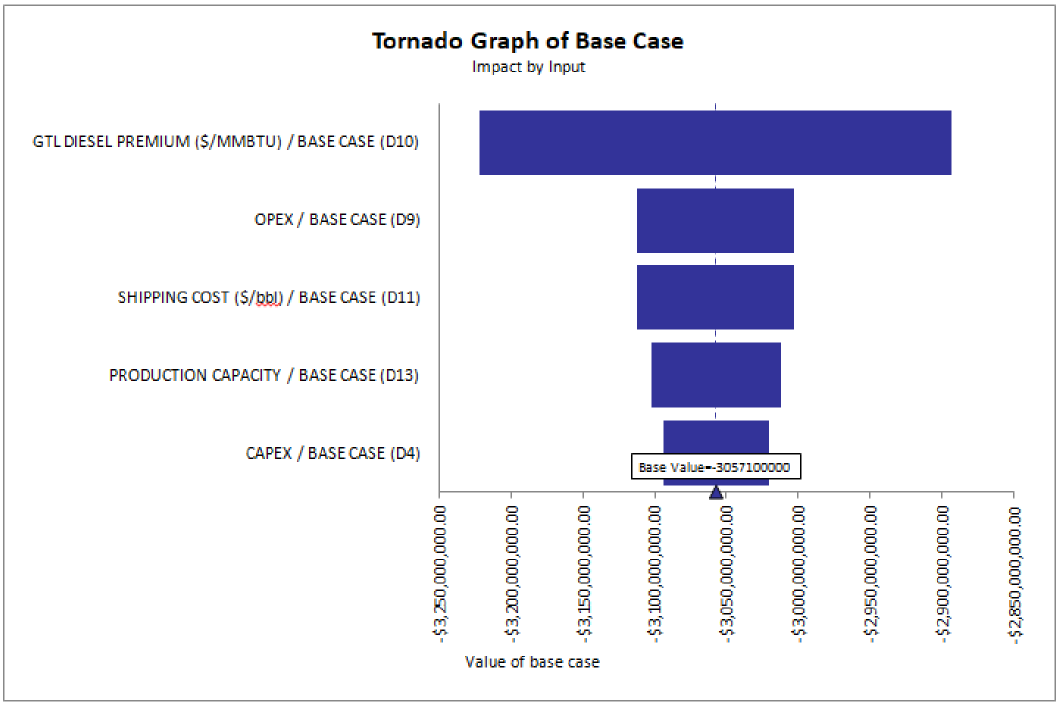

Figure 18. Tornado Plot of Sensitivity of the Factors on NPV for Base Case

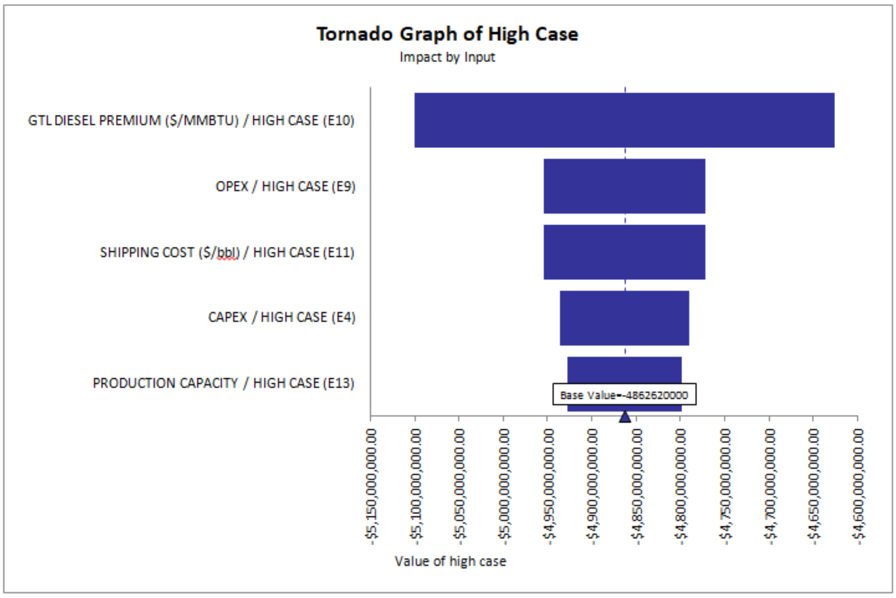

Figure 19. Tornado Plot of Sensitivity of the Factors on NPV for High Case

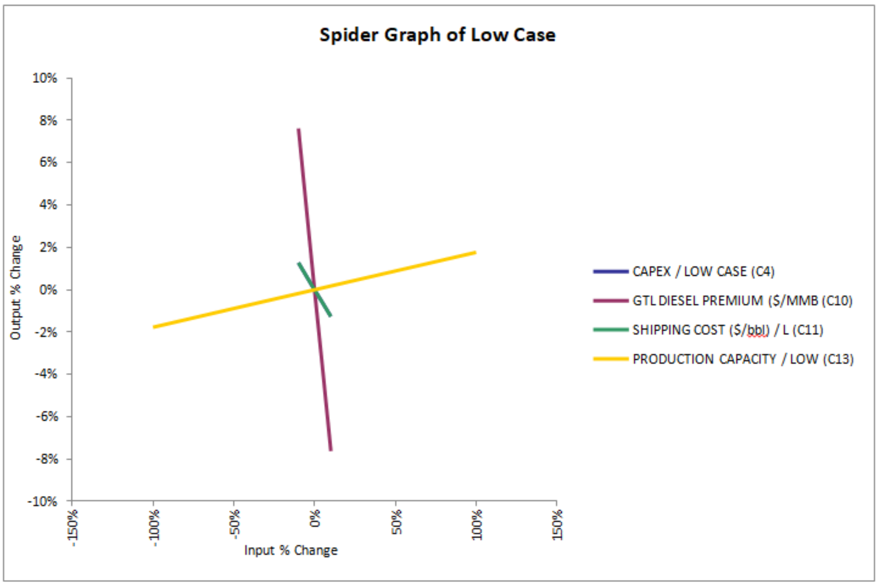

Figure 20. Spider Plot of Impact of some factors on the NPV for Low Case

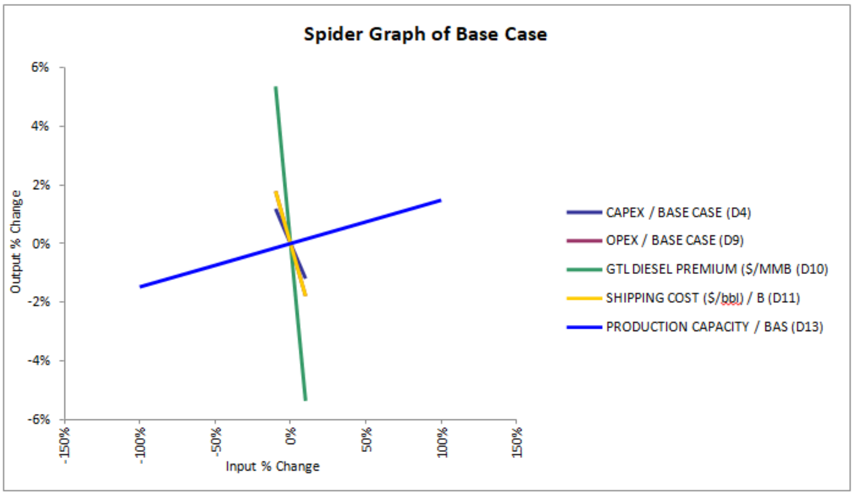

Figure 21. Spider Plot of Impact of some factors on the NPV for Base Case

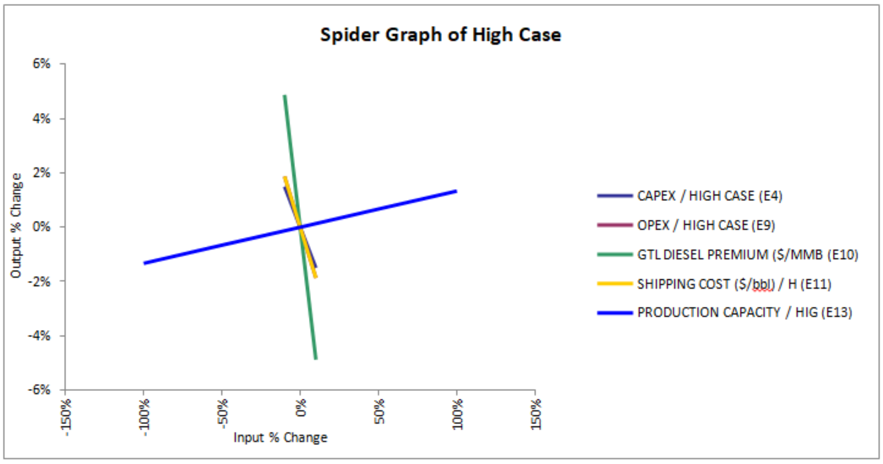

Figure 22. Spider Plot of Impact of some factors on the NPV for High Case

The spider plots were used to further show the sensitivity of some factors to NPV for the three case scenarios considered and are presented in figures 20 to 22. The point of overlapping is indicating that the factors have similar values, and the GTL diesel premium dominate in all three cases. A closer look at figures 17 through 22, the sensitivity of the factors differs and this is because the conditions are changing due to the different fiscal policies for the cases. That is to conclude that for profitability to be ensured, the prices of crude oil should be increased while other factors are kept constant.

Conclusion

The economic analysis of the implementation of the FT-GTL plant in Niger Delta, Nigeria showed a positive trend. DCF of the proposed project analysis produced performance criteria such as net present value (NPV) and internal rate of return (IRR) which were obtained from the cash flow of the projects under consideration, suggesting that the project is viable. The results of the economic analysis obtained at the different case scenarios using the most likely values of the economic input parameters indicate that FT-GTL profitability is highly dependent on the crude oil price, Capital Expenditure (CAPEX), Operating Expenditure (OPEX) and discounting factor and hence they should each be given proper considerations and review before embarking on future GTL projects. The following conclusions were arrived at as regards the best way Nigeria can monetize its stranded natural resources using the GTL technology.

1. Higher crude oil prices lead to increased NPV and IRR, indicating greater profitability, while lower prices have the opposite effect.
2. The payback period tends to be shorter when crude oil prices are high, as cash flows are more favorable.
3. Higher capital expenditures result in lower NPV and IRR, potentially making the project less economically attractive and elevated CAPEX lead to a longer payback period, which increases project risk.
4. Increased operating expenditures from the FT-GTL technology reduced the NPV and IRR thereby affecting project profitability and extend the payback period, increasing the time to recoup initial investments.
5. A higher discount rate factor decreases the present value of future cash flows, resulting in a lower NPV and potentially lower IRR. While a lower discount rate has the opposite effect, increasing the attractiveness of the FT-GTL plant project in terms of NPV and IRR.

Recommendation

Given the economic potential of GTL technology projects in Nigeria, as demonstrated in this research, it is recommended that project stakeholders implement a comprehensive risk management strategy for the FT-GTL plant project in Nigeria. This approach should include hedging, flexible pricing arrangements, cost-effective capital expenditures, and operational efficiency measures to mitigate risks and optimize project economics. By adopting this strategy, project stakeholders can refine their financial modeling to ensure alignment with industry's best practices and make informed decisions to drive long-term profitability. Continuous monitoring of market conditions, cost trends, and operational performance will also be crucial in identifying areas for improvement and adjusting the project's financial model accordingly. This proactive approach will ultimately enhance the project's chances of success and provide a solid foundation for sustainable growth in Nigeria's energy sector.

Acknowledgement: *The authors of this work acknowledge the immense contributions of Peter Oluwaseyi Ojegbile of the Department of Petroleum Engineering, University of Ibadan, Oyo State as well as the Department Petroleum Engineering, University of Benin, Benin City during the research stages of this work.*

Compliance with Ethical Standards *Ethical responsibilities of Authors: The authors have read, understood, and complied as applicable with the statement on "Ethical responsibilities of Authors" as found in the Instructions for Authors".*

Conflict of Interest: *The authors declare that they do not have any conflict of interest.*

Change of Authorship: *The authors have read, understood, and complied as applicable with the statement on "Ethical responsibilities of Authors" as found in the Instructions for Authors and is aware that with minor exceptions, no changes can be made to authorship once the paper is submitted.*

References

Ahmed MM, Bello AA, Idris MN, (2012), Natural Gas Utilization and the Nigerian Gas-To-Liquid Project; An Opportunity to End Gas Flaring, *Int. Emer. Trends Engin. & Dev*., **2**(2). 240-256. https://www.researchgate.net/publication/285736728_Natural_gas_utilization_and_the_Nigerian_gas-to-liquid_project_an_opportunity_to_end_gas_flaring

Akpomera E, Oghenekevwe O, (2017), Economic Assessment of Gas to Liquid (GTL) Technology in Nigeria. *J. Natural Sci. Res*., **7**(22). 8-18.

Al-Saadoon FT, (2005) Economics of GTL Plants. SPE 94380 Paper Presented at the *SPE Hydrocarbon Economics and Evaluation Symposium in April 3-5 2005*, Dallas, Texas, USA, Society of Petroleum Engineers. https://doi.org/10.2118/94380-MS

Al-Shalchi W, (2006), Gas to Liquids Technology (GTL) *Petroleum Expert*, Baghdad 2006, https://pdfroom.com/books/gas-to-liquids-technology-2006/jb5qOBWBgxQ/download

Capuano L, (2018) *Annual Energy Outlook 2018*, U.S. Energy Information Administration, Independent Statistics and Analysis, www.eia.gov

Chikwe AO, Ukpai UCE, Elechi DU, Onyia OS, (2021) Comparative Economic Analysis of Liquefied Natural Gas Technology and Gas to Liquid Technology, *Europ. J. Adv. Engin. & Tech*., **8**(10), 9-16. https://www.ijser.org/researchpaper/Comparative-Economic-Analysis-of-Gas-to-Liquid-and-Liquefied-Natural-Gas-Technologies.pdf

Diugwu IA, Ikaiya MA, Musa M, Egila AE, (2013), The Effect of Gas Production, Utilization and Flaring on the Economic Growth of Nigeria. *Natural Resour J.*, **4**. 341–348. https://digitalrepository.unm.edu/nrj/

Dodaro J, (2015) Fischer-Tropsch Process. Submitted as Coursework for PH240, *Stanford University. http://large.stanford.edu/courses/2010/ph240/liu1/*

Economides MJ, Aguirre M , Morales A , Naha S , Tijani H, Vargas L, (2005) The Economics of Gas to Liquids Compared to Liquefied Natural Gas, *World Energy*, **8**(1). 136-140. https://ntnuopen.ntnu.no/ntnu-xmlui/bitstream/handle/11250/3053156/Yaz%25C4%25B1r.pdf?sequence=1&isAllowed=y

Glebova O, (2013) Gas to Liquids: Historical Development and Future Prospects: *The Oxford Institute for Energy Studies*, University of Oxford, 1–47 https://ora.ox.ac.uk/objects/uuid:574a2d88-61ee-4097-8642-f154e7bbf813

Global Gas Flaring Reduction Partnership. (2018), World Bank. GGFR Technology Overview – Utilization of Small-Scale Associated Gas. https://pubdocs.worldbank.org/en/495311492808037862/GGFR-Technology-Overview-April-2017.pdf

Gradassi JM, (2001) Gas-To-Liquid R & D: Setting Cost Reduction Targets, *Elsevier Science* B.V, p 7. https://www.ijser.org/researchpaper/Comparative-Economic-Analysis-of-Gas-to-Liquid-and-

Liquefied-Natural-Gas-Technologies.pdf

Hendrix C, Au T, (2003) Project Management for Construction: Fundamental Concepts for Owners, *Engineers, Architects and Builders*. Retrieved on January 15 2007 from www.ce.cmu.edulpmbooklO5 cost estimation.html. https://books.google.com.tr/books?id=N5mVq8GrT0kC&printsec=frontcover&hl=tr

Idigbe KI, Onwuachi-Iheagwara PN, (2014) Driving Sustainable Growth through Natural Gas Assets in Nigeria. *Journal of Emerging Trends in Engineering and Applied Sciences* (JETEAS) **5**(2). 140-147. https://www.scholarlinkinstitute.org/jeteas/listofissues.php

Ikoku, Chi I. (1992), Natural Gas Production Engineering, Book, Reprint Edition. *Krieger Publishing Company*, Krieger Drive, Malabar, Florida 32950, 1–17. https://www.amazon.com/Natural-Gas-Production-Engineering-Ikoku/dp/0894646397

International Energy Agency, The World Energy Out-look, (2009). Kerzner, H. (2001), Project Management: A System Approach to Planning, Scheduling, and Controlling. 7th Edition. John Wiley & Sons, Inc. New York, USA. p.952 https://ftp.idu.ac.id/wp-content/uploads/ebook/ip/BUKU%20MANAJEMEN%20PROYEK/project-management-harold-kerzner1.pdf

Mian MA, (2010) Project Economics and Decision Analysis (2nd Edition, Volume 1), *PennWell Corporation*, Tulsa, Oklahoma. https://www.amazon.in/Project-Economics-Decision-Analysis-Determinisitic/dp/1593702086

Nagi CA, Dulu A, Godwin C, (2016), Comparative Economic Analysis of Gas to Liquid and Liquefied Natural Gas Technologies, *Int. J. Sci. & Engin. Res.*, **7**(6). 258 – 275, ISSN 2229-5518 https://ejaet.com/PDF/8-10/EJAET-8-10-9-16.pdf

Nwankwo JE, (2008) Gas Utilization in Nigeria - an Economic Comparison of Gas-to-Liquid and Liquefied Natural Gas Technologies, M.Sc. Thesis, North-West University, South Africa. https://www.connecting-africa.net/query_2.php?rid=B00009605

Nwaoha C, Iyoke UJ, (2013) A Review on Natural Gas Utilization and Cutting Carbon Emissions: How Viable is Compressed Natural Gas for Road Vehicle Fuel?, *J. Energy Tech. & Policy*, **3**(5). 37-46. https://www.iiste.org/Journals/index.php/JETP/article/download/5596/5708

Onyelucheya OE, Ibe EC, (2015) Profitability Challenge of the Excravous GTL Plant. *Proceedings of the 45th Annual Conference of NSChE*, 5th- 7th Nov., 2015, Warri, Nigeria. P019. https://www.researchgate.net/publication/335608733_Profitability_Challenges_of_the_Escravos_GTL_Plant

Oredein O, (2013) Hopes of Monetizing GTL Resources in Nigeria are again Delayed. Special E&P, *Hart Energy*, January 22, 2013, https://www.hartenergy.com/exclusves/hopes-monetizing-gtl-resources-nigeria-are-again-delayed-19219.

Patel B, (2005) Gas Monetization: A Techno-Economic Comparison of Gas-to-Liquid and LNG, *Foster Wheeler Energy Ltd*, Reading UK, Paper Presented at the 7th World Congress of Chemical Engineers in Glasgow, 1-11. https://www.econstor.eu/bitstream/10419/246518/1/978-1-907555-74-9.pdf

Smith R, Asaro M, (2005), Fuels of the Future: Technology Intelligence for Gas to Liquids Strategies. *SRI Consulting*, Menlo Park. https://link.springer.com/10.1007/978-1-4419-0851-3_72

Stanley IO, (2009) Gas to Liquid Technology: Prospect for Natural Gas Utilization in Nigeria, Elsevier, *J. Nat. Gas Sci. & Engin.*, **1**(6). 190–194. https://doi.org/10.1016/j.jngse.2009.12.001

Toochukwu, E. S., Chinedu, I. N., Ubanozie, O. J., Kerunwa, A., Ohia, N. P., Odo, J. E. and Obah, B. (2019), Economics of Gas-to-Liquids (GTL) Plants, *Petroleum Science and Engineering*, **3**(2). 85-93, doi.10.11648/j.pse.20190302.17

Ubanzie JO, Toochukwu ES, Abanobi CI, Eluagu RC, Igbojionu AC, (2021) Evaluation of the Economic Potentials of a Mini Gas-to-Liquid (GTL) Plant in Nigeria. *Int. J. Oil, Gas & Coal Engin.*, **9**(6). 98-110, doi.10.11648/j.ogce.20210906.13

Uzuegbunam F, (2014), Escravous GTL Project Finally Gets off Ground, Accessed at https://archive.businessday.ng/oilandgas/article/chevrons-escravos-gtl-project-finally-gets-off-ground/

J. Int. Environmental Application & Science, Vol. 20: 56-69 (2025)
Research Paper

Prediction and Optimization of Compressive Strength of Cement Concrete with Box- Behnken Model

Michael Toryila Tiza[1, *], Jonah Agunwamba[2], Fidelis Okafor [3], Shina Solomon[4]

[1]Physical Planning Unit, Federal Polytechnic Wannune, Benue State, Nigeria; [2& 3]Department of Civil Engineering, University of Nigeria, Nigeria; [4]Digital Engineering Faculty of Civil & Environmental Engineering, Bauhaus-Universität Weimar Germany.

Received October 11, 2024; Accepted March 3, 2025

Abstract: In this study a Box-Behnken's Model is employed to optimize the compressive strength of concrete material, by analysing factors like Water, Cement, Sand, Reclaimed Asphalt Pavement (RAP) and Coarse Aggregates. Optimization is performed with Minitab software by target strength and maximization approaches. Analysis of experimental data demonstrates that the target strength approach provides a more realistic fundability profile and reasonable funding probabilities. The statistical analyses i.e. regression analysis and ANOVA are employed to analyse the significance of factors and their interactions on compressive strength. The regression equation from the model gives information about the numerical relationship of the factors to compressive strength. Furthermore, residual analysis and normal probability plots confirm the performance of the model and data distribution. These visualizations are the surface plot, main effects plot and interaction plots that provide more detail on the effect of each factor itself and with other factors between them on compressive strength. According to the study, it is casted that optimizing concrete mix proportions using target strength approach leads to desirable compressive strength around 30 N/mm² with optimal proportions of 24.72% for A, 9.99% for B, 25.26% for C, 33.18% for D and75 % for E and actual values then can be adjusted according to certain constraints in order more realistically find proportioned properties fulfilling this experimental result. These observations will assist in improving the reliability and application of concrete mix design processes, which would help engineers and researchers to deliver optimal properties while designing various mixes.

Keywords: *Compressive strength, Box-Behnken model, Optimization, Concrete mix design, Reclaimed asphalt pavement (RAP).*

Introduction

Growing attention on sustainable practices in the building sector in recent years has driven research into substitute materials for concrete manufacture (Xiao *et al*., 2007). Emerging as a potential candidate for increasing sustainability while preserving or improving concrete performance are reclaimed asphalt pavement aggregates (RAP) (Michael *et al*., 2021). Ensuring structural integrity and durability (Taha et al., 2002) depends on RAP concrete's compressive strength being optimized. Often time-consuming and resource-intensive, traditional approaches for mix design optimization led to the use of advanced modelling techniques such as the response surface methodology (Pradani *et al*., 2023), the Box-Behnken design. Using the Box-Behnken model, this work attempts to forecast and maximize the compressive strength of RAP concrete by methodically changing parameters including RAP substitution percentage, water-cement ratio, and curing time (Tiza *et al*., 2022).The aim of the study is to create empirical models to precisely predict compressive strength under various circumstances, so offering insightful analysis of the viability and efficiency of RAA inclusion in concrete mixes (Yryshkin, 2022).These results can guide practitioners and engineers in maximizing concrete compositions for particular performance criteria, so promoting sustainable building methods and lowering environmental impact and guaranteeing structural integrity (Tavva & Reddy, 2024).

**Corresponding: E-Mail: tizamichael@gmail.comu, Tel: +2347036280738*

Figure 1. Crumbs of RAP in raw state

Figure 2. RAP in Manual Crushed State

Preparation of RAP

Following the acquisition of reclaimed asphalt pavement (RAP) from the Gboko-Makurdi route rehabilitation in Wannune, the material was transported to a clean cement concrete platform for hand crushing, so guaranteeing the elimination of foreign materials and uniform aggregates. The sieved crushed RAP aggregates then helped to separate them from the asphalt in asphaltic concrete (Tiza, 2022). Applied to the samples to remove the asphalt coating on the aggregates, diesel fuel-characterised by the chemical formula $C_{12}H_{23}$—then clearly reduced asphalt presence. Ultimately, the RAP was sundried to help diesel coatings from the aggregates dry off (Yaro *et al.*, 2023). This sequential process guaranteed the readiness of uniform, clean RAP aggregates for possible use in several building projects. Figures 4a and 4b show the Reclaimed Asphalt Pavement (RAP) after treatment with Diesel, aimed at eradicating asphaltic coatings; Figure 1 shows the crumbs of Reclaimed Asphalt Pavement (RAP) in their raw state; Figure 2 shows RAP after manual crushing; Figure 3. shows the stepwise process followed for obtaining and treating the recycled asphalt aggregates.

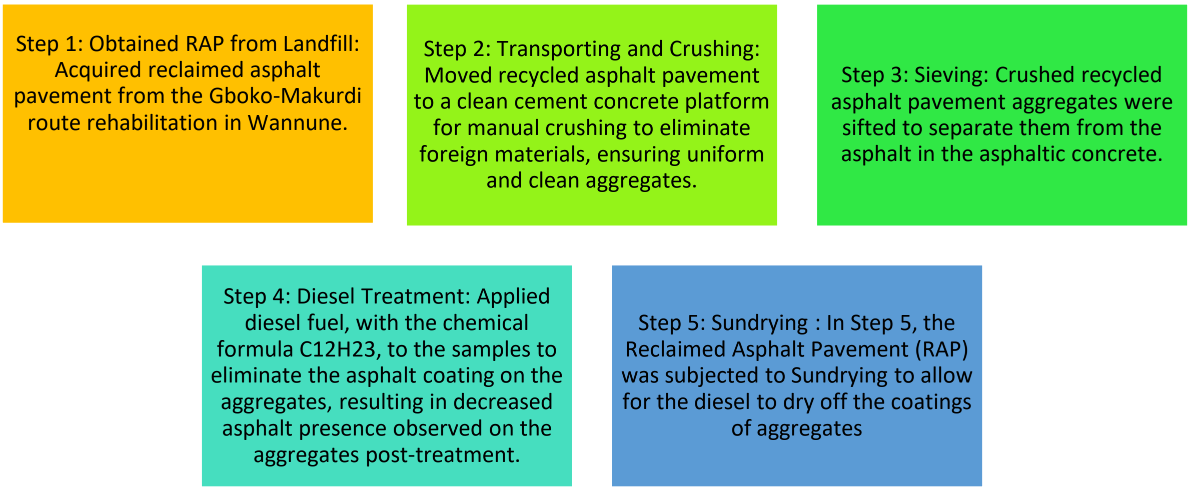

Figure 3: The step-by-step process for obtaining and treating the recycled asphalt aggregates.

Figure 4 a & b: Reclaimed Asphalt Pavement After treating with Diesel to remove asphaltic coatings

Materials and Methods

This study paid close attention to choosing materials that complied with British Standards Institution (BSI) criteria so guaranteeing the quality and effectiveness of concrete manufacture. River sand satisfied BS EN 12620:2013; Dangote 3X Cement (CEMII 42.5R) was chosen in line with BS EN 197-1:2011. Following BS EN 1008:2002, borehole water was obtained in compliance; natural coarse aggregates were selected using BS EN 12620:2013 recommendations. Reclaimed asphalt pavement (RAP) from Wannune also met BS EN 12620:2013 criteria. To reduce asphalt coating before inclusion, the RAP was manually crushed and diesel treated. This rigorous respect to criteria guaranteed the fit and quality of every component for their purposes in the concrete manufacturing process (Tiza, 2023).

Figure 5a. Compression testing machine

Figure 5b. Sample Cubes used for the study

Figure 5c. Sample under compression test

Figure 5d. Sample under Failure

Figure 5a above displays the compression testing machine utilized in this study, while Figure 5b showcases the sample cubes employed for the research. Furthermore, Figure 5c exhibits a sample undergoing compression testing, and Figure 5d illustrates a sample experiencing failure during the test.

Box-Behnken Design

The experimental plan in Minitab utilized the Box-Behnken Design by setting specific low and high levels for each component of the concrete mix (Özgen & Yıldız, 2010). Water and cement were defined as percentages of the total mix weight, with water ranging from 15% to 25% and cement from 7% to 10% of the total mix weight. Sand and Reclaimed Asphalt Pavement (RAP) were designated as percentages of the total aggregate weight, varying between 25% and 45% for sand, and 10% and 50% for RAP. Coarse aggregates were structured with low, medium, and high levels, encompassing 55%, 65%, and 75% of the total aggregate weight, respectively. Minitab's design interface systematically varied these components within their specified ranges, enabling an organized exploration of how alterations in these percentages impact diverse properties of concrete mixes. This structured approach facilitated the optimization of concrete mix designs, allowing researchers to tailor compositions for desired characteristics more effectively (Asadzadeh & Khoshbayan, 2018; Kumar, 2020).

Table 1: Experimental Design for Concrete Mix Proportions Using Box-Behnken Design

Std Order	Run Order	Pt Type	Blocks (%)	Water (%)	Cement (%)	Sand (%)	RAP (%)	Coarse Aggregates (%)
37	1	2	1	20	7	35	10	65
42	2	0	1	20	8.5	35	30	65
29	3	2	1	20	8.5	25	30	55
36	4	2	1	25	8.5	35	30	75
25	5	2	1	15	8.5	35	10	65
7	6	2	1	20	8.5	25	50	65
41	7	0	1	20	8.5	35	30	65
43	8	0	1	20	8.5	35	30	65
6	9	2	1	20	8.5	45	10	65
30	10	2	1	20	8.5	45	30	55
24	11	2	1	20	10	45	30	65
5	12	2	1	20	8.5	25	10	65
20	13	2	1	20	8.5	35	50	75
4	14	2	1	25	10	35	30	65
18	15	2	1	20	8.5	35	50	55
26	16	2	1	25	8.5	35	10	65
1	17	2	1	15	7	35	30	65
17	18	2	1	20	8.5	35	10	55
12	19	2	1	20	10	35	30	75
10	20	2	1	20	10	35	30	55
15	21	2	1	15	8.5	45	30	65
33	22	2	1	15	8.5	35	30	55
8	23	2	1	20	8.5	45	50	65
3	24	2	1	15	10	35	30	65
13	25	2	1	15	8.5	25	30	65
45	26	0	1	20	8.5	35	30	65
44	27	0	1	20	8.5	35	30	65
16	28	2	1	25	8.5	45	30	65
31	29	2	1	20	8.5	25	30	75
46	30	0	1	20	8.5	35	30	65
19	31	2	1	20	8.5	35	10	75
34	32	2	1	25	8.5	35	30	55
28	33	2	1	25	8.5	35	50	65
32	34	2	1	20	8.5	45	30	75
14	35	2	1	25	8.5	25	30	65
40	36	2	1	20	10	35	50	65
22	37	2	1	20	10	25	30	65
27	38	2	1	15	8.5	35	50	65
11	39	2	1	20	7	35	30	75
9	40	2	1	20	7	35	30	55
39	41	2	1	20	7	35	50	65
38	42	2	1	20	10	35	10	65
2	43	2	1	25	7	35	30	65
21	44	2	1	20	7	25	30	65
23	45	2	1	20	7	45	30	65
35	46	2	1	15	8.5	35	30	75

Legend: *Natural Aggregates (NA); Reclaimed Asphalt Pavement (RAP), Fine Aggregates (FA)*

Although Minitab 22 produced the results as shown in Table 1 Experimental Design for Concrete Mix Proportions Using Box-Behnken Design, the outcome had to be proportioned into kilograms(kg) to facilitate the experimental process. Each value for water, cement, sand, RAP, and coarse aggregates had to be proportionally distributed to represent the equivalent of the original result the table above. This proportioning was necessary to ensure that the experimental conditions accurately reflected the intended research parameters, and the result of proportioning is as represented below in table 2.

Table 2. Proportioned values from Box-Behnken Minitab Result for Compressive Strength (Concrete Cubes)

Std Order	Run Order	Pt Type	Blocks (%)	Water (kg)	Cement (kg)	Sand(kg)	RAP (kg)	Coarse Aggregates (kg)
37	1	2	1	1.168	0.41	2.04	0.584	3.79
42	2	0	1	1.01	0.43	1.76	1.51	3.28
29	3	2	1	1.156	0.49	1.44	1.734	3.17
36	4	2	1	1.1525	0.39	1.61	1.383	3.45
25	5	2	1	0.8985	0.51	2.09	0.599	3.89
7	6	2	1	0.95	0.40	1.18	2.375	3.08
41	7	0	1	1.01	0.42	1.76	1.515	3.28
43	8	0	1	1.01	0.42	1.76	1.515	3.28
6	9	2	1	1.078	0.45	2.42	0.539	3.49
30	10	2	1	1.01	0.42	2.27	1.515	2.77
24	11	2	1	0.942	0.47	2.11	1.413	3.06
5	12	2	1	1.246	0.52	1.55	0.62	4.049
20	13	2	1	0.85	0.36	1.48	2.12	3.18
4	14	2	1	1.2125	0.48	1.69	1.45	3.15
18	15	2	1	0.95	0.40	1.66	2.37	2.61
26	16	2	1	1.3925	0.47	1.94	0.55	3.62
1	17	2	1	0.789	0.36	1.84	1.57	3.41
17	18	2	1	1.246	0.52	2.18	0.62	3.42
12	19	2	1	0.942	0.47	1.64	1.41	3.53
10	20	2	1	1.066	0.53	1.86	1.59	2.91
15	21	2	1	0.7335	0.41	2.20	1.46	3.17
33	22	2	1	0.8355	0.47	1.94	1.67	3.06
8	23	2	1	0.85	0.36	1.91	2.12	2.7625
3	24	2	1	0.774	0.51	1.80	1.54	3.35
13	25	2	1	0.83	0.47	1.39	1.67	3.62
45	26	0	1	1.01	0.42	1.76	1.51	3.28
44	27	0	1	1.01	0.42	1.76	1.51	3.28
16	28	2	1	1.1525	0.39	2.07	1.383	2.99
31	29	2	1	1.01	0.42	1.26	1.515	3.78
46	30	0	1	1.01	0.42	1.26	1.515	3.78
19	31	2	1	1.078	0.45	1.88	0.539	4.04
34	32	2	1	1.3075	0.44	1.8305	1.569	2.87
28	33	2	1	1.0875	0.36	1.52	2.175	2.82
32	34	2	1	0.898	0.38	2.02	1.34	3.36
14	35	2	1	1.3075	0.44	1.30	1.56	3.39
40	36	2	1	0.888	0.44	1.55	2.22	2.88
22	37	2	1	1.066	0.53	1.33	1.59	3.46
27	38	2	1	0.6915	0.39	1.61	2.30	2.99
11	39	2	1	0.958	0.33	1.67	1.43	3.59
9	40	2	1	1.088	0.38	1.90	1.63	2.99
39	41	2	1	0.904	0.31	1.58	2.26	2.93
38	42	2	1	1.142	0.57	1.99	0.57	3.70
2	43	2	1	1.235	0.34	1.72	1.48	3.21
21	44	2	1	1.088	0.38	1.36	1.63	3.53
23	45	2	1	0.958	0.33	2.15	1.43	3.11
35	46	2	1	0.735	0.41	1.71	1.47	3.67

Box Behnken's Regression Model for Compressive Strength

In this Box-Behnken design conducted using Minitab 22, a comprehensive investigation was undertaken to understand the effects of various continuous factors, denoted as water, cement, sand, RAP (reclaimed asphalt pavement), and coarse aggregates, on a response variable. Employing the full quadratic model allowed for a thorough exploration of these relationships, considering linear, quadratic, and potential interaction effects. The study maintained a 95% confidence level for all intervals and carefully defined the ranges and constraints for each factor, ensuring practical and meaningful experimentation. Overall, this approach enabled a robust analysis of the factors' impacts on the response variable, offering valuable insights into the underlying dynamics of the system under study (Lam et al., 2023).The details are in table 3 below.

It should be noted that the factors used in this design are in coded forms where A is water, B is Cement, C is Sharp Sand, D is RAP and E is Coarse Aggregates, and this applies throughout this study for the Box Behnken's design.

Table 3. Box Behnken's design for Compressive Strength

Std Order	Run Order	Pt Type	Water (kg)	Cement (kg)	Sand (kg)	RAP (kg)	Coarse Aggregates (kg)	Av. of 3 Lab Response
37	1	2	1.168	0.41	2.04	0.584	3.79	30.25
42	2	0	1.01	0.43	1.76	1.51	3.28	30.5
29	3	2	1.156	0.49	1.44	1.734	3.17	30.75
36	4	2	1.1525	0.39	1.61	1.383	3.45	31
25	5	2	0.8985	0.51	2.09	0.599	3.89	31.25
7	6	2	0.95	0.4	1.18	2.375	3.08	31.75
41	7	0	1.01	0.42	1.76	1.515	3.28	32
43	8	0	1.01	0.42	1.76	1.515	3.28	32.25
6	9	2	1.078	0.45	2.42	0.539	3.49	32.25
30	10	2	1.01	0.42	2.27	1.515	2.77	32.75
24	11	2	0.942	0.47	2.11	1.413	3.06	33.25
5	12	2	1.246	0.52	1.55	0.62	4.049	33.5
20	13	2	0.85	0.36	1.48	2.12	3.18	33.75
4	14	2	1.2125	0.48	1.69	1.45	3.15	34
18	15	2	0.95	0.4	1.66	2.37	2.61	34.25
26	16	2	1.3925	0.47	1.94	0.55	3.62	34.5
1	17	2	0.789	0.36	1.84	1.57	3.41	34.75
17	18	2	1.246	0.52	2.18	0.62	3.42	35
12	19	2	0.942	0.47	1.64	1.41	3.53	35.25
10	20	2	1.066	0.53	1.86	1.59	2.91	35.5
15	21	2	0.7335	0.41	2.2	1.46	3.17	35.75
33	22	2	0.8355	0.47	1.94	1.67	3.06	36
8	23	2	0.85	0.36	1.91	2.12	2.7625	30.25
3	24	2	0.774	0.51	1.8	1.54	3.35	30.5
13	25	2	0.83	0.47	1.39	1.67	3.62	30.75
45	26	0	1.01	0.42	1.76	1.51	3.28	31
44	27	0	1.01	0.42	1.76	1.51	3.28	31.25
16	28	2	1.1525	0.39	2.07	1.383	2.99	31.5
31	29	2	1.01	0.42	1.26	1.515	3.78	31.75
46	30	0	1.01	0.42	1.26	1.515	3.78	32
19	31	2	1.078	0.45	1.88	0.539	4.04	32.25
34	32	2	1.3075	0.44	1.8305	1.569	2.87	32
28	33	2	1.0875	0.36	1.52	2.175	2.82	32.5
32	34	2	0.898	0.38	2.02	1.34	3.36	32.75
14	35	2	1.3075	0.44	1.3	1.56	3.39	33
40	36	2	0.888	0.44	1.55	2.22	2.88	33.25
22	37	2	1.066	0.53	1.33	1.59	3.46	33.5
27	38	2	0.6915	0.39	1.61	2.3	2.99	33.75
11	39	2	0.958	0.33	1.67	1.43	3.59	34
9	40	2	1.088	0.38	1.9	1.63	2.99	34.25
39	41	2	0.904	0.31	1.58	2.26	2.93	34.5
38	42	2	1.142	0.57	1.99	0.57	3.7	34.75
2	43	2	1.235	0.34	1.72	1.48	3.21	34.75
21	44	2	1.088	0.38	1.36	1.63	3.53	35.25
23	45	2	0.958	0.33	2.15	1.43	3.11	35.25
35	46	2	0.735	0.41	1.71	1.47	3.67	35.5

The coded coefficients provide in table 4 represent the coefficients of the terms in the full quadratic model used for the Box-Behnken design. Each term corresponds to a specific factor or combination of factors, with their coefficients indicating the strength and direction of their impact on the response variable. The constant term represents the baseline value of the response when all factors are at their zero levels. The coefficient values, standard errors, t-values, and p-values are crucial for assessing the significance of each term. A positive coefficient suggests a positive effect on the response variable, while a negative coefficient implies a negative effect. Additionally, the t-values and p-values help determine the statistical significance of each coefficient. Terms with p-values below a chosen significance level (e.g., 0.05) are considered statistically significant. In this analysis, several terms have statistically significant coefficients, indicating their importance in explaining the variability in the response variable. However, further interpretation and validation of these results should be conducted in the context of the specific study and its objectives (Guo et al., 2022). Additionally, consideration of multicollinearity, as indicated by the variance inflation factor (VIF), is important to ensure the reliability of the model estimates (Li et al., 2023).

Table 4. Coded Coefficients for the Box Behnken's Compressive Strength

Term	Coef	SE Coef	T-Value	P-Value	VIF
Constant	104.7	49.2	2.13	0.043	
A	0.80	1.35	0.59	0.558	473.78
B	-11.52	4.75	-2.43	0.023	527.48
C	0.432	0.666	0.65	0.523	461.28
D	0.094	0.321	0.29	0.771	427.94
E	-1.260	0.735	-1.71	0.099	561.28
A*A	0.0431	0.0168	2.57	0.017	118.53
B*B	0.905	0.187	4.85	0.000	236.68
C*C	0.00432	0.00420	1.03	0.313	91.03
D*D	0.00186	0.00105	1.77	0.088	17.70
E*E	0.00995	0.00420	2.37	0.026	311.03
A*B	-0.1000	0.0828	-1.21	0.238	193.44
A*C	-0.0338	0.0124	-2.72	0.012	114.00
A*D	-0.01000	0.00621	-1.61	0.120	74.00
A*E	-0.0050	0.0124	-0.40	0.691	234.00
B*C	-0.0125	0.0414	-0.30	0.765	178.44
B*D	-0.0458	0.0207	-2.22	0.036	138.44
B*E	-0.0000	0.0414	-0.00	1.000	298.44
C*D	0.00625	0.00310	2.01	0.055	59.00
C*E	-0.00125	0.00621	-0.20	0.842	219.00
D*E	0.00281	0.00310	0.91	0.373	179.00

Table 5. Box Behnken's Model Summary

S	R-sq	R-sq(adj)	R-sq(pred)
1.24126	69.89%	45.81%	0.00%

The model summary in Table 5 presents key metrics evaluating the performance of the regression model. With a standard error of 1.24126, the model's R-squared value of 69.89% indicates that approximately 69.89% of the variability in the response variable is accounted for by the independent variables. However, the adjusted R-squared value of 45.81% suggests that the model's explanatory power may be slightly diminished when considering the number of predictors (Dai et al., 2019; Maaze & Shrivastava, 2023).

The analysis of variance (ANOVA) of Box Behnken's Compressive Strength design

The analysis of variance (ANOVA) provides valuable insights into the significance of the factors and their interactions in the regression model (Tiza et al., 2023). The "Model" section indicates that the overall model is statistically significant, with an F-value of 2.90 and a corresponding p-value of 0.006, suggesting that at least one of the factors has a significant effect on the response variable. The "Linear" and "Square" subsections further delve into the significance of the linear and quadratic terms, respectively. Notably, the "Square" subsection demonstrates significant effects for terms A*A and B*B, with p-values of 0.017 and 0.000, respectively, indicating the presence of nonlinear relationships between these factors and the response variable. Additionally, the "2-Way Interaction" section reveals some significant interactions between factors, such as A*C and B*D.

Regression Equation in coded Units

Compressive Strength =200.0 + 0.238 A - 14.18 B + 0.0606 C + 0.0174 D - 0.1370 E + 0.001725 A^2 + 0.4023 B^2 + 0.000043 C^2 + 0.000005 D^2 + 0.000099 E^2- 0.0133 A*B - 0.000675 A*C - 0.000100 A*D - 0.000100 A*E - 0.00083 B*C - 0.001528 B*D - 0.00000 B*E+ 0.000031 C*D - 0.000013 C*E + 0.000014 D*E (1)

In this equation, *A, B, C, D, and E represent the actual values of the factors (A is Water,B is Cement, C is Sand, D is RAP, and E is Coarse Aggregates), while A^2, B^2, C^2, D^2, and E^2 represent the squared values of these factors. Each coefficient represents the change in compressive strength associated with a one-unit change in the respective factor, holding all other factors constant.*

Table 6. Analysis of Box Behnken's Compressive Strength Residuals

Run Order	Water (kg)	Cement (kg)	Sand (kg)	RAP (kg)	Coarse Aggregates (kg)	Av. of 3 Lab Response Value (N/mm^2)	Predicted Value (N/mm^2)	Residual (N/mm^2)
1	1.16	0.41	2.04	0.584	3.79	30.25	32.135	-1.88
2	1.01	0.43	1.76	1.51	3.28	30.5	31.167	-0.667
3	1.15	0.49	1.44	1.734	3.17	30.75	32.141	-1.391
4	1.15	0.39	1.61	1.383	3.45	31	32.083	-1.083
5	0.89	0.51	2.09	0.599	3.89	31.25	32.271	-1.021
6	0.95	0.4	1.18	2.375	3.08	31.05	30.859	0.641
7	1.01	0.42	1.76	1.515	3.28	31.75	31.167	0.583
8	1.01	0.42	1.76	1.515	3.28	32	31.167	0.833
9	1.07	0.45	2.42	0.539	3.49	32.25	31.328	0.922
10	1.01	0.42	2.27	1.515	2.77	32.05	33.578	-1.078
11	0.94	0.47	2.11	1.413	3.06	32.75	34.12	-1.37
12	1.24	0.52	1.55	0.62	4.049	33	32.641	0.359
13	0.85	0.36	1.48	2.12	3.18	33.25	33.563	-0.313
14	1.21	0.48	1.69	1.45	3.15	33.05	32.969	0.531
15	0.95	0.4	1.66	2.37	2.61	33.75	32.969	0.781
16	1.39	0.47	1.94	0.55	3.62	34	32.99	1.01
17	0.78	0.36	1.84	1.57	3.41	34.75	34.094	0.156
18	1.24	0.52	2.18	0.62	3.42	35	33.375	1.125
19	0.94	0.47	1.64	1.41	3.53	35.25	34.01	0.74
20	1.06	0.53	1.86	1.59	2.91	35	34.542	0.458
21	0.73	0.41	2.2	1.46	3.17	35.25	35.599	-0.349
22	0.83	0.47	1.94	1.67	3.06	35.5	33.896	1.604
23	0.85	0.36	1.91	2.12	2.7625	35.75	34.547	1.203
24	0.77	0.51	1.8	1.54	3.35	36	35.75	0.25
25	0.83	0.47	1.39	1.67	3.62	30.25	31.036	-0.786
26	1.01	0.42	1.76	1.51	3.28	30.05	31.167	-0.667
27	1.01	0.42	1.76	1.51	3.28	30.75	31.167	-0.417
28	1.15	0.39	2.07	1.383	2.99	31	30.943	0.057
29	1.01	0.42	1.26	1.515	3.78	31.25	31.859	-0.609
30	1.01	0.42	1.26	1.515	3.78	31.05	31.167	0.333
31	1.078	0.45	1.88	0.539	4.04	31.75	31.719	0.031
32	1.3075	0.44	1.8305	1.569	2.87	32	33.115	-1.115
33	1.0875	0.36	1.52	2.175	2.82	32.25	31.708	0.542
34	0.898	0.38	2.02	1.34	3.36	32.05	32.797	-0.297
35	1.3075	0.44	1.3	1.56	3.39	32.75	33.13	-0.38
36	0.888	0.44	1.55	2.22	2.88	33		
37	1.066	0.53	1.33	1.59	3.46	33.25	33.307	-0.057
38	0.6915	0.39	1.61	2.3	2.99	33.05	34.99	-1.49
39	0.958	0.33	1.67	1.43	3.59	33.75	33.854	-0.104
40	1.088	0.38	1.9	1.63	2.99	34	34.385	-0.385
41	0.904	0.31	1.58	2.26	2.93	34.25	35.604	-1.354
42	1.142	0.57	1.99	0.57	3.7	34.05	35.042	-0.542
43	1.235	0.34	1.72	1.48	3.21	34.75	34.312	0.438
44	1.088	0.38	1.36	1.63	3.53	35	32.776	2.224
45	0.958	0.33	2.15	1.43	3.11	35.25	34.339	0.911
46	0.735	0.41	1.71	1.47	3.67	35.5	33.86	1.635

The table 6 above presents a comparison between the average of three lab response values and their corresponding predicted values, along with residuals and percentage errors. Overall, the model appears to perform reasonably well, with most percentage errors being relatively low, indicating accurate predictions.

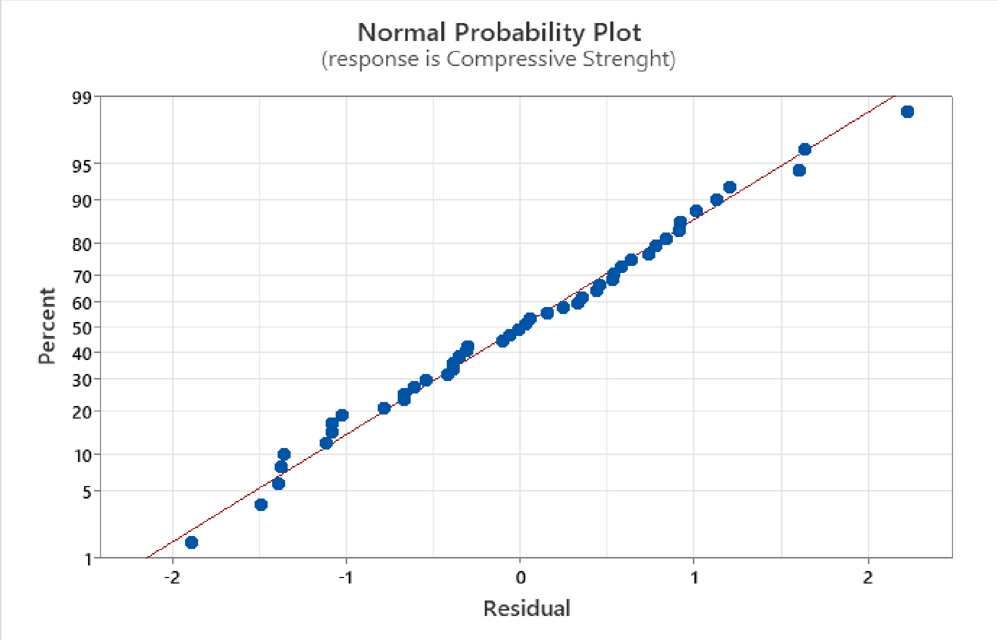

Figure 6. Normal Probability Plot

The Normal Probability Plot in figure 6 above visually assesses whether the data points align with a normal distribution by comparing them to the expected alignment represented by the red line. In this plot, the blue dots represent individual data points of compressive strength, and their proximity to the red line indicates the degree of conformity to a normal distribution. The closely packed arrangement of the dots suggests a good level of adherence to normality, indicating that the compressive strength data follows a relatively normal distribution. However, slight deviations from the red line may still be observed, suggesting minor departures from perfect normality. Overall, the pattern observed in the plot suggests that the compressive strength data is reasonably well-distributed and conforms reasonably well to a normal distribution (Liu et al., 2019).

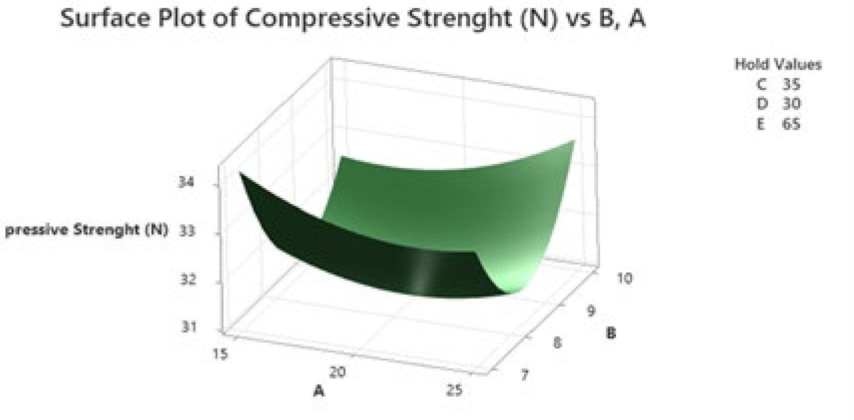

Figure 7. Surface Plot of Compressive Strength

The Figure 7 above shows **t**he 3D surface plot depicts the relationship between two variables, A and B, and their influence on compressive strength in cement concrete. The x-axis represents variable A, ranging from 15 to 25, while the y-axis represents variable B, ranging from 7 to 10. The vertical z-axis illustrates compressive strength in Newtons (N), ranging from 31 to 34. The surface shape of the graph showcases a curved structure, indicative of how compressive strength varies with different combinations of A and B. An intriguing observation is that as variable B decreases and variable A increases, there is a discernible trend of increased compressive strength. This trend is visually evident from the upward curvature of the surface plot. It implies that adjustments in these variables can significantly impact the compressive strength of the material.

Furthermore, the "Hold Values" table in the top right corner provides specific numerical values for variables C, D, and E, namely 35, 30, and 65, respectively. These values likely represent constants or fixed parameters within the experimental setup, influencing the behavior of A and B in relation to compressive strength. In summary, the surface plot highlights the interplay between variables A and B and their effect on compressive strength. The visualization suggests that higher values of A and lower values of B contribute to stronger compressive strength in the cement concrete mixture, providing valuable insights for optimizing concrete formulations to achieve desired strength characteristics.

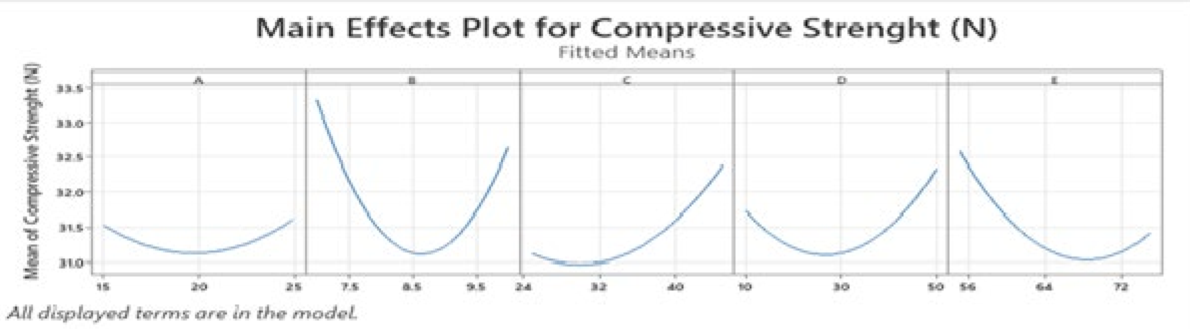

Figure 8: The Main Effects Plot for Compressive Strength

The Main Effects Plot for Compressive Strength in figure 8 with Fitted Means provides insights into the impact of different scenarios labeled A to E on the compressive strength of the material. Although the variable represented on the x-axis is unspecified in the image, it is evident that each scenario corresponds to a specific value of this variable, with the y-axis representing the mean compressive strength in N/mm^2.

Each scenario exhibits a U-shaped curve, starting from a low point, rising to a peak, and then decreasing. This characteristic curve shape indicates that there are optimal values of the variable where compressive strength is maximized.

Scenario A: The curve peaks around a certain value of the variable, suggesting an optimal point where compressive strength reaches its highest level.

Scenario B: Similar to scenario A, but with a different peak, indicating another optimal value of the variable that maximizes compressive strength.

Scenario C: In contrast to scenarios A and B, the curve for scenario C is relatively flat, implying less sensitivity to changes in the variable and a more consistent compressive strength across different values.

Scenario D: This scenario exhibits another peak, albeit at a different value of the variable, signifying a different optimal point for maximizing compressive strength.

Scenario E: In this scenario, the curve shows a gradual decline, indicating that increasing or decreasing the variable leads to a decrease in compressive strength.

The text at the bottom of the plot states that "All displayed terms are in the model," suggesting that the graph represents the effects of specific terms within a statistical model. This implies that the observed variations in compressive strength across different scenarios are accounted for by the terms included in the model, providing a comprehensive understanding of the factors influencing compressive strength in the material.

The main plot in Figure 9 titled "Interaction Plot for Compressive Strength (N)" with a subtitle "Fitted Means." Within the main plot, there were nine smaller plots, each representing interactions between two variables (e.g., AB, AC, BC, AD, BD, CD, AE, BE, and C*E). The Y-axis represented the mean compressive strength in Newtons, ranging from approximately 30 to 35. The X-axis corresponded to the values of variables A to E, each with specific numeric scales. Legends on the right side indicated values associated with line styles and colors. A note at the bottom stated: "All displayed terms are in the model." This suggested that the graph represented the effects of specific terms within a statistical model, providing insights into the interactions between different variables and their impact on compressive strength.

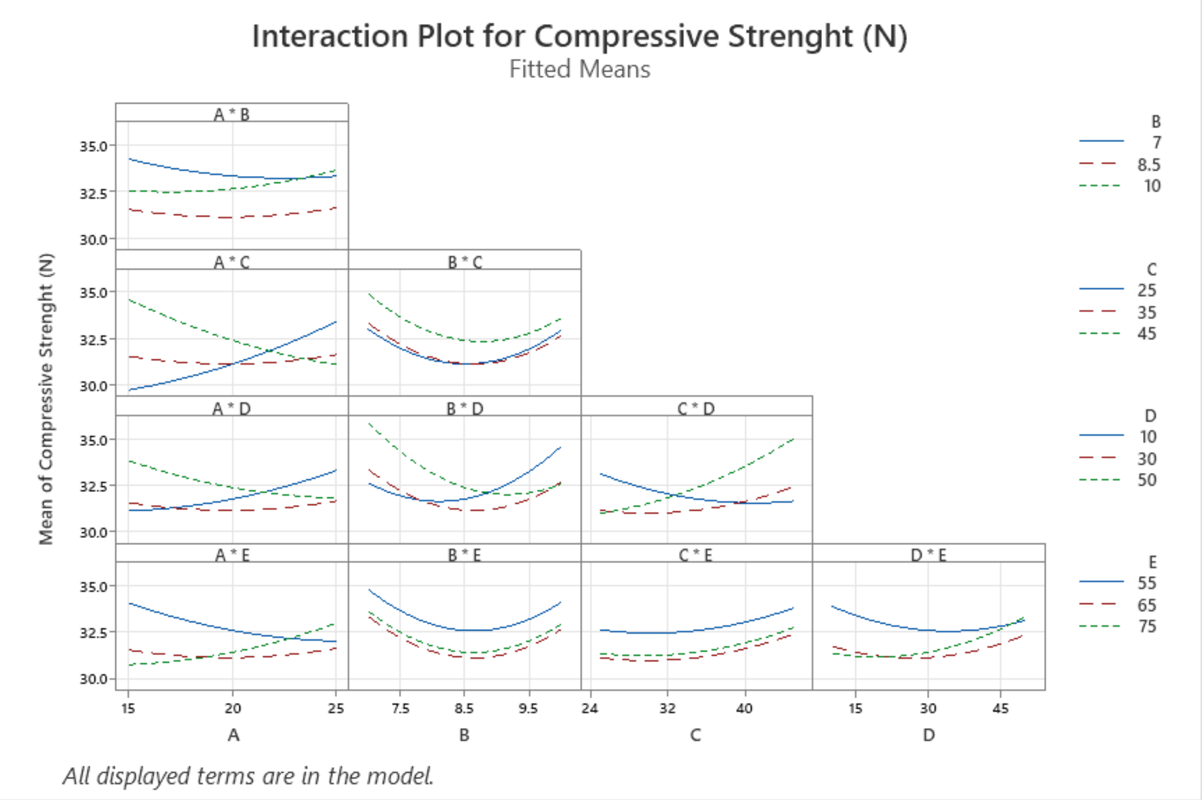

Figure 9. Interaction Plot for Compressive Strength

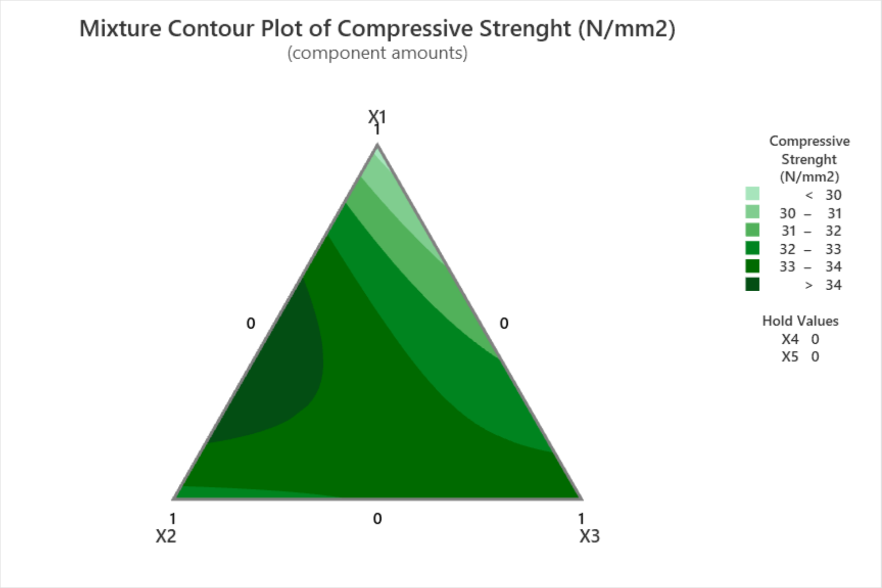

Figure 10. Mixture Contour Plot of Compressive Strength (N/mm^2)

The main plot is titled "Mixture Contour Plot of Compressive Strength (N/mm^2)" with a subtitle "(component amounts)." Within the plot, a triangular representation is observed, with each corner corresponding to a component labeled as X1, X2, and X3. The varying shades of green filling the triangle indicate different levels of compressive strength, with darker greens representing higher strengths. The Y-axis denotes the mean compressive strength in N/mm^2, ranging from approximately 30 to 34. A legend on the right side explains that lighter greens signify lower compressive strengths (around 30 N/mm^2), while darker greens indicate higher strengths (around 34 N/mm^2). Hold values are listed for X4 and X5, both set to 0. This plot visually depicts the relationship between these components and their effect on compressive strength. Practical Application: Engineers or researchers can utilize this information to optimize the mixture of components for achieving the desired compressive strength in materials. By adjusting the proportions of X1, X2, and X3, they can enhance the material's performance.

Optimization of Compressive Strength Using Box Behnken's Model

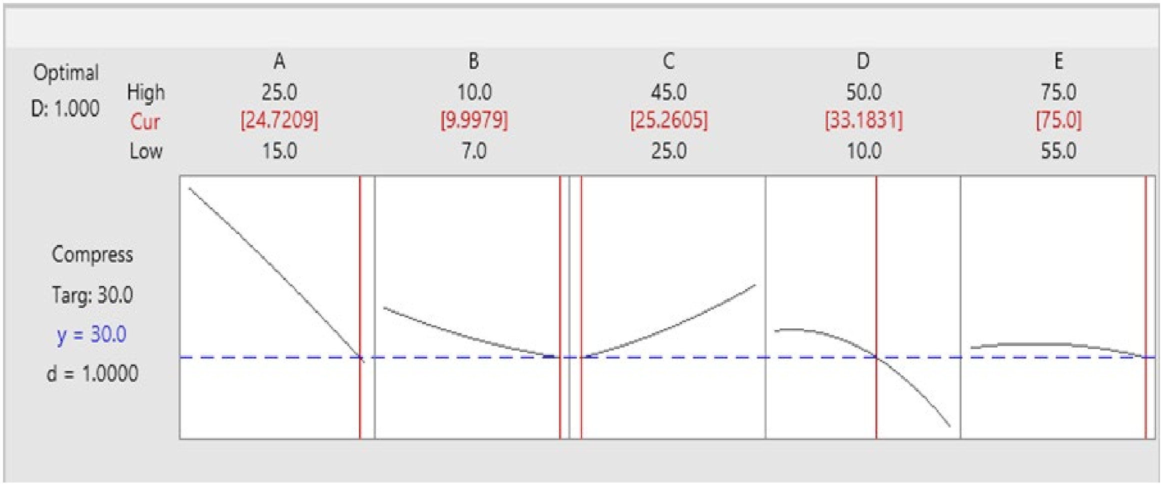

Figure 11. Optimization Results of Compressive Strength Using Box Behnken's Model

The graph presented in Figure 11 illustrates the ideal blend proportions for maximizing compressive strength in concrete, with distinct sections representing Water, Cement, Sand, RAP (Reclaimed Asphalt Pavement), and Coarse Aggregates, expressed in percentages. Each material level—High, Optimal, and Low—represents the required quantities for achieving varying compressive strength outcomes. The blue dashed line signifies the optimal mix, resulting in approximately 30.00 N/mm² of compressive strength. The decision to employ the target strength approach in optimization using Minitab for the Box-Behnken model is founded on a practical assessment of experimental data and the quest for a feasible solution (Hari & Mini, 2023). Given that most experimental values cluster around 30 N/mm², opting for a maximization approach often yields excessively high values, potentially straying from practical feasibility. By setting a target strength, the optimization process seeks to align with observed experimental trends, ensuring that the optimized solution remains within realistic and attainable parameters. This approach mitigates the risk of overestimation or underestimation of the desired outcome, thereby enhancing the reliability and applicability of the optimization process for concrete mix design. Specifically, at 30 N/mm², the optimal proportions were found to be 24.72% for A, 9.99% for B, 25.26% for C, 33.18% for D, and 75% for E. To obtain the actual values, this result will be adjusted to 100% constraint and then proportioned accordingly to match experimental realities, in this context, the results yields 14.68% for A, 5.94% for B, 15.00% for C, 19.69% for D, and 44.69% for E.

Conclusion

In conclusion, this study has investigated the potential of reclaimed asphalt pavement aggregates (RAP) in enhancing the sustainability of concrete production while optimizing its compressive strength. Through the utilization of advanced modeling techniques such as the Box-Behnken design, we systematically varied parameters including RAP substitution percentage, water-cement ratio, and curing time to predict and optimize compressive strength. Our findings suggest that RAP incorporation can indeed improve the sustainability of concrete mixes without compromising structural integrity or durability. The developed empirical models accurately forecast compressive strength under diverse conditions, providing valuable insights into the feasibility and effectiveness of RAP incorporation in concrete mixes. These results hold significant implications for engineers and practitioners seeking to optimize concrete compositions for specific performance requirements while advancing sustainable construction practices and reducing environmental impact. Ultimately, this research contributes to the growing body of knowledge on sustainable construction materials and practices, paving the way for more environmentally friendly and resilient infrastructure in the future.

Recommendations

To advance research and practical applications in sustainable concrete production using reclaimed asphalt pavement aggregates (RAP), several recommendations are proposed. Continued research efforts should focus on long-term performance and durability assessments of RAP concrete, alongside exploration of optimization techniques to refine mix design processes. Comprehensive material characterization is essential to understand RAP aggregate properties fully. Standardization efforts are necessary to establish clear guidelines for RAP concrete usage, while industry collaboration can facilitate technology transfer and knowledge dissemination. Education and training programs should be developed to raise awareness among construction professionals, while supportive policies and incentives are crucial to incentivize the adoption of RAP concrete in construction projects. Through concerted efforts across research, industry, and policy spheres, the widespread adoption of RAP aggregates in concrete production can be promoted, fostering sustainability and resilience in infrastructure development.

Acknowledgments: *The authors, extends gratitude to all authors whose research laid the foundation for this study.*
Funding: *No external funding was obtained for this study.*
Conflict of Interest: *The author declares no conflict of interest.*

References

Asadzadeh S, Khoshbayan S, (2018) Multi-objective optimization of influential factors on the production process of foamed concrete using the Box-Behnken approach. *Constr. Build. Mater.* **170**, 101–110. https://doi.org/10.1016/j.conbuildmat.2018.02.189

Dai C, Wu A, Qi Y, Chen Z, (2019) The optimization of mix proportions for cement paste backfill materials via Box–Behnken experimental method. *J. Inst. Eng. India Ser. D*, **100**(2), 307–316. https://doi.org/10.1007/s40033-019-00180-7

Guo L, Guo Y, Zhong L, (2022) Research on the back analysis and failure mechanism of recycled concrete aggregate meso-parameters based on Box-Behnken Design response surface model. *J. Build. Eng.* **51**, 104317. https://doi.org/10.1016/j.jobe.2022.104317

Hari R, Mini KM, (2023) Mechanical and durability properties of basalt-steel wool hybrid fiber reinforced pervious concrete – A Box Behnken approach. *J. Build. Eng*. **70**, 106307. https://doi.org/10.1016/j.jobe.2023.106307

Kumar R, (2020) Modified mix design and statistical modelling of lightweight concrete with high volume micro fines waste additive via the Box-Behnken design approach. *Cem. Concr. Compos.* 113, 103706. https://doi.org/10.1016/j.cemconcomp.2020.103706

Lam MN-T, Le D-H, Nguyen D-L, (2023) Reuse of clay brick and ceramic waste in concrete: A study on compressive strength and durability using the Taguchi and Box–Behnken design method. *Constr. Build. Mater*. **373**, 130801. https://doi.org/10.1016/j.conbuildmat.2023.130801

Li H, Zhang L, Liu J, Chu F, Tian Y, (2023) Study on the characteristics of composite recycled aggregate concrete based on Box–Behnken Design Response Surface Model. *Fractals Fract*. **7**(9), 648. https://doi.org/10.3390/fractalfract7090648

Liu H, Liu S, Wang S, Gao X, Gong Y, (2019) Effect of mix proportion parameters on behaviors of basalt fiber RPC based on Box-Behnken model. *Appl. Sci*. **9**(10), 2031. https://doi.org/10.3390/app9102031

Maaze MR, Shrivastava S, (2023) Design optimization of a recycled concrete waste-based brick through alkali activation using Box-Behnken design methodology. *J. Build. Eng*. **75**, 106863. https://doi.org/10.1016/j.jobe.2023.106863

Michael T, (2021) Characterization of Reclaimed Asphalt Pavement and Optimization in Polymer Modified Asphalt Blends: A Review. *J. Civ. Eng. Beyond Limits (CEBEL)*. **2**(2), 27–34. https://doi.org/10.36937/cebel.2021.002.004

Özgen S, Yıldız A, (2010) Application of Box–Behnken design to modeling the effect of smectite content on swelling to hydrocyclone processing of bentonites with various geologic properties. *Clays Clay Miner*. **58**(3), 431–448. https://doi.org/10.1346/ccmn.2010.0580312

Pradani N, Irmawaty R, Tjaronge MW, Rahim IR, (2023) The effect of recycled material and Buton granular asphalt (BGA) on asphalt concrete mixture performance. *Civ. Eng. J.* **9**(6), 1412–1426. https://doi.org/10.28991/cej-2023-09-06-09

Taha R, Al-Harthy A, Al-Shamsi K, Al-Zubeidi M, (2002) Cement Stabilization of Reclaimed Asphalt Pavement Aggregate for Road Bases and Subbases. *J. Mat. Civ. Eng.* **14**(3), 239–245. https://doi.org/10.1061/(asce)0899-1561(2002)14:3(239)

Tavva TL, Reddy KS, (2024) Corrigendum to 'A mechanistic-empirical approach to estimate the degree of reclaimed asphalt pavement (RAP) bitumen activity'. *Constr. Build. Mater.* **400**, 132912. https://doi.org/10.1016/j.conbuildmat.2024.135533

Tiza M, (2022) Sustainability in the civil engineering and construction industry: A review. *J. Sustain. Constr. Mater. Technol*. https://doi.org/10.14744/jscmt.2022.11

Tiza MT, (2023) Integrating sustainability into civil engineering and the construction industry. *J. Cem. Based Compos.* **4**(1), 1–11. https://doi.org/10.36937/cebacom.2023.5756

Tiza TM, Kpur G, Ogunleye E, Sharma S, Singh SK, Likassa DM, (2023) Enhanced industrial applications of functionalized nanomaterials. *Mater. Today Proc. Elsevier*.

Tiza TM, Mogbo O, Singh SK, Shaik N, Shettar MP, (2022) Bituminous pavement sustainability improvement strategies. *Energy Nexus* **6**, 100065. https://doi.org/10.1016/j.nexus.2022.100065

Xiao F, Amirkhanian S, Juang CH, (2007) Rutting Resistance of Rubberized Asphalt Concrete Pavements Containing Reclaimed Asphalt Pavement Mixtures. *J. Mat. Civ. Eng*. **19**(6), 475–483. https://doi.org/10.1061/(asce)0899-1561(2007)19:6(475)

Yaro NSA, et al., (2023) A comprehensive overview of the utilization of recycled waste materials and technologies in asphalt pavements: *Towards environmental and sustainable low-carbon roads.* Processes **11**(7). https://doi.org/10.3390/pr11072095

Yryshkin I, (2022) Influence of the regenerated road concrete mix on the wheel tracking of highways. Transportnye Sooruženiâ **9**(4). https://doi.org/10.15862/09sats422

J. Int. Environmental Application & Science, Vol. 20: 70-79 (2025)
Research Paper

Investigation of Effect of Aluminium Oxides Nanoparticles on Some Rheological Properties of Water Based Mud

Igbinere, Sunday Agbons[1,*]; Oisakede, Maureen Olere[2]

Department of Petroleum Engineering, University of Benin, Benin City, Nigeria[1]; Department of Materials and Metallurgical Engineering, University of Benin, Benin City, Nigeria[2]

Received February 10, 2025; Accepted March 3, 2025

Abstract: The success of well-drilling operations is heavily dependent on the drilling fluid because, it cools down and lubricates the drill bit, remove cuttings, prevent formation damage, suspend cuttings and cake off the permeable formation, thus retarding the passage of fluid into the formation. Drilling through subsurface formations with induced and natural fractures attracts huge drilling fluid losses that lead to higher operational expenses. It is therefore vital to design the drilling fluid in such a way that minimizes the mud invasion into formation to prevent lost circulation. This research investigates the effects of a nano base fluid as additives on the rheological properties of water base mud. Baravis and polyanionic cellulose (PAC) were also used as additives and added to fresh water-based mud. The nano base fluid was obtained from aluminium oxide nanoparticles (Al_2O_3 NPs) and its effects on rheological properties of water-based mud were compared with water based mud mixed with baravis and polyanionic cellulose. The laboratory measurements included measuring filtrate losses and some rheological properties as well as filtration properties of water-based nano mud and local additives drilling fluids under static conditions. The lowest filtrate loss value of 14.4ml occurred for an addition of 1.0g of aluminium oxide nanoparticles without any additional materials or additives, and this result was obtained when Al_2O_3 NPs was acting as the loss circulation materials. More than 70% reduction in fluid loss was achieved in the presence of 0.5-2.0 grams of Al_2O_3 NPs. These results have also shown that the filter cake developed during the nano and local additives-based drilling fluid filtration was thin, which implies high potential for reducing the differential pressure sticking problem, formation damage and torque and drag problems while drilling. Nano-based drilling fluid with specific characteristics is thus expected to play a promising role in solving the circulation loss and other technical challenges faced with commercial drilling fluid during oil and gas drilling operation in any subsurface formation.

Keywords: *Aluminum Oxide Nanoparticle, Water Based Mud, Baravis, Polyanionic Cellulose, Rheological Properties,*

Introduction

The production of hydrocarbon fluids from subsurface formations requires drilling and completing a well into the reservoir. The drilling operation of a well involves the application of drilling fluid, which may be water, oil, air or synthetic base fluid. The importance of drilling fluids in drilling a well or hole cannot be overemphasized and its application in recent times has necessitated further study in getting appropriate

**Corresponding: E-Mail: agbons.igbinere@uniben.edu, Tel: +234 09070858395*

drilling fluid properties that bring about improve process of drilling a well through various hole conditions or materials present at different depths. Anyanwu and Unubi (2016) studied the impact of aluminium oxide nanoparticles size distribution on filtration lost in drilling fluid. The application of drilling fluid in drilling an oil and gas wells is very key to the sustainability of the important role played by the drilling fluid during borehole construction. Nanoparticles can also be applied as fluid loss additives in a surfactant polymer-based drilling fluid (Srivatsa & Ziaja 2011). The drilling fluids used when drilling subsurface formations must keep the hole clean by removing cuttings and other debris, suspend the cuttings when the need arises, cool the drill bits, maintain the needed hydrostatic pressure to prevent the flow of reservoir fluids into the bottom of the well. The type of drilling fluid adopted is a function of the subsurface location, because different formations have different interactions with the constituents of the drilling fluids, and this led to loss circulation and filtration loss as well as other related issues associated with drilling fluids in subsurface formations.

The challenges from drilling fluids in deep waters, harsh formation associated with high pressure and high temperature will always attracts more research into better ways of drilling and into high performance drilling fluids appropriate for different subsurface formations, and these operations in deep waters has attracted advancing technologies (Smith et al., 2018). The growing demand for more oil and gas reserves has necessitated the drilling of more wells (Smith, 2001) in unconventional locations (Xu et al., 2017), and the need for high performing drilling fluids is on the increase. Often, oil-based muds are applied in deep waters because of the high pressure and high temperature (HPHT) associated with it, and has a better performance in HPHT environment when compared to water-based muds. However, the high costs associated with the use of oil based muds, and the environmental concerns of such oil base fluids are the major drawbacks why operators seek for alternative drilling fluids in drilling through the reservoir location in recent time. Amarfio and Abdulkadir (2016) and Aybar *et al*., (2015) focused on the thermal stability of water-based mud with added aluminium oxide NPs, while (Bybee 2001; Elward-Barry and Thomas 1994) looked at the application of nanotechnology in oil and gas deep-water drilling and ultra-deep formations.

This work focusses on the investigation of the formulation of potential application of nano-fluid obtained from the mixture of aluminium oxides nanoparticles and water based mud in HPHT reservoir conditions as well as low pressure and low temperature. Smith *et al*., (2018) stated that offshore exploration drilling and appraisal wells are among the highest capital costs, it cost as high as 60% in the development of an oil field. Adding nano materials to drilling fluids is aimed at increasing wellbore stability and drilling efficiency by enhancing the rheological properties of the drilling fluid at low pressure and low temperature, which reduces drilling cost (Mao *et al*., 2015; Shaughnessy *et al*., 2003). This is achieved through reduced filtration of drilling fluids (reduced filter cake thickness) which can prevent differential sticking, improved rheological properties that affect the transport of cuttings to the surface, reduced friction and hence lower torque and drag on the drill pipes, and reduced wear during horizontal and directional drilling operations. Drilling problems were reduced by using synthesized nanoclays in drilling fluids formulation (Abdo and Haneef, 2013). Furthermore, nanoparticles can improve heat transfer properties of drilling fluids which will reduce thermal degradation of down-hole equipment. Lower drilling costs through the use of nanoparticles instead of expensive additives would then allow drilling operations to become economically viable.

Materials and Methods

This research focused on the use of aluminium oxides nanoparticles (Al_2O_3 NPs) in the formulation of different concentrations of mud samples, other materials include baravis and polyanionic cellulose (PAC) and both materials were used as additives to fresh water-based mud. The powder form and scanning electron microscope (SEM) image as shown in figure 1 (Hawraa *et. al*. 2020; Smith *et al*., 2018), represent aluminium oxide nanoparticles and have hydrophilic surfaces; it is chemically inert, non-toxic, hard and tough, it has been widely used in high performance materials as fillers to increase toughness, ductility scratch resistance and also as an absorbent material for thermocouples (Ogolo and Onyekonwu, 2022). Furthermore, Al_2O_3 NPs have exceptional physico-chemical and structural features such as resistance to wear chemicals and mechanical stresses. They also have optical properties, low-cost preparation and easy handling and it is thermally stable, ductile, and is not flammable (Ogolo & Onyekonwu, 2022). It constitutes a good abrasive, adsorbent, low friction, composite and blasting material, presented in figure 1. It is a high-temperature component for heat resistance, a desiccant for drying gases, and is used as an electrical insulator, a catalyst carrier and adsorbent in the petroleum and chemical industries (Ogolo & Onyekonwu, 2022). The methodological concept applied and executed in this study is based on sample preparation of both water and nano based mud samples. These samples were subjected to several static periods and temperatures, and the rheological properties of these subjected mud samples were measured based on temperature and stability. The data used were local content materials easily manufactured and manipulated in the laboratory. These experimental procedures designed and adopted in this research is to help investigate standard procedural concepts to aid in the understanding and examining the data generated from laboratory condition. Water based drilling fluid samples were prepared based on the typical formulation currently used in drilling operations. Table 1 shows the water-based fluid (WBF) formulation with concentrations of aluminium oxide NPs with concentrations ranging from 0.5 wt% up to 2.0 wt%.

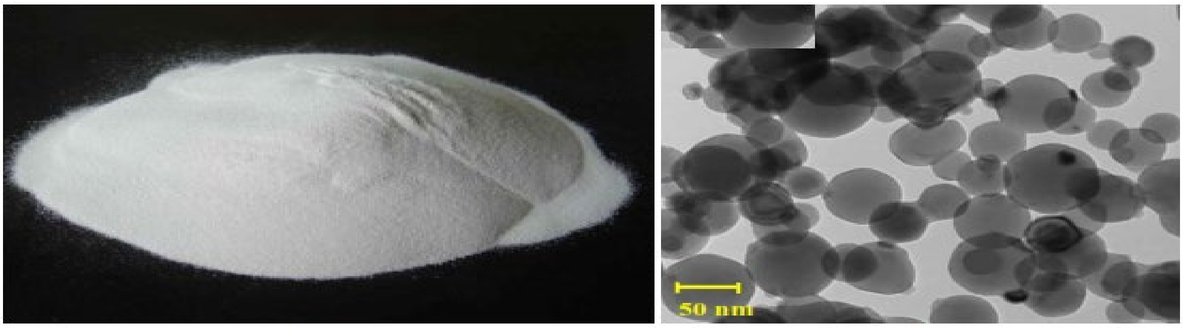

a **b**

Figure 1. Aluminum Oxide Nanoparticles Al_2O_3 (**a**) Powder (**b**) SEM Image (Hawraa *et. al*. 2020; Smith *et al*., 2018)

Experimental Procedures

Fresh water-based mud was prepared, and the sample preparation procedure involves stirring and mixing after adding each component (water, bentonite, barite) for 15 minutes (Smith *et al*., 2017). To improve the rheological properties of water-based fluids typically baravis and polyanionic cellulose (PAC) were added. Baravis and polyanionic cellulose added to the fresh water-based mud were in the concentration of 0.5g, 1.0g and 2.0g. Then modified samples with addition of Al_2O_3 NPs were prepared and their rheological (apparent viscosity, plastic viscosity, yield point, 10sec gel-strength and 10min gel-strength) and filtration properties were tested. The rheological properties of water-based mud sample were tested, before adding nanoparticles, and the concentration of nanoparticles that was used in formulating drilling fluid samples are 0.5g, 1.0g, and 2.0g and these measurements were done at room temperature. Metal oxides dispersed in distilled water are used for water based. Basic rheological properties were carried out such as mud weight, plastic viscosity, yield point, gel strength, filter cake thickness and filtrate loss. The application of filter press to investigate the filtration properties of these different water-based mud samples were done for normal pressure and normal temperature as well as that of high pressure and high temperature, taking into consideration the API standard for filtration test. The fresh water-based mud prepared was the reference sample, while three samples each from baravis, polyanionic cellulose and aluminium oxide nanoparticles where formulated, making it a total of ten samples of mud used in the investigation.

Rheological Model Applications

The approach for this research requires the determination of some of the rheological properties of the different samples prepared and these samples include fresh WBM, fresh WBM containing baravis as additives, fresh WBM containing polyanionic cellulose additives and fresh WBM containing Al_2O_3 NPs. Some properties measured in laboratory conditions were used to determine the apparent viscosity (AV), plastic viscosity (PV) and yield point (YP). Equations 1 to 4 were used to generate the rheological properties as presented in table 1.

$$\beta = \frac{RPM_{600}}{2} \quad (1)$$

$$\alpha = RPM_{600} - RPM_{300} \quad (2)$$

$$\sigma = RPM_{300} - PV \quad (3)$$

$$\tau = k\gamma^n \quad (4)$$

Where β is the apparent viscosity (AV), α is the plastic viscosity (PV), σ is the yield point (YP), while RPM_{300} and RPM_{600} are the revolutions per minute at 300 and 600 respectively. Also, τ is the shear stress ($1bf/100ft^2$), k is the consistency index ($Pa\text{-}S^n$), γ is the shear rate (S^{-1}) and n is the flow behave index (dimensionless). The apparent viscosity was calculated based on the experimental effects of the measured 600 revolutions per minute (RPM_{600}) for the different samples of water base mud, while the PV were calculated based on the 600 revolutions per minute (RPM_{600}) and 300 revolutions per minute (RPM_{300}), also from the mud samples already prepared. Furthermore, YP were calculated based on the 300 revolutions per minute (RPM_{600}) together with already calculated value for PV. While equation 4 is referred to as the power law model, lower values of 'n' are an indication of a more non-Newtonian behaviour or a shear thinning fluid and Increasing values of the consistency index (k) imply an increased annular viscosity, and thereby an increased hole-cleaning capacity (William *et al*., 2014).

Results and Discussions

The results obtained as presented here in table 1 are some of the rheological properties for the different samples, which include the plastic viscosity, apparent viscosity, yield point, gel strength as well as the corresponding power law data for each of the properties measured and calculated. The charts presented in figure 1 to 6 described the influence of the different concentration of the Al_2O_3 NPs on the apparent viscosity and the plastic viscosity as well as on the yield point, including samples of fresh mud, fresh mud with additives such as polyanionic cellulose (PAC), baravis and Al_2O_3 NPs. After a careful survey of some research questions during the study, the data had to been filtered out and presented in a proper landscape for easier identification and explanation. And to fully fulfil the demands of this research, some laid down outlines would be followed through, these outlines best demonstrate the focus of this study. The experimental results of fresh muds and muds formulated using aqua gel (baroid) bentonite clay with Al_2O_3 nanoparticles additives and PAC and baravis is as given below in table 1. The results were compared with a base case drilling fluid with no nanomaterial, and they showed that there is an optimum concentration for aluminium oxide nanoparticles that can be used to improve the rheological and filtration properties of drilling fluids. These results demonstrated that nano-enhanced drilling fluids have an improved thermal stability at heightened temperatures and can withstand the harsh conditions in advanced drilling operations while they impose a lower environmental impact and capital costs.

Table 1. Rheological Properties of the Different Water Based Mud Samples

Mud Rheological Properties	Samples									
	Fresh Mud (Control)	Mud + PAC			Mud + BARAVIS			Mud + Al_2O_3		
		0.5g	1.0g	2.0g	0.5g	1.0g	2.0g	0.5g	1.0g	2.0g
pH	7	6.5	6.5	6.5	6	6	6	5	5	5
600 rpm	23	151	245	>300	115	90	163	120	137	147
300 rpm	12	110	184	>300	101	62	76	80	120	102
200 rpm	9	93	159	286	67	47	60	70	114	74
100 rpm	5	69	123	245	46	32	43	56	103	64
6 rpm	1	31	60	141	17	14	25	40	41	34
3 rpm	0.5	28	54	131	15	13	23	40	34	23
10 sec Gel (lb/100ft^2)	2	38	58	123	38	28	41	34	31	31
10 min Gel (lb/100ft^2)	11	80	113	162	77	38	72	54	47	39
P.V.	11	41	61	69	14	28	87	40	17	45
A.V.	11.5	75.5	122.5	150	57.5	52	81.5	60	68.5	73.5
Y.P.	1	69	123	73.00	87.00	34	21	40	103	57
Power law (n)	0.94	0.46	0.41	-	0.19	0.54	1.1	0.58	0.19	0.53
Consistency (k)	0.17	31.85	73.07	-	157.52	10.9	0.48	11.0	187.6	19.1

The effect of different mud samples with nanoparticles of different concentration on some rheological properties are presented below. These behaviours help in understanding the responses associated to increase or reduction of the nanoparticles concentration, and the composition of the muds in terms of the additives is also shown in figure 2 to 8.

Plastic Viscosity

The result shows that the plastic viscosity of water-based drilling fluid reduces after exposed to 250°F. Figure 2 shows that the trend of mud sample decreases when the concentration Al_2O_3 NPs increases. However, the plastic viscosity of water-based drilling fluid with aluminum oxide nanoparticles was found to be 23 centipoises (cp), which is slightly higher than the controlled sample (fresh mud) without nanoparticles.

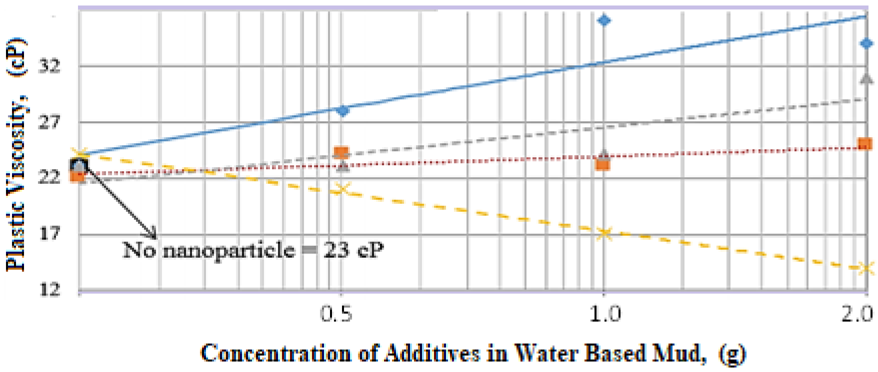

Figure 2. Effect of Baravis, Polyanionic Cellulose and Al_2O_3 NPs Concentration on Plastic Viscosity

Nanoparticles consist of large surface areas per volume, and it will increase the interaction of the nanoparticles with the matrix and surrounding water-based drilling fluid. This surface area may serve as sites for bonding with functional groups can influence chain entanglement and thus can generate a variety of properties in the matrix. Thus, the nanoparticles and base fluid may be linked or bonded together directly or through certain intermediate chemical linkages to improve the plastic viscosity of water-based drilling fluid.

However, repulsive force occurs between aluminium oxides nanoparticle and water molecular, thus is caused the plastic viscosity to reduce as concentration increase due to greater repulsive force occur. In drilling fluid, it will maintain viscosity of drilling fluid at high pressure and high temperature. Then, the rheological behaviour may depend on the particle type, size, and concentration and interparticle distance of nanoparticles with the fluid because of the large surface area of nanoparticles compared to micron-sized and larger particles. For example, only about 1 lb/gal of nanoparticles may do the job of 10 lb/gal of other materials. The reduced solid volumes with increased surface area would thus help maintain equivalent viscosities of drilling fluids.

Yield Point

Figure 3 shows the effect of nanoparticle concentration on yield point in water-based drilling fluid. The yield point of aluminium oxide increases as nanoparticle concentration increases. The higher yield point of the nano-based fluid will provide better dynamic suspension of drilling cuttings and efficient cleaning of the wellbore while drilling.

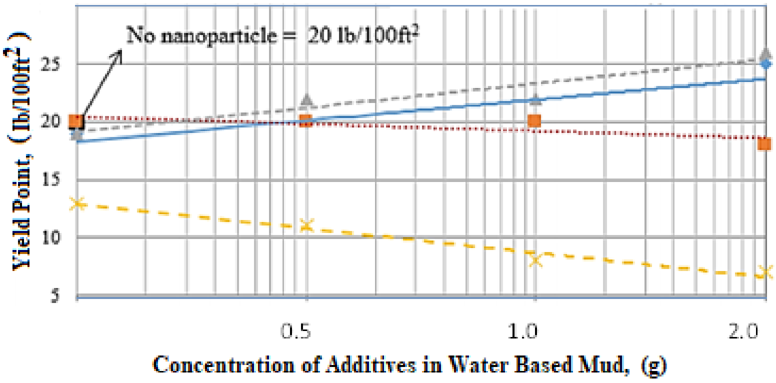

Figure 3. Effect of Baravis, Polyanionic Cellulose and Al_2O_3 NPs Concentrations on Yield Point

Gel Strength

The results in figures 4 and 5 show the effect of aluminium oxide nanoparticles on gel strength at different concentrations at 10 seconds and 10 minutes respectively. aluminium oxide shows an increasing trend as concentration increased. This phenomenon occurs due to the electrostatic force between the nanoparticles that the attractive force causes the nanoparticles link together with base fluid within 10 sec and 10 min period to form a rigid structure, thus it will increase the gelling effect. This trend, however, was not followed by other drilling fluid samples where gel strength was found to reduce gradually as concentration increased.

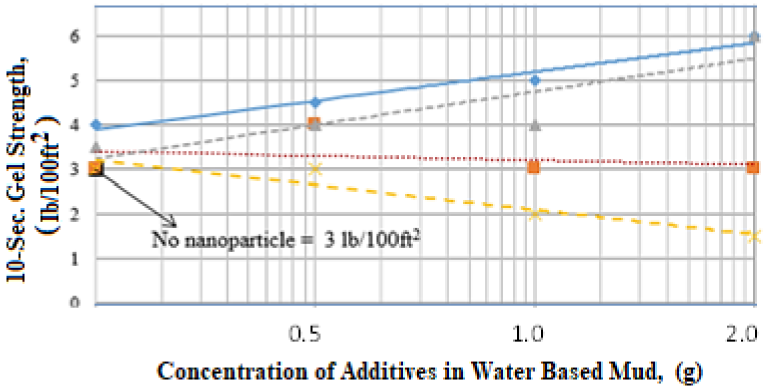

Figure 4. Effect of Baravis, Polyanionic Cellulose and Al_2O_3 NPs Concentrations on Gel-Strength (10-sec)

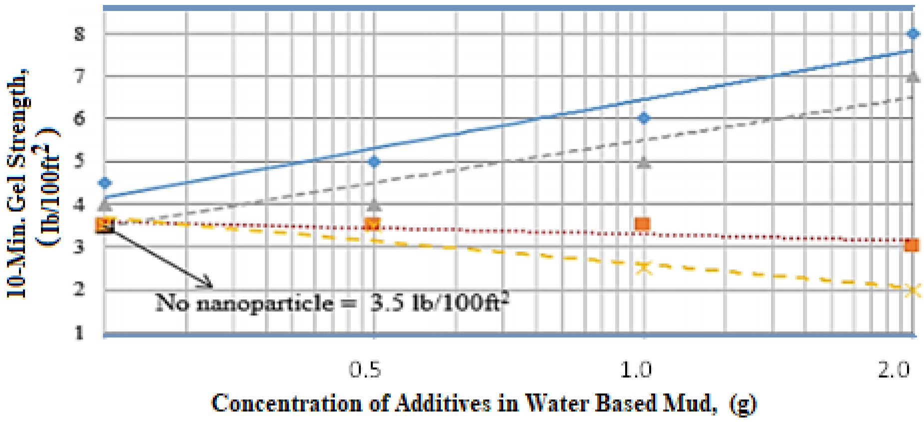

Figure 5. Effect of Baravis, Polyanionic Cellulose and Al_2O_3 NPs Concentrations on Gel-Strength (10-min)

Apparent Viscosity

The one half of the dial reading of the RMP_{600} is presented in table 1, the results showed that there is a corresponding increase in the apparent viscosity as the concentration of aluminium oxide nanoparticles increases as presented in figure 6, and this is also observed when baravis and polyanionic cellulose were added to the fresh water-based mud. This trend is like what was obtained in other rheological properties. This is connected to the ability of the based fluid to enhance intermolecular forces in the nano fluid, and this leads to high and effective resistance to flow and the high surface area lead to an increase interactions with water based mud. The polyanionic cellulose has faster impacts on the apparent viscosity when compared with other two mud samples gotten from the Al_2O_3 NPs and baravis. Furthermore, water-based mud containing baravis has the tendency to increase apparent viscosity with higher concentration of baravis additives

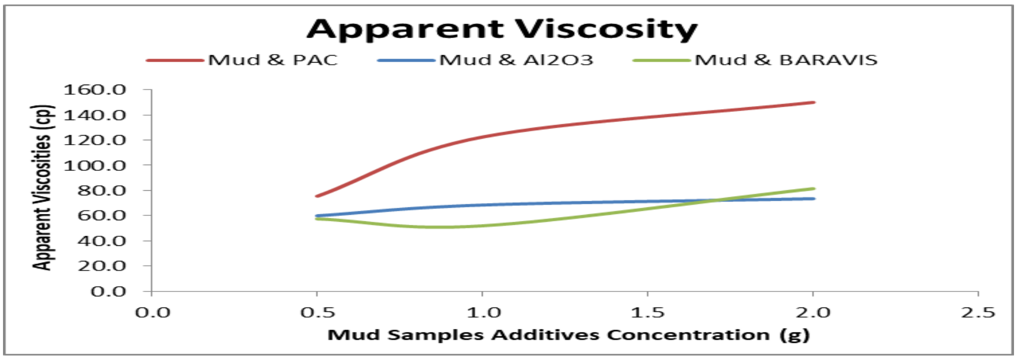

Figure 6. Apparent Viscosity of the three Mud Samples

High Pressure High Temperature Filtration Loss

The comparison of the HPHT fluid loss behaviour of the water base drilling fluid with different concentration of aluminium oxide nanoparticles is illustrated in Figure 7. An increased in nanoparticle concentration for mud sample gave lower filtration loss that shows a very good result. The dispersed mud sample acted as plaster between each particle, and consequently, seals the permeable filter cake at high temperature to reduce the filtration loss. The addition of metal oxide nanoparticles (aluminium oxide) is only good until 0.01 g and then increases after that value. Filtrate loss must be low enough to prevent excessive filter cake thickness and reduce the change of different pressure sticking.

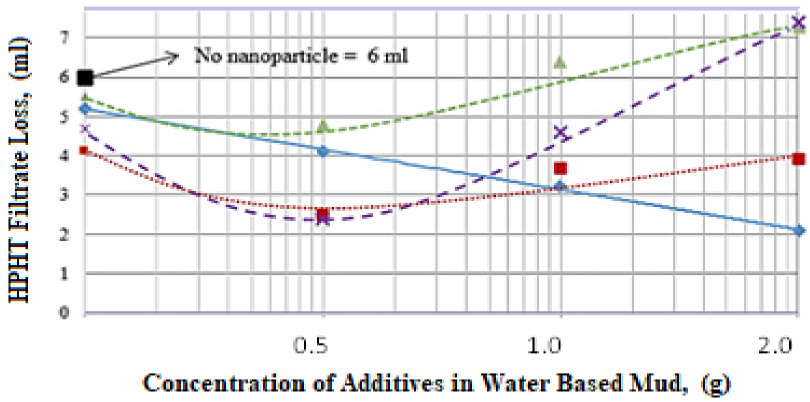

Figure 7. Effect of Baravis, Polyanionic Cellulose and Al_2O_3 NPs Concentrations on HPHT Filtration Loss

Filter Cake Thickness

Figure 8 illustrated the results of filter cake thickness of different water-based drilling fluid samples against the different concentration of aluminium oxides nanoparticles. Mud sample showed a decreasing trend where the filter cake thickness decreases when the concentration of mud sample increases. However, aluminium oxide showed similar trend where they reached the optimum value of 0.1 g and then increased sharply as the concentration increases.

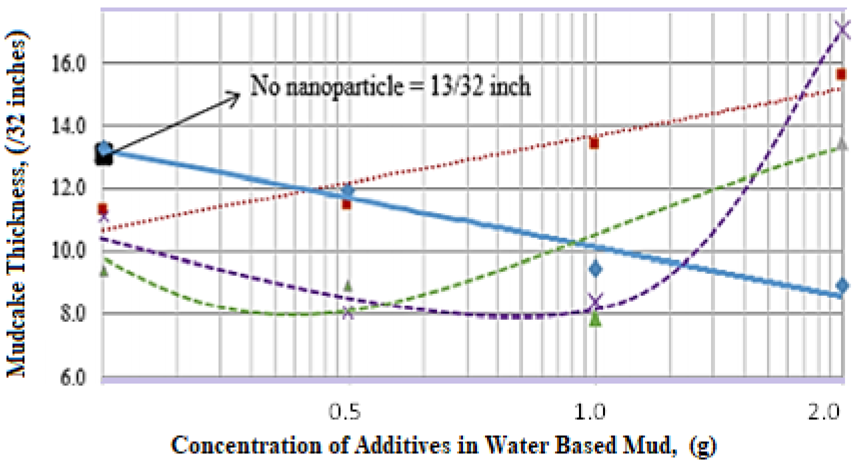

Figure 8. Effect of Baravis, Polyanionic Cellulose and Al_2O_3 NPs Concentrations on Filter Cake Thickness

Conclusion

This study has been able to show the effects of aluminium oxide nanoparticles on water-based mud and also when the baravis and polyanionic cellulose are added to act as anti-filtration loss materials. The determined rheological properties showed that the concentration of the different nano-fluids affect the properties of water based mud both at reservoir and laboratory conditions. The nano samples have favourable characteristics to hold cuttings under dynamic suspension and, aluminium oxide shows an increasing trend as concentration increased during the gel strength investigation for both 10 seconds and 10 minutes. This gel like structural behaviour will help the nano-based drilling fluid to prevent settling of cuttings and other solids from settling down during static periods. Furthermore, increasing the concentration of aluminium oxide nanoparticles leads to a reduction in filtration loss volume, and this filtration volume were also observed with the presence of baravis and polyanionic cellulose in fresh water-based mud. This behaviour of the nanofluid is connected to the high surface area of aluminium oxide nanoparticles because the viscosity of the nanofluid WBM is different from a fresh WBM. The thermal stability of the water based mud increased as a result of the addition of aluminium oxide nanoparticles when compared with reference samples. This was shown from the results presented in table 1 and in figure 1 through 6, the high pressure high temperature filtration outcome for the sample with aluminium oxide NPs had a reduced filtrate volume than the reference sample, and with this sample also showing some level of increase in shear stress for the sample with aluminium oxide NPs compared to the base sample (fresh water-based mud) during the rheological properties investigation. The following conclusion can be seen from this research study.

1. The lowest filtrate loss value of 14.4ml occurred for an addition of 1.0g of aluminium oxide nanoparticles and leads to a 70% reduction, suggesting that aluminium oxide nanoparticles can be used to reduce filtration loss of drilling fluids in subsurface or reservoir formation.
2. The addition of aluminium oxide nanoparticles and baravis and polyanionic cellulose in fresh water-based mud develop thin filter cake.
3. The rheological properties (apparent viscosity, plastic viscosity and yield point) and gel strength have direct relationship with aluminium oxide nanoparticles concentration.
4. Aluminium oxide nanoparticles have the tendencies to reduce filtration loss at high pressure high temperature and also at low pressure and low temperature.

Acknowledgement: *The authors of this work acknowledge the immense contributions of Mr. Elvis Oghenevwegba Ogheneovo of the Department of Petroleum Engineering, University of Benin, Benin City during the research stages of this work.*

Compliance with Ethical Standards *Ethical responsibilities of Authors: The authors have read, understood, and complied as applicable with the statement on "Ethical responsibilities of Authors" as found in the Instructions for Authors".*

Conflict of Interest: *The authors declare that they do not have any conflict of interest.*

Change of Authorship*: The authors have read, understood, and complied as applicable with the statement on "Ethical responsibilities of Authors" as found in the Instructions for Authors and are aware that with minor exceptions, no changes can be made to authorship once the paper is submitted.*

References

Abdo J, Haneef MD. (2013) Clay nanoparticles modified drilling fluids for drilling of deep hydrocarbon wells, *Appl. Clay Sci.,* **86**, 76-82. https://doi.org/10.1016/j.clay.2013.10.017

Amarfio EM, Abdulkadir M, (2016) Effect of Al_2O_3 Nanoparticles on the Rheological Properties of Water Based Mud. *Int. J. Sci. & Engin. Appl.,* **5**(1), 2016, 7–11. http://dx.doi.org/10.7753/ISEA0501.1002

Anyanwu C, Unubi MM, (2016) Experimental Evaluation of Particle Sizing in Drilling Fluid to Minimize Filtrate Losses and Formation Damage, paper presented at: *SPE Nigeria Annual International Conference and Exhibition*, 2-4 August 2016, Lagos, Nigeria. https://www.proceedings.com/32211.html

Aybar HS, Sharifpur M., Azizian MR., Mehrabi M, Meyer JP. (2015) A Review of Thermal Conductivity Models for Nanofluids. *Heat Transfer Eng.*, **36**(13), 2015, 1085-1110. https://doi.org/10.1080/01457632.2015.987586

Bybee K, (2001) Water-Based Drilling-Fluid Systems for Deepwater Norway, *JPT*, **53**(11), 2001, 36-36. https://jpt.spe.org/

Elward-Berry J., Thomas EW. (1994) Rheologically Stable Deepwater Drilling Fluid Development and

Application, Paper SPE-27453-MS Presented at *IADC/SPE Drilling Conference*, Dallas, Texas, 15-18. https://onepetro.org/SPEDC/94DC/conference/94DC

Hawraa KH, Ruba F A, Emad ME., Neda IM, (2020) Applications of Aluminum Oxide and Nano Aluminum Oxide as Adsorbents: Review. *Samarra J. Pure & App. Sci.*, **2**(2), 19-32. https://doi.org/10.2118/27453-MS

Mao H, Qiu Z, Shen Z, Huang W, Zhong H, Dai W, (2015) Novel Hydrophobic Associated Polymer Based Nano-Silica Composite with Core–Shell Structure for Intelligent Drilling Fluid under Ultra-High Temperature and Ultra-High Pressure. *Prog. Natural Sci.: Mat. Int.* **25**(1), 2015, 90-93. https://doi.org/10.1016/j.pnsc.2015.01.013

Ogolo NA, Onyekonwu MO, (2022) Potential Applications of Aluminum Oxide Nanoparticles in the Oil and Gas Industry, *J. Oil, Gas & Petrochem. Tech.*, **9**(1), 2022, 8-20. https://doi.org/10.22034/jogpt.2022.325676.1102 .

Shaughnessy JM, Romo LA, America BP, Soza RL, Resources B, (2003) Problems of Ultra-Deep High-Temperature, High-Pressure Drilling, Paper Presented at *SPE Annual Technical Conference and Exhibition*, 5-8 October 2003, Denver, Colorado, USA. https://onepetro.org/SPEATCE/03ATCE/conference/03ATCE

Smith JR, (2001) Energy Demand Creates New Opportunities and Challenges for Drilling. *Journal of Bulletin of Canadian Petroleum Geology*, **40**(05) https://doi.org/10.2118/01-05-DAS

Smith SR, Rafati R, Haddad AS, Cooper A, Hamidi H, (2018) Application of Aluminium Oxide Nanoparticles to Enhance Rheological and Filtration Properties of Water Based Muds at HPHT Conditions. *Colloids and Surfaces A: Physicochemical and Engineering Aspects*, **537**, 361-371 https://doi.org/10.1016/j.colsurfa.2017.10.050

Srivatsa JT, Ziaja MB, (2011) An Experimental Investigation on use of Nanoparticles as Fluid Loss Additives in a Surfactant-Polymer Based Drilling Fluids, paper presented at *International Petroleum Technology Conference*, 15-17 November 2011 Bangkok, Thailand. https://onepetro.org/IPTCONF/11IPTC/conference/All-11IPTC

William JKM, Ponmani S, Samuel R, Nagarajan R, Sangwai JS, (2014) Effect of CuO and ZnO Nanfluids in Xanthan Gum on Thermal, Electrical and High-Pressure Rheology of Water-Based Drilling Fluids. *J. Petrol. Sci. Eng,, Elsevier*, **117**, 15-27. https://doi.org/10.1016/j.petrol.2014.03.005

Xu JG, Qiu Z, Zhao X, Huang W, (2017) Hydrophobic Modified Polymer Based Silica Nanocomposite for Improving Shale Stability in Water-Based Drilling Fluids. *J. Petrol. Sci. Eng,* **153**, 325-330. https://doi.org/10.1016/j.petrol.2017.04.013

J. Int. Environmental Application & Science, Vol. 20: 80-87 (2025)
Research Paper

Impact of Programming Language on Air Quality Estimation[#]

Emre Dalkiliç[1, *], Şükrü Dursun[1];

[1,2]*Environmental Engineering Department, Engineering & Natural Sciences Faculty, Konya Technical University, Konya, Türkiye.*

Received March 13, 2025; Accepted March 19, 2025

Abstract: The world has started to gain extra awareness about human health and environmental health after the coronavirus outbreak. In parallel with the increasing environmental awareness, components such as the use of natural resources and the possibility of causing global environmental problems to have started to play an effective role in decision-making processes rather than the financial side of the projects that come to the agenda. States carry out various environmental policies through their ministries, such as preparing legislation on air quality protection and sources affecting air pollution, odor emissions, determining targets, principles, policies and strategies, determining, implementing and having implemented procedures, principles and criteria for the creation of air pollution maps and the preparation of clean air action plans. However, the current situation is no longer sufficient for policymaking, and it is necessary to foresee the future and take steps in this direction. Being able to see today through the eyes of tomorrow provides great convenience in combating problems before they reach the threshold of a crisis in military, political and economic terms as well as environmental terms. Machine learning, a sub-branch of computer science developed in the early 20th century from digital learning and pattern recognition studies in artificial intelligence, is a system that investigates the operability and writing of algorithms that can learn as a structural function and make predictions on data. Written algorithms are designed to learn, instead of following program instructions to the letter, to create data-based predictions from the inputs provided to the system and to act as a decision maker. In the future, there is a need for algorithms that can be written using programming languages to predict air pollution and to determine its effects on public health. Today, using machine learning methods to predict air pollution has become more popular with data and data processing capabilities, which are among the most invaluable capitals. In this study, studies on predictability of air pollution with programming languages will be presented.

Keywords: *Programming Languages, Air Pollution, Forecast, Algorithm*

Introduction

Air pollution, known as the cancer of our age and ranked first in the world problems, is a natural problem that affects humanity itself because of its desire to increase its level of welfare and live in a more comfortable environment. Although the unplanned and unprepared focus of the development and industrialization race that accelerated after the industrial revolution and focused solely on economy overshadowed environmental and environmental health problems for a while, air pollution that emerged over time has become a danger that we breathe, visible or invisible, physically, biologically or chemically, and that grows every day and will affect humanity at the cost of its life (Varınca *et al.,* 2008). Air pollution causes changes in air compounds in the atmosphere, climate change, acid rain, structural deterioration in the ozone layer, and the effects on human and wild environments. Factors such as locating residential and industrial areas without considering environmental factors (pressure, temperature, wind, humidity, precipitation, solar radiation, *etc.*) of settlements, inadequate green areas, inadequate pollutant control equipment used in industries, poor quality fuel used in vehicles and heating, and lack of maintenance and incomplete combustion of combustion devices used greatly affect air pollution in regions (Kampa & Castanas, 2008; Toros & Bağış, 2017; Yılmaz *et al.*, 2020). Artificial intelligence has become a frequently mentioned focus of attention in the media in the last few years. It is frequently encountered, especially in technology-focused publications, that it will be an indispensable

**Corresponding: E-Mail: emredalkilic95@gmail.com, Tel: +905051414994;*
[#]*This paper has been presented from Ph.D. Thesis of Emre Dalkılıç*

part of the future and can be adapted and used in every sector. Intelligent virtual assistants, unmanned land, air and sea vehicles, and chatbots are preparing humanity for an imaginary future. The idea of a world where labor will decrease and where we can realistically consult and get realistic ideas before or after starting any work foresees a sometimes frightening and sometimes promising future (Chollet & Chollet, 2021). Scientific research is always a pioneering resource in every subject and carries research forward. Compiling these facilitates our inferences on the subject. The aim of this study is to compile studies on the predictability of air pollution with machine learning methods and thus its place in environmental awareness. The accuracy of data for the future is a development that excites the scientific world.

Machine Learning

Intelligent Machines was a term that introduced the world to another area in the 1950s where machines were trying to be intelligent like us humans. This was the first step towards a new era. In 1948, Turing and Champernowne invented 'paper and pencil' chess. It was the world's first chess playing computer program. The first AI program that included learning was called "response learning program" and "shopping program" written by Anthony Oettinger in 1951. This was the main effort to learn machines (Shinde & Shah, 2018).

Machine Learning Steps

Vapnik and Cortes' reaching a definite result and robust assumptions with support vector machines in 1995 is remembered as the greatest first success of machine learning (Angra & Ahuja, 2017). Following those years, Freund and Schapire developed strengthened weak classifiers, also known as AdaBoost, in 1997. AdaBoost, in which each node is selected from a random subset of features and each of which is formed by a random subset of examples, was discovered by Breiman in 2001. As we approach the present day, Deep Learning systems began to develop and are currently widely used machine learning algorithms such as Naive Bayes (NB), k-Nearest Neighbor (k-NN), Decision Tree, Support Vector Machines (SVM), Bayesian Network, Random Forest, Linear Classifier, Artificial Neural Network (ANN), Logistic Regression and Bootstrap Aggregation (Bagging) (Singh *et al,* 2016). As of 2017, the products available are: Colaboratory (or "Colab" for short), Google Cloud AutoML, KNIME, TensorFlow, WEKA, Torch/Pytorch, RapidMiner, Azure Machine Learning Studio, Accord.NET, Scikit-Learn, Apache Singa, Shogun, Apache Mahout, Apache Spark MLib. Any machine learning application can be implemented using the above interfaces.

Air Pollution Forecasting Using Machine Learning Methods

The decrease in the cost of measuring air pollutants and the increase in environmental data and laboratory analysis data has increased the number of pollutant data sets from the past to the present. These set values have many results and complicated correlations. Traditional epidemiological models are becoming very complex and difficult to analyze and interpret the results of large data sets. As a result, in order to facilitate our understanding of the data, data mining and machine learning methods, which are not new but have an expanding scope of analysis methods, offer methods that perform well on similar problems, provide a wide perspective and are highly reliable (Bellinger *et al*., 2017).

Machine Learning Algorithms and Data Mining

The ever-evolving big data algorithm belongs to the prediction model. Choosing the prediction models that are created is a big issue on its own. In order to help those who are new to this subject and in the beginning stage in the application of machine learning algorithms, Domingos also discusses some important issues (Domingos, 2012). When choosing the algorithm, the programmer should consider the data complexity of the current problem, and the number of data sets available. For example, a complex, nonlinear classifier will be ineffective on a simple, linear classification problem. Large amounts of data will facilitate the use of advanced learning algorithms such as deep neural networks, but will also force users to consider questions about storage, memory, and training time (LeCun *et al.*, 2015).

As a result, it is widely understood that there is no magic bullet when it comes to choosing machine learning algorithms. From an implementation perspective, it is good practice to select a small, diverse set of algorithms from the paradigm of related methods, test them individually, and choose the one that best meets the performance goals. Alternatively, grouping several sets of models to create an ensemble of predictions has been shown to be an effective solution in theory and practice (LeCun *et al*., 2015). For example, an ensemble of neural networks, support vector machines, Gaussian processes, decision trees, and random forests were applied in the reviewed literatüre (Lary *et al*., 2014).

As a result of the research, the selected algorithms are tested on the existing data set. The resulting models are evaluated to select the model that gives the closest and lowest deviation to the correct result in the forward-looking prediction task. Data mining is the computational basis for the process of analyzing existing big data to solve a problem, determining the limits, revealing valid data and taking these into account to predict the consequences of future and yet unknown events.

Machine Learning, Artificial Intelligence, Mathematics, Database Systems and Statistics are multidisciplinary computational methods used in the estimation process. In addition to basic computational methods, it may be necessary to apply the data mining process and various preprocessing steps to be able to reach a conclusion. A post-processing stage is typically used to visualize the recognized patterns or the received information in an intuitive and easy-to-communicate way.

The most commonly used learning algorithms in air pollution epidemiology can be categorized as predictive or data mining methods (Köktürk *et al*., 2009). Value estimation is a frequently used area of data mining, as it involves determining variables from data taken from specific sample data sets and estimating different data sets considering them. Depending on the variables and structure of the application area, either a data mining algorithm that makes classifier predictions (k-means, k-medians, *etc*.) or numerical predictions (linear regression, MARS, *etc*.) will be selected.

Typical classification, numerical predictions and many methods are given in Table 1. The most appropriate method to choose the data mining method to be used to solve a problem encountered will be to try many algorithms repeatedly and choose the algorithm that gives the best performance values. In other words, prediction algorithms are generally initiated through a controlled learning process. Therefore, the aim is to make b predictions about a example of the target problem. For this, a parameterized function F: a → b is induced.

Table 1 Machine Learning Algorithms

No	**Deep Learning**	**Neural Networks**	**Regularization**
1	Boltzmann Machine	Perceptron	LASSO
2	Deep Belief Networks	Back-Propagation	Elastic Net
3	Convolutional Neural Network	Hopfield Network	Least Angle Regression (LARS)
4	Stack Auto-Encoders	Ridge Regression	
No	**Rule System**	**Instance Based**	**Clustearing**
1	Cubist	k-Nearest Neighbour	k-Means
2	One Rule (OneR)	LVQ	k-Medians
3	Zero Rule (ZeroR)	SOM	Expectation Maximization
4	RIPPER	LWL	Hierarchical Clustering
No	**Ensemble**	**Regression**	**Bayesian**
1	Random Forest	Linear Regression	Naive Bayes
2	GBM	OLSR	AODE
3	Boosting	Stepwise Regression	Bayesian Belief Networks (BBN)
4	Boorstrapped Aggregation (Bagging)	MARS	Gaussian Naive Bayes
5	AdaBoost	LOESS	Bayesian Network (BN)
6	Stacked Generalizationneralization	Logistic Regression	
7	GBRT		
No	**Decision Tree**	**Dimensionality Reduction**	
1	Classification and Regression Tree	PCA	
2	ID3	PLSR	
3	C4.5	Sammon Mapping	
4	C5.0	Multidimensional Scaling	
5	CHAID	Projection Pursuit	
6	Decision Stump	PCR	
7	Conditional Decision Trees	PLSDA	
8	M5	MDA	
9		QDA	
10		RDA	
11		FDA	
12		LDA	

For the value estimates to be continuous, it can be applied to real numbers such as b ∈ R, but also to integers such as b ∈ I. The most preferred algorithms in supervised learning algorithms are support vector machines, artificial neural networks, Bayesian methods and decision trees. The main reason why decision tree algorithms are shown as an effective classifier is that they have independent variables and rules. It creates a simple estimation method by dividing data sets into sections with the divide and conquer strategy. Nowadays, there are many methodologies and algorithms for machine learning. Machine learning is divided into three groups according to the learning method: Supervised, Unsupervised and Reinforcement.

Supervised Machine Learning Algorithms

Supervised machine learning algorithms are the most widely used algorithms among machine learning algorithms. In these model algorithms, the data scientist teaches the algorithm what results to produce in a teacher-like manner. The algorithm is trained with data sets with pre-labeled outputs, like a small child trying to learn the multiplication table by heart.

Supervised machine learning algorithms vary depending on the problem to be addressed. The algorithms we will choose for each problem differ from each other in terms of their features. Naive Bayes classifier, k-nearest neighbor, SVM (Support vector machines), Linear regression, Decision trees, Neural networks are some of the supervised learning algorithms.

Unsupervised Machine Learning Algorithms

In unsupervised learning, outputs are not included in the study. Observed units are brought together according to their similar features. Unsupervised learning, which uses machine learning algorithms to interpret and classify unidentified data sets, classifies data without requiring any intervention.

Result and Discussion

In the article titled Time Series Analysis and Forecast for Air Pollution in Ankara: Box-Jenkins Approach by (Turgut & Temiz, 2015), they aimed to estimate the future values of PM10 pollutant in Ankara using Box-Jenkins methodology. Box-Jenkins methodology works as a single variable model in estimating the future status of a parameter. It is a successful method in near-term estimations. In the study, 232 data were used using 5-year weekly data from Ankara Sıhhiye station and time series were used using Minitab Package program. Autocorrelation graphs were created, and it was observed that the time series were stationary and Extended Dickey-Fuller Unit Root Test, EViews package program was used for proof. According to Dickey-Fuller Unit Root test, since the critical values were greater than the statistical value, $H0$ hypothesis was rejected. In other words, the time series is stationary. By examining the graphs and proof results, it was decided to apply ARIMA (3,0,0) model of Box-Jenkins approach accordingly. When 232 data were processed into the model program and the result output was obtained, it was estimated that the PM10 pollutant in the Ankara Sıhhiye region would be at an average level of 83.21 mg/m3. It was concluded that it was at a medium pollution level.

Özel (2019) titled Air Pollution Prediction for Ankara Province Using Markov Chain, it was aimed to estimate long-term air pollution values using Markov chains by using PM_{10} air quality index values at Bahçeli station in Ankara city center. Markov process is a system that does not need past data other than previous processes. With the help of air quality and daily changes data obtained from the ministry page, the transition matrix giving the probabilities was reached by using the number of these changes. For example, when the air quality is good in Ankara, the probability of the weather being good the next day is 40%, the probability of it being middle class is 40%, the probability of it being sensitive is 17% and the probability of it being unhealthy is 3%. To obtain the limit distribution that will show the long-term structure of the Markov chain, the equilibrium distribution was reached by using the MATLAB program. As a result, the long-term probability of air quality in Ankara being good is 46%, the probability of being moderate is 19%, the probability of being sensitive is 14%, the probability of being unhealthy is 4.5%, the probability of being poor is 2.1% and the probability of being hazardous is 15%.

Kaplan *et al.*, (2014) in their study titled "Prediction of PM_{10} and SO_2 substances causing air pollution using artificial neural networks and calculation of error rate", it was aimed to predict PM_{10} and SO_2 pollutants causing air pollution using Levenberg-Marquardt learning algorithm. Levenberg-Marquardt algorithm, which is one of the learning algorithms of feedback model in artificial neural networks, is a system that approaches the error surface parabolically at each iteration stage and the minimum parabola angle represents the result for that step. In this study, Wind, Humidity, PM_{10} and SO_2 data taken every hour for 5 days belonging to Kütahya province were used. 96 of the data used were used as training and 24 as test data. A 3-layer feedback network structure was created using MATLAB artificial neural networks toolbox. The tangent sigmoid function was used as the activation function, and 30 neurons were selected in the intermediate layer, and the weights were changed in the feedback using the Levenberg-Marquart learning algorithm. As a result, because of using 5-day air pollutant concentration and meteorological data in Kütahya province, the pollutant estimate of the 6th day was realized, and the estimates largely coincided with the real data. According to this model, the normalized PM10 root mean square error value was 0.0161 and the SO_2 root mean square error value was 0.0372.

In the study titled "A Comparative Evaluation of Air Pollution Prediction with Machine Learning Algorithms" conducted by (Gültepe, 2019) on developing models to predict air pollution with various machine learning algorithms in Kastamonu province, Artificial Neural Networks (ANN), Random Forest, K-Nearest Neighborhood, Logistic Regression, Decision Tree, Linear Regression and Naive Bayes methods were used as prediction models. In the performance evaluations of the methods used on the Kastamonu DataSet, it was determined that there were statistically significant differences in terms of the Explanatory Coefficient (R2), Mean Squared Error (MSE), Root Mean Square Error (RMSE) and Mean Absolute Error (MAE) metrics. Studies have shown that the artificial neural network model provides 87% success in predictive data accuracy, while Random Forest and Decision Tree algorithms work at 99% predictive data accuracy. The Linear Regression method exhibited a very poor performance with an accuracy rate of 30%.

Study titled "Estimating CO2 emissions in OECD countries with machine learning" studied the estimation of CO2 emissions of 10 OECD countries with machine learning. 80% of the data was used for training and 20% for testing (Garip, 2017). Three methods; M5P, support vector machine (SVM) and artificial neural networks (ANN) were used as machine learning methods. After the estimations were made, statistical functions such as Mean Absolute Error (MAE), Mean Square Error (MSE), Mean Absolute Percentage Error (MAPE) and Root Mean Square Error (RMSE) were used to evaluate the performance of the applied machine learning methods. As a result of the estimations, it was seen that the SVM machine learning method made quite successful estimations in 7 out of 10 countries. It was understood that SVM was more successful than ANN and M5P.

Dokuz et al., (2020) provided a study that can prevent selection confusion regarding the problem of which parameters should be examined with which method and how in machine learning, which is used as a tool in improving air quality. In the study titled "Using machine learning methods for the estimation and spatial distribution of air quality parameters", machine learning algorithms were introduced and many studies that performed air pollution estimation with machine learning were examined. As a result of the examinations, it was determined that the data volume to be used in algorithm selection significantly affects the algorithm success; pollutant parameter selection for the application area; the presence of a real air quality station to verify the algorithm result; a good data volume that can take meteorological variability into account; importance should be given to data regularity, quality and precision; The analysis technique should be determined according to the spatial distribution of the estimated concentration amounts obtained, whether it is an urban or rural area, the necessity of defining the topography and the type of land use. Paying attention to these headings will increase the accuracy percentage of the study to be conducted.

Rybarczyk and Zalakeviciute, (2016) in their article titled "Machine learning approach to predict urban pollution" used a model based on machine learning to predict PM2.5 concentrations from air pollutant parameters in Quito, Ecuador, by accepting wind (speed and direction) and precipitation meteorological data as variables. Data collection processes were carried out with PM2.5 and meteorological data measuring devices from two regions determined in Quito. WEKA data mining program was used for machine learning. In addition, modeling studies were conducted with decision tree algorithms. For both regions, PM2.5 concentrations were predicted with a classification based on 15 µg/m3 threshold and 65% accuracy was obtained. Since the complexity in predicting pollution originating from vegetation and meteorological data in Ecuador and the difficulties in producing a model with minimum parameters and maximum accuracy are quite high, 65% accuracy was accepted as a very high accuracy.

Zhan et al., (2017) used a new machine learning algorithm, Geographically Weighted Gradient Boosting Machine (GW-GBM), in their study titled "Spatiotemporal estimation of continuous daily PM2.5 concentrations across China using a spatially explicit machine learning algorithm" in China, where acute human health problems are most frequently encountered in the world. The model used aerosol optical depth and meteorological data as variables to investigate the spatial variation of PM 2.5 concentrations. As a result, it was observed that 95% of the Chinese population lives in areas where PM 2.5 concentration is higher than 35 mg m^{-3}.

In the article titled "*Using Ensemble Regression Algorithms to Increase the Prediction Success of Air Quality Index*" by Irmak and Aydilek (2019), the air quality index of Adana province was estimated. The calculations were made with Spyder, a Python programming language compiler that includes useful libraries for data mining and machine learning. They collected hourly measurement values of PM10, SO_2, NO_2, O_3 and CO air pollutants between 2013-2017 from 4 different stations. The regression methods used are random forest regression, decision tree regression, support vector regression, K-EN nearest neighbor regression, linear regression and artificial neural network regression, batch regression, adaptive booster regression, gradient booster regression and sampled total regression. After the calculation process was completed, a data set containing 43838 records for the years 2013-2017 was obtained. A training data set of 75% and a test data set of 25% were created by randomly selecting from this data set. Machine learning algorithms were run on the Spyder compiler with the help of Pandas and Sklearn libraries. Regression algorithms were first trained with the training data set. Then, test data was applied to the same algorithm and error values were recorded. The same operations were applied to each algorithm and their values were recorded. As a result, the algorithm that could best predict the air quality index was random forest regression. Community-based regression algorithms produced more successful results than other algorithms. The fastest algorithm was linear regression with 0.00699 seconds.

In their paper titled "A Machine Learning Approach to Predict Air Quality in California", Castelli *et al*., (2020) used support vector regression (SVR), a popular machine learning method, to predict pollutant and particulate levels and estimate the air quality index (AQI). The Radial Basis Function was the kernel type that allowed SVR to predict with the highest success rate among the alternative algorithms tested. Using all available variables instead of determining features using principal component analysis was a move that increased success in the study. It was observed that SVR with the RBF kernel gave 94.1% success in predicting hourly pollutant concentrations of nitrogen dioxide, carbon monoxide, ground-level ozone, particulate matter 2.5, and sulfur dioxide, as well as the air quality index of California.

They wanted to predict future PM2.5 and PM10 concentrations using daily PM2.5 and PM10 concentration data in Kunming and Yuxi cities of China between 2015 and 2016 using a new hybrid model (CI-FPA-SVM) written by (Li, Kong, & Wu, 2017). At the beginning of the study, it was difficult to obtain results due to the difficulty of understanding the relationship between variables with different definitions. For this reason, they created a hybrid model by combining different models. Here, various parameters were optimized with FPA and a nonlinear system was obtained with SVM. In order to test the hybrid model, six benchmark models were considered, including FPA-SVM, CI-SVM, CI-GA-SVM, CI-PSO-SVM, CI-FPA-NN, and multiple linear regression model. The empirical study results show that the proposed CI-FPA-SVM model is far superior to all the evaluated benchmark models in terms of high prediction accuracy and the application of the model for prediction can lead to more effective air quality monitoring and management.

Sotomayor-Olmedo *et al*., (2013) in their study "Predicting Urban Air Pollution in Mexico City Using Support Vector Machines: Kernel Performance Approach" presents a forecast pollution model using support vector machines and kernel functions such as Gaussian, Polynomial and Spline. In the study where these techniques were used, ozone (O_3), particulate matter (PM_{10}) and nitrogen dioxide (NO_2) in Mexico City were estimated. As a result of the study, it was observed that the Gaussian kernel gave more realistic results for the necessary calculations. It was revealed that the polynomial kernel gave less successful results than the Gaussian.

In a study conducted in 2012 to make short-term estimates of air pollution in Macau, data sets were created by organizing daily meteorological and air pollution data collected from continuous monitoring stations. While SVM had a good coverage ability in the study where Support Vector Machine was preferred in regression and time series estimation, it was observed that the performance of the SVM model generally depends on the kernel selection. In the experiments conducted with different kernel types, the estimation results of the linear model and the RBF model gave results that were quite close to the real data sets for the test of SO2 and NO2 data. Similarly, in the tests of seasonal data, the two models provided a higher accuracy rate than the other three models. However, some delays and underestimations occurred in these two models in the winter experiment. In the studies conducted, it was concluded that using the Linear model and the RBF model in the air pollutant and meteorological data estimations in the city of Macau in five different models yielded good results with lower errors compared to the other data sets. In addition, it was recommended that users who want to make air pollutant estimations in similar cities use these models (Vong *et al*., 2012).

As a result of many factors such as industrialization, uncontrolled urbanization, climate change, violation of regulations by industrial facilities and inadequate inspection activities of supervisory institutions and organizations, the air quality of cities is getting worse over time. Although research shows that air quality is extremely important for human and environmental health, the extent to which this situation will be taken in the future is no longer an unknown through algorithm and modeling programs such as machine learning.

Due to many reasons such as the fact that industrial areas in cities are located within the city center, the city's wind paths are blocked by high-rise buildings, natural gas has not yet become a dominant fuel type in the city, the city administration units such as governorships, mayors, provincial directorates and clean air center directorates are drowning in bureaucratic work and the city's inability to manage air quality well, air quality is above the limit values specified in the regulations in almost all air pollutant parameters, especially in the winter months.

Revealing how this situation will proceed in the coming years is considered as a project that will positively affect the air quality of the city in the future, contribute to the literature and human health. Considering these situations, collecting air quality data and meteorological parameters from previous years covering city centers and districts, processing them and using the appropriate algorithm machine learning algorithm written in the programming tool, estimating the status of pollutant parameters in the coming years will be a project that will take cities quite a bit further in terms of action plans. It is a definite opinion that it would be better if the studies carried out were taken one step further and converted into web or mobile applications, made accessible to the public and operated. In addition, the support of municipalities and ministries in such projects is essential. It is obvious that choosing the right algorithm in machine learning will give the most suitable model for our data. Of course, it is not an easy process to try algorithms one by one for this. Also, doing this manually can leave us with a result such as struggling with the data and eventually getting discouraged.

It is not practical to try everything, so of course it is necessary to use machine learning tool providers AutoML systems. The best ones show themselves with scans on feature engineering algorithms and normalizations. The hyper-parameter setting of the best model or models is left after the algorithm selection. It should be known that this situation is easily solved by AutoML and in my opinion, it is the process that requires the most thought. In summary, machine learning algorithms are only a part of the machine learning puzzle. In addition to algorithm selection (manual or automatic), you need to deal with optimizers, data cleaning, feature selection, feature normalization and (optionally) hyperparameter settings. Once we have considered all of these and created a model that works for our data, it is time to deploy the model and update it as conditions change.

Acknowledgment: *I would like to thank Environmental Engineer Feride Dalkilic for her contributions to this study.*

Compliance with Ethical Standards Ethical responsibilities of Authors: *The author has read, understood, and complied as applicable with the statement on "Ethical responsibilities of Authors" as found in the Instructions for Authors".*

Funding: *There is no funding this study.*

Conflict of Interest: *The authors declare that they do not have any conflict of interest.*

Change of Authorship: *The author has read, understood, and complied as applicable with the statement on "Ethical responsibilities of Authors" as found in the Instructions for Authors and is aware that with minor exceptions, no changes can be made to authorship once the paper is submitted.*

References

Angra S, Ahuja S, (2017) Machine learning and its applications: A review. Paper presented at the *2017 international conference on big data analytics and computational intelligence (ICBDAC).* https://doi.org/10.1109/ICBDACI.2017.8070809

Bellinger C, Mohomed Jabbar MS, Zaïane O, Osornio-Vargas A, (2017) A systematic review of data mining and machine learning for air pollution epidemiology. *BMC Public Health*, **17**, 1-19. https://doi.org/10.1186/s12889-017-4914-3

Castelli M, Clemente FM, PopovičA, Silva S, Vanneschi L, (2020) *A machine learning approach to predict air quality in California. Complexity,* 2020(1), 8049504. https://doi.org/10.1155/2020/8049504

Chollet F, Chollet F, (2021) Deep learning with Python: Simon and Schuster. https://sourestdeeds.github.io/pdf/Deep%20Learning%20with%20Python.pdf

Dokuz Y, Bozdağ A, Gökçek B, (2020) Hava Kalitesi Parametrelerinin Tahmini ve Mekansal Dağilimi Için Makine Öğrenmesi Yöntemlerinin Kullanilmasi. *Niğde Ömer Halisdemir Ün. Müh. Bil. Der.,* **9**(1), 37-47. https://dergipark.org.tr/tr/pub/ngumuh/issue/52170/654092

Domingos, P. (2012) A few useful things to know about machine learning. *Communications of the ACM,* **55**(10), 78-87. https://dl.acm.org/doi/pdf/10.1145/2347736.2347755

Garip E, (2017) OECD ülkelerindeki CO_2 emisyonunun makina öğrenmesi ile tahmin edilmesi. İstanbul *Medeniyet Üni. Fen Bil. Enst. Müh. Tezler.* https://acikbilim.yok.gov.tr/

Gültepe Y, (2019) Makine öğrenmesi algoritmaları ile hava kirliliği tahmini üzerine karşılaştırmalı bir değerlendirme. *Av. Bil. ve Tek. Derg.* (16), 8-15. https://dergipark.org.tr/tr/pub/ejosat/issue/45333/530347

Irmak ME, Aydilek İB, (2019) Hava kalite indeksinin tahmin başarısının artırılması için topluluk regresyon algoritmalarının kullanılması. Academic platform-*J. Engin. & Sci.,* **7**(3), 507-514. https://dergipark.org.tr/tr/pub/apjes/issue/44190/478038

Kampa M, Castanas E, (2008) Human health effects of air pollution. *Environ. Pollut.,* **151**(2), 362-367. https://doi.org/10.1016/j.envpol.2007.06.012

Kaplan Y, Saray U, Azkeskin E, (2014) Hava kirliliğine neden olan PM10 ve SO2 maddesinin yapay sinir ağı kullanılarak tahmininin yapılması ve hata oranının hesaplanması. *AKU J. Sci.Eng.***14** (2014) 025201 (1-6) https://dergipark.org.tr/tr/pub/akufemubid/issue/1611/20175

Köktürk F, Ankarali H, Sümbüloğlu V, (2009) Veri madenciliği yöntemlerine genel bakış. *Turkiye Klinikleri J. Biostat*., **1**(1), 20-25. https://www.turkiyeklinikleri.com/article/en-veri-madenciligi-yontemlerine-genel-bakis-53374.html

Lary DJ, Faruque FS, Malakar N, Moore A, Roscoe B, Adams ZL, Eggelston Y, (2014) Estimating the global abundance of ground level presence of particulate matter ($PM_{2.5}$). Geospatial health, 8(3), S611. https://doi.org/10.4081/gh.2014.292

LeCun Y, Bengio Y, Hinton G, (2015) Deep learning. **Nature**, **521**(7553), 436-444. https://www.nature.com/articles/nature14539

Li W, Kong D, Wu J, (2017) A new hybrid model FPA-SVM considering Cointegration for particular matter concentration forecasting: A case study of Kunming and Yuxi, C*hina. Comput. Intellig. & Neurosci.,* 2017(1), 2843651. https://doi.org/10.1155/2017/2843651

Özel G, (2019) Markov zinciri kullanarak Ankara ili için hava kirliliği tahmini. *Int. J. Sci. & Tech. Res.*, **3**(2), 144-151. https://dergipark.org.tr/tr/pub/bilgesci/article/546317

Rybarczyk Y, Zalakeviciute R, (2016) Machine learning approach to forecasting urban pollution. Paper presented at the *2016 IEEE Ecuador Technical Chapters Meeting* (ETCM). https://doi.org/10.1109/ETCM.2016.7750810

Shinde PP, Shah S, (2018) A review of machine learning and deep learning applications. Paper presented at the 2018 Fourth international conference on computing communication control and automation (ICCUBEA). https://doi.org/10.1109/ICCUBEA.2018.8697857

Singh A, Thakur N, Sharma A, (2016) A review of supervised machine learning algorithms. Paper presented at the 2016 *3rd International Conference on Computing for Sustainable Global Development (INDIACom*). https://ieeexplore.ieee.org/stamp/stamp.jsp?tp=&arnumber=7724478

Sotomayor-Olmedo A, Aceves-Fernández MA, Gorrostieta-Hurtado E, Pedraza-Ortega C, Ramos-Arreguín JM, Vargas-Soto JE, (2013) Forecast urban air pollution in Mexico City by using support vector machines: A kernel performance approach. *Int. J. Intel. Sci.* **3**, (3) 126-135 http://dx.doi.org/10.4236/ijis.2013.33014

Toros H, Bağış S, (2017) Hava kirlilik modellerinde kullanılacak emisyon envanteri oluşturulması için yaklaşımlar ve İstanbul hava kirliliği dağılımı örneği. *Çukurova Ün. Müh.-Mim. Fak. Der.*, **32**(2), 1-12. https://dergipark.org.tr/tr/pub/cukurovaummfd/issue/32170/357001

Turgut D, Temiz İ, (2015) Ankara'daki hava kirliliği için zaman serileri analizi ve tahmin: box-jenkins yaklaşımı. *Alphanum. J.*, 3(2), 131-138. https://dergipark.org.tr/tr/pub/alphanumeric/article/20803

Varınca, K. B., Güneş, G., & Ertürk F, (2008) Hava kirleticilerinin insan sağlığı ve iklim değişikliği üzerine etkileri. *U UHAKS,* Konya. https://www.academia.edu/1424169/Hava_Kirleticilerinin

Vong, C.-M., Ip, W.-F., Wong PK, Yang JY, (2012) Short-term prediction of air pollution in Macau using support vector machines. Journal of Control Science and Engineering, 2012(1), 518032. https://doi.org/10.1155/2012%2F518032

Yılmaz M., Toros H., İncecik, Öztürk, Z., Kirkil, G., Öztaş, D, Beba, HE. (2020) Dilovası Hava Kirliliğinin Trafik Emisyonları Açısından Değerlendirilmesi. *Ulusal Çevre Bil. Araş. Der.*, **3**(1), 43-51. https://dergipark.org.tr/tr/pub/ucbad/issue/54360/738990

Zhan Y, Luo Y, Deng X, Chen H, Grieneisen ML, Shen X, Zhang M, (2017) Spatiotemporal prediction of continuous daily PM2. 5 concentrations across China using a spatially explicit machine learning algorithm. *Atmos. Environ.*, **155**, 129-139. http://dx.doi.org/10.1016/j.atmosenv.2017.02.023

J. Int. Environmental Application & Science, Vol. 20: 88-97 (2025)
Research Paper

Estimated Carbon Footprint for the Construction and Operational Phases of a Wastewater Treatment Plant

Muhammed Hasan Eken[1], Özlem Tunç Dede[2*]

[1] *Konya Technical University, Technology Transfer Office Application and Research Centre, Konya, Turkiye;*
[2]*Giresun University, Faculty of Engineering, Environmental Engineering Department, Giresun, Turkiye*

Received February 10, 2025; Accepted March 11, 2025

Abstract: In this paper, the carbon footprint of the construction and operational phases of a WWTP in Giresun was evaluated in accordance with TSE EN ISO 14064 Guidelines for Calculation of Greenhouse Gases, within the framework of GHG Protocol standards and CCaLC2 software. The carbon footprint of the plant during the construction phase was calculated as 1077.55 tCO_2e for 2022 and 1110.52 tCO_2e for 2023. The estimated carbon footprint for operational phase was determined to be 800.64 tCO_2e. The primary contribution to greenhouse gas emissions stems from fuel consumption and wastewater treatment for construction and operational phases, respectively. The calculated carbon footprint value was relatively low compared to other WWTPs reported in the literature, primarily due to the lack of real-time operational data. However, the research incorporating both design data and operational data from the plant will further elucidate the findings of this study and enable the examination of carbon footprints under various operating conditions.
Keywords: *carbon footprint, greenhouse gas, emission, energy, wastewater.*

Introduction

Water is a fundamental element of life and is indispensable for the sustainability of ecosystems and human health. Increasing population, industrialization, agricultural and urbanization processes intensify pressure on water resources, leading to water scarcity and pollution problems. Wastewater, which refers to polluted water because of domestic, industrial and agricultural activities, can cause serious environmental problems if discharged directly to receiving environments. In this context, wastewater treatment plants (WWTPs) play a critical role in protecting water resources, securing human health and sustainability of ecosystems. Furthermore, with the escalating climate crisis, energy saving and energy efficiency have become more prominent. WWTPs are recognized as significant energy consumer and sources of greenhouse gas (GHG) emissions (Campos *et al.*, 2016; Chai *et al.*, 2015; Goliopoulos *et al.*, 2022; Robescu & Presură, 2017). Energy consumption in WWTPs is influenced by factors such as location, size, extent of the sewerage network, treatment configuration, aeration type, equipment energy efficiency and overall WWTP efficiency. Aeration, a primary energy-consuming component, accounts for 25-60% of total energy consumption (Goliopoulos *et al.*, 2022). The energy consumption of WWTPs is estimated to be about 4% of the electricity consumption of the water industry, depending on the country. (Goliopoulos et al., 2022; Gupta et al., 2024). According to the Intergovernmental Panel on Climate Change (IPCC) Sixth Assessment Report, the global GHG emissions from the waste/wastewater sector constituted 3.9% of 59 $GtCO_2e$ total emissions in 2019 (IPCC, 2022). GHG emissions from WWTPs can originate from direct sources, such as the sewage collection system, treatment processes, and disposal, and indirect sources, such as electricity consumption, transportation of various chemicals and sludge, consumption of chemicals, disposal of residues (Goliopoulos *et al.*, 2022) (Karakas et al., 2024). WWTPs directly produce various GHGs, such as carbon dioxide (CO_2), nitrous oxide (N_2O), and methane (CH_4), as a result of treatment and directly contribute to CO_2 and methane emissions through energy consumption (Campos *et al.*, 2016; Chai *et al.*, 2015; Goliopoulos *et al*., 2022). However, direct CO_2 emissions from WWTPs are often excluded in the calculation of GHG emissions as they are deemed part of the natural carbon cycle (biogenic origin). For that reason, CO_2 emission sources in WWTPs are primarily related to energy consumption (Karakas et al., 2024).

The environmental impacts of WWTPs are not limited to the operational phase; the construction phase of the plant can also contribute significant carbon emissions, although typically less than the operational phase (Chai *et al.*, 2015). In general, the construction industry, a significant contributor to

Corresponding author: e-mail: ozlem.dede@giresun.edu.tr, Tel:+90 454 310 1000/4039

global GHG emissions, has a substantial impact on global warming (Arıoğlu Akan *et al.*, 2017; Hammond and Jones, 2008; Hong et al., 2015; Labaran et al., 2021; Purnell and Black, 2012). It has been reported that the building and construction sector contributed to approximately 37% of global carbon emissions in 2022 (United Nations Environment Programme, 2024) (Wang et al., 2022) Emissions during the construction phase of WWTPs generally result from various activities such as material production, transportation, the use of construction vehicles, and land preparation. On-site electricity use and the production of construction materials are the two largest contributors to GHG emissions (Hong et al., 2015; Purnell and Black, 2012; Stokes and Horvath, 2006) Assessing carbon emissions during the construction phase is also important to more comprehensively understand the environmental impacts of WWTPs throughout their lifecycle and to develop mitigation strategies.

Carbon footprint analysis serves as a critical tool for evaluating the climate change impact of WWTPs. It also facilitates the identification of strategies to reduce GHG emissions and the evaluation of their effectiveness. In general terms, carbon footprint is the measurement of the amount of GHGs generated because of the activities, expressed in units of CO_2e. GHG emission sources that contribute to the carbon footprint can be analysed in two categories: direct and indirect. Direct sources are CO_2 emissions from the use of fossil fuels, including energy consumption related to electricity, fuel, transportation, etc., while indirect sources are CO_2 emissions from the production of materials used and the eventual degradation of these products (Karakas *et al.*, 2024).

Different standards and methods can be used in the calculation of a carbon footprint. The most widely accepted methodologies in this field are the Greenhouse Gas Protocol (GHG), prepared by the Business Council for Sustainable Development and ISO 14064 Greenhouse Gas Calculation and Verification Management System, published by the International Organization for Standardization. In GHG inventory calculations, data are generally evaluated using IPCC Tier-1 and Tier-2 methodologies and ANNEX, DEFRA conversion factors, within the framework of the GHG Protocol and ISO 14064 standard (IPCC, 2006; Lin, 2020; Tosun and Tunç Dede, 2024; TSE, 2019a, 2019b). Another method encountered in the literature is the CCaLC2 program, created by the University of Manchester based on ISO 14044 and PAS 2050 rules, which aims to perform life cycle analysis (Azapagic, 2012).

The present research forecasts the environmental impacts of the construction and operational phases of the WWTP under construction in Batlama Neighbourhood of Central District of Giresun Province. The GHG of construction phase of a WWTPs are limited in the literature and the available studies are mainly focused on the operational phases. This study aims to present a holistic overview of the WWTP's energy consumption and GHG emissions during both construction and operational phases and could shed light on the WWTP, energy and GHG emission relationship.

Materials And Methods

Study Area

The WWTP is situated in the west-central part of Giresun city, Turkiye. The plant covers an area of approximately 2.2 hectares (ha) in the central Batlama district. The land elevation varies between 5-25 m, and approximately 2 ha are located on nearly flat terrain. The distance of the land to the coast is approximately 300 m. The plant will treat domestic and industrial wastewater collected by the combined sewer system of Giresun city centre. The design parameters of the WWTP are 141 982 population equivalents (PE), with a daily flowrate of 19 653 m^3/day. A general view of the WWTP is given in Fig. 1. The WWTP is designed to incorporate a coarse screen, inlet pumping station, fine screen, grit and grease removal, primary sedimentation tank, anaerobic mixing tanks, activated sludge tank, membrane bioreactor (MBR) units, secondary sedimentation tank, disinfection, and filtration units. The plant is currently under construction and is planned to be operational after March 2025. GHG emissions from the construction phase are calculated based mainly on energy consumption, while GHG emissions for the operational phase are calculated based on feasibility report data.

Carbon Footprint Calculations

Within the scope of this study, the carbon footprint of the Giresun WWTP, currently under construction in Batlama, Central District of Giresun Province, was assessed. GHG emissions and carbon footprint calculations for the construction and operational phases of WWTP were determined according to TSE EN ISO 14064 Guidelines for the Calculation of Greenhouse Gases and CCaLC2 software within the framework of GHG Protocol standards (IPCC, 2006; TSE, 2019b, 2019a, 2019c). The CCaLC2 program was developed by researchers at the University of Manchester to calculate the carbon footprint of products over their life cycle as a part of project. This software, developed within the scope of a project, divides the sectors that produce carbon emissions into groups. Within the program's interface, the product life cycle is analysed in four sections: raw materials, production, storage and use. The waste component is divided into sub-sections within each section. The program includes a database on wastewater treatment, and the carbon emission value of sewage sludge is automatically calculated according to the amount of sludge. The researcher follows ISO 14044 and PAS 2050, the internationally accepted life cycle methodology, for the development of the program and supported with over 50 case studies (Azapagic, 2012). The potential direct and indirect sources of GHG emissions from the construction and operational phases of any WWTP can be summarized as shown in Table 1.

Figure 1. The general view of the Giresun WWTP

Considering the information provided in Table 1, GHG emission and carbon footprint calculations of Giresun WWTP were conducted separately for the construction and operational phases. The available data on the WWTP primarily included energy consumption data, and the calculations focused on GHG emissions resulting from energy consumption. For the construction phase, the years 2022 and 2023 were used as a baseline, and data on electricity consumption, fuel consumption of construction vehicles and rental vehicles were used. All data used in the calculations were declared by the authorities of the construction company. Other data (construction materials, transportation, etc.) were not included in the calculations due to their unavailability.

For the operational phase, since the plant is still under construction, calculations were made based on the feasibility report and in line with the available data declared by construction company (electricity use, amount of wastewater treated, use of polyelectrolyte and $FeCl_3$ chemicals, sludge formation and disposal) for the planned operation of the plant. The formulas and the emission factors used in the calculations were determined according to relevant guidelines and are presented in Table 2.

Results and Discussions

Assessment of the carbon footprint for construction phase

The activities that may cause emissions during the construction phase of the Giresun WWTP are primarily fuel consumption, electricity consumption, building materials production, and construction waste generation. Within the scope of this paper, fuel consumption (both direct and indirect) and electricity consumption data were included in the carbon footprint calculations. Due to the unavailability of detailed information on building materials and waste, these data could not be incorporated into calculations. The carbon footprint of the Giresun WWTP during the construction phase was calculated for the years 2022 and 2023 by determining the carbon dioxide equivalents (tCO_2e) of GHG emissions. Emission values for 2022 and 2023 are tabulated in Table 3 and Table 4, respectively. In 2022 and 2023, the construction company reported an average daily fuel consumption of 1000 L for construction vehicles and 100 L for rental vehicles. As all construction vehicles and rental vehicles used diesel fuel, calculations were made accordingly, using the annual fuel consumption amounts, assuming 360 working days per year based on information received from company authorities. The annual electricity consumption were 56 026 kWh and 125 000 kWh for 2022 and 2023, respectively. Based on Table 3, the total GHG emission from the WWTP during the construction phase in 2022 was determined to be 1077.55 tCO_2e. The emission sources and their percentage contribution are visualized in Fig(2). As illustrated, the largest contribution to GHG emissions originated from the fuel consumption of construction vehicles, accounting for 88.6% of the total in 2022. This was followed by emissions from indirect consumption, contributing 8.9% and emissions from electricity consumption with 2.5%.

Table 1. Possible sources of GHG emissions from construction and operational phases of WWTPs (Chai et al., 2015; Hong et al., 2015; Labaran et al., 2021; Parravicini et al., 2016)

	Source of Direct GHG Emissions	**Source of Indirect GHG Emissions**
Construction phase	- Energy consumption of construction vehicles - On-site transportation - Construction electricity usage - Construction chemical use - On-site worker activities	- Construction materials (production, transportation, demolition and other non-building activities) - Transportation of construction vehicles - Off-site worker activities (electricity use, transportation, other necessities)
Operational phase	- Wastewater collection system - Treatment process • *CO_2 emissions from organic matter degradation* • *N_2O emissions from the nitrification/ de-nitrification process* • *CH_4 and N_2O emissions from anaerobic digestion* - Discharging	- Electricity usage - Chemical and additives usage -Transportation (chemicals, sludge) - Sludge final disposal

Table 2. The factors used in the calculation of GHG emissions (IPCC, 2022, 2006; TUIK, 2024)

Factors	**Source**	**Emissions**			
Consumption data	Scope 1: Transportation (work vehicle)	Diesel			
	Scope 2: Electric	Electricity			
	Scope 3: Transportation (rental vehicles	Diesel			
Emission	GHG = Activity data x emission factor	Diesel[1]	CO_2 (kg/TJ)	CH_4 (kg/TJ)	N_2O (kg/TJ)
			74 100	3	0.6
		Electric[2] (kg/kWh)		0.478	
Net calorific value[3]	Fuel type	Diesel (TJ/Gg)		43.0	
Global warming potential (GWP)[4]	Greenhouse gas type	CO_2: 1 CH_4: 27 (non-fossil) and 29.8 (fossil) N_2O: 273			
Density	Fuel type	Diesel: 0.83 kg/m^3			
Percentage of oxidized carbon[5]	Fuel type	Diesel: 0.984=1 (In IPCC Tier-1 approaches, all values are taken as 1)			
Emission (E)	E = FV x EF x YF	FV: Activity data EF: Emission factor (kg/TJ) YF: Oxidation factor			
	FV = Fuel amount x NKD	NKD: Net calorific value (TJ/Gg)			

[1] Tablo 2.2 Default Emission Factors for Stationary Combustion in the Energy Industries from IPCC Report (IPCC, 2006)
[2] Electricity Consumption Point Emission Factors (The Ministry of Energy and Natural Resources, 2024a).
[3] Table 3.17 Average NCVs of fuels from Turkish Greenhouse Gas Inventory 1990 – 2022 (The Ministry of Energy and Natural Resources, 2024b).
[4] IPCC Report - Climate Change 2022 (IPCC, 2022)
[5] Table 3.6 Country specific oxidation factor of fuels from Turkish Greenhouse Gas Inventory 1990 – 2022 (The Ministry of Energy and Natural Resources, 2024b).

Table 3. Carbon emission values for the construction period of WWTP for 2022

Energy source		Density	Consumption	NKD	Energy Consumption	Emission Factor	Emission	Percent of oxidized carbon	GWP	CO_2 Emission
		(kg/m^3)	(kg)	(TJ/Gg)	(TJ)	(kg/TJ)	(t)			(tCO_2e)
CO_2 emissions from construction vehicles										
CO_2	Diesel (L) 360 000	0.83	298 800	43	12.85	74 100	952.18	1	1	952.18
CH_4	Diesel (L) 360 000	0.83	298 800	43	12.85	3	0.038	1	29.8	1.13
N_2O	Diesel (L) 360 000	0.83	298 800	43	12.85	0.6	0.007	1	273	1.91
								Total emission (tCO_2e)		**955.22**
CO_2 emissions from energy consumption										
Electric (kWh)	56 026					0.478 (kg/kWh)				26.78
								Total emission (tCO_2e)		**26.78**
Indirect consumption (rental cars)										
CO_2	Diesel (L) 36 000	0.83	29 880	43	1.285	74 100	95.22	1	1	95.22
CH_4	Diesel (L) 36 000	0.83	29 880	43	1.285	3	0.0038	1	29.8	0.11
N_2O	Diesel (L) 36 000	0.83	29 880	43	1.285	0.6	0.0008	1	273	0.22
								Total emission (tCO_2e)		**95.55**
								Total CO_2 emission for 2022 = 1077.55 tCO_2e		

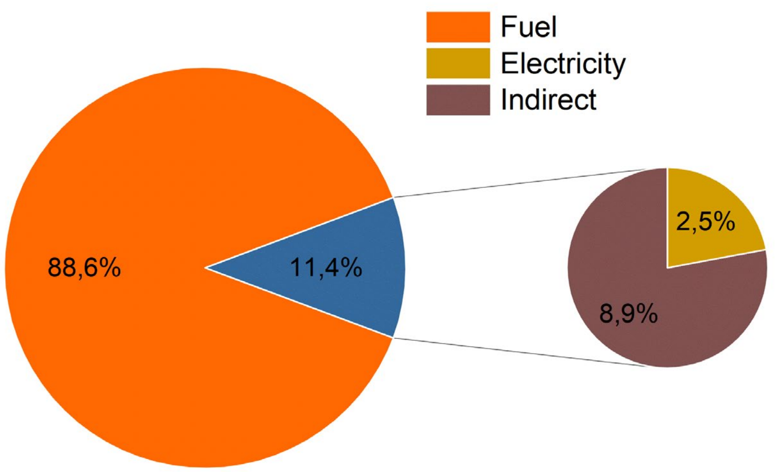

Figure 2. The distribution of emission sources for construction phase of WWTP in 2022

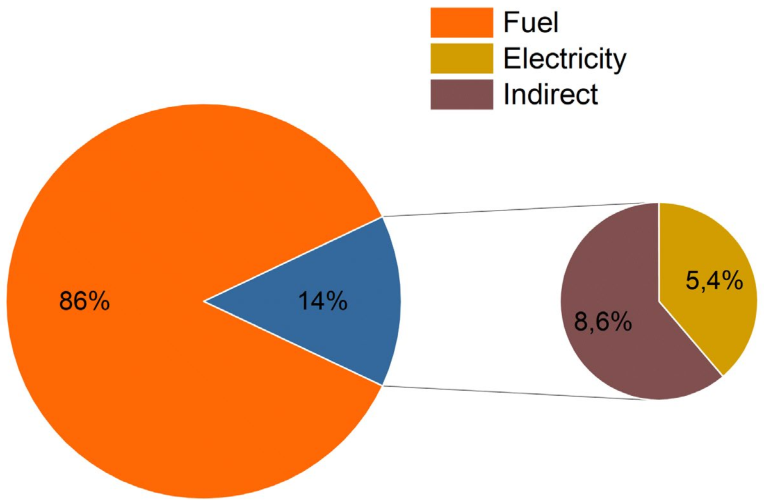

Figure 3. The distribution of emission sources for construction phase of WWTP in 2023

Table 4. Carbon emission values for the construction period of WWTP for 2023

Energy source			Density	Consumption	NKD	Energy Consumption	Emission Factor	Emission	Percent of oxidized carbon	GWP	CO_2 Emission
			(kg/m^3)	(kg)	(TJ/Gg)	(TJ)	(kg/TJ)	(t)			(tCO_2e)
CO_2 emissions from construction vehicles											
CO_2	Diesel (L)	360 000	0.83	298 800	43	12.85	74 100	952.18	1	1	952.18
CH_4	Diesel (L)	360 000	0.83	298 800	43	12.85	3	0.038	1	29.8	1.13
N_2O	Diesel (L)	360 000	0.83	298 800	43	12.85	0.6	0.007	1	273	1.91
									Total emission (tCO_2e)		**955.22**
CO_2 emissions from energy consumption											
Electric (kWh)		125 000					0.478 (kg/kWh)				59.75
									Total emission (tCO_2e)		**59.75**
Indirect consumption (rental cars)											
CO_2	Diesel (L)	36 000	0.83	29 880	43	1.285	74 100	95.22	1	1	95.22
CH_4	Diesel (L)	36 000	0.83	29 880	43	1.285	3	0.0038	1	29.8	0.11
N_2O	Diesel (L)	36 000	0.83	29 880	43	1.285	0.6	0.0008	1	273	0.22
									Total emission (tCO_2e)		**95.55**
									Total CO_2 emission for 2023 = 1110.52 tCO_2e		

Based on Table 4, the total GHG emission from the WWTP during construction phase in 2023 was determined to be 1110.52 tCO_2e. The emission sources and their percentage contributions are visualized in Fig. 3. As illustrated, the largest contribution to GHG emissions came from the fuel consumption of construction vehicles, accounting for 86% of the total in 2023. This was followed by emissions from indirect consumption with 8.6% and emissions from electricity consumption contributing 5.4%. Total CO_2 emission for 2023 is slightly higher than in 2022, due to increased electricity consumption in 2023.

Assessment of the carbon footprint for operational phase

The activities that may cause emissions during the operational phase of the Giresun WWTP are mainly involve electricity consumption, fuel consumption, waste sludge management, and the use of polyelectrolyte and $FeCl_3$, as well as wastewater emissions. As the plant is still under construction, the data for the operation phase were obtained from the feasibility report and incorporated in the carbon footprint calculations. Carbon footprint calculations were performed in accordance with GHG Protocol and using CCaLC2 program. Emission sources and carbon dioxide equivalents (tCO_2e) of GHG for the operational phase of the WWTP are tabulated in Table 5. Emission values from sewage sludge and wastewater treatment were generated using the CCaLC2 software and are also presented in Table 5. The feasibility report indicated that the generated sludge (5.35 ton/day) would be transferred to a nearby cement factory (approximately 80 km from the WWTP) for disposal. To calculate the carbon emissions from sludge transportation, it was assumed that a 6-wheeled truck (consuming an average of 13 L diesel fuel per 100 kilometres) with a volume of approximately 20 tons would make two trips per week. Accordingly, the average daily fuel consumption for sludge transport was included in the calculations as 10.4 L, totalling 1082 L annually.

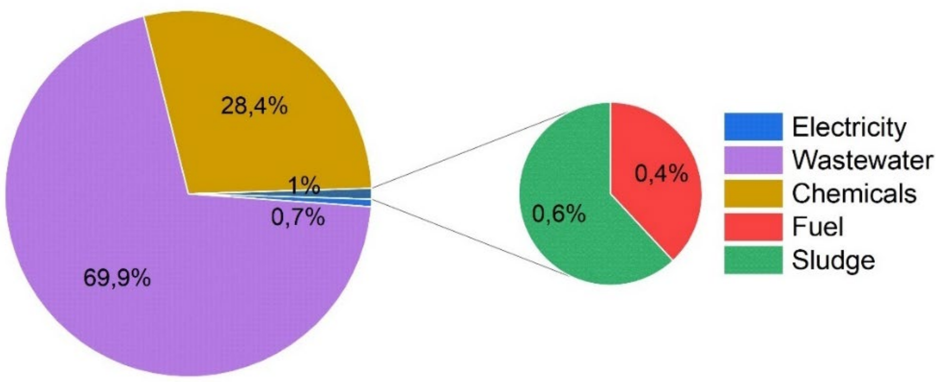

Figure 4. The distribution of emission sources for operational phase of WWTP

Based on Table 5, the total GHG emission from the WWTP during the operational phase was found to be 800.64 tCO_2e. Emission sources and their percentage contributions are illustrated in Fig. 4. It is seen that the largest contribution to GHG emissions originated from the wastewater treatment, accounting for 69.9%. This is followed by emissions from chemical consumption with 28.4%. However, the use of a biogas unit for electricity production has a positive impact, decreasing the carbon emission value by 2.18 tCO_2e/year.

Table 5. The annual carbon emission values for operational period of WWTP

Energy source		**Density** (kg/m^3)	**Consumption** (kg)	**NKD** (TJ/Gg)	**Energy Consumption** (TJ)	**Emission Factor** (kg/TJ)	**Emission** (t)	**Percent of oxidized carbon**	**GWP**	**CO_2 Emission** (tCO_2e)
Transportation of activated sludge										
CO_2	Diesel (L) 1 082	0.83	898.1	43	0.039	74 100	2.89	1	1	2.89
CH_4	Diesel (L) 1 082	0.83	898.1	43	0.039	3	0.0001	1	29.8	0.003
N_2O	Diesel (L) 1 082	0.83	898.1	43	0.039	0.6	0.00002	1	273	0.005
								Total emission (tCO_2e)		**2.90**
CO_2 emissions from energy consumption										
Electric (kWh/year)	10 975					0.478 (kg/kWh)				**5.25**
CO_2 emissions from waste										
Sludge amount (t/year)	1953									**4.72**
CO_2 emissions from wastewater										
Amount of wastewater (m^3/day)	19 653									**560**
CO_2 emissions from chemicals						**Emission factor (kg CO_2e)**				
Polyelectrolyte amount (t/year)		15.77				1.182				**18.64**
$FeCl_3$ amount (t/year)		388				0.539				**209.13**
								Total CO_2 emission = 800.64 tCO_2e		

Biogas electric production		**Emission factor (kg/kWh)**	**Reduction in CO_2 emission due to electricity production (tCO_2e/year)**
Electric (kWh/year)	4 568	0.478	**2.18**

Conclusion

Wastewater treatment plants play a crucial role in waste disposal and pollutants treatment, rendering wastewater harmless to the environment. However, it is paramount to examine the carbon emissions resulting from activities within wastewater treatment plants, which directly contribute to global warming.

Within the scope of this study, the environmental impacts of the construction phase (based on 2022 and 2023) of the WWTP in the Batlama Neighbourhood of the Central District of Giresun Province were evaluated in terms of GHG emissions, and the carbon footprint of the plant was calculated. In addition, estimated carbon footprint calculations of the operational phase were conducted based on design data provided in the feasibility report. Carbon footprint calculations were performed using TSE EN ISO 14064 Greenhouse Gas Calculation Guidelines and CCaLC2 software, within the framework of GHG Protocol standards.

For the construction phase, fuel consumption (both direct and indirect) and electricity consumption data were included in the carbon footprint calculations, while for the operational phase, estimated values of electricity consumption, fuel consumption, waste sludge, the chemicals polyelectrolyte and $FeCl_3$, and wastewater treatment amount were utilized.

The calculated carbon footprint during the construction phase was 1077.55 tCO_2e for 2022 and 1110.52 tCO_2e for 2023. Emissions from fuel consumption made the highest contribution to the carbon footprint for both years. The estimated total carbon emission for the operational phase was calculated as 800.64 tCO_2e, with the main contribution stemming from wastewater treatment, followed by chemical consumption. Furthermore, electricity generation from biogas unit was estimated to prevent 2.18 tCO_2e/year of emissions.

In line with the literature, the carbon emission values obtained for the construction phase are lower than those for the operational phase (Chai et al., 2015). However, the calculations can be further elaborated by including information on the construction material used, on-site and off-site worker activities and transportation data. The estimated CO_2 emission value calculated for the operational phase of the WWTP was compared with similar studies in the literature and is tabulated in Table 6. WWTPs having the similar capacity were used for the comparison purposes. All research studies have been used IPCC (2006) method in their calculations while some have additionally used the CCALC2 method (Güller & Balcı, 2018; Ateş, 2021; Erşan, 2022). It is seen that the calculated carbon footprint value is relatively low in comparison with other WWTPs in the literature. The main reason for this difference is the lack of real-time operational data. Nevertheless, the calculations made using the design data will provide a valuable resource for future studies.

The carbon footprint calculations conducted in this research indicate that GHG emissions are directly proportional to energy consumption. The calculations demonstrate the contribution of activities carried out during both the construction and operational phases of a WWTP to carbon emissions. It is therefore essential to evaluate activities within WWTPs, which play a vital role in treating wastewater and discharging it into the environment, in terms of carbon emissions. Various measures are being implemented globally and nationally reduce carbon footprint.

Creating carbon sink areas by planting trees is an effective solution to reduce carbon emissions. The company can contribute to emission reduction by afforesting the areas surrounding its facilities. In fact, the amount of emission sequestration varies based on the type and age of each tree, but detailed research is required to determine specific values. As the construction company has indicated that the plant will be completed and begin operating shortly, recommendations have been made based on the carbon emission value for the operational phase. The emission value of 800.64 tCO_2e/year for the operational phase corresponds to approximately 72 785 trees (assuming one tree absorbs 11 kg CO_2 per year) (Tosun and Tunç Dede, 2024).

Another recommendation to reduce carbon emissions is to provide electricity from renewable energy sources, such as photovoltaic panels, to absorb emissions from energy consumption sources as much as possible. Photovoltaic panels are devices that capture solar energy and convert it into electrical energy. If a 540 W panel generates an average of 0.54 kW of electricity in 1 hour of sunshine per day and considering that the average annual sunshine duration for Giresun province is 2.2 hours/day according to the National General Directorate of Meteorology, the annual average electrical energy generation capacity of a 540 W panel would be 433.6 kW. Given that the annual electricity consumption value of the plant was reported as 10 975 kWh, it was determined that this value corresponds to the use of approximately 25 photovoltaic panels with 500 W capacity.

Table 6. The annual carbon emission values for different WWTPs

Place	Wastewater (m^3/day)	Carbon footprint (tCO_2e/year)	Reference
WWTPs from China	20 000	5 817-9 928	(Chai et al., 2015)
WWTP Puducherry, India	25 000	3 716	(Vijayan et al., 2017)
WWTP Muğla, Turkiye	17 111	77 316-82 946	(Güller and Balcı, 2018)
WWTP Bingöl, Turkiye	15 840	45 238	(Ateş, 2021)
WWTP, Sivas, Turkiye	78 516	76 141-74 520	(Erşan, 2022)
WWTPs from China	20 000	2 345-3 586	(Chen et al., 2023)
WWTP in Erzurum, Turkiye	13 000	10 389-53 529	(Karakas et al., 2024)
WWTP Giresun, Turkiye	19 653	800.64	This study

Despite evaluating the carbon footprint of the WWTP in Giresun, this paper acknowledges several limitations and areas for additional research. The calculations for construction phase are mainly based on energy and electricity consumption. The construction materials and transportation emissions can contribute to GHG emissions. However, these data could not be included in the calculations due to unavailability. The operational phase analysis relies solely on estimated data, as the system is still under construction and has not yet operational. Due to the dynamic nature of operational conditions, alterations in these parameters can influence emission factors, energy consumption patterns, and chemical consumption patterns. Once the WWTP is operational, the calculations should be renewed according to actual data. Therefore, further research is imperative to expand the scope of the findings and investigate carbon footprints under various operating conditions. Optimizing wastewater treatment plant operation can be important at the local level and can help improve the carbon footprint of urban areas.

Acknowledgement: *This paper has been prepared as a part of Muhammed Hasan Eken's MSc. Thesis. The authors would like to thank the authorities of the construction company of WWTP for their cooperation. The authors would like to thank Prof. Dr. Adisa Azapagic and her team at the University of Manchester for making CCalC2 software freely available.*

Funding: *This research has not been funded with any project.*

Author contributions: *Ozlem Tunc Dede: Conceptualization, Methodology, Writing-Original draft preparation, Reviewing and Editing; Muhammed Hasan Eken: Investigation, Data curation, Methodology, Writing-Original draft preparation.*

Conflicts of interest: *The authors declare no conflicts of interest.*

References

Arıoğlu Akan MÖ, Dhavale DG, Sarkis J, (2017) Greenhouse gas emissions in the construction industry: An analysis and evaluation of a concrete supply chain. J. Clean. Prod. 167, 1195–1207. https://doi.org/10.1016/j.jclepro.2017.07.225

Ateş F, (2021) Evaluation of Bingöl wastewater treatment plant carbon footprint according to CCALC2 and GPS-X methods. MSc Thesis, Fırat University. https://tez.yok.gov.tr/UlusalTezMerkezi/ 674741

Azapagic A, (2012) CCaLC2 carbon footprint tool. http://www.ccalc.org.uk/latestccalc2.php?lsce=EEY8D00G

Campos JL, Valenzuela-Heredia D, Pedrouso A, Val Del Río A, Belmonte M, Mosquera-Corral A, (2016) Greenhouse Gases Emissions from Wastewater Treatment Plants: Minimization, Treatment, and Prevention. J. Chem. 2016. https://doi.org/10.1155/2016/3796352

Chai C, Zhang D, Yu Y, Feng Y, Wong MS, (2015) Carbon footprint analyses of mainstream wastewater treatment technologies under different sludge treatment scenarios in China. Water (Switzerland) 7, 918–938. https://doi.org/10.3390/w7030918

Chen, H., Zheng, Y., Zhou, K., Cheng, R., Zheng, X., Ma, Z., Shi, L., (2023) Carbon emission efficiency evaluation of wastewater treatment plants: evidence from China. Environ. Sci. Pollut. Res. 30, 76606–76616. https://doi.org/10.1007/s11356-023-27685-9

Erşan, F., (2022) Evaluation of greenhouse gas emissions originating from biological treatment units of Sivas domestic wastewater treatment plant. Msc. Thesis, Sivas Cumhuriyet University. https://tez.yok.gov.tr/UlusalTezMerkezi/ 752072

Goliopoulos N, Mamais D, Noutsopoulos C, Dimopoulou A, Kounadis C, (2022) Energy Consumption and Carbon Footprint of Greek Wastewater Treatment Plants. Water (Switzerland) 14. https://doi.org/10.3390/w14030320

Güller S, Balcı A, (2018) Carbon Footprint Assessment of Mugla Waste Water Treatment Plant. üleyman Demirel Univ. J. Nat. Appl. Sci. 22, 547. https://doi.org/10.19113/sdufbed.11001

Gupta R, Lee S, Lui J, Sloan WT, You S, (2024) Carbon footprint assessment of water and wastewater treatment works in Scottish islands. J. Clean. Prod. 450, 141650. https://doi.org/10.1016/j.jclepro.2024.141650

Hammond GP, Jones CI, (2008) Embodied energy and carbon in construction materials. Proc. Inst. Civ. Eng. Energy 161, 87–98. https://doi.org/10.1680/ener.2008.161.2.87

Hong J, Shen GQ, Feng Y, Lau WST, Mao C, (2015) Greenhouse gas emissions during the construction phase of a building: A case study in China. J. Clean. Prod. 103, 249–259. https://doi.org/10.1016/j.jclepro.2014.11.023

IPCC, (2022) Climate Change 2022 - Mitigation of Climate Change - Full Report, Cambridge University Press. https://doi.org/10.1017/9781009157926

IPCC, (2006) IPCC Guidelines for National Greenhouse Gas Inventories, IPCC Guidelines for National Greenhouse Gas Inventories. https://www.ipcc-nggip.iges.or.jp/public/2006gl/

Karakas A, Tozum-Akgul S, Komesli OT, Kaplan-Bekaroglu SS, (2024) Carbon footprint analysis of advanced biological wastewater treatment plant. J. Water Process Eng. 61, 1–8. https://doi.org/10.1016/j.jwpe.2024.105254

Labaran YH, Mathur VS, Farouq MM, (2021) The carbon footprint of construction industry: A review of direct and indirect emission. *J. Sustain. Constr. Mater. Technol.* 6, 101–115.

https://doi.org/10.29187/jscmt.2021.66

Lin, L., (2020) Carbon emission assessment of wastewater treatment plant based on accounting perspective. E3S Web Conf. 194, 0–4. https://doi.org/10.1051/e3sconf/202019404049

Parravicini V, Svardal K, Krampe J, (2016) Greenhouse Gas Emissions from Wastewater Treatment Plants. Energy Procedia 97, 246–253. https://doi.org/10.1016/j.egypro.2016.10.067

Purnell P, Black L, (2012) Embodied carbon dioxide in concrete: Variation with common mix design parameters. Cem. Concr. Res. 42, 874–877. https://doi.org/10.1016/j.cemconres.2012.02.005

Robescu LD, Presură E, (2017) Reducing carbon footprint of a wastewater treatment plant using advanced treatment and renewable energy sources. Environ. Eng. Manag. J. 16, 1055–1062. https://doi.org/10.30638/eemj.2017.108

Stokes J, Horvath A, (2006) Life cycle energy assessment of alternative water supply systems. Int. J. Life Cycle Assess. 11, 335–343. https://doi.org/10.1065/lca2005.06.214

Tosun, G., Tunç Dede, Ö., (2024) Karbon Ayak İzi Hesaplamalarında Enerji Tüketiminin Örnek Bir Çalışma ile İncelenmesi. Karadeniz Fen Bilim. Derg. 14, 932–943. https://doi.org/10.31466/kfbd.1458712

The Ministry of Energy and Natural Resources, (2024a), Turkey Electricity Generation and Electricity Consumption Point Emission Factors - 2022. https://enerji.gov.tr/Media/Dizin/EVCED/tr/ÇevreVeİklim/İklimDeğişikliği/EmisyonFaktorleri/TEUVETN_Emisyon_Faktörleri_Bilgi_Formu.pdf. Accessed date: 15.02.2025

The Ministry of Energy and Natural Resources, (2024b), Turkish Greenhouse Gas Inventory 1990 – 2022. https://enerji.gov.tr//Media/Dizin/EVCED/tr/ÇevreVeİklim/İklimDeğişikliği/UlusalSeraGazıEmisyonEnvanteri/Belgeler/EK-1.pdf. Accessed date: 15.02.2025

TSE, (2019a) Greenhouse gases - Part 1: Specification with guidance at the organization level for quantification and reporting of greenhouse gas emissions and removals. Ankara. https://www.tse.org.tr/

TSE, (2019b) Greenhouse gases - Part 2: Specification with guidance at the project level for quantification, monitoring and reporting of greenhouse gas emission reductions or removal enhancements. Ankara. https://www.tse.org.tr/

TSE, (2019c) Greenhouse gases - Part 3: Specification with guidance for the verification and validation of greenhouse gas statements. Ankara. https://www.tse.org.tr/

TUIK, (2024) Turkish Greenhouse Gas Inventory 1990-2022, Oil: a Cultural and Geographic Encyclopedia of Black Gold: Volume 1-2. https://doi.org/10.1007/978-3-642-41714-6_72140

United Nations Environment Programme, (2024) Global Status Report for Buildings and Construction: Beyond foundations: Mainstreaming sustainable solutions to cut emissions from the buildings sector. Nairobi., 2023 Global Status Report for Buildings and Construction: Beyond foundations - Mainstreaming sustainable solutions to cut emissions from the buildings sector. https://doi.org/https://doi.org/10.59117/20.500.11822/45095

Vijayan G, Saravanane R, Sundararajan T, (2017) Carbon Footprint Analyses of Wastewater Treatment Systems in Puducherry. Comput. Water, Energy, Environ. Eng. 06, 281–303. https://doi.org/10.4236/cweee.2017.63019

Wang T, Li K, Liu D, Yang Y, Wu D, (2022) Estimating the Carbon Emission of Construction Waste Recycling Using Grey Model and Life Cycle Assessment: A Case Study of Shanghai. Int. J. Environ. Res. Public Health 19. https://doi.org/10.3390/ijerph19148507

J. Int. Environmental Application & Science, Vol. 20: 98-115 (2025)
Research Paper

Remote Sensing of Spatial and Temporal Mapping of Flare Impacts in the Niger Delta, Nigeria

Barnabas O. Morakinyo*

Department of Surveying & Geoinformatics, Faculty of Environmental Sciences, BAZE University, Abuja, Nigeria

Received October 15, 2024; Accepted March 6, 2025

Abstract: This research focuses on the mapping of spatial and temporal effects of flare on vegetation cover. The data (11 Landsat 5 TM, 49 Landsat 7 ETM+, 27 Landsat 8 OLI-TIRS, and 15Landsat 9 OLI-TIRS) dated from 10/10/1984 to 17/12/2023 with < 3 % cloud cover was used to study 11 flaring sites in the Niger Delta. Data processing and analysis were carried out using MATLAB codes. Normalized Difference Vegetation Index (NDVI)for Landsat 5 and 7 bands (1-4) and Landsat 8 and 9 bands (2-5) was determined from the atmospherically corrected multispectral bands.The results show that the temporal in NDVI is specific to each site, and that the effect of the flares on the vegetation cover does not majorly depend on the size of facility. Eleme I (-2.71×10^{-5}-2.32×10^{-5}) and II (-1.740×10^{-4}-2.074×10^{-5}) presented significant results for a small portion of the area. Umurolu (-1.679×10^{-5}-5.868×10^{-5}) and Bonny (-3.089×10^{-5}-2.423×10^{-5}) show significant results for a wider area which could be because of the number of flare stacks within them 4 and 5 respectively. All small and medium facilities show statistically significant results which could be attributed to the rate and volume of gas burning from them. Therefore, it can be concluded that Landsat data can be used to map the spatial and temporal impacts of flare on vegetation cover in the Niger Delta.

Keywords: *Remote Sensing, Environmental Science, Thematic Mapping, Land Cover, Environmental Studies.*

Introduction

The Niger Delta region is in the Southern part of Nigeria; and it consists of Akwa Ibom, Bayelsa, Cross River, Delta and Edo states from South South region; Abia and Imo states from South East region; and Ondo State from South West region (Morakinyo, 2015; Onosode, 2003). The Niger Delta is an arcuate shaped basin that consists of diverse vegetation and four different ecological zones such as coastal ridge barriers, brackish/freshwater swamp forests, mangrove forests and lowland rain forests (Odukoya, 2006).

The Niger Delta is the home for oil and gas exploration, exploitation and processing activities in Nigeria. Hence, activities of multinational oil companies such as Shell Petroleum Company, AGIP, Total, ELF, etc.are ongoing. The effects of oil and gas activities in the environment of the Niger Delta includes increase in temperature (Lu et al., 2020; Morakinyo *et al*., 2019); environmental pollution (Morakinyo et al., 2023a;Morakinyo et al., 2023b; Umbugala & Morakinyo, 2023; Lu et al., 2020); contamination of vegetation (Morakinyo, 2015); destruction of vegetation and agricultural pursuits (Morakinyo *et al*., 2020a,b; Nwaogu & Onyeze, 20208), stunted growth and or death of farm produce, reduction and destruction of agricultural activities and vegetation (Musa *et al*., 2024; Morakinyo*et al.*, 2023a;Morakinyo, 2023c;Morakinyo*et al*., 2021;Morakinyo et al., 2020 a, b).

Remote sensing technology deals with the mapping of the environment using space borne platforms (Jansen &Gregorio, 2004). It is essential in the production of large, repetitive geospatial data of the environment. The geospatial information acquired at different locations can be employed for the characterization and assessment of changes in the environment (Yuan *et al.,* 2005). Characteristics of remotely sensed data are spatial, temporal, and spectral and are used for mapping of land cover dynamics, landuse land cover (LULC) changes, retrieval of land surface temperature (LST) (Morakinyo *et al*., 2022), planning etc. for decision making purposes(Berlanga-Robles and Ruiz-Luna 2002).The availability of satellite data has made it possible to observe LC from space (Molliconeet al.

**Corresponding: E-Mail:barnabas.ojo@bazeuniversity.edu.ng, Tel: +234(0)8103676990*

2003); and geospatial information needed for evaluation of changes on Earth's surface are collected at different time intervals(Jensen 2005).

Landsat data has been useful in the study of the environment in several ways such as assessment of LULC (Jensen 2005); monitoring of vegetation health (Morakinyo *et al.,* 2023a); LST retrieval (Lu *et al.*, 2020); forest and agricultural areas monitoring (Campbell 2007); urbanization and planning processes (Jensen & Cowen 1999); urban studies (Wang *et al*. 2020). Open access to satellite data enables spatially valid datasets over large areas with great spatial information and temporal frequency (Xiao et al. 2006). Improvements in remote sensing data gathering with increased spatial accuracy; and availability of various free satellites data provides opportunities and improve quantitative studies of activities on Earth surface for example land cover dynamics, the rate and pattern of LULC change, vegetation monitoring (Epstein *et al.*, 2002).

Many studies have been conducted on Normalized Difference Vegetation Index (NDVI) because of its usefulness in assessing vegetation, simplicity and can be easily obtained from any multispectral sensor with a visible and a near Infra-Red band, hence the reason for its general application(Huang *et al*., 2020)for the assessment of vegetation such as land use studies, land cover changes, commercial agriculture, assessments of the climate effects on vegetation dynamics (Kalisa et al., 2029); drought monitoring (Hua *et al*., 2019, Wei *et al*., 2021;Karnieli et al., 2010; Polat et al., 2024); forest health and vegetation changes (Gessner *et al.*, 2023; Kloos et al., 2021; Chang *et al.,* 2022;Chrysopolitou*et al*., 2013); monitoring land cover dynamics (Lavender, 2016); ecological environmental change (Jiang 2021); LULC changes (Hu et al., 2023); systematic planning of urban environment (Guha, 2021; Guha *et al*., 2020); and global vegetation monitoring (Roßberg& Schmitt, 2023); the study of chlorophyll concentration in leaves (Pastor-Guzman, 2015); productivity of plant(Vicente-Serrano *et al*., 2016) and plant stress Chavez, 2016).The robustness of the NDVI-related models is directly determined by the reliability of the NDVI (Butt, 2018).

Spatial and temporal mapping of flare effects using remote sensing technology is the focus for this study. The significance of this study is to help evaluate the spatial and temporal variation of flare impact on vegetative cover detected by Landsat sensors. There are three (3) principal research questions for this study: (1). Can Landsat data be used for spatial and temporal mapping of flare effects on vegetation cover at the flare sites in the Niger Delta? (2). What is the spatial and temporal variability in the detection of flare effects on vegetation cover at each flare site? (3) How accurately can regression analysis be used for the evaluation of the flare effects on vegetation cover? Therefore, the overall aim of this study is to evaluate of the ability of Landsat 5, 7, 8 and 9 data for spatial and temporal mapping of flare effects on vegetation cover at gas flaring sites in the Niger Delta. The objectives for this study are: (1) Computation of NDVI from atmospherically corrected Landsat data for each site; (2) Regression analysis against time to produce 3 maps (Annual change in NDVI (regression slope), regression coefficient, r and p-value for the regression at each pixel for each site.(3) Computation of mean and standard deviation (SD) of NDVI for further analysis.

Materials and Methods

Study Area

Eleven (11) flaring sites including two (2) refineries (Eleme 1 and Eleme 2); seven (7) flow stations (Onne, Umurolu, Alua, Rukpokwu, Obigbo, Chokocho & Umudioga); One (1) Liquefied Natural Gas (LNG) plant (Bonny) and One (1) oil well (Sara) all from Rivers State, Niger Delta region (Figure 1) were studied for the spatial and temporal mapping of flare effects on vegetation. All sites are located within the Latitude 4 ° 40 ¹ and 5 ° 01 ¹ N and Longitude 6 ° 50 ¹ and 7 ° 01 ¹ E (Morakinyo *et al*., 2022a; Morakinyo, 2015).

Study Data

Eleven (11) Landsat 5 TM data, forty-nine (49) Landsat 7 ETM+ data, twenty-seven (27) Landsat 8 OLI-TIRS data, and Fifteen (15) Landsat 9 OLI-TIRS data dated from 10/10/1984 to 17/12/2023 with $<$ 3 % cloud cover was used for this study. The USGS website where these data were downloaded is (https://earthexplorer.usgs.gov/).

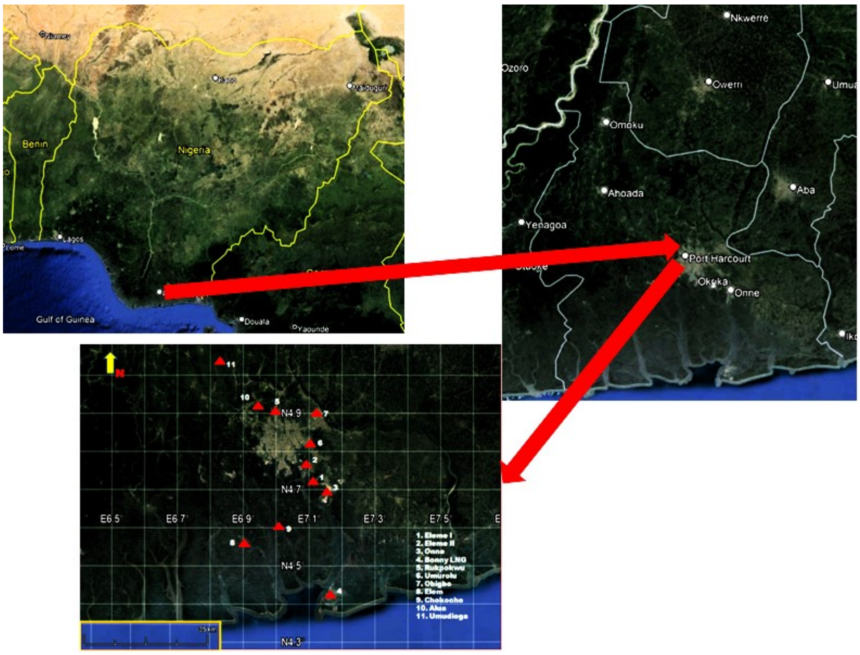

Figure 1. Above Left Map of Nigeria, (ESRI, 2024); Above Right) Map of Rivers State (ESRI, 2024); Below) 11 gas flaring studied sites (ESRI, 2024).

Methods

Processing of Landsat Data

1. Geo-location points were verified: Ten (10) ground control points (GCPs) were selected over the Niger Delta using Google Earth (Table 1). Twenty (20) images with five (5) images each from Landsat 5, Landsat 7**,** Landsat 8 and Landsat 9 were uploaded into the ArcGIS and the selected GCPs were identified. The comparison of the coordinates of these controls obtained from the Google Earth and ArcGIS was carried out with a negligible difference found (1.0×10^{-6} to 7.3×10^{-6} m) (Table 1). This was taken as an acceptable error range for the geo-location of the imagery.
2. Removal of zero and out of range values from the data using MATLAB code; and their replacement with not a number (nan) in order to avoid divide by zero errors in calculations. Values at the upper and lower limits of the 8-bit, 12 bit and 14 bit data range which cannot be distinguished from noise were all removed.

Table 1. Geo-location points verification for Landsat 5, 7, 8 and 9 data

S/N	Google Earth Latitude (θ)	Google Earth Longitude (λ)	Landsat 5, 7, 8 and 9Latitude (θ)	Landsat 5, 7, 8 and 9Longitude (λ)	Remarks
1	04 24 35.42	07 09 36.00	04 24 35.40	07 09 36.00	An edge of a two-storey building
2	04 25 48.34	07 11 15.41	04 25 48.34	07 11 15.39	A point on a tower
3	04 44 18.04	06 46 26.03	04 44 18.04	06 46 26.00	A two-point road junction
4	04 58 17.09	06 37 51.89	04 58 17.01	06 37 51.23	Edge of a fence.
5	04 52 59.09	06 52 09.95	04 52 59.09	06 52 09.00	A point on a LNG terminal
6	04 51 40.12	06 57 57.93	04 51 40.00	06 57 57.00	A three-point road junction
7	05 03 08.89	06 55 15.91	05 03 08.10	05 55 15.21	A three-point road junction
8	05 00 59.28	06 57 15.5	05 00 59.20	06 57 15.30	Edge of a building at Rivers International Airport
9	04 45 26.24	07 07 04.29	04 45 26.20	07 07 04.30	Edge of Eleme II fence
10	04 47 56.02	07 03 26.73	04 47 56.01	07 03 26.50	Edge of a building

3. The radiometric calibration of the multispectral bands of the data was done. The Digital Number (DN) values were converted to the top of atmosphere (TOA) radiance values based on the sensor calibration parameters provided within the metadata files from USGSaccording to the Landsat 5 (Chander & Markham, 2003), Landsat 7 (NASA, 2002), Landsat 8 and Landsat 9 Science Data Users Handbooks (Ihlen, 2019) using equations1.

$$L_\lambda = ((LMAX_\lambda - LMIN_\lambda) / (QCALMAX - QCALMIN)) \times (QCAL - QCALMIN) + LMIN_\lambda \quad (1)$$

Where:
L_λ= Spectral radiance at the sensor's aperture ($Wm^{-2}sr^{-1}\mu m^{-1}$);
QCAL =The quantized calibrated pixel value in DN (Digital Number);
$LMIN_\lambda$=Spectral radiance scaled to QCALMIN ($Wm^{-2}sr^{-1}\mu m^{-1}$);
$LMAX_\lambda$=Spectral radiance scaled to QCALMAX ($Wm^{-2}sr^{-1}\mu m^{-1}$);
QCALMIN =Minimum quantized calibrated pixel value in DN = 1 for LPGS (a processing software version) products;
QCALMAX = The maximum quantized calibrated pixel value in DN = 255.

For Landsat 8 and 9, the DN can be converted to spectral radiance using equation 2

$L_\lambda = M_L \times Q_{cal} + A_L$ (Ihlen, 2019) (2)

Where:
L_λ= Spectral radiance ($Wm^{-2}sr^{-1}\mu m^{-1}$);
M_L= Radiance multiplicative scaling factor for the band from the metadata;
A_L= Radiance additive scaling factor for the band from the metadata;
Q_{cal}= Level 1-pixel value in DN.

4. Computation of TOA reflectance for multispectral bands 1 to 4 for Landsat 5 and 7including the application of simple sun angle correction is done with equation (3) which assumes Lambertian surface reflectance(NASA, 2002;Markham & Barker, 1986):

$\rho_p = (\pi \times L_\lambda \times d^2) \div (ESUN_\lambda \times \cos\theta s)$ (3)

Where:
ρ_p = Unitless effective at-satellite planetary reflectance;
L is measured per unit solid angle;
πL = Upwelling radiance over a full hemisphere;
d = Earth-Sun distance in astronomical units;
$ESUN_\lambda$= Mean solar exo-atmospheric irradiances;
θs = Solar zenith incident angle in degrees (Chander & Markham, 2003).

For Landsat 8 and 9, Level 1 DN of multispectral bands 2-5 can be converted to TOA uncorrected reflectance for solar elevation angle using equation 4.

$\rho_\lambda' = M_\rho \times Q_{cal} + A_\rho$ (Ihlen, 2019) (4)

Where:
ρ_λ' = TOA Planetary Spectral Reflectance, without correction for solar angle(Unitless);
M_ρ= Reflectance multiplicative scaling factor for the band from the metadata;
A_ρ= Reflectance additive scaling factor for the band from the metadata;
Q_{cal}= Level 1-pixel value in DN.

The Landsat 8 and 9 corrected reflectance for solar elevation angle is as follows:

$\rho_\lambda = \rho_\lambda'/\cos(\theta_{SZ}) = \rho_\lambda'/\sin(\theta_{SE})$ (Ihlen, 2019) (5)

Where:
$\rho\lambda$=TOA planetary reflectance
θ_{SZ}=Local sun elevation angle; the scene centre sun elevation angle in degrees is provided in the metadata;
θ_{SE}=Local solar zenith angle; $\theta_{SZ}=90° - \theta_{SE}$.

5. Atmospheric correction method: Dark object subtraction (DOS)method (Lavender, 2016, Liang et al., 2001) was adopted for this study; and it assumes within the image some pixels are in complete shadow and their radiances received at the satellite are due to the atmospheric scattering. Also, this assumption is combined with the fact that very few targets on the Earth's surface are absolute black, so an assumed 1 % minimum reflectance is better than 0 % (Chavez, 1996). Furthermore, this principle is employed for the development of algorithms for atmospheric correction for MODerate Resolution Imaging Spectroradiometer (MODIS) and Medium

Resolution Imaging Spectroradiometer (MERIS) sensors (Chavez, 1996). However, this method assumes that the error is uniform for the entire image.

With the application of DOS processes to this study, the pixels for the darkest location (Atlantic Ocean) were selected for bands 1-4 for Landsat 5 and 7, and bands 2-5 for Landsat 8 and 9(Table 2). The computation of reflectance for these dark pixels was carried out and the lowest value recorded for each band was used as an estimate of the atmospheric reflectance for the respective band. To reduce the atmospheric effects these small errors were subtracted from the computed reflectance for each pixel of the entire image.

Table 2: Coordinates of dark pixels over Atlantic Ocean (L5, L7, L8 and L9) data

Image ID	Band 1 (Lat/Long.)	Band 2 (Lat/Long.)	Band 3 (Lat/Long.)	Band 4 (Lat/Long.)
LT51880571986017AAA04	04 20 02.07	04 20 11.21	04 21 36.79	04 21 25.05
	07 15 03.13	07 15 58.84	07 15 51.34	07 16 22.45
LT51880571987004XXX04	04 10 00.26	03 48 04.22	03 49 09.90	03 51 01.14
	07 04 43.95	07 42 00.92	07 42 01.96	07 42 23.63
LT51880571986353XXX10	04 16 48.94	04 11 40.48	04 10 16.93	04 08 08.69
	07 21 40.25	07 39 48.02	07 21 20.77	07 09 02.10
LE71880571999333AGS00	03 40 37.29	03 41 14.57	03 45 10.61	03 43 54.41
	06 35 44.23	06 35 31.92	06 34 32.91	06 32 27.08
LE71880572000352EDC00	03 57 55.38	04 17 17.76	04 18 50.68	04 19 24.42
	06 24 15.44	08 09 37.65	08 10 15.89	08 11 31.37
LE71880572003008SGS00	04 18 00.97	03 36 14.95	03 38 15.29	03 41 09.19
	07 26 14.16	07 57 22.38	07 57 45.13	07 58 49.59
	Band 2 (Lat/Long.)	Band 3 (Lat/Long.)	Band 4 (Lat/Long.)	Band 5 (Lat/Long.)
LC81880572018361LGN00	04 22 38.41	04 22 43.01	04 22 39.58	04 22 36.42
	07 04 41.30	07 04 26.11	07 04 48.01	07 04 15.20
LC81880572019364LGN00	04 16 36.71	04 18 54.00	04 17 22.05	04 16 49.02
	08 10 10.49	08 10 32.05	08 10 47.00	08 10 19.67
LC81880572021353LGN00	03 35 25.09	03 34 22.50	03 35 44.80	03 34 19.28
	07 56 24.71	07 56 12.06	07 55 31.42	07 55 37.52
LC09L1TP18805720211211	04 22 37.00	04 23 00.05	04 22 49.61	04 22 26.08
	07 04 41.13	07 04 23.05	07 04 37.01	07 04 43.59
LC09L1T18805720220317	04 06 42.08	04 06 06.59	04 06 43.39	04 04 52.90
	06 38 18.60	06 48 45.38	06 49 22.24	06 46 54.80
LC09L1T18805720231225	03 58 05.19	03 58 42.27	03 58 57.30	03 59 11.23
	06 23 32.19	06 25 23.40	06 25 41.18	06 25 59.42

6. Atmospherically corrected reflectance: This is the result obtained after the application of DOS method in section 5 above.
7. Classification of Land Surface Cover (LSC):The atmospherically corrected reflectance bands 1-4 for Landsat 5 and 7; and bands 2-5 for Landsat 8 and 9 using the K-means function (Morakinyo et al., 2023c, Morakinyo *et al*., 2021, Morakinyo *et al*., 2020b, Şatır & Berberoğlu, 2012) of the MATLAB tool were used for the first unsupervised cluster analysis for the land cover types classification. Three (3) classes of land cover (LC) types with cloud classified as the fourth class was obtained. Any of the3LC (Vegetation, water, soil and built-up area) and the cloud as the fourth class were identified. Also, MATLAB codes were used for the elimination of the cloud class by masking. The cloud-masked reflectance was used for the second cluster analysis and 4 LC retrieved are vegetation, soil, built up area and water (Morakinyo et al., 2021,Maaharjan, 2018, Morakinyo, 2015).However, Landsat SWIR bands 5 and 7 (Landsat 5 and 7), and bands 6 and 7 (Landsat 8 and 9) were also employed for the classification of land cover types but they could not give useful results as the bands used, therefore, they were dropped for further analysis. Furthermore, Visual examination of Worldview-1 and 2, and IKONOS pseudo-true colour images (RGB) from Google Earth and Digital Global (http://browse.digitalglobe.com/imagefinder/public.do) were also used to study and clarified the LC obtained. Results obtained from LC classification were used to summarize the LC types around each site.

8. Retrieval of Normalized Differential Vegetation Index (NDVI) in the N, E, S and W directions:The cloud-masked reflectance bands 3 and 4 for Landsat 5 and 7, and bands 4 and 5 for Landsat 8 and 9 were used for the retrieval of NDVI (Morakinyo *et al*., 2023a). For Landsat 5 and 7, band 3 is Red (R)and band 4 is Near Infra-Red(NIR) while for Landsat 8 and 9, band 4 is R and band 5 is NIR. Mathematical formula for NDVI is as stated in equation (6) (Huete et al., 2002).

$$NDVI = (NIR - R)/(NIR + R) \qquad (6)$$

Where,
NIR = Near Infra-Red reflectance;
R = Red reflectance.

The MATLAB codes used for data processing and analyses in this study are implemented as follow:

Retrieval of reflectance

- Each imagery was read from the folder i.e. a folder was created for Landsat 5, Landsat 7, Landsat 8, and Landsat 9 respectively. 1 = L5_folder310513; 2 = L7_folder010613; 3 = L8_folder020613; and 4 = L9_folder030613;
- Read in XL radiometric calibration file; fill in all gaps in XL file with Nan (i.e. Not a number).
- For each Scene Name, convert the specific characters into numerical path, row, year, day.
- Plot (scene Path, 'x'); plot (scene Year, 'X'); plot (scene Day, 'X')
- Read Landsat data files;
- Read .mtl files;
- Write a loop to automatically go through each line of the file. Instead of printing out;
- This process is repeated from while to the line counter to process for each X & Y;
- Choice of dimension of area around the flare station for investigation; i.e. the 12 × 12 km;
- Removal of zero values or bad values;
- Dark pixel method of Atmospheric Correction for the Landsat reflective bands;
- Channel the reading of both scene and radiometric calibration files;
- Radiometric calibrations for multispectral bands 1, 2, 3 and 4 for Landsat 5, and Landsat 7; and bands 2, 3, 4, and 5 for Landsat 8, and Landsat 9.
- Convert digital numbers (DN) back to the top-of-atmosphere radiances (Lt) for all Landsat bands.
- Computation of at sensor radiance for dark pixels
- Apply a simple sun angle correction to calculate reflectance Rt at the flaring sites from the top-of-atmosphere radiance
- Application of atmospheric correction to reflective bands 1-4
- Computation of dark pixel reflectance for bands 1-4 for Landsat 5 and Landsat 7; and bands 2-5 for Landsat 8 and 9;
- True reflectance for bands 1 to 4 1-4 for Landsat 5 and Landsat 7; and bands 2-5 for Landsat 8 and 9 i.e. application of atmospheric correction;

Cluster processing (I)

- k-means for unsupervised and supervised land cover classifications;
- Application of MATLAB 'Statistics Toolbox' for k-means clustering;

Masking of cloud

- To identify cloud and mask it from the data;

Cluster processing (II) & Land cover classifications

- To look at the four (4) classes as a map;
- To look at the centroid and range of each band and each cluster;
- And compare the 'spectra' for the 4 classes:
- To give each land cover classification as vegetation; water; soil; built up

Retrieval of Normalized Differential Vegetation Index (NDVI)

- Computation of the NDVI;
- NDVI for vegetation i.e. Masking of water, soil and built up classes to remain only vegetation;
- Computation of mean NDVI for vegetation;

Conversion from Julian day to month and day

- Formal function for converting julian day into month + day;

- Month for a given year (leap / not leap year);
- Years divisible by 4 are leap years;
- Catch days in January;

Spatio-temporal regression analysis
- Create a directory for the results files;
- Stop at 307 for the processing of NDVI;
- Load(d1(ifile).name, 'ndvi_mask', 'IDX3','water', 'vegetation', 'builtup', 'soil') ;
- Conversion to julian days
- Initialize output variables: slopes(ibad) = nan; rvalues(ibad) = nan; pvalues(ibad) = nan; n(ibad) = nan;
- Plot the maps: Slope, r-values and p-values maps respectively;
- print('-f150','-r600','-dpng', 'spatial_regression_Stn_1.png').

A summary of stages for the processing of Landsat 5, 7, 8 and 9 is shown in Figure 2.

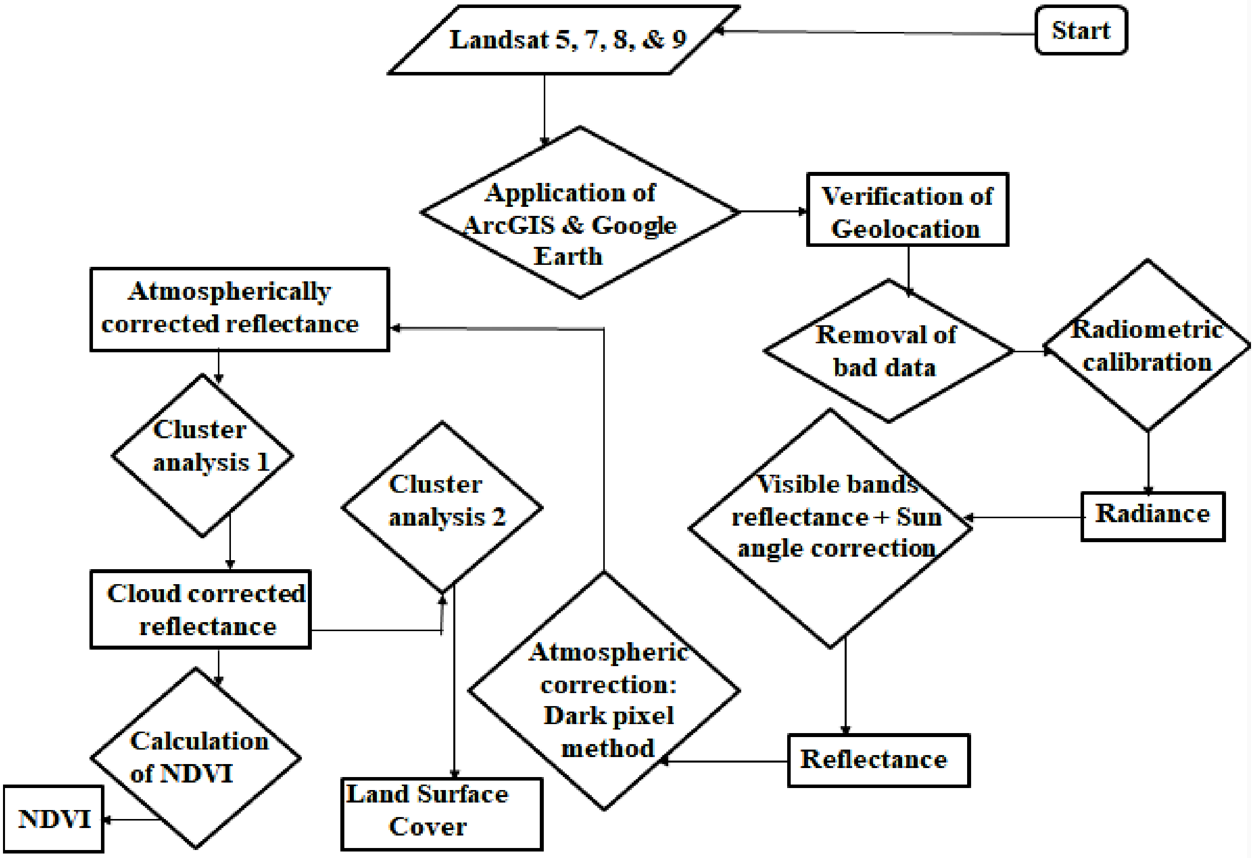

Figure 2. Methodology for processing of Landsat 5, 7, 8 and 9 data.

Insitu measurement for validation of Landsat data

Methods and processes for the evaluation of satellite data to check if such data meet their stated accuracy requirements and objectives is referred to as the validation of satellite products. For this study, the validation measurements were carried out at Eleme Refineries I and II, and Onne, Alua, Chokocho & Obigbo Flow Stations on 27/07/2012 for reconnaissance activities. On 04/08/2012 to 21/09/2012 (Morakinyo, 2015), the first ground measurements and observations took place; and were also repeated from 05/08/2019 to 22/09/2019 (Morakinyo, 2025b; Morakinyo, 2024a, b, c; Morakinyo *et al*., 2021). The third field measurement occurred from 05/08/2023 to 22/09/2023. The insitu data acquired are coordinates of features and points, relative humidity, air temperature, and photographs of features and locations. In addition, fieldwork activities at these 6 flaring sites confirmed that their LC (vegetation, some buildings, open land and water bodies) types are similar; and that they are the same with all other remaining flaring sites examined due to the similarity in the topography of the Niger Delta.

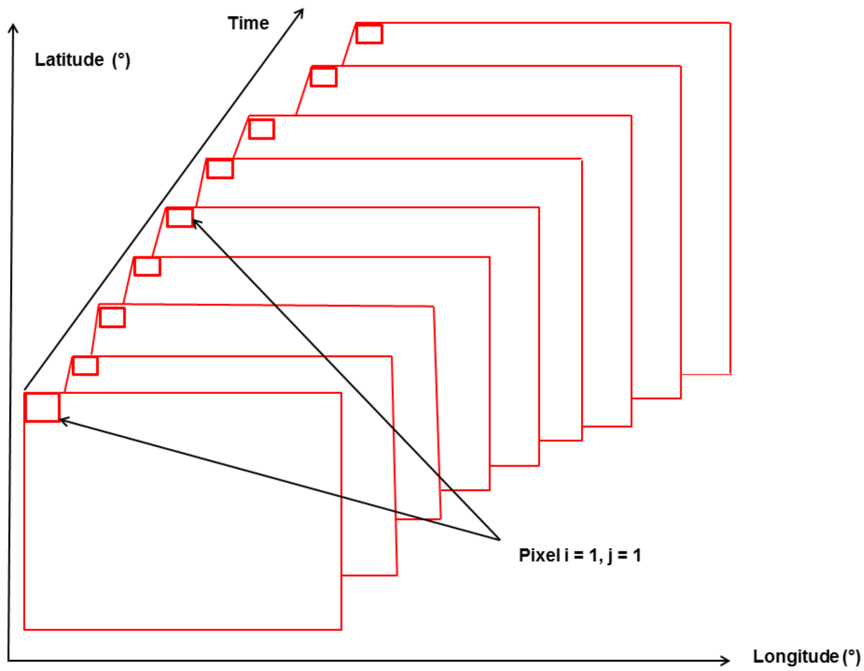

Figure 3. Schematic diagram for spatio-temporal analysis

Results and Discussion

Retrieval of NDVI

NDVI values were obtained for each pixel covering each site of 12 by 12 km i.e. 400 ×400 pixel.

Regression Analysis

This analysis is necessary in order to evaluate the spatial and temporal variation in detection of flare effects on the vegetation cover by Landsat data (Figure 3). The spatially-resolved linear regression of NDVI against time from 1984 to 2023 for each site was carried out for the purpose of generating three maps for each site (Annual change in NDVI (regression slope), regression coefficient, r and p-value for the regression at each pixel). Data calculated are mean (positive (+), negative (−) and all) and standard deviation (SD) (positive (+), negative (−) and all) of NDVI trend values. Tables3-13 presents the mean and SD for (+), (−)and net slopes of NDVI at each site.

Table 3. Eleme 3: Mean and SD for (+), (−) and net slopes of NDVI (Change in NDVI/ year).

S/N	Parameters	Value obtained
1.	Mean (pixels with + slope)	2.3164×10^{-5}
2.	Mean (pixels with − slope)	-2.7076×10^{-5}
3.	SD (pixels with + slope)	3.3855×10^{-5}
4.	SD (pixels with − slope)	3.8550×10^{-4}
5.	Mean (all)	1.9166×10^{-5}
6.	SD (all)	2.0689×10^{-4}

Table 4. Eleme 2: Mean and SD for (+), (−) and net slopes of NDVI (Change in NDVI/ year).

S/N	Parameters	Value obtained
1.	Mean (pixels with + slope)	2.0741×10^{-5}
2.	Mean (pixels with − slope)	-1.7400×10^{-4}
3.	SD (pixels with + slope)	3.0926×10^{-5}
4.	SD (pixels with − slope)	2.5439×10^{-4}
5.	Mean (all)	1.5010×10^{-5}
6.	SD (all)	1.3596×10^{-4}

Table 5. Onne: Mean and SD for (+), (−) and net slopes of NDVI (Change in NDVI/ year).

S/N	Parameters	Value obtained
1.	Mean (pixels with + slope)	1.0817×10^{-5}
2.	Mean (pixels with − slope)	-2.4278×10^{-5}
3.	SD (pixels with + slope)	2.9639×10^{-5}
4.	SD (pixels with − slope)	1.0757×10^{-4}
5.	Mean (all)	2.2849×10^{-6}
6.	SD (all)	7.9515×10^{-5}

Table 6. Umurolu: Mean and SD for (+), (−) and net slopes of NDVI (Change in NDVI/ year).

S/N	Parameters	Value obtained
1.	Mean (pixels with + slope)	5.8684×10^{-5}
2.	Mean (pixels with − slope)	-1.6787×10^{-5}
3.	SD (pixels with + slope)	3.7938×10^{-5}
4.	SD (pixels with − slope)	4.2276×10^{-4}
5.	Mean (all)	5.8057×10^{-5}
6.	SD (all)	7.4988×10^{-5}

Table 7. Bonny: Mean and SD for (+), (−) and net slopes of NDVI (Change in NDVI/ year).

S/N	Parameters	Value obtained
1.	Mean (pixels with + slope)	2.4228×10^{-5}
2.	Mean (pixels with − slope)	-3.0889×10^{-5}
3.	SD (pixels with + slope)	3.3757×10^{-5}
4.	SD (pixels with − slope)	1.8121×10^{-4}
5.	Mean (all)	2.1294×10^{-5}
6.	SD (all)	8.2903×10^{-5}

Table 8. Alua: Mean and SD for (+), (−) and net slopes of NDVI (Change in NDVI/ year).

S/N	Parameters	Value obtained
1.	Mean (pixels with + slope)	8.8056×10^{-5}
2.	Mean (pixels with − slope)	-2.4815×10^{-4}
3.	SD (pixels with + slope)	5.2640×10^{-5}
4.	SD (pixels with − slope)	0.0011
5.	Mean (all)	8.7469×10^{-5}
6.	SD (all)	1.4516×10^{-4}

Table 9. Rukpokwu: Mean and SD for (+), (−) and net slopes of NDVI (Change in NDVI/ year).

S/N	Parameters	Value obtained
1.	Mean (pixels with + slope)	7.6961×10^{-5}
2.	Mean (pixels with − slope)	-4.3011×10^{-5}
3.	SD (pixels with + slope)	4.1556×10^{-5}
4.	SD (pixels with − slope)	1.7924×10^{-4}
5.	Mean (all)	7.3986×10^{-5}
6.	SD (all)	6.2093×10^{-5}

Table 10. Obigbo: Mean and SD for (+), (−) and net slopes of NDVI (Change in NDVI/ year).

S/N	Parameters	Value obtained
1.	Mean (pixels with + slope)	7.9023×10^{-5}
2.	Mean (pixels with − slope)	-3.5435×10^{-4}
3.	SD (pixels with + slope)	4.5078×10^{-5}
4.	SD (pixels with − slope)	7.1281×10^{-4}
5.	Mean (all)	7.8273×10^{-5}
6.	SD (all)	1.1192×10^{-4}

Figures 4-14 show Maps of annual change in NDVI (regression slopes), regression coefficient, R-values and p-values for each of the flaring site are presented in Figs 4-14. α >0.05 is the significant level adopted for the analysis. The p-value maps are Ps which shows where the relationship is statistically significant. The yellow colour area in the map slope shows portions within the site where the temporal trend in NDVI is statistically significant. Also, portions that are always cloudy or that are not vegetation are white in the map P.

Table 11. Chokocho: Mean and SD for (+), (−) and net slopes of NDVI (Change in NDVI/ year).

S/N	Parameters	Value obtained
1.	Mean (pixels with + slope)	1.0546×10^{-4}
2.	Mean (pixels with − slope)	-2.1310×10^{-4}
3.	SD (pixels with + slope)	3.9183×10^{-5}
4.	SD (pixels with − slope)	4.3901×10^{-5}
5.	Mean (all)	1.0520×10^{-4}
6.	SD (all)	5.0786×10^{-5}

Table 12. Umudioga: Mean and SD for (+), (−) and net slopes of NDVI (Change in NDVI/ year).

S/N	Parameters	Value obtained
1.	Mean (pixels with + slope)	4.8557×10^{-5}
2.	Mean (pixels with − slope)	-4.0582×10^{-5}
3.	SD (pixels with + slope)	5.8950×10^{-5}
4.	SD (pixels with − slope)	8.9129×10^{-5}
5.	Mean (all)	-3.0408×10^{-5}
6.	SD (all)	1.0120×10^{-4}

Table 13. Sara: Mean and SD for (+), (−) and net slopes of NDVI (Change in NDVI/ year).

S/N	Parameters	Value obtained
1.	Mean (pixels with + slope)	3.3600×10^{-5}
2.	Mean (pixels with − slope)	-2.9388×10^{-5}
3.	SD (pixels with + slope)	2.4634×10^{-5}
4.	SD (pixels with − slope)	9.2132×10^{-5}
5.	Mean (all)	1.4015×10^{-5}
6.	SD (all)	7.6382×10^{-5}

For Figure 4 (Eleme Refinery I) there is a little portion with yellow colour in the slope map which spread in the N, E, S and NW directions within the site that presented significant temporal trend in the NDVI.-2.71×10^{-5}-$2.32 \times 10^{-5}$is the range of value with a mean of$\pm 3.38 \times 10^{-5}$and the p-value is from 0.05 and above. However, the significant trend for a small portion occurred (slope map) in the NW, S and SW directions within the site Eleme Refinery II Figure 5); and the value obtained ranges from (-1.740×10^{-4}-2.074×10^{-5}) with a mean of ($\pm 3.093 \times 10^{-5}$) and p-value from 0.05 and above. For Onne station (Figure 6), little portions in the E, SE, S and W directions presented a significant result. The range of the trend in NDVI is (-2.428×10^{-5}-2.9639×10^{-5}) with SD of ($\pm 7.952 \times 10^{-5}$) and p-value from 0.05 and above.

Figure 7 (Umurolu) slope shows that there is a significant positive temporal trend in NDVI within Umurolu site (portion with yellow colour).The spatially coherent portion in NDVI within the Umurolu site which include boundary of the flow station and an area within the site up to a distance of 90 m from the flare (mostly E direction) is between (-1.679×10^{-5} and 5.868×10^{-5}) with SD of ($\pm 7.499 \times 10^{-5}$); and with the p-value from 0.05 and above. For Figure 8 (Bonny LNG) some portions within the site in the N, NE, E, S and SE directions (area with yellow colour) gives significant results with -3.089×10^{-5}-2.423×10^{-5} as the range of NDVI and the same p-value as for Umurolu. Also, Alua site (Figure 9) presented a significant result around the flow station and at a distance towards E, NE, W and NW directions (sections with yellow colour) where the slope $\neq 0$ (between -2.482×10^{-4}-8.806×10^{-5}, with a SD$\pm$ 1.452×10^{-4}); and p-value from 0.05 and above.

Rukpokwu (Fig. 10) has significant trend in NDVI with the locations that are spatially coherent (portions with yellow colour). Such portions are around the facility, towards N, NW and SW where the changes in NDVI are more pronounced. NDVI range for Rukpokwu is (-4.301×10^{-5}-7.696×10^{-5}), SD of ($\pm 6.209 \times 10^{-5}$) and value of p is 0.05 and above. In addition, Obigbo(Figure 11) also show statistically significant results (yellow colour portions) with much effect in the N, NE, E and S. NDVI is (-3.544×10^{-4}-7.902×10^{-5}), SD ($\pm 1.119 \times 10^{-4}$) and p-value is 0.05 and above. For Chokocho (Figures 12) most portions such as flow station surroundings within the site presented significant results Chokocho's NDVI range in the trend is (-2.131×10^{-4}-1.055×10^{-5}), SD ($\pm 5.079 \times 10^{-5}$), and p-value is 0.05 and above.

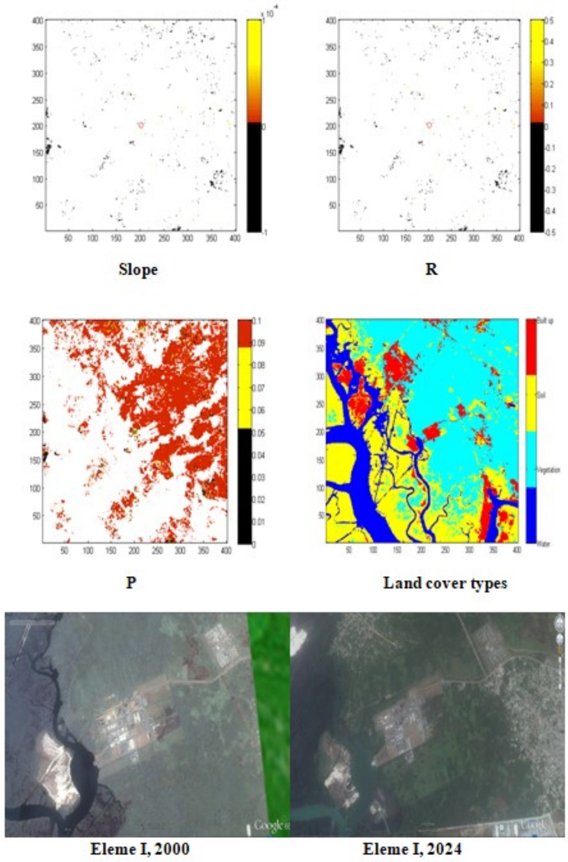

Figure 4. Maps of slope, r & p values; & land cover types for Eleme I

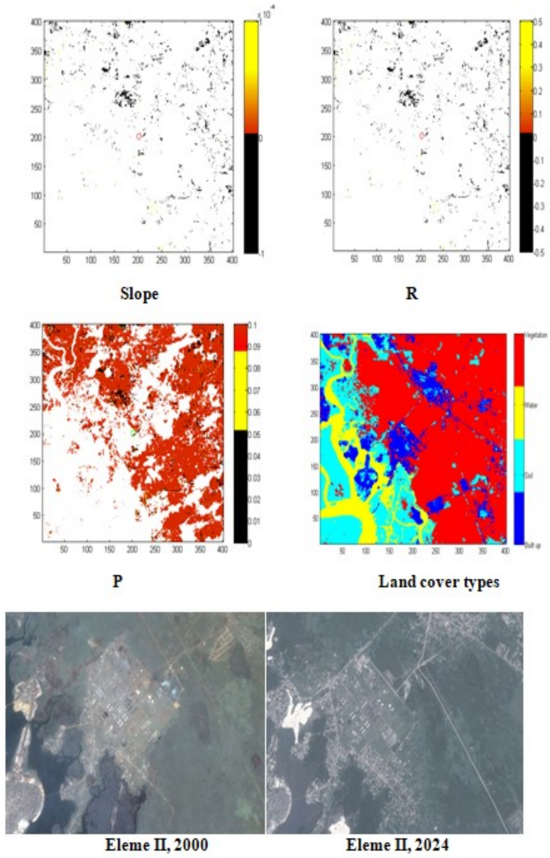

Figure 5. Maps of slope, r & p values; & land cover types for Eleme II

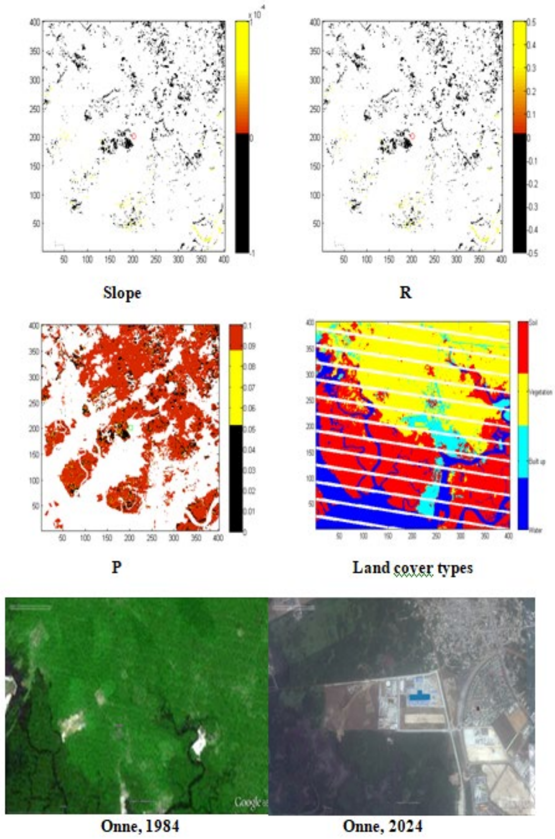

Figure 6. Maps of slope, r & p values; & land cover types for Onne

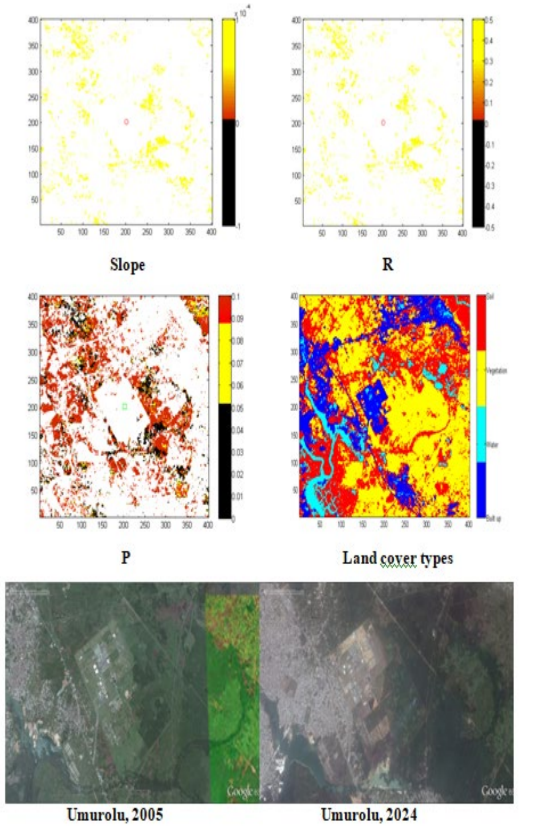

Figure 7: Maps of slope, r & p values; & land cover types for Umurolu

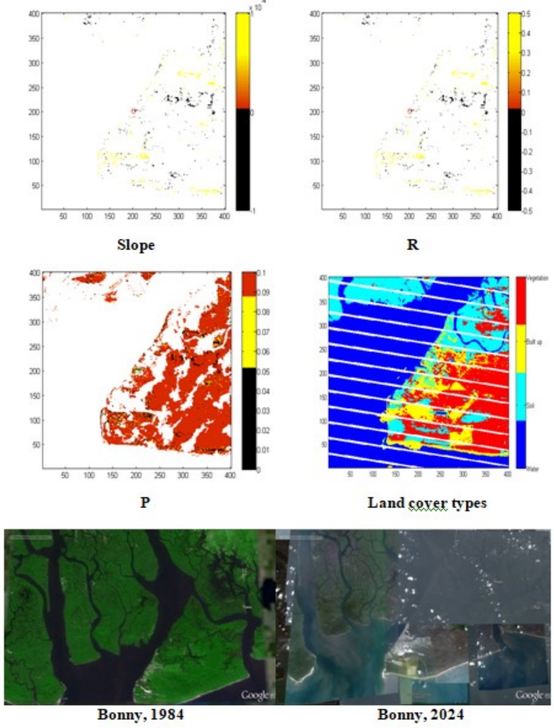

Figure 8. Maps of slope, r & p values; & land cover types for Bonny

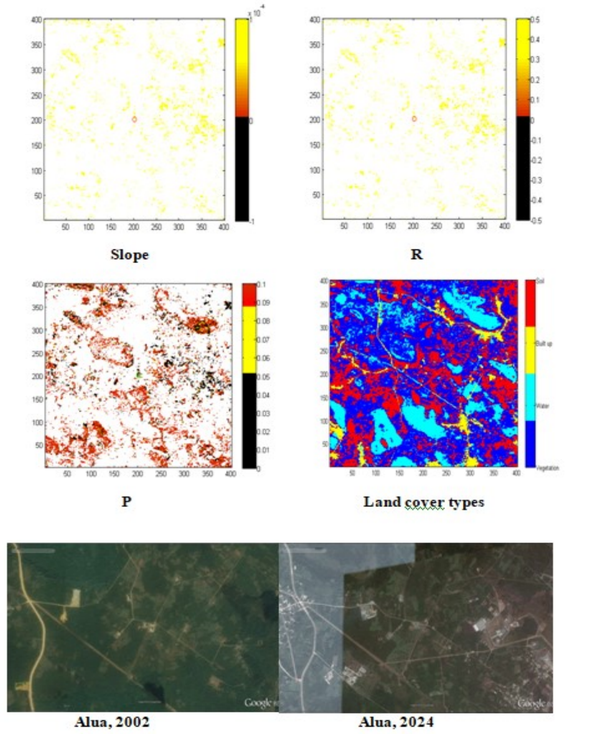

Figure 9. Maps of slope, r & p values; & land cover types for Alua

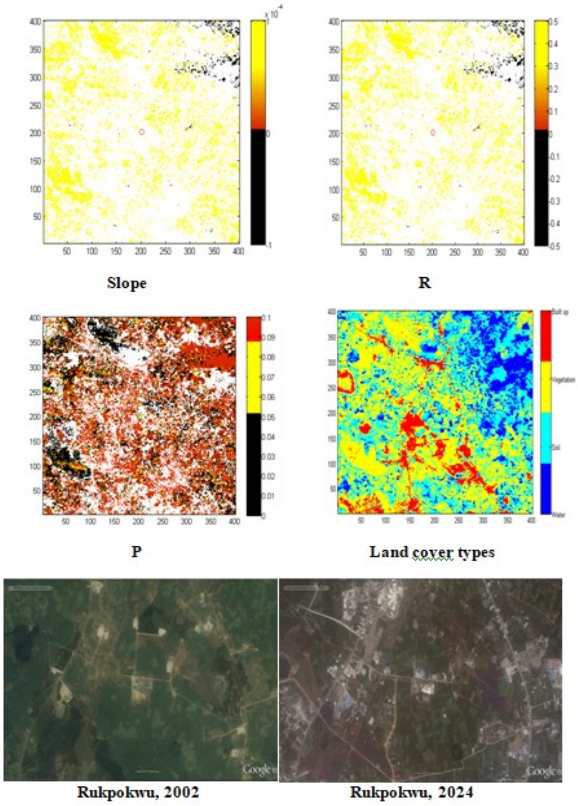

Figure 10. Maps of slope, r &*p* values; & land cover types for Rukpokwu

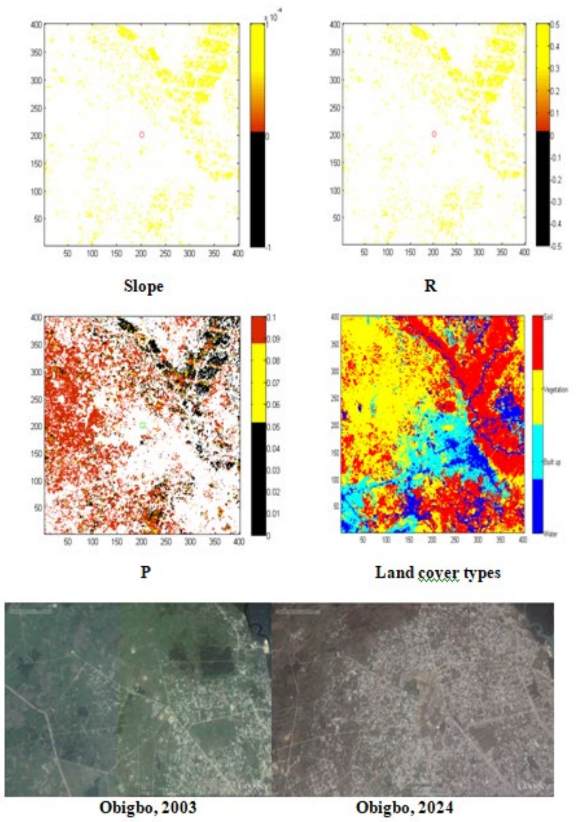

Figure 11. Maps of slope, r &*p* values; & land cover types for Obigbo

For Figure 12 slope, sufficient data to proof that the gas flaring effects only is the factor for the trend in NDVI throughout the site. Factors such as burning of refuse, clearing of bush for farming, burning of bush for killing of animals etc could be contributing to the result.

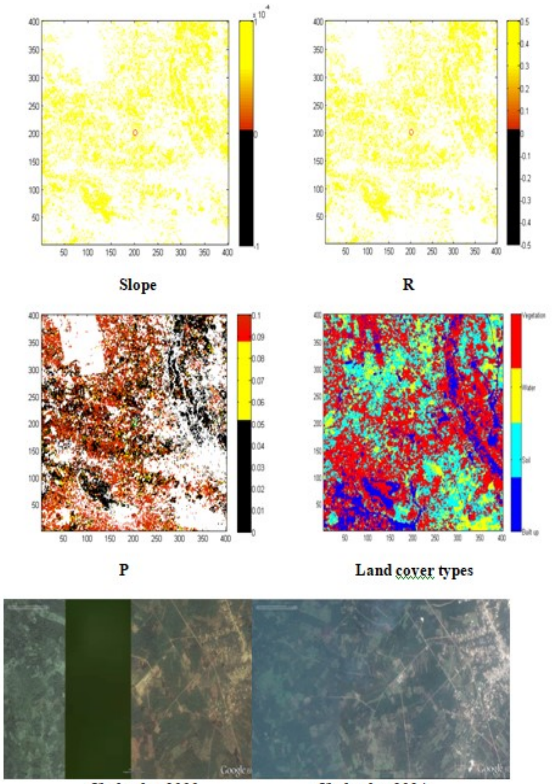

Figure 12. Maps of slope, r & p values; & land cover types for Chokocho

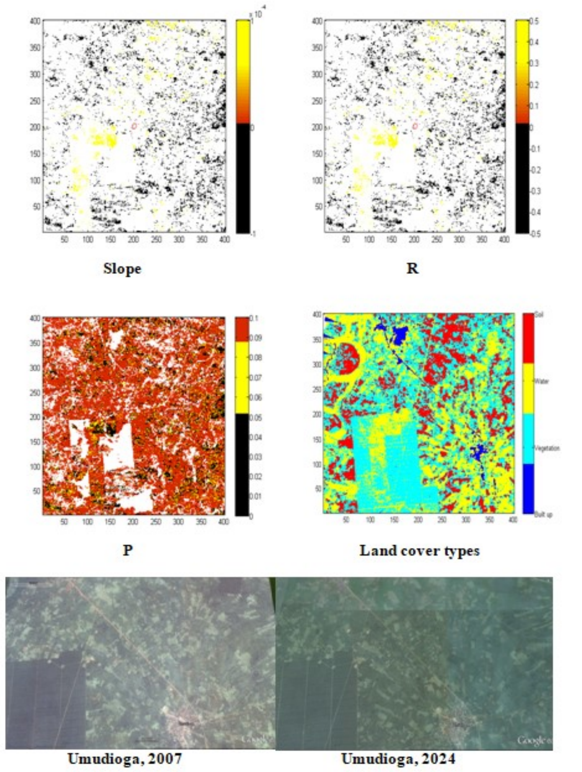

Figure 13. Maps of slope, r & p values; & land cover types for Umudioga

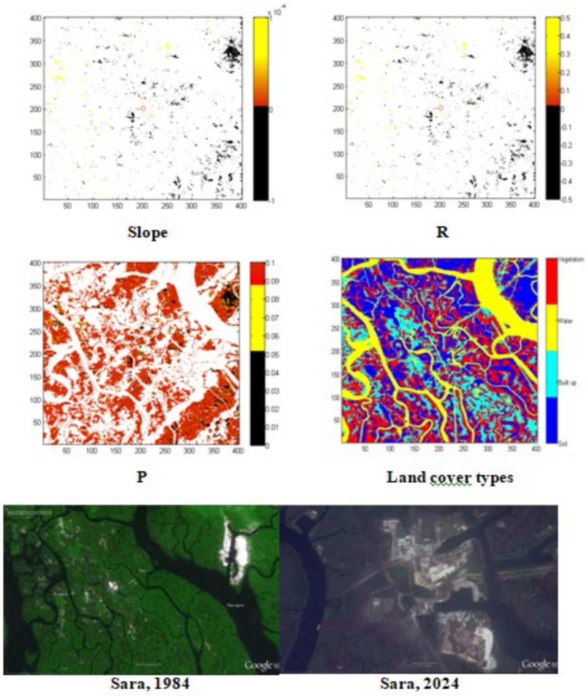

Figure 14. Maps of slope, r & p values; & land cover types for Sara

Umudioga (Figure 13) presented statistically significant results within the site which is more pronounced around the facility towards W except in the NW direction. The N of the site shows a partially significant trend. The NDVI trend range for the site is (-4.058×10^{-5}-4.856×10^{-5}), SD ($\pm 1.012 \times 10^{-4}$) and p-value is 0.05 and above. Furthermore, Sara site (Figures 14), located at the coastal boundary of River Bonny presented that a little portion within the site has a statistically significant result with not much in the S and SW directions. The result obtained could be as a result of its coastal location. NDVI trend range (-2.939×10^{-5}-3.360×10^{-5}), SD (7.638×10^{-5}), and p-value of 0.05 and above are recorded.

The significant (+) trends results in the NDVI for a larger area within each site were presented by the inland facilities (Umurolu, Alua, Rukpokwu, Obigbo, Chokocho and Umudioga). Coastal facilities (Bonny, Eleme I and II, Onne, and Sara) show the significant (+) trends in the NDVI over a small area. However, Bonny facility show wider (+) significant trend than all other coastal facilities because it gas has 5 flare stacks within the facility. Also, for Bonny site the + significant trend in the E direction of the site could be as a result of the impact of human activities e.g. urban growth.

The results show that the temporal in NDVI is specific to each site, and that the effect of the flares on the vegetation cover does not majorly depend on the size of facility. Both Eleme I (-2.71×10^{-5}-2.32×10^{-5}) and II (-1.740×10^{-4}-2.074×10^{-5}) presented significant results for a small portion of the area. Umurolu (-1.679×10^{-5}-5.868×10^{-5}) and Bonny (-3.089×10^{-5}-2.423×10^{-5}) show significant results which could be as a result ofthe number of flare stacks within them 4 and 5 respectively. Furthermore, all small and medium facilities show statistically significant results which could be attributed to the rate and volume of gas burning from them. Sara site with statistically significant results (-2.939×10^{-5} to 3.360×10^{-5}) over a narrow area is a result of its swampy location with many tributaries.

The results of previous studies similar to this research are in support of the results obtained for this research. From Figures 4-14, the marked yellow colour portions in the slope maps shows the area within the site where the NDVI temporal trend is statistically significant. This means that as a result of nearly zero or lowest value of NDVI, the vegetation is sparse, nearly dead or dead due to the effect of gas flaring in the area. This is supported by several researchers including Nwaogu & Onyeze (2020); they stated that destruction of vegetation and agricultural produce are some of impacts of flaring in the environment. Musa et al. (2024) also concluded that stunted growth, death of vegetation and farm produce are part of results of flaring gas effects in the environment. Furthermore, Lu et al. (2020); Umbugala & Morakinyo (2023); Morakinyo (2024a); Morakinyo (2025b) concluded that environmental pollution occurs at flaring sites. In addition, many researchers have concluded that NDVI is the most useful vegetation index for vegetation assessment. Other previous results that are in supports of this study includes (Kalisa et al., 2019); Huang et al., 2020; Hua et al., 2019, Wei et al., 2021; Karnieli et al., 2010; Polat et al., 2024; Gessner et al., 2023; Kloos et al., 2021; Chang et al., 2022; Chrysopolitou *et al.*, 2013); Lavender, 2016); Jiang, 2021); Hu et al., 2023; Guha, 2021; Guha et al., 2020; Roßberg & Schmitt, 2023; Pastor-Guzman, 2015; Vicente-Serrano et al., 2016; Chavez, 2016).

The limitation of this study is that Landsat data used cover only dry season in Nigeria. Hence, the results obtained cannot determine the effects of the flare on the vegetation in all seasons. How each vegetation type responds to the flare could not be assessed due to lack of data on the vegetation types and their photosynthetic rate. The rate and volume of the gas burning at each site does could not be applied to this study due to their unavailability and so this study could not give the exact total influence of flare on the vegetation.

Conclusions

Generally, the results show a fall from healthy vegetation as the flare stacks are being spatially approached in the all sites and so the vegetation closer to the flare is dead.The impact of gas flare is felt up to 120 m from the stack with an annual reduction in NDVI values over the timescale analyzed. Onne site show an unstable trend from 1984 to 2007 (years before it was built) which could be as a result ofvegetation density, vegetation types and their photosynthetic rate as there was no flaring activities during this period.

The results obtained showthat each site is specific with its own temporal trend in NDVI from 1984 to 2024. Hence, it can be concluded that Landsat data can be used to map the spatial and temporal impacts of flare on vegetation cover in the Niger Delta. However, the spatial and temporal variability in Landsat data linked to the detectable flare impact on vegetation cover is specific to each site and its activities, and dependent on the landscape of the site, e.g. Sara facility is built in the swampy terrain. Flaring is still ongoing in Nigeria and its associated challenges evident with Nigerian Government yet to determine to have zero flare in Nigeria. Therefore, I wish to make the following recommendations:

- Nigerian Government should carry out the **s**tringent enforcement of the Nigerian Petroleum Industry Act of 2021.
- Nigerian Environmental protection laws should have adequate provisions for combating oil and gas pollution, degradation, and gas flaring. The National Environmental Standard Regulation Enforcement Agency (Establishment) Act (NESREA), 2007, should be amended to widen its scope to oil and gas sector activities.
- The Nigerian Constitution should be amended to make environmental infringements justiciable in order to guarantee a healthy and sustainable environment.
- Enactment of the comprehensive regulatory framework governing gas utilization and development of gas pipeline networks to all the six (6) geo-political zones in Nigeria for proper gas distribution.
- The Nigerian Government should increase generation of electricity in Nigeria using gas.
- Oil companies should update their equipment to modern technologies and methods to be in accordance with theinternational standards.
- Nigerian Government should encourage investors in the energy sector by providing the enabling environment.
- A gas flaring price targeting natural gas companies should be more effective in mitigating gas flaring than the wider 'carbon price' or pollution price/tax policy.
- The Federal Government should provide alternative energy sources to mitigate the effect of gas flaring on the people and salvage the environment.

Acknowledgement: *The Author is grateful to the USGS for the provision of Landsat data. Many thanks to Jill Schwarz for MATLAB coding and guidance.*
Conflict of Interest: *The Author declares no conflict of interest.*

References

Berlanga-Robles CA, Ruiz-Luna A, (2002). Land use mapping and change detection in the coastal zone of northwest Mexico using remote sensing techniques. *J. Coastal Resour.***18**(3):514-522. https://www.jstor.org/stable/4299098

Butt B, (2018) Environmental indicators and governance. *Current Opinion on Environ. Sus.* **32**: 84-89. https://doi.org/10.1016/j.cosust.2018.05.006

Campbell JB, (2007) Introduction to remote sensing, 4thEdn. The Guil ford Press, New York. https://istncrg.wordpress.com/wp-content/uploads/2019/09/introduction_to_remote _sensing_www.gisman.ir_.pdf

Chander G, Markham K, (2003). Revised Landsat 5 TM Radiometric Calibration Procedures and Post Calibration Ranges. *IEEE Trans. of Geosci.& Remote Sens.***41**(11): 2674-2677. https://doi.org/10.1109/TGRS.2003.818464

Chang J, Liu Q, Wang S, Huang C, (2022) Vegetation Dynamics and Their Influencing Factors in China from 1998 to 2019. *Remote Sensing***14**, 3390. https://doi.org/10.3390/rs14143390

Chavez PS, (1996) Image-based Atmospheric Corrections-Revisited and Improved. *Photogrammetry Engineering & Remote Sensing***62**(9): 1025-1036. https://www.researchgate.net/publication/236769129_Image-Based_Atmospheric_Corrections_-_Revisited_and_Improved

ChrysopolitouV, ApostolakisA, AvtzisD, AvtzisN, DiamandisS, KemitzoglouD, PapadimosD, PerlerouC,TsiaoussiV, DafisS, (2013) Studies on forest health and vegetation changes in Greece under the effects of climate changes. *Biodiv. Conser.*, **22**:1133-1150, https://link.springer.com/article/10.1007/s10531-013-0451-2.

Epstein J, Payne K Kramer E, (2002) Techniques for mapping suburban sprawl. *Photogrammetry Engineering Remote Sensing* 68(9):913-918 EROS (2021) Earth Resources Observation and Science (EROS)

ESRI. (2024) Map of Nigeria, map of Rivers State and map of 11 gas flaring studied sites.https://www.esri.com/en-us/arcgis/products/arcgis-storymaps/contest/overview

Gessner U, Reinermann S, Asam S, Kuenzer C, (2023) Vegetation Stress Monitor-Assessment of Drought and Temperature-Related Effects on Vegetation in Germany Analyzing MODIS Time Series over 23 Years. *Remote Sensing* 15, 5428. https://doi.org/10.3390/rs15225428

Guha S, (2021) A long-term monthly assessment of land surface temperature and normalized difference vegetation index using Landsat data. *urbe. Revista Brasileira de Gestão Urbana*, v.13, e20200345. https://doi.org/10.1590/2175-3369.013.e20200345

Guha S, GovilH, DiwanP, (2020) Monitoring LST-NDVI Relationship Using Premonsoon Landsat Datasets. *Advan. in Meteo.*2020, Article ID 4539684, 15 https://doi.org/10.1155/2020/4539684

Hu Y, Raza A, Syed, NR, AcharkiS, Ray RL, Hussain S, Dehghanisanij H, Zubair M, Elbeltagi A, (2023) Land Use/Land Cover Change Detection and NDVI Estimation in Pakistan's Southern Punjab Province. *Sustain.*, 15**,** 3572,https://doi.org/10.3390/su15043572

HuaX, RenaH, TanseyK, ZhengaY, GhentD, LiuX, YanL, (2019) Agricultural drought monitoring using European Space Agency Sentinel 3A land surface temperature and normalized difference vegetation index imageries. *Agri.& Forest Meteor.***279**, 107707. https://www.scilit.com/publications/ab36ace649bb150860f2a1b0058149ec

HuangS, TangL, HupyP, WangY, ShaoG, (2020) A commentary review on the use of normalized difference vegetation index (NDVI) in the era of popular remote sensing. *J. Forestry Res.* **32**(1): 1-6,https://doi.org/10.1007/s11676-020-01155-1

HueteA, DidanK, MiuraT, RodriguezEP, X Gao, FerreiraLG, (2002) Overview of the radiometric and biophysical performance of the MODIS vegetation indices. *Remote Sens. Environ.* 83 (1-2): 195-213, https://doi.org/10.1016/S0034-4257(02) 00096-2

IhlenV, (2019) Landsat 8 (L8) Data Users Handbook, Version 5.0. Department of the Interior, U.S. Geological Survey. https://www.usgs.gov/landsat-missions/landsat-8-data-users-handbook

Jensen JR, (2005) Introductory digital image processing: a remote sensing perspective, 3rd edn. Prentice Hall, Upper Saddle River Campbell JB (2007) Introduction to remote sensing, 4thedn. The Guilford Press, New York. https://www.scribd.com/document/667034923/JENSEN-J-R-Introductory-Digital-Image-Processing-a-Remote-Sensing-Perspective

Jansen LJM, Di-Gregorio A, (2004) Obtaining land-use information from a remotely sensed land cover map: results from a case study in Lebanon. *Int. J. App. Earth Obser. & Geoin.* 5 (2):141-157. https://doi.org/10.1016/j.jag.2004.02.001

Jensen JR, Cowen DC, (1999) Remote sensing of urban/suburban infrastructure and socio-economic attributes. *Photogr. Eng. Remote Sensing* **65**:611-622. https://www.asprs.org/wp-content/uploads/pers/99journal/may/1999_may_611-622.pdf

JiangL, LiuY, WuS, YangC, (2021) Analyzing ecological Environmental change and associated driving factors in China based on NDVI time series data. *Ecol. Indi.***129**, 107933. https://doi.org/10.1016/j.ecolind.2021.107933

Kalisa W, Igbawua T, Henchiri M, Ali S, Zhang S, Bai Y, Zhang J, (2019) Assessment of climate impact on vegetation dynamics over East Africa from 1982 to 2015. *Sci. Reports* **9**:16865,https://doi.org/10.1038/s41598-019-53150-0

KarnieliA, AgamN, PinkerRT, AndersonM, ImhoffML, GutmanGG, PanovN, GoldbergA, (2010) Use of NDVI and Land Surface Temperature for Drought Assessment: Merits and Limitations. *J. Climate* 23: 618-633. https://doi.org/10.1175/2009JCLI2900.1

KloosS, YuanY, CastelliM, MenzelA, (2021) Agricultural Drought Detection with MODIS Based Vegetation Health Indices in Southeast Germany. *Remote Sens.***13**, 3907. https://doi.org/10.3390/rs13193907

Liang S, Fang H, Chen M, (2001) Atmospheric Correction of Landsat ETM+ Land Surface Imagery - Part I: Methods. *IEEE Transactions on Geoscience and Remote Sensing* 39(11): 2490-2498. https://doi.org/10.1109/36.964986

LavenderSJ, (2016) Monitoring land cover dynamics at varying spatial scales using high to very high resolution optical imagery. The International Archives of the Photogrammetry, *Remote Sensing and Spatial Informa. Sci.*, Vol. XLI-B8, 23rdISPRS Congress, 12-19 July, Prague, Czech Republic.https://isprs-archives.copernicus.org/articles/XLI-B8/937/2016/isprs-archives-XLI-B8-937-2016.pdf

Lu W, Liu Y, Wang J, Xu W, Wu W, Liu Y, Zhao B, Li H, Li P, (2020) Global proliferation of offshore gas flaring areas. *J. Maps* 16(2): 396-404, DOI: 10.1080/17445647.2020.1762773

Maaharjan, A. (2018) Land use/land cover of Katrimandu valley by using Remote Sensing and GIS. M.Sc. Dissertation submitted to Central Department of Environmental Sciences, Inst. Sci.& Tech., Tribhuvan Uni., Kirtipur, Kathmandu, Nepal. https://www.academia.edu/37299127/land_use_land_cover_of_kathmandu_valley_by_using_remote_sensing_and_gis

MolliconeD, AchardF, EvaH, BelwardAS, FedericiS, Lumicisi A, (2003) Land use change monitoring in the Framework of the UNFCCC and its Kyoto Protocol: report on current capabilities of satellite remote sensing technology. European Communities, Luxembourg. EUR, 20867.https://publications.jrc.ec.europa.eu/repository/handle/JRC26418

MorakinyoBO, (2025b) Geospatial Information for Land Use Planning and Sustainable Management. *FUDMA Journal of Sciences (FJS)***9**(2): 105-118, DOI: https://doi.org/10.33003/fjs-2025-0902-3146

MorakinyoBO, (2024a) Time Series Analysis from 1984 to 2023 of Earth Observation Satellites Data for Evaluating Changes in Vegetation Cover and Health at Flaring Sites in the Niger Delta, Nigeria. *Academic Platform Journal of Natural Hazards and Disaster Management***5**(2): 76-100, DOI: 10.52114/apjhad.1557231

MorakinyoBO, (2024b) Determination of Mean Sea Level from 1980 TO 2018 Using Tidal Observation Data, Bonny Primary Port, Nigeria. *Science World Journal***19**(4): 1176-1184.

Morakinyo BO, (2024c) Analysis from 1980 TO 2018 of Tidal Observation Data for Assessing the Stability of Tidal Constants for Primary Port. *FUDMA Journal of Sciences (FJS)***8(**6): 503-513, DOI: https://doi.org/10.33003/fjs-2024-0806-3043

MorakinyoBO, (2023c) Detection of Impacts of Gas Flaring in the Environment: Application of Landsat Earth Observation Data. *BAZE University J. Entrepreneurship and Interdisciplinary Studies* **2**(1): 74-89.http://dx.doi.org/10.61955/XQBJFP

MorakinyoBO, (2023b) Assessments of the impacts of environmental factors on vegetation cover at gas flaring sites in the Niger Delta, Nigeria. *Review of Environ. and Earth Sci.* 10(1): 8-18.http://dx.doi.org/10.18488/80.v10i1.3390

MorakinyoBO, LavenderS, AbbottV, (2023a) Detection of potentially gas flaring related pollution on vegetation cover and its health using remotely sensed data in the Niger Delta, Nigeria. *Asian Review of Environ.& Earth Sci.***10**(1): 1-13. https://doi.org/10.20448/arees.v10i1.4407

MorakinyoBO, LavenderS, AbbottV,. (2022b) Evaluation of factors influencing changes in land surface temperature at gas flaring sites in the Niger Delta, Nigeria. *BAZE University J. Entrepreneurship and Interdisciplinary Studies* 1(2): 1-19.http://dx.doi.org/10.61955/RIIKUF

MorakinyoBO, LavenderS, AbbottV, (2022a) Investigation of potential prevailing wind impact on land surface temperature at gas flaring sites in the Niger Delta, Nigeria.*Int. J. Environ. A&ndGeoinfor.* **9**(1): 179-190,https://doi.org/10.30897/ijegeo.968687

MorakinyoBO, LavenderS, AbbottV,. (2021) The methodology and results from ground validation of satellite observations at gas Flaring Sites in Nigeria.*Int. J. Environ. and Geoinformatics* 8(3): 290-300, https://doi.org/10.30897/ijegeo.749664

MorakinyoBO, LavenderS, AbbottV, (2020b) Retrieval of land surface temperature from Earth observation satellites for gas flaring sites in the Niger Delta, Nigeria.*Int. J. Environmental Monitoring and Analysis*8(3): 59-74. https://doi.org/10.11648/j.ijema.20200803.13

MorakinyoBO, LavenderS, AbbottV, (2020a) Assessment of uncertainties in the computation of atmospheric correction parameters for Landsat 5 TM and Landsat 7 ETM+ thermal band from atmospheric correction parameter (ATMCORR calculator) *British J. Environ. Sci.***8**(1): 20-30. https://eajournals.org/bjes/vol-8-issue-1-february-2020/assessment-of-uncertainties-in-the-computation-of-atmospheric-correction-parameters-for-landsat-5-tm-and-landsat-7-etm-thermal-band-from-atmospheric-correction-parameter-atmcorr-calculator/

MorakinyoBO, LavenderS, SchwarzJ, AbbottV,. (2019) Mapping of land cover and estimation of their emissivity values for gas flaring sites in the Niger Delta. *British J. Environ. Sci.* 7(2): 31-58. https://www.eajournals.org/wp-content/uploads/Mapping-of-land-cover-and-estimation-of-their-emissivity-values-for-gas-flaring-sites-in-the-Niger-Delta.pdf

MorakinyoBO, (2015) Flaring and pollution detection in the Niger Delta using remote sensing. PhD Thesis, University of Plymouth, Plymouth, United Kingdom.https://dx.doi.org/10.24382/4528

Markham BL, Barker JL, (1986) Landsat MSS and TM post-calibration dynamic ranges, exoatmosphericreflectances and at-satellite temperature. EOSAT Landsat Technical Notes: 3-8.https://www.scirp.org/reference/referencespapers?referenceid=1578935

Musa,DG., Oruonye, E. D., Anger, R. T., Ojeh, V. N & Delphine, D. (2024) Effect of Gas Flaring on Human Well-Being and Environ. in Obodo-Ugwa, Ndokwa West, Local Government Area, Delta State, Nigeria. *J. Eng. & Environ. Sci.* **2**(1): 000108. *https://medwinpublishers.com/JEESc/effect-of-gas-flaring-on-human-well-being-and-environment-in-obodo-ugwa,-ndokwa-west,-local-government-area,-delta-state,-nigeria.pdf*

NASA. (2002) National Aeronautics and Space Administration. Landsat 7 ETM+ Science Data Users Handbook.http://www.landsathandbook.gsfc.nasa.gov/data_prod/prog_sect11_3.html [Accessed 23rdJan. 2022].

NwaoguLA, OnyezeGOC, (2020) Environmental Impacts of Gas Flaring on Ebocha-Egbema, Niger Delta, Nigeria. *Energy & Environ. Res.***8**(1): 1-11.https://dergipark.org.tr/tr/pub/apjhad/issue/89412/1557231

Odukoya OA, (2006) Oil and sustainable development in Nigeria: A case study of the Niger Delta. *Human Ecology* 20(4): 249-258.DOI: 10.31901/24566608.2006/20.04.03

Onosode GO, (2003) Environmental Issues and challenges of the Niger Delta (Perspectives from the Niger Delta Environmental Survey Process) Lagos, Lilybank Property & Trust Limited. https://books.google.com/books/about/Environmental_Issues_and_Challenges_of_t.html?id=MmQ7AQAAIAAJ

Pastor-Guzman, J., Atkinson, P., Dash, J & Rioja-Nieto, R. (2015) Spatio-temporal variation in mangrove chlorophyll concentration using Landsat 8. *Remote Sensing of Environ.* **7**(11): 14530-14558.http://dx.doi.org/10.3390/rs71114530

PettorelliN, VikJO, MysterudA, GaillardJM, TuckerCJ, StensethNC, (2005) Using the satellite-derived NDVI to assess ecological responses to environmental change. *Trends of Ecol.Evol.***20**(9): 503-510.https://doi.org/10.1016/J.TREE.2005.05.011

Polat AB, Akcay O, Kontas F, (2024) Drought monitoring in Burdur Lake, Turkey using multi-sensor remote sensing data sets. *Ad. Geodesy &Geoinfor. (formerly Geodesy and Cartography)* 73(1), article no. e47, DOI:10.24425/agg.2023.146159

RoßbergT, SchmittM, (2023) A Globally Applicable Method for NDVI Estimation from Sentinel-1 SAR Backscatter Using a Deep Neural Network and the SEN12TP Dataset. PFG, 91: 171-188.http://dx.doi.org/10.1007/s41064-023-00238-y

SanterR, CarrereV, DubuissonP, RogerJC, (1999) Atmospheric correction over land for MERIS. *Int. J. Remote Sens.***20**: 1819-1840. https://earth.esa.int/eogateway/documents/20142/37627/ MERIS%20ATBD%202-15

Şatır O, Berberoğlu S, (2012) Land Use/Cover Classification Techniques Using Optical Remotely Sensed Data in Landscape Planning, Landscape Planning, Dr. Murat Ozyavuz (Ed.), ISBN: 978-953-51-0654-8, InTech. [Online]. *http://www.intechopen.com/books/landscape-planning/land-use-cover-classificationtechniques-using-optical-remotely-sensed-data-in-landscape-plannin* [Accessed 15th May 2023]

TianJ, WangL, LiX, GongH, ShiC, ZhongR, LiuX, (2017) Comparison of UAV and WorldView-2 imagery for mapping leaf area index of mangrove forest. *Int. J. Appl. Earth Obser.&Geoinfor.***61**: 22-31. h*ttp://dx.doi.org/10.1016/*j.jag.2017.05.002

Umbugala,UD&MorakinyoBO, (2023) Detection of Oil and Gas Platforms in the Niger Delta, Nigeria: Role of Digital Technology in Facilities Management. *BAZE University J. Entrep.&Interdis. Stud.***2**(2): 11-22. https://boldscholar.com/Home/ArticleLists?volID=21&journalID=12

Vicente-Serrano, S. M., Camarero, J. J., Olano, J. M., Martín-Hernández, N., Peña-Gallardo, M., Tomás-BurgueraM, GazolA, Azorin-MolinaC, BhuyanU, El-KenawyA, (2016) Diverse relationships between forest growth and the normalized difference vegetation index at a global scale. *Remote Sens Environ.* **187**: 14-29.https://doi.org/10.1016%2Fj.rse.2016.10.001

Wei W, Zhang H, Zhou J, Zhou L, Xie B, Li C, (2021) Drought monitoring in arid and semi-arid region based on multi-satellite datasets in Northwest China. *Environ Sci & Poll.Res.* **28**: 51556-51574.https://doi.org/10.1007/s11356-021-14122-y

Xiao J, Shen Y, Ge J, Tateishi R, Tang C, Liang Y, Huang Z, (2006) Evaluating urban expansion and land use change in Shijiazhuang, China, by using GIS and remote sensing. *Lands. Urban Plan***75**(1-2):69-80.https://doi.org/10.1016/j.landurbplan.2004.12.005

Yuan F, Sawaya KE, Loeffelholz BC, Bauer ME, (2005) Land cover classification and change analysis of the Twin Cities (Minnesota) Metropolitan Area by multi-temporal Landsat remote sensing. *Remote Sens. Environ.***98**(2-3):317-328. https://doi.org/10.1016/j.rse.2005.08.006